Detour pathways of descending motor systems

Emma Mitchell

BSc (Hons)

A Thesis submitted in fulfilment of the requirements for the degree of Doctor
of Philosophy to the Institute of Neuroscience and Psychology,
College of Medical, Veterinary and Life Sciences,
University of Glasgow

September 2015

University
of Glasgow

VIA VERITAS VITA

Abstract

The motor cortex makes a substantial contribution to contralateral limb function via the corticospinal tract (CST). The extent to which the motor cortex influences ipsilateral limb function is less clear. Interest in ipsilateral cortical control stems from studies of stroke survivors, demonstrating increased activation of the ipsilateral motor cortex during movement of the affected limb. This raises the possibility that ipsilateral pathways contribute to recovery of function following damage to the contralateral CST. The overarching aim of this thesis was to extend the knowledge of neural systems that might mediate ipsilateral actions of the motor cortex, both under normal circumstances and after stroke.

In rodent models of stroke, there is evidence that CST axons originating from the non-ischaemic hemisphere sprout into the denervated (ipsilateral) side of the spinal cord, and the extent of sprouting correlates with the degree of motor recovery. However, it is yet to be confirmed whether the CST from the non-ischaemic hemisphere establishes new terminals in the denervated (ipsilateral) side of the spinal cord to replace connections lost after stroke. Hence, the first major aim of this thesis was to assess for CST terminal remodelling between the non-ischaemic hemisphere and the denervated (ipsilateral) side of the cervical spinal cord following recovery from experimental stroke in the rat. Rats underwent 60 min middle cerebral artery occlusion (MCAo) or sham occlusion surgery. Behavioural testing was conducted prior to MCAo and postoperatively for 28 days to monitor functional deficit and recovery. At day 28, the anterograde tracer cholera toxin b (CTb) subunit was injected into the forelimb motor cortex of the non-ischaemic hemisphere. Spinal sections containing anterogradely labelled terminals were reacted with antibodies against CTb and immunoreactive terminals were quantified. MCAo was associated with loss of approximately 35% of CST axons originating from the ischaemic hemisphere and infarcts were localised to subcortical structures. Rats exhibited sensorimotor deficits in the early phase after MCAo but recovered over time such that there were no significant differences in sensorimotor performances between sham-operated and MCAo rats at post-operative day 28. Despite functional recovery demonstrated by MCAo rats, the number of CTb-labelled terminals in the

cervical spinal cord originating from the non-ischaemic hemisphere was not altered compared to shams. The results of this first study suggest that after subcortical stroke, the motor cortex from the non-ischaemic hemisphere does not contribute to recovery of the affected limb via increasing its direct CST connections to the denervated (ipsilateral) side of the spinal cord. If the motor cortex from the non-ischaemic hemisphere does take over control of ipsilateral spinal circuitry after stroke, it likely utilises an indirect route.

In the intact animal, a number of indirect routes via which the motor cortex may gain access to ipsilateral spinal circuitry have been identified. These pathways are complex and involve intercalated neurons located in the brainstem and contralateral spinal cord. However, there are numerous putative indirect routes which have yet to be investigated. One such route involves contralaterally descending CST axons targeting spinal commissural interneurons (CINs), which in turn would either mono- or polysynaptically affect motor neurons on the opposite side of the spinal cord. CINs are a heterogeneous population of cells important for inter-limb coordination. Despite the importance of CINs to locomotion and their potential role in providing the motor cortex indirect access to ipsilateral spinal circuits, supraspinal input to CINs is poorly defined. Hence, the second major aim of this thesis was to characterise contacts to CINs from different supraspinal sources (the CST and reticulospinal tract (ReST)) in the cervical spinal cord of the intact rat. The CINs included i) those that issue long-range axonal projections to lumbar segments, termed long-descending propriospinal neurons (LDPNs), and ii) those that issue short-range axonal projections confined to a single segment, termed intrasegmental CINs. Axons were labelled anterogradely by injecting CTb into the forelimb motor cortex or medial longitudinal fasciculus (MLF), to label CST and ReST axons, respectively. Fluorogold (FG) was injected unilaterally into segments L1/L2 or C3/C4 in order to retrogradely label LDPNs or intrasegmental CINs, respectively. Spinal sections containing labelled cells and terminals were immunoreacted with various antibody combinations and were then examined with confocal microscopy. Both LDPNs and intrasegmental CINs received very few contacts from CST terminals but had significant numbers of contacts from ReST terminals. Use of vesicular glutamate and vesicular GABA transporters revealed that both cell types received approximately 80% of excitatory and 20% of inhibitory ReST contacts.

The results suggest that in the intact animal, the CST has a minimal direct influence on LDPNs and intrasegmental CINs but the ReST has a powerful direct influence. Therefore, following loss of CST axons (e.g. after stroke), the cortico-reticulospinal-commissural pathway has the capacity to deliver information from the intact hemisphere to the denervated side of the spinal cord.

Acknowledgments

Firstly, I would like to thank my supervisors, Professor David J Maxwell and Dr Deborah Dewar for accepting me as a PhD student and for their guidance over the last 4 years. I would also like to acknowledge the Medical Research Council for funding my PhD research.

Thank you to the technical staff at the Wellcome Surgical Institute; Lindsay Gallagher, for passing on her surgical skills; Linda Carberry and George Graham, for all of their practical support. I would also like to thank everyone within the spinal cord research group who has helped me, especially Robert Kerr and Christine Watt for their technical assistance.

Thank you to all my fellow students at the Wellcome Surgical Institute and spinal cord research group (Lisa, Huma, Emma, Ashleigh, Amy and many more) for keeping spirits high and for making this such an enjoyable experience.

I would like to extend my thanks to my parents Lesley and Mike and my sister Hollie who have provided unrivalled support throughout my time at university. Lastly, thank you to Ross for his encouragement and endless patience.

Author's declaration

All work in this thesis was carried out exclusively by me, apart from some surgical procedures and MRI RARE T_2 weighted imaging. Professor David J Maxwell contributed to this work by performing brain and spinal injections in rats. Lindsay Gallagher contributed to this work by performing MRI RARE T_2 weighted imaging on rats. I confirm that this thesis has not been submitted in any previous applications for a higher degree.

The copyright of this thesis belongs to the author under the terms of the United Kingdom Copyright Acts as qualified by University of Glasgow Regulation. Due acknowledgement must always be made of the use of any material contained in, or derived from this thesis.

Emma Mitchell

Signature:

Date:

Table of Contents

List of Tables

List of Figures

Chapter 5

Chapter 6

Abbreviations

AMPA	α-amino-3-hydroxy-5-methyl-4-isoxazolepropionic acid
ANOVA	analysis of variance
ATP	adenosine triphosphate
BDA	biotinylated dextran amine
Ca^{2+}	calcium ion
ChAT	choline acetyltransferase
CIN	commissural interneuron
Cl^-	chlorine ion
CNS	central nervous system
CPG	central pattern generators
CST	corticospinal tract
CTb	b subunit of cholera toxin
DAB	3, 3'-diaminobenzidine
DNA	deoxyribonucleic acid
ER	endoplasmic reticulum
EtOH	Ethanol
FG	Fluorogold
GABA	gamma amino butyric acid
H_2O_2	hydrogen peroxide
H&E	haematoxylin and eosin
ICC	Immunocytochemistry
IgG	immunoglobin
K^+	potassium ion
LAPN	long ascending propriospinal neuron
LDPN	long descending propriospinal neuron
M1	primary motor cortex
M2	secondary motor cortex
MCA	middle cerebral artery
MCAo	middle cerebral artery occlusion
MLF	medial longitudinal fasciculus
MRI	magnetic resonance imaging
Na^+	Sodium ion

NMDA	N-Methyl-D-aspartate
NO	Nitric oxide
PBS, PBST	phosphate buffered saline, PBS with 0.3% TritonX-100
PET	positron emission tomography
PLIC	Posterior limb of the internal capsule
PKC-γ	protein kinase C gamma
RARE	rapid acquisition with refocused echoes
ReST	reticulospinal tract
RST	rubrospinal tract
RM ANOVA	repeated measures analysis of variance
ROS	Reactive oxygen species
rtPA	recombinant tissue plasminogen activator
S1 FL	primary somatosensory-forelimb region
S1 HL	primary somatosensory-hindlimb region
SD	standard deviation
T_2	transverse relaxation time
TMS	transcranial magnetic stimulation
VGAT	vesicular GABA transporter
VGLUT	vesicular glutamate transporter
VSCC	Voltage sensitive calcium channel
VST	vestibulospinal tract

Chapter 1

Introduction

The motor cortex exerts a strong influence on contralateral limb function via the corticospinal tract (CST). From its origin in the cortex, the CST passes through the ipsilateral medullary pyramid before crossing at the pyramidal decussation and innervating contralateral spinal circuits (Porter & Lemon, 1993). Injury to the CST rostral to the pyramidal decussation, for example after stroke, results in prominent motor deficits in the contralateral side of the body such as paralysis or a loss of digit fractionation (Geyer & Gomez, 2009). The extent to which the motor cortex contributes to ipsilateral limb function however is less clear. The motor cortex may gain access to ipsilateral motor neurons via relay networks located in the brainstem and spinal cord but these pathways are currently ill-defined (Jankowska & Edgley, 2006). Interest in ipsilateral cortical control stems from studies of stroke survivors; movement of the stroke-affected limb elicits abnormally enhanced activity in the motor cortex of the ipsilateral (undamaged) hemisphere, raising the possibility that ipsilateral descending pathways might contribute to recovery of movement, by taking over the actions of damaged crossed CST fibres (Stoeckel & Binofski, 2010). This thesis aims to extend the knowledge of the neural systems that might mediate ipsilateral actions of the motor cortex, both under normal circumstances and after stroke. The experiments conducted to fulfil the aims of this thesis were performed on rats.

1.1 Descending supraspinal pathways in motor control

The cerebral cortex gains access to the spinal cord directly via the CST, and indirectly via tracts descending from brainstem structures. Each descending tract has distinct anatomical, neurochemical and functional characteristics which are just beginning to be elucidated (Lemon, 2008). The purpose of this section is to provide a brief overview of the defining features of each of the major descending tracts.

1.1.1 Corticospinal tract (CST)

The CST has the longest axonal trajectory of the mammalian nervous system and is the most direct pathway by which the cerebral cortex affects spinal circuitry (Armand, 1982). The CST makes a substantial contribution to volitional movements and precisely coordinated actions, such as fractionated movement of the digits (Lawrence & Kuypers, 1968). In the rat, the CST mainly arises from

large layer 5 pyramidal cells located in the primary motor cortex and in the forelimb and hindlimb regions of the primary sensory cortex (Miller, 1987). Neurons in the forelimb area of the motor and sensory cortex project to the cervical enlargement, while those in the hindlimb area project to the lumbar enlargement (Li et al., 1990). CST fibres pass through the internal capsule (posterior limb) and cerebral peduncle, to form the longitudinal fibres of the pons. After exiting the basilar pons they pass through the medullary pyramid. In the rat, the majority of axons (>96%) then cross the midline at the pyramidal decussation, and subsequently travel in the contralateral dorsal column down to the most caudal level of the spinal cord (Terashima, 1995). It is noteworthy that in primates including humans, CST axons are not present in the dorsal column and instead descend mainly via the contralateral dorsolateral funiculus with a few uncrossed axons descending in the ipsilateral dorsolateral funiculus and ventromedial funiculus (Rosenzweig et al., 2009; Ralston & Ralston, 1985; Schoen, 1964). Anterograde tracing studies performed in the rat have shown that CST axons terminate in all spinal laminae contralateral to their cells of origin, with dense terminations in laminae II to VII and sparse terminations in laminae I, II and the ventral horn (Gribnau & Dederen, 1989; Casale et al., 1988; Liang, 1991; Du Beau et al., 2012). In addition to the principal CST in the contralateral dorsal column, the rat spinal cord also contains CST fibres in the contralateral lateral, ipsilateral ventral and ipsilateral dorsal funiculi (Liang, 1991; Brösamle & Schwab, 2000; see **Figure 1-1**). CST terminals ipsilateral to the hemisphere of origin are very sparse in the rat and are largely found in the intermediate grey matter (Brösamle & Schwab, 2000). In primates, contralaterally projecting CST fibres terminate mainly in Rexed's laminae II to VII and to a lesser extent in the ventral horn; ipsilaterally projecting fibres terminate in laminae V to IX (Lacroix et al., 2004; Rosenzweig et al., 2009; Ralston & Ralston, 1985). According to a recent tract tracing study in rhesus monkeys, the proportion of CST fibres that descend the spinal cord ipsilaterally (~13%) is higher than that of the rat (~4%) (Rosenzweig et al., 2009). Occasionally contralaterally descending fibres have collaterals that re-cross the midline at the level of the spinal cord to terminate ipsilaterally (**Figure 1-1**); these re-crossing axons are sparse in rats (Liang et al., 1991) and somewhat more common in primates (Rosenzweig et al., 2009). In addition to its spinal projections, the CST issues collaterals to numerous subcortical targets including the striatum, red nucleus, reticular nuclei and

dorsal column nuclei to provide these structures with a copy of the cortical motor outflow (O'Leary & Terashima, 1988; Antal, 1984).

The CST pathway is widely accepted to be excitatory (Lemon, 2008). CST terminals of the rat are enriched with glutamate (Valtschanoff et al., 1993) and a recent immunolabelling study demonstrated that 96% of rat CST axons contain vesicular glutamate transporter 1 (VGLUT-1; Du Beau et al., 2012).

pyramidal
neurons

Contralateral   Ipsilateral
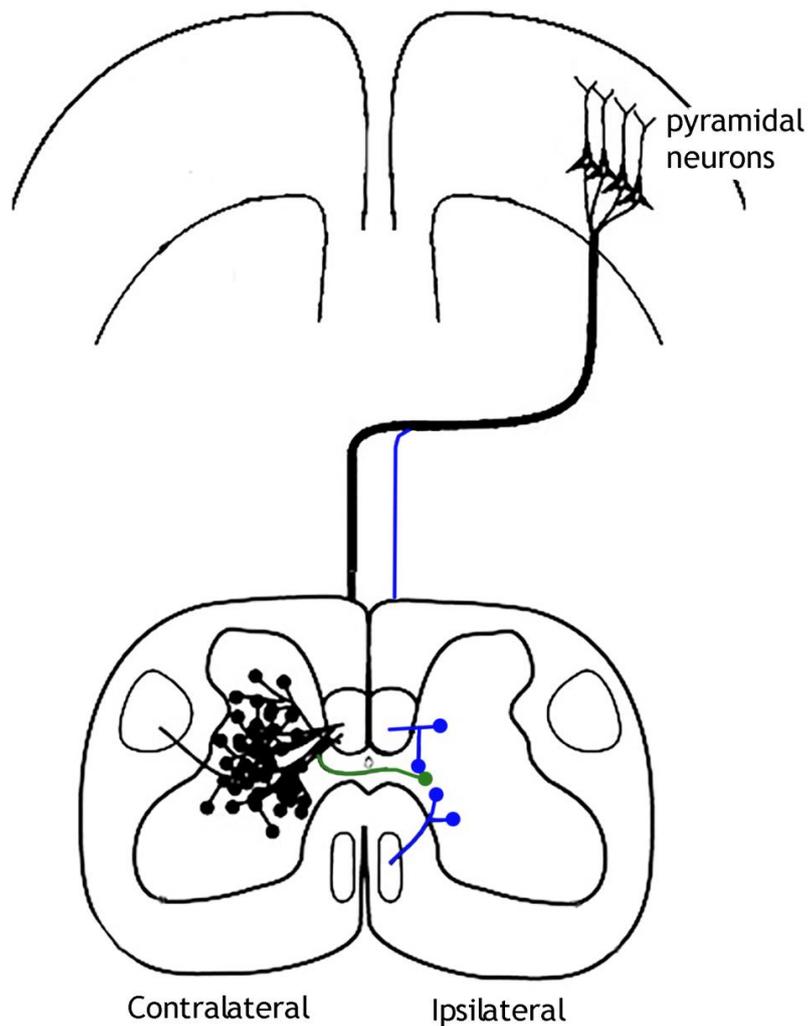
Figure 1-1 Termination patterns of the corticospinal tract (CST) in the rat

The CST is primarily a crossed pathway, with ~96% of axons terminating on the contralateral side of the spinal cord (black). A sparse number of axons descend in the spinal cord ipsilaterally and terminate ipsilaterally (blue). Occasionally, contralateral axons re-cross the midline at the spinal level, resulting in a "double crossed" pathway (green) (Modified from Carmel & Martin, 2014).

Contralateral actions of the CST

In humans and non-human primates, CST fibres have been reported to synapse directly onto motor neurons in the contralateral ventral horn and these monosynaptic cortico-motorneuronal connections have long been considered to be decisive in the control of skilled voluntary movements such as digit fractionation (Lemon et al., 2004; Kuypers, 1960; Lawrence & Kuypers, 1968; Palmer & Ashby, 1992). The issue of whether similar monosynaptic connections exist in non-primate mammals, particularly in the rat, is controversial. According to an earlier anatomical tracing study, CST axons contact contralateral motor neurons in the rat, as they do in primates (Liang et al., 1991); however, this was not confirmed by electron microscopy (Yang & Lemon, 2003). In an experiment in the rat by Alstermark et al., (2004), corticofugal fibre stimulation at the level of the pyramid failed to evoke monosynaptic excitation of contralateral forelimb motor neurons. Instead, pyramidal stimulation excited contralateral motor neurons via two indirect pathways; the first pathway involved the CST acting on interneurons located within the same spinal segments as the forelimb motor neurons and the second pathway involved the reticulospinal tract (ReST) (**Figure 1-2**). The pontomedullary reticular formation (from which the ReST originates) receives input from the sensorimotor cortex via collaterals from the CST and via a direct cortico-reticular pathway (Newman et al., 1989; Antal, 1984; Canedo & Lamas, 1993); and in turn ReST fibres make mono- and polysynaptic connections with motor neurons (see **section 1.1.3**). A large number of studies have been devoted to uncovering cortico-motorneuronal pathways of the cat, which like the rat, lacks monosynaptic connections between the cortex and spinal motor neurons. In the cat, the shortest pathway from the cortex to contralateral forelimb motor neurons is disynaptic (Illert et al., 1976). Behavioural experiments performed in the cat have shown that target-reaching involves the CST acting on cervical segment C3/C4 propriospinal interneurons, which in turn activate forelimb motor neurons; whereas food grasping involves the CST (and rubrospinal tract; RST) acting on premotor interneurons located within the forelimb segments (C6 to Th1) (Alstermark et al., 1985; Alstermark et al., 1981). Importantly, these "phylogenetically older" polysynaptic cortico-motorneuronal connections of the rat and cat still exist in primates and they may play

important functional roles in parallel with the newly developed monosynaptic cortico-motorneuronal connections (reviewed by Isa et al., 2013).

The observation that rats have very few, if any, monosynaptic cortico-motorneuronal connections (Yang & Lemon, 2003; Alstermark et al., 2004) has been employed to explain a perceived relative lack of ability for fine motor control (Courtine et al., 2007). However, detailed behavioural analysis suggests that rats have more dexterity than is generally appreciated; for instance, during food handling rats exhibit a complex repertoire of skilled movements including digit fractionation (Ivanco et al., 1996; Whishaw & Coles, 1996). A lesion of the motor cortex results in impaired digit manipulation of the paw contralateral to the lesion during food handling (Whishaw & Coles, 1996; Whishaw et al., 1986). Furthermore, a lesion of the dorsal columns, which carry crossed CST axons, impairs performance during a food pellet retrieval task (Weidner et al., 2001). Thus, rats exhibit fine motor control which appears to be dependent on the integrity of the motor cortex and its crossed CST projections. It is noteworthy however, that a recent study failed to detect reaching/grasping deficits in rats following dorsal column lesions; the authors raised the possibility that skilled forepaw function in the rat may not be critically dependant on spinal circuits controlled by the CST and that other pathways, such as the cortico-reticulospinal-motorneuronal pathway might be more important (Alstermark & Pettersson, 2014). The precise function of the CST in the rat is therefore not yet fully understood.
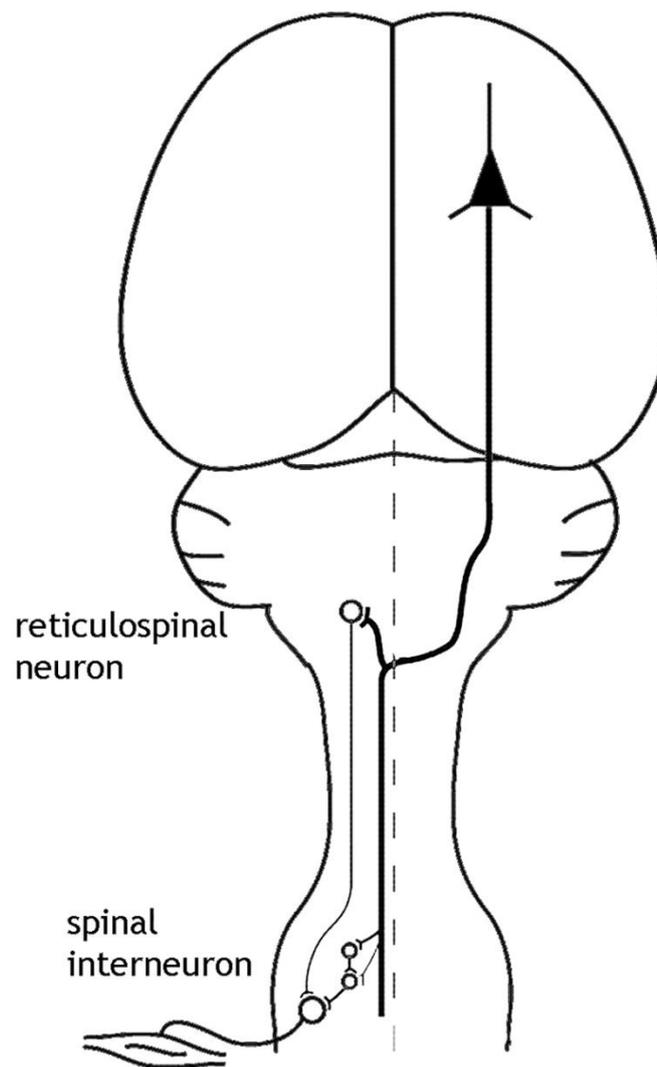
Figure 1-2 Major pathways contributing to the contralateral actions of the motor cortex in the rat

Originating from the sensorimotor cortex, the CST (thick black line), makes connections with motor neurons on the contralateral side of the spinal cord via spinal interneurons. Additionally, corticofugal fibres contact reticulospinal neurons that in turn relay the cortical command to contralateral motor neurons (Modified from Umeda et al., 2010).

Ipsilateral actions of the CST

Traditionally, research has focussed on the contralateral actions of the CST, due to the predominance of CST axons that cross the pyramidal decussation and terminate in the contralateral side of the spinal cord (Porter & Lemon, 1993). However, ipsilateral CST terminals - arising from ipsilaterally descending axons as well as from "double crossed" axons (**Figure 1-1**) – are well established. Anatomical tracing studies in the rat have described ipsilateral CST terminals in laminae III to VII (Liang et al., 1991; Brösamle & Schwab, 1997). Ipsilateral CST terminals have also been identified in the cat in laminae VII to VIII (Armand et al., 1985) and in the primate in laminae V to IX (Lacroix et al., 2004). According to Soteropoulos et al., (2011), stimulation of the primate primary motor cortex (or medullary pyramid) failed to elicit monosynaptic excitation of ipsilateral motor neurons supplying forearm and hand muscles. However, Montgomery et al., (2013) stimulated the primate primary motor cortex (premotor cortex or supplementary motor area) using a longer stimulus train sufficient enough to activate both mono- and polysynaptic pathways and this elicited ipsilateral wrist, forearm and shoulder movements. Thus, based on primate electrophysiological studies, it appears that under normal circumstances, CST pathways do not directly influence ipsilateral motor neurons; however, the motor cortex has the capacity to influence ipsilateral motor neurons indirectly. There are several potential routes through which the motor cortex could gain access to ipsilateral motor neurons. For instance, the small number of ipsilaterally terminating CST fibres may contact ipsilaterally operating spinal interneurons that in turn excite (or inhibit) motor neurons (Jankowska & Edgley, 2006). Evidence to support this notion comes from Jankowska & Stecina (2007); in the cat lumbar spinal cord, a small proportion of premotor interneurons mediating group I/II afferent reflexes can be monosynaptically excited by stimulation of the ipsilateral medullary pyramid. Furthermore, using electron microscopy in the rat, ipsilaterally terminating CST fibres were shown to form synaptic contacts with cells in the intermediate grey matter (Brösamle & Schwab, 2000). In addition to the CST fibres that terminate ipsilaterally, the motor cortex may also influence ipsilateral motor neurons via relay neurons located in the brainstem and contralateral spinal cord (Jankowska & Edgley, 2006; Edgely et al., 2004: Jankowska & Stecina, 2007; Stecina & Jankowska,

2007); these more complex indirect pathways are considered later, in **section 1.3**.

1.1.2 Rubrospinal tract (RST)

The rubrospinal tract (RST) is a phylogenetically old supraspinal system arising mainly from the magnocellular region of the red nucleus; a nucleus located on either side of the midbrain tegmentum (ten Donkelaar, 1988). In addition to major input from cerebellar nuclei, the red nucleus of the cat and primate receives extensive projections from the sensorimotor cortex in the form of a direct corticorubral pathway and via collateral branches of CST axons (Brown, 1974; Humphrey, 1984; Giuffrida et al., 1991). These projections are mainly ipsilateral but there is a minor contralateral component. In the rat, cerebellar afferents to RST neurons are well established but afferents from the sensorimotor cortex are less well documented (Dekker, 1981). Anatomical studies have reported that the rat sensorimotor cortex provides projections to the parvocellular part of the red nucleus only (Gwyn et al., 1974; Brown, 1974); however, according to Giuffrida et al., (1988), stimulation of the rat motor cortex evokes monosynaptic excitation (and disynaptic inhibition) of neurons located in both the magnocellular and parvocellular parts of the ipsilateral red nucleus.

In the rat, the majority of RST axons cross at the ventral tegmental decussation and descend the dorsolateral funiculus to terminate in laminae V to VII contralateral to their cells of origin; but a small number of ipsilateral projections are also present (Ruigrok et al., 2008; Antal et al., 1992). The RST is also a predominantly crossed pathway in carnivores and primates and it occupies a position ventral to the CST in the dorsolateral funiculus before terminating in laminae V to VII (Holstege & Kuypers 1987; Murray & Haines, 1975). According to electrophysiological studies performed in the rat, cat and primate, RST neurons mainly influence contralateral motor neurons indirectly, through activation of excitatory or inhibitory premotor interneurons (Al-Izk et al., 2008; Hongo et al., 1972; Jankowska, 1988; Shapovalov, 1966), although a small number of monosynaptic connections between RST axons and contralateral motor neurons have been detected in the cat and primate (Holsteg & Kuypers, 1987).

In rats, damage to the dorsolateral funiculus, where the RST lies, impairs performance during a pellet- reaching task (Muir et al., 2007; Morris et al., 2011) and detailed behavioural analysis suggests that the RST is more involved in paw rotation as opposed to digit use (Morris et al., 2011). Electrophysiological recordings from primates during reaching and grasping have demonstrated that neurons of the magnocellular red nucleus discharge vigorously in association with grouped digit movements (Houk et al., 1988; Van Kan & McCurdy, 2002). Thus, it has been theorised that RST neurons control the muscle synergies that produce group digit extensions on which CST neurons superimpose control for individuated digit movements (Schieber, 1990; Van Kan & McCurdy, 2002). Some authors have placed emphasis on the importance of the RST in maintaining limb function after damage to the CST (Lawrence & Kuypers, 1968) and indeed, RST output to affected (contralateral) forearm flexor muscles has been reported to increase following unilateral ablation of the pyramidal tract in primates (Belhaj-Saif & Cheney, 2000). However, the RST is virtually absent in humans (Nathan & Smith, 1955), making the contribution of this pathway to recovery in humans with pyramidal tract damage (e.g. stroke survivors) unlikely.

The RST is purely an excitatory system. According to Antal et al., (1992) RST terminals of the rat are not immunoreactive for GABA or glycine. Moreover, a recent immunolabelling study revealed that 97% of RST terminals contain vesicular glutamate transporter 2 (VGLUT-2; Du Beau et al., 2012).

### 1.1.3 Reticulospinal tract (ReST)

Another phylogenetically old supraspinal system is the ReST, a heterogeneous tract originating from dispersed nuclei of the brainstem reticular formation. The reticular nuclei receive widespread convergence from multiple structures including the spinal cord, cerebral cortex, cerebellum, red nucleus and vestibular apparatus (Alstermark & Ekerot, 2013). Input from the sensorimotor cortex occurs in the form of CST collaterals and via a direct corticoreticular pathway and these fibres have extensive terminations within the medial pontomedullary reticular formation, the region from with ReST axons originate (Newman et al., 1989; Keizer & Kuypers, 1984; Keizer & Kuypers, 1989). According to anatomical tracing studies performed in the rat, cat and primate, the pontomedullary reticular formation receives projections from both the

ipsilateral and contralateral sensorimotor cortex (Newman et al., 1986; Keizer &
Kuypers, 1984: Keizer & Kuypers, 1989). Investigations at the single cell level in
the cat have demonstrated that an individual cortical neuron can branch
profusely to give off widespread terminations on both sides of the
pontomedullary reticular formation (Kably & Drew, 1998; Matsuyama & Drew,
1997). In the cat, ReST neurons are monosynaptically activated following
stimulation of the ipsilateral or contralateral cerebral cortex (Peterson et al.,
1974).

Anatomical and physiological studies mainly in cats, but more recently in rats
and primates, have identified two major subdivisions of the ReST; the medial
ReST and lateral ReST (Peterson, 1979; Reed et al., 2008; Sakai et al., 2009).
The medial ReST originates from neurons primarily in the medial pontine
reticular formation and the rostral gigantocellularis (Ito, 1970). The fibres
descend through, or close to the medial longitudinal fasciculus (MLF) in the
caudal brainstem, continue in the spinal ventromedial funiculus and terminate in
laminae VI to IX of all segmental levels of the spinal cord (Petras, 1967).
Anterograde tracing of single pontine ReST axons in the cat showed that the
majority of axons project to the ipsilateral spinal grey matter, but a small
number of axons (~15%) project bilaterally as they exhibit additional branches
that extend across the midline into the contralateral grey matter (Matsuyama et
al., 1999). The lateral ReST originates from neurons located in the ventrocaudal
part of the medial medullary reticular formation (Peterson, 1979). According to
an anterograde degeneration study in cats, lateral ReST neurons send their axons
to all spinal segments via both the ipsilateral and contralateral funiculus
(Nyberg-Hansen, 1965) and an individual fibre can give off multiple bilateral
collaterals with major arborisations in laminae V to IX (Holstege & Kuypers,
1982). Therefore, the ReST has remarkable potential for exerting widespread
effects, as a single neuron can project to both sides of the spinal cord at
multiple segments. Although the majority of the above studies were performed
in cats, similar complex bilateral termination patterns have also been reported
for the ReST of rats (Reed et al., 2008) and primates (Sakai et al., 2009).

In rats, cats and primates, stimulation of ReST fibres evokes monosynaptic
excitation of ipsilateral neck, axial and limb motor neurons (Shapovalov &

Gurevitch, 1970; Peterson, 1979; Peterson et al., 1979; Riddle et al., 2009). In addition to monosynaptic activation, ReST axons also elicit disynaptic excitation and inhibition of motor neurons via intercalated spinal interneurons (Floeter et al., 1993; Shapovalov & Gurevitch, 1970; Riddle et al., 2009; Takakusaki et al., 2001). In the cat lumbar spinal cord, Jankowska et al., (2003) demonstrated that ReST neurons can influence contralateral motor neurons disynaptically, via uncrossed ReST axons activating commissural interneurons (CINs) which in turn excite or inhibit motor neurons on the opposite side of the spinal cord (Jankowska et al., 2003). Immunocytochemical analysis of lumbar CINs monosynaptically excited by ReST neurons revealed that this population includes both glutamatergic and glycinergic neurons (Bannatyne et al., 2003).

Functionally, the ReST is traditionally considered to control proximal and axial muscles, and most research has focused on its contribution to gross movements such as locomotion (Mori et al., 2001) or postural adjustments (Schepens et al., 2008). However, an increasing body of evidence suggests that ReST axons may contribute to voluntary movements. For instance, in the mouse, selective ablation of ReST neurons in the lower brainstem produces a grasping impairment during a food pellet retrieval task (Esposito et al., 2014). In primates, ReST neurons make mono- and disynaptic connections with ipsilateral motor neurons that innervate intrinsic hand muscles (Riddle et al., 2009), and neurons of the pontomedullary reticular formation have been shown to modulate their activity in response to ipsilateral fine finger movements (Soteropoulos et al., 2012). Moreover, following unilateral pyramidal tract transection in primates, ReST fibres descending through the MLF strengthen their output to affected flexor motor neurons (Zaaimi et al., 2012); this raises the possibility that the ReST contributes to some of the recovery that occurs after loss of CST fibres (e.g. after stroke).

Many ReST axons have strong excitatory actions on spinal neurons (Jankowska et al., 2003; Edgley et al., 2004). However, anterograde labelling studies have revealed some ReST axons to be GABAergic (Holstege, 1991) or glycinergic (Holstege & Bongers, 1991). A recent immunocytochemistry study performed in the rat reported that 59% of axons descending via the MLF contain vesicular glutamate transporter 2 (VGLUT-2) and 20% contain vesicular GABA transporter

(VGAT; Du Beau et al., 2012). Furthermore, in the rat, a proportion of ReST projections arising from the gigantocellular complex have been shown to be serotonergic (Bowker et al., 1981). Thus, the ReST systems are heterogeneous in terms of the neurotransmitters they contain.

1.1.4 Other descending supraspinal pathways

The vestibulospinal tract (VST), arising from all 4 subdivisions of the vestibular nuclear complex, controls postural extensor activity in the limbs, neck and trunk mainly via a medial and lateral pathway (Wilson et al.,1967; Bankoul & Neuhuber, 1992; Pompeiano, 1972). Tectospinal axons originate in the deep and intermediate layers of the superior colliculus and are implicated in head movements (Yasui et al., 1998).

1.2 Spinal commissural interneurons (CINs)

At the spinal level, CINs are defined by an axonal projection that crosses the midline to the contralateral side of the spinal cord. They constitute a highly heterogeneous population in terms of their location, their postsynaptic targets, and their presynaptic inputs (Kiehn & Butt, 2003). As will be discussed later (**section 1.3**), neural pathways involving CINs represent a potential substrate for recovery of function following injury to the CST (e.g. after stroke) (Jankowska & Edgley, 2006; Edgley et al., 2004). Therefore, it is important to examine the connectivity of CINs and their inputs from supraspinal sources. The purpose of this section is to provide an overview of the most extensively studied CIN systems.

1.2.1 Lumbar commissural interneurons (CINs)

CINs have been widely investigated in the lumbar spinal cord. Anatomical studies have described various types of CINs, mainly in laminae VI to VIII of lumbar segments, where the walking central pattern generator (CPG) is located (Kiehn, 2006); 1) long-range CINs that project at least one and a half segments either rostrally (ascending) or caudally (descending), or bifurcate in both directions and 2) short-range CINs that project less than one and a half segments (intrasegmental CINs; Stokke et al., 2002; Matsuyama et al., 2006).

The best-described CINs in the rat are descending CINs located in the laminae VI to VIII of segment L2/L3 and which have axons projecting contralaterally at least as far as segment L4 (Butt et al., 2002a; Butt et al., 2002b; Butt & Kiehn, 2003). These cells have been shown to play a role in flexor-extensor synergies across and along the spinal cord during locomotion and they are composed of a mixed population of glutamatergic and glycinergic neurons (Kiehn, 2006). They influence contralateral flexor and extensor motor neurons via 1) monosynaptic excitation 2) monosynaptic inhibition 3) polysynaptic inhibition mediated by glutamatergic CINs synapsing onto inhibitory interneurons located ipsilateral to motor neurons (Butt & Kiehn, 2003). A similar population of CINs exist in the cat lumbar spinal cord; they have somata located in L3 to L5 and axons projecting contralaterally at least as far as L7 and they provide monosynaptic excitatory and inhibitory as well as polysynaptic inhibitory inputs to motor neurons (Jankowska et al., 2003; Bannatyne et al., 2003). These CINs fall into two major subpopulations; those with monosynaptic input from ReST neurons, VST neurons and group I afferents, and those with monosynaptic input from group II afferents (Jankowska et al., 2005; Jankowska, 2008). Reconstructions of the axonal projections of these CINs have revealed that they have widespread projections over multiple segments and also innervate neurons located outside motor nuclei as well as motor neurons (Bannatyne et al., 2003; Matsuyama et al., 2004).

Anatomical tracing in the rat has shown that approximately 10 per cent of CINs in the lumbar spinal cord are intrasegmental, with axons confined to a single segment (Stokke et al., 2002). Intrasegmental connections likely play a direct role in organising left-right coordination between segmental homonymous muscles (Kiehn, 2006). Intrasegmental CINs in laminae VII and VIII directly excite, directly inhibit or indirectly inhibit contralateral motor neurons (Quinlan & Kiehn, 2007; Kjaerulff & Kiehn, 1997). Indirect inhibition is likely mediated via Ia inhibitory interneurons and Renshaw cells (Jankowska et al., 2005; Nishimaru et al., 2006).

Other studied populations of lumbar CINs include those in the dorsal horn targeted by group II muscle spindles, which are mainly inhibitory and project to the intermediate zone and ventral horn (Bannatyne et al., 2006). In mice, cholinergic partition cells in lamina X/VII of the lumbar spinal cord have been

shown to issue commissural projections; these cells have axons ascending or descending several segments and they influence motor neurons monosynaptically via large "C-bouton" synapses (Stepien et al., 2010; Miles et al., 2007). Genetic inactivation of cholinergic partition cells in mice impairs locomotion (Zagoraiou et al., 2009). Anterograde tracing studies performed in rats and cats have identified neurons in lumbar segments that issue commissural (and uncrossed) projections to cervical segments (Dutton et al., 2006; Brockett et al., 2013; English et al., 1985); these cells (termed long-range ascending propriospinal neurons; LAPNs) likely participate in the synchronisation of lumbar and cervical CPGs. Indeed, an experiment in neonatal rats showed that the hindlimb CPG issues rhythmic inputs to the forelimb CPG and part of this drive is crossed inhibition (Juvin et al., 2005).

1.2.2 Cervical commissural interneurons (CINs)

At variance with the numerous studies on CINs of the lumbar spinal cord, little information is available on CINs of the cervical spinal cord. One group studied in the cat comprises CINs in laminae VII and VIII of the upper cervical cord (C1 to C3); they synapse with motor neurons at least one segment rostral or caudal from their somata and they participate in bilaterally organised vestibulocollic reflexes (Bolton, 1991; Sugiuchi et al., 1992). Another population identified in the cat, are those in segments C3/C4 with axons projecting to contralateral forelimb motor neurons (C6 to Th1); these cells are active during targeted reaching, and they are postulated to provide postural stability to the contralateral limb when the ipsilateral limb is lifted (Alstermark & Kümmel, 1990).

Anatomical and physiological studies performed in cats, rats and mice have identified neurons within the cervical enlargement that issue long-distance axonal projections to the lumbar enlargement. These cells, referred to as long-range descending propriospinal neurons (LDPNs), have both commissural and uncrossed projections (Alstermark et al., 1987; Alstermark et al., 1991; Brockett et al., 2013; Reed et al., 2009; Ni et al., 2014). Although the precise function of the different types of LDPNs (e.g. commissural versus uncrossed) is poorly understood, it is known that LDPNs work reciprocally with LAPNs to synchronise cervical and lumbar circuits during locomotion (Ballion et al., 2001; Juvin et al.,

2005; Zaporozhets et al., 2006). It is likely that different types of LDPNs contribute to the adjustment of hindlimb postures during specific movements of the forebody (Alstermark et al., 1987). In the rat, unilateral injection of a retrograde tracer into the L1 or L3 segment was found to label cells in all cervical segments and approximately half of the labelled cells were commissural i.e. they were located in the grey matter contralateral to the tracer injection site (Brockett et al., 2013). Similarly, bilaterally labelled cells were detected throughout all cervical segments in mice following unilateral injection of a transsynaptic tracer into hindlimb muscles, suggesting that both commissural and uncrossed LDPNs make monosynaptic connections with motor neurons (Ni et al., 2014). Some of the commissural (and uncrossed) LDPNs were found to have contacts from CST axons and brain-stem derived serotonergic axons, but the bouton numbers were very low (0 to 2 per cell), so the authors concluded that these supraspinal systems are not major regulators of LDPNs in mice (Ni et al., 2014). Although, in an electrophysiological study in cats, commissural (and uncrossed) LDPNs located in segments C3 to C5 were monosynaptically excited by stimulation of the contralateral medullary pyramid (Alstermark et al., 1987), suggesting that these cells are under direct control from the CST. These cells were also disynaptically activated by stimulation of the ipsilateral medullary pyramid (via ReST neurons, which are the main source of input to them together with VST input; Alstermark et al., 1987; Alstermark et al., 1991). Supraspinal inputs to commissural (and uncrossed) LDPNs have yet to be fully characterised in the rat. However, recent interest in LDPNs stems from a study performed in rats: thoracically axotomised CST fibres were reported to sprout in the cervical spinal cord and increase their arborisation onto LDPNs, and the LDPNs in turn increased their innervation onto lumbar motor neurons, effectively forming a "bridge" so that descending commands could bypass the injury site (Bareyre et al., 2004). Furthermore, the formation of this new LDPN-mediated detour circuit led to the restoration of hindlimb function. Although it is unclear whether the CST sprouting observed by Bareyre and colleagues was onto commissural, uncrossed or both types of LDPNs, the study raises the possibility that LDPNs might be involved in supporting recovery after CST injury and highlights the need for a detailed characterisation of these cells and their supraspinal inputs.

As mentioned above (**section 1.2.1**), intrasegmental CINs with axons confined to a single segment have been characterised both anatomically and physiologically in the lumbar cord of rats and mice and these cells are postulated to be directly involved in the synchronisation of left-right homonymous muscles (Stokke et al., 2002; Quinlan & Kiehn, 2007; Kjaerulff & Kiehn, 1997). Despite the proposed functional significance of intrasegmental CINs, information on these cells at the cervical level is currently lacking. Although a recent electrophysiological experiment in primates has established the existence of a short-range commissural system in the lower cervical enlargement of primates (C6 to Th1; Soteropoulos et al., 2013); these cells were shown to innervate motor neurons of intrinsic hand muscles and they also have inputs from the periphery and from fibres descending close to the MLF.

1.3 Role of the motor cortex in ipsilateral movement control

The motor cortex exerts a strong influence on contralateral limb function via the CST, which provides layer 5 pyramidal neurons with direct access to contralateral spinal circuits (**section 1.1.1**). However, the role of the motor cortex in ipsilateral limb control is less well understood. As mentioned previously (**section 1.1.1**), electrophysiological studies performed in primates suggest that under normal circumstances, the motor cortex does not influence ipsilateral motor neurons directly (monosynaptically; Soteropoulos et al., 2011) but may have the capacity to influence ipsilateral motor neurons indirectly (polysynaptically; Montgomery et al., 2013). As will be discussed later (s**ection 1.4.2**), it is important to uncover the neural systems that mediate ipsilateral actions of the motor cortex because these systems might underlie some of the recovery of function that occurs after damage to the crossed CST (e.g. after stroke; Jankowska & Edgley, 2006). The purpose of this section is to outline potential neural pathways that might allow the motor cortex to gain access to ipsilateral motor neurons.

As discussed previously (**section 1.1.1**), a small proportion of CST fibres terminate on the side of the spinal cord ipsilateral to their cells of origin (Lacroix et al., 2004; Armand & Kuypers, 1980; Brösamle & Schwab). Currently, there is little information available on the cellular targets of these fibres other

than electrophysiological evidence from cats showing that a small number of premotor interneurons involved in group I/I afferent reflexes are monosynaptically activated by stimulation of the ipsilateral medullary pyramid (Jankowska & Stecia, 2007); and anatomical evidence from rats showing that ipsilaterally terminating CST fibres synapse onto cells in the intermediate grey matter (Brösamle & Schwab, 2000). Ipsilaterally terminating CST fibres are a readily available source through which sprouting could strengthen cortical control of the ipsilateral limb during recovery following injury of the crossed CST (e.g. after stroke; Jankowska & Edgley, 2006).

A series of electrophysiological studies have been performed in the cat lumbar spinal cord in order to ascertain which neural systems could mediate ipsilateral actions of the motor cortex; the pathways investigated thus far are depicted in **Figure 1-3**. The motor cortex has the capacity to influence motor neurons via ipsilaterally descending CST fibres acting through premotor interneurons; and via ipsilateral ReST neurons with axons running through the MLF acting directly on motor neurons or though premotor interneurons (Stecina & Jankowska, 2007). In parallel to these uncrossed pathways, the motor cortex can also gain access to ipsilateral motor neurons via a "double-crossed" pathway, involving contralateral ReST neurons which in turn activate spinal CINs that project back across to motor neurons and interneurons ipsilateral to the stimulated pyramidal tract (Edgley et al., 2004). Candidate CINs that form synapses with contralateral motor neurons have been described in mid-lumbar segments (see **section 1.2.1**; Bannatyne et al., 2003; Jankowska et al., 2003). The ipsilateral premotor interneurons relaying the descending command to ipsilateral motor neurons include those that mediate group I/II afferent reflexes along with other interneurons that remain unidentified (Stecina et al., 2008).
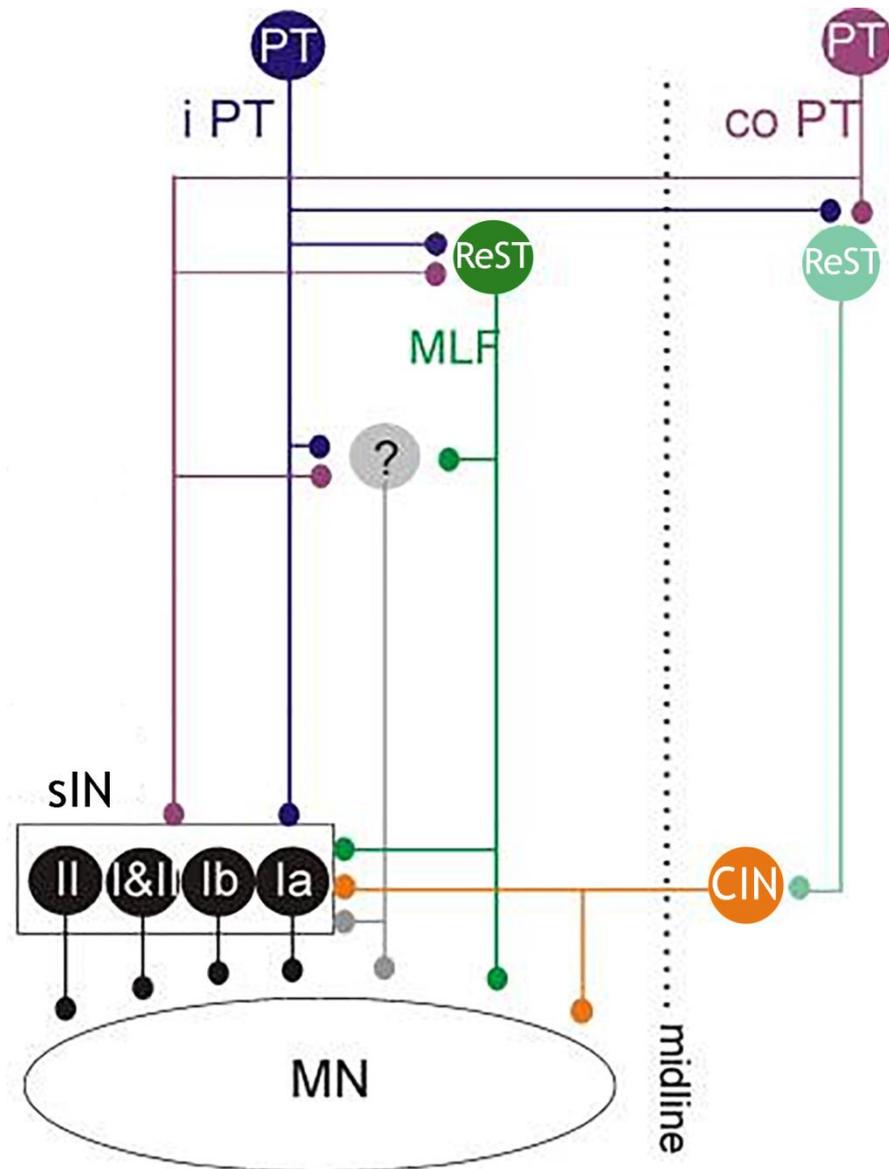
Figure 1-3 Neural pathways between the cortex and ipsilateral motor neurons identified in the cat

Uncrossed pathways include ipsilaterally projecting CST fibres acting on group I/II sINs and so far unidentified other interneurons (represented by ?). An additional uncrossed pathway involves ipsilateral ReST neurons acting directly on MNs as well as on sINs. A double crossed pathway comprises contralateral ReST neurons activating CINs that in turn re-cross the spinal midline. (Modified from Jankowska & Stecina, 2007).

iPT = ipsilateral pyramidal tract; coPT = contralateral pyramidal tract; ReST = reticulospinal tract; MLF = medial longitudinal fasciculus; sIN = segmental interneurons; CIN = commissural interneurons; MN = motor neurons

Under normal circumstances, the ipsilateral actions of the motor cortex described above are much weaker than the contralateral actions of the motor cortex. However, if crossed CST axons become damaged (e.g. after stroke), recovery of function might involve the strengthening of ipsilateral connectivity at spinal and/or bulbar levels; this would allow for the intact motor cortex to drive motor output to the impaired side of the body (Jankowska & Edgley, 2006).

The connectivity diagram in **Figure 1-3** is far from complete, as there are numerous putative pathways from the motor cortex to ipsilateral motor neurons that have yet to be examined. For instance, in rats, cats and primates, a moderate proportion of the contralaterally descending CST axons terminate in laminae VI to VII (Gribnau & Dederen, 1989; Liang, 1991; Lacroix et al., 2004; Rosenzweig et al., 2009) and a major cell group located within these laminae are CINs. One possibility, therefore, is that contralaterally descending CST fibres target CINs, which in turn either mono- or polysynaptically affect motor neurons on the opposite side of the spinal cord. However, there is so far only one preliminary observation to support this notion; as discussed earlier (**section 1.2.2**), commissural LDPNs in segments C3 to C5 of the cat are monosynaptically excited by stimulation of the contralateral medullary pyramid (Alstermark et al., 1987; **section 1.2.2**). Although anatomical evidence from mice suggests that the CST is not a major regulator of these cells (Ni et al., 2014). The disagreement in the available literature warrants further examination of CST inputs to commissural LDPNs. Additionally (as discussed in **section 1.2**), CINs are a highly heterogeneous population and a comparison of CST (and other supraspinal) inputs to different subpopulations of CINs has yet to be performed.

Another putative route via which the motor cortex might influence ipsilateral motor neurons is via RST neurons located in the red nucleus. RST neurons receive direct input from the ipsilateral motor cortex (Giuffrida et al., 1988; Fanardjian, 1988) and the red nucleus has a small number of ipsilateral projections to the spinal cord (Antal et al., 1992; Ruigrok et al., 2008; **see section 1.1.2**). Although, a comparison of the postsynaptic potentials in motor neurons evoked by stimulation of the medullary pyramid versus red nucleus in cats suggests that the RST does not act as a relay for the ipsilateral actions of the motor cortex under normal circumstances (Stecina et al., 2008).

1.4 Stroke

In the UK, stroke is the fourth leading cause of death and the most common cause of adult disability (www.stroke.org.uk, Stroke Statistics, 2015). Of those affected, 75% survive beyond the first year and many of those survivors experience sensorimotor and/or cognitive deficits depending on the extent and localisation of injury. The most common deficit among stroke survivors is contralateral motor dysfunction; with 80-90% of survivors exhibiting paresis or loss of dexterity on the side of the body opposite to the infarct (Lawrence et al., 2001). Most survivors experience a degree of spontaneous motor recovery. The greatest phase of recovery typically occurs from 1 week to 1 month after stroke; then to a lesser extent between 2 to 3 months after stroke (Verheyden et al., 2008). Unfortunately, the extent of recovery is highly limited, with >50% of survivors still exhibiting severe limb deficits 1 year after the initial stroke event (Dobkin, 2005). An understanding of the mechanisms of spontaneous motor recovery after stroke may reveal novel targets for improving functional outcome. However the neural events supporting recovery are poorly understood.

Recovery after stroke involves three processes; resolution of acute tissue damage, behavioural compensation, and brain reorganisation (Carmichael, 2003). Recovery within the first few days after stroke is attributed to resolution of oedema and cessation of inflammation associated with the initial infarct (Wieloch & Nikolick, 2006). Later improvements in function are partially due to compensation, whereby a subject adopts a new behavioural strategy to complete a task. Compensatory behaviours reflect learned activity patterns rather than changes in brain circuitry, and they are often inefficient and energetically expensive (Dobkin, 2005). Late recovery is also attributed to brain reorganisation. Reorganisation in this context refers to the recruitment of areas previously not engaged in a given task, in order to substitute for damaged areas (Nudo et al., 2006). There has been great interest in the possibility that the motor cortex of the non-ischaemic hemisphere assumes control of the recovered limb after stroke. The following section will firstly outline the pathophysiology of stroke. Then, the notion that ipsilateral motor pathways arising from the non-ischaemic hemisphere contribute to recovery will be discussed.

1.4.1 Stroke pathophysiology

Stroke is the rapid loss of cerebral function following a severe reduction in blood flow. Although they can be haemorrhagic (caused by an arterial aneurysm rupture or arteriovenous malformation) the majority of strokes are ischaemic, accounting for 85% of cases (Chen et al., 2010). In ischaemic stroke, a cerebral artery occlusion arises from the production of an atherosclerotic plaque, thrombus or from a dislodged embolus such as a blood clot that ascends from the heart to the cerebral circulation. Within seconds following preclusion of blood flow to the affected area, the ischaemic cascade is initiated within the brain parenchyma. This encompasses a complex sequence of deleterious events that converge to mediate irreversible injury. The major pathological mechanisms include excitotoxicity, peri-infarct spreading depolarisations, inflammation, necrosis and apoptosis (**Figure 1-4**).

Excitotoxicity

Adenosine triphosphate (ATP) levels in the perfusion territory of the affected artery fall, impairing the ability of membrane ion-motive ATPases to maintain ionic gradients (Siesjo, 1992). As a consequence, intracellular Na^+ levels rise leading to depolarisation of the membrane potential. This triggers the opening of presynaptic voltage-gated Ca^{2+} channels and glutamate is released into the extracellular space. Activation of N-Methyl-D-aspartate (NMDA), α-amino-3-hydroxy-5-methyl-4-isoxazolepropionic acid (AMPA) and metabotropic receptors exacerbates cytosolic Ca^{2+} overload. Na^+ influx drives Cl^- influx via chloride channels, resulting in inflow of water and cytotoxic oedema (Liang et al., 2007). The cytosolic Ca^{2+} overload impinges cell function via activation of endonucleases, phospholipases and cysteine proteins including calpains (Chan & Mattson, 1999). Additionally, Ca^{2+} induces a surge in superoxide and hydroxyl radicals along with nitric oxide which combines with superoxide to form a highly potent anion termed peryoxynitrate that induces DNA strand breakage (Garthwaite & Boulton, 1995).
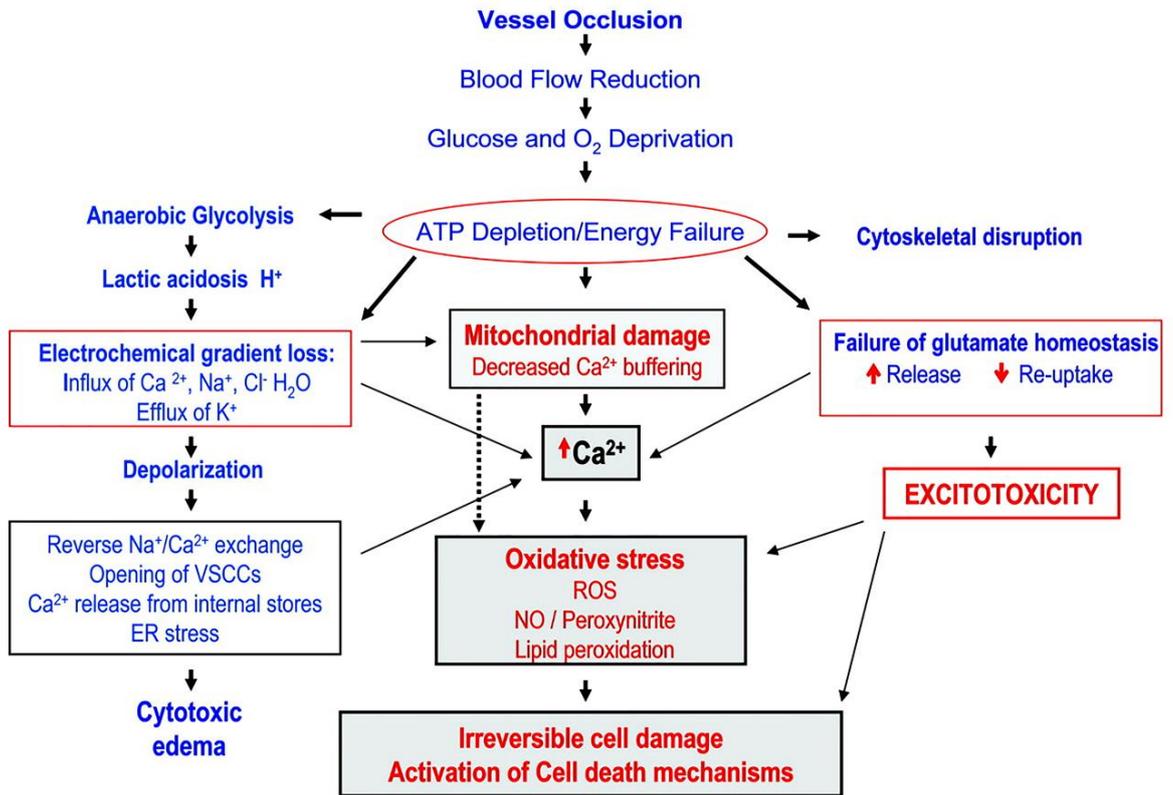
Figure 1-4 The ischaemic cascade

Occlusion of a cerebral blood vessel triggers a wide spectrum of biochemical events that culminate in cell death. (Modified from Chavez et al., 2009).

Peri-infarct depolarisations

In the ischaemic core, energy failure is so profound that cells undergo anoxic depolarisation and are incapable of repolarising. This irreversibly damaged area is surrounded by a gradient of moderately hypo-perfused non-functional but still viable tissue known as the penumbra. In penumbral tissue, cells retain the ability to repolarise but at the expense of further energy consumption (Markus, 2004). Once repolarised the same cells again depolarise in response to increasing glutamate and K^+ levels which accumulate in the extracellular space. In the absence of reperfusion, the cycle continues as recurring waves of depolarisations called peri-infarct depolarisations, until the penumbral tissue is recruited into the core region destined to infarct. As the penumbra has recovery potential, it is a target for interventional therapy in acute ischaemic stroke (Rohl et al., 2001).

Inflammation

Inflammatory mediators such as tumour necrosis factor-alpha, interleukin-1 and interleukin-6 become overly expressed as a result of enhanced cystolic Ca^{2+}. Neutrophils, macrophages and monocytes migrate into the ischaemic brain, guided by a variety of chemoattractants produced by cells at the site of the lesion (Dirnagl et al., 1999). Although the primary role of inflammatory cells is to clear necrotic cells, the activated macrophages express and release toxic factors including reactive oxygen species, proteinase and cytokines that further contribute to ischaemic damage (Arvin et al., 1996).

Necrotic and apoptotic cell death

Ischaemic cell death occurs via necrosis or apoptosis depending on the severity of the insult or the nature of the excitotoxic signalling pathways. Necrosis is a passive process secondary to energy depletion and predominates in the ischaemic core, where mitochondria are dysfunctional for ATP production. It is accelerated by Ca^{2+}-dependant proteases and is typified by organelle swelling and spillage of intracellular contents including toxic mediators into the extracellular milieu, affecting the surrounding cells (Brouns and De Deyn, 2009). Apoptosis is a programmed mechanism that orchestrates cell death in the penumbra and peri-infarct regions (Dirnagl et al., 1999). Apoptosis remains

inactive until it is stimulated by appropriate death signals including free radicals, tumor necrosis factor, DNA damage, p53 induction and cytochrome c release from mitochondria (Ueda et al., 2004).

The middle cerebral artery (MCA)

In ischaemic stroke, the territory of the occluded vessel determines the brain areas affected and the subsequent neurological outcome. The middle cerebral artery (MCA) and its branches are the most commonly affected vessels in stroke, accounting for over 70% of cases (Geyer & Gomez, 2009). The MCA has the largest vascular territory of all of the major intracranial arteries; it supplies almost the entire convex surface of the brain as well as most of the basal ganglia and internal capsule (Tatu et al., 1998). In humans, the MCA arises from the internal carotid artery as the larger of the two main terminal branches (the MCA and anterior cerebral artery; **Figure 1-5A**). Approximately 5-15 penetrating lenticulostriate arteries branch off the MCA stem and supply the globus pallidus, caudate nucleus, putamen and internal capsule. The MCA stem then bifurcates into superior and inferior subdivisions that give rise to 12 branches that distribute in a "fan-like" fashion to supply the lateral surface of the hemisphere and underlying white matter (Bogousslavsky, 2001). Occlusion of the MCA commonly occurs within the main stem or within one of the terminal superior or inferior subdivisions. A blockage within the main stem can result in a large infarct affecting both deep and superficial structures. Although the deep structures (i.e. the basal ganglia and internal capsule) are particularly vulnerable to ischaemia, given that they are supplied by lenticulostriate end arteries without anastomoses (Decavel, 2012). It is possible for a small embolus to occlude a single lenticulostriate branch, resulting in a small infarct or "lacune" within the basal ganglia or internal capsule; although this only occurs occasionally, as the majority of lacunes are caused by small vessel wall thickening termed Lipohyalinosis (Wardlaw, 2005).

Models of focal cerebral ischaemia have been established in a number of species (Macrae, 1992; Macrae, 2011; Traystman, 2003). The most commonly used species is the rat due to low animal and maintenance costs and similarities in cerebrovascular anatomy between humans and rats (Macrae, 2011). In a pattern comparable to humans, the MCA of the rat gives off deeply penetrating

lenticulostriate arteries before curving over the lateral surface of the cerebral hemisphere (**Figure 1-5B**; Scremin, 2004). Accordingly, blocking the MCA in rats can produce deep infarcts (involving the striatum and internal capsule) and/or superficial infarcts (involving the lateral cortex and underlying white matter) depending on the occlusion site and duration of ischaemia (Uluç et al., 2011; Garcia et al., 1993).

In humans, at 2 weeks after the onset of MCA territory stroke, the extent of pyramidal tract damage at the level of the cerebral penduncle correlates with the degree of contralateral motor dysfunction (Thomalla et al, 2004). Furthermore, in subjects with MCA territory stroke, the degree of acute damage (<12 h) to the posterior limb of the internal capsule (PLIC) predicts the severity of contralateral limb weakness present at 3 months after the stroke event (Puig et al., 2011). Injury to the PLIC can arise from i) striatocapsular stroke, in which there is direct involvement of the PLIC in the infarct, and ii) cortical/subcortical stroke, in which there is no direct involvement of the PLIC in the infarct, but presumed anterograde degeneration of the descending pathways passing through the PLIC (Pendlebury et al., 1999). Thus, the integrity of the pyramidal tract, particularly at the level of the PLIC, plays a key role in motor outcome following MCA territory stroke. As such, damage to the pyramidal tract should be an important feature of animal models of MCA territory stroke and this will be addressed in Chapters 3 and 4.
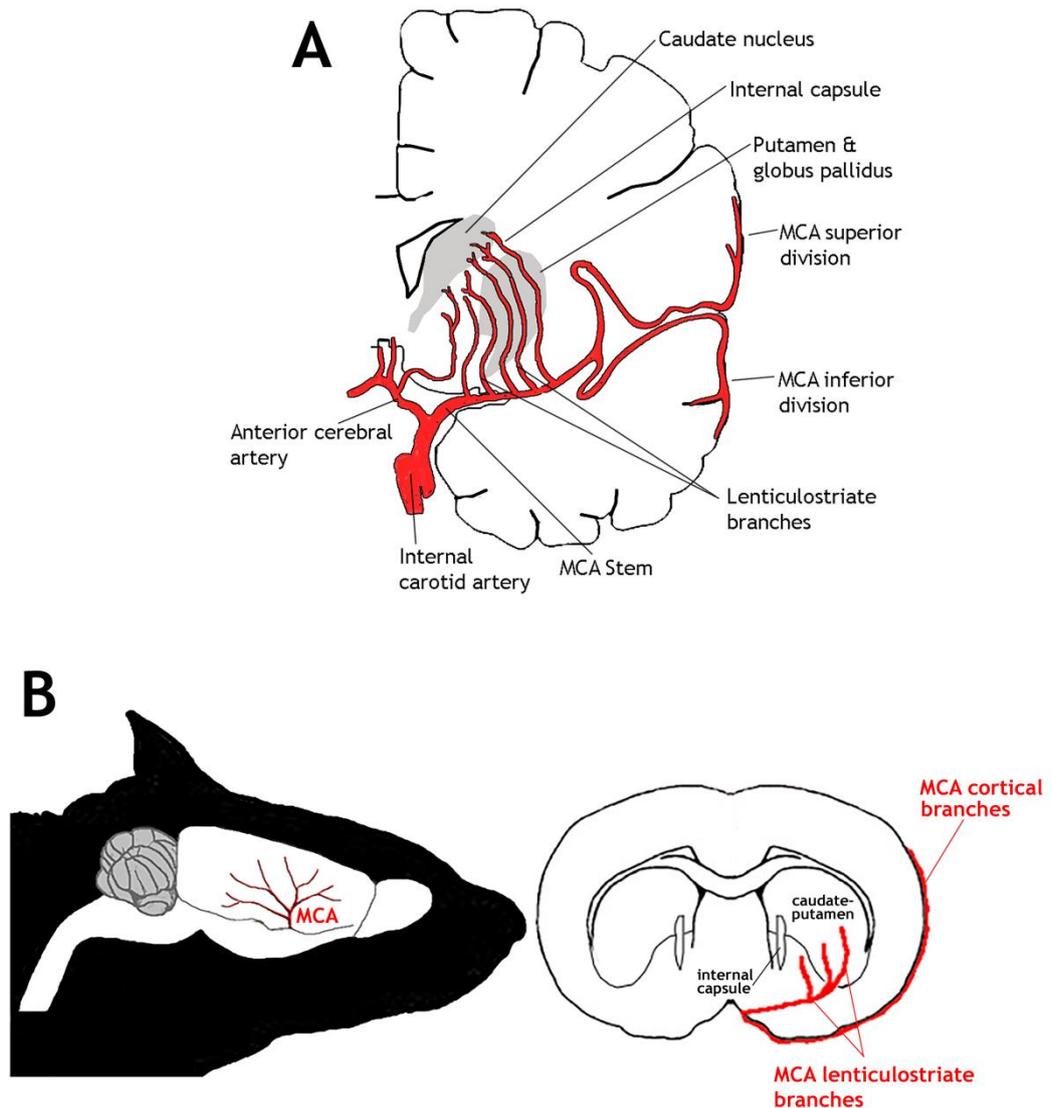
Figure 1-5 Anatomy of the middle cerebral artery (MCA) in humans and rats

A: In humans, the lenticulostriate branches of the MCA supply the caudate nucleus, internal capsule, putamen and globus pallidus. The distal subdivisions of the MCA supply much of the lateral surface of the hemisphere and underlying white matter.

B: Similarly, the MCA of the rat gives off deeply penetrating lenticulostriate vessels before branching out across the convex surface of the hemisphere. The left image depicts the MCA on the lateral cortical surface. The right image is a coronal view of the MCA lenticulostriate and cortical branch locations. (Modified from Davis et al., 2013).

1.4.2 Current treatment strategies for stroke

Effective treatment options for ischaemic stroke are extremely limited. The only Food & Drug Administration- approved treatment is recombinant tissue plasminogen activator (rtPA). This enzyme catalyses the conversion of plasminogen to plasmin, allowing for clot lysis and subsequent reperfusion of brain tissue before irreversible injury occurs. According to the National Institute of Neurological Disorders & Stroke, for every 100 patients treated with rtPA, 32 will attain a better outcome (Saver, 2004). However, many patients are ineligible for rtPA therapy due to its limited 4.5 h treatment window and adverse effects on oedema and haemorrhagic transformation (Cronin, 2010). As such, only 9-12% of all patients are thrombolysed (Stroke Statistics 2015, www.stroke.org.uk).   It is noteworthy that a series of recent clinical trials have demonstrated significant benefits of intra-arterial thrombectomy in acute ischaemic stroke patients, with reports of enhanced reperfusion and improved functional outcome (Goyal et al., 2015; Berkhemer et al., 2015).

For decades, research has primarily focussed on salvaging the ischaemic penumbra. Over 1000 putative neuroprotective agents have been investigated in animal models of ischaemia; including glutamate receptor antagonists, Ca^{2+} channel blockers, free radical scavengers and anti-inflammatory agents (Ginsberg, 2009). Unfortunately, this has yet to be translated into gains for stroke survivors, despite the completion of over 200 clinical trials (Stroke Trials Registry, www.strokecenter.org). Currently, post-stroke treatment remains limited to physical and occupational therapy.

An alternative approach to stroke treatment would be to enhance the brains innate capacity to reorganise itself after stroke. Studies of humans and experimental animals have uncovered a plethora of repair-related events to occur in response to stroke (Cramer, 2008; Benowitz & Carmichael, 2010). Many of these events correspond temporally with spontaneous functional recovery. A better understanding of repair-related mechanisms may reveal novel targets for therapeutic interventions.

1.4.3 Role of the non-ischaemic (ipsilateral) hemisphere in recovery of the affected limb

Stroke induces long-lasting adaptive processes in regions both proximal and distal to the infarct. An extensive literature suggests that the non-ischaemic (ipsilateral) hemisphere may be involved in control of the spontaneously recovered limb (Dancause, 2006). Brain mapping studies of both humans and animals have provided insights into how the non-ischaemic hemisphere responds to stroke at a systems level. Additionally, anatomical tracing studies in animals have demonstrated how neural pathways from the non-ischaemic hemisphere might become strengthened in order to take over control of the impaired limb.

Insights from brain mapping studies

According to fMRI and PET studies in stroke survivors, movement of the stroke affected hand elicits abnormally enhanced neural activity in the non-ischaemic (ipsilateral) hemisphere, which is not detected in healthy subjects (Grefkes & Fink, 2011; Ward & Frackowiak, 2006; Rehme et al., 2011; Chollet et al., 1991; Grefkes et al., 2008). For example, in subjects with chronic (> 5 weeks) subcortical MCA territory infarcts, movement of the stroke-affected hand evokes activity in the ipsilateral primary motor cortex, premotor cortex and supplementary motor area that is not seen in healthy controls (Grefkes et al., 2008). Such findings have contributed to the notion that these ipsilateral motor areas mediate spontaneous recovery of the stroke-affected limb. However, identification of movement-related activation with functional imaging does not establish the functional significance of a particular brain area; ipsilateral activation could also reflect a nonspecific epiphenomenon of stroke, or even a maladaptive process that hinders recovery (Cramer, 2008).

The most compelling evidence for the involvement of ipsilateral motor areas in limb recovery comes from studies examining the effects of disrupting these areas. Multiple pulse transcranial magnetic stimulation (TMS) transiently interferes with a target cortical site; a TMS-induced disturbance of a specific motor behaviour is indicative of a contributory role of the stimulated cortical site to that behaviour. In well-recovered chronic stroke patients (>8 months) with internal capsule infarcts, performance of a finger tapping task using the

recovered hand was found to deteriorate when inhibitory TMS was applied over the ipsilateral primary motor cortex (or premotor cortex; Lotze et al., 2006) i.e. blocking ipsilateral cortical activity reinstated the original deficit. Similarly, inhibitory TMS over the ipsilateral premotor cortex was also shown to slow down reaction times of the stroke-affected hand in chronic stroke subjects (6 months) with subcortical or cortical MCA territory infarcts (Johansen-berg et al., 2002). This is highly suggestive that motor areas in the non-ischaemic (ipsilateral) hemisphere participate in control of the recovered limb. Interestingly, Johansen-berg and colleagues (2002) noted that TMS to the ipsilateral premotor cortex was more disruptive in subjects with greater impairments. Thus, from one point of view hand recruitment of ipsilateral areas seemed to be related to poor outcome; from another point of view ipsilateral activation was better present than absent, particularly in the most affected patients. The effect of infarct size/location on response in the non-ischaemic (ipsilateral) hemisphere requires more detailed investigation.

In contrast with the above findings, some authors argue that recruitment of ipsilateral motor areas during paretic-limb movement is maladaptive. The underlying hypothesis is that activation in the non-ischaemic hemisphere is increased due to reduced transcallosal inhibition from the ischaemic to the non-ischaemic hemisphere. In turn, over-active non-ischaemic hemisphere exerts a heightened transcallosal inhibitory influence on the ischaemic hemisphere, thereby deteriorating function of the affected limb beyond the initial deficit caused by the infarct (Nowak et al., 2009). Support for this comes from the work of Takeuchi et al., (2005) who studied chronic stroke subjects (> 7 months) with subcortical infarcts and reported that inhibitory TMS over the non-ischaemic (ipsilateral) primary motor cortex immediately improved performance of the stroke-affected hand during a pinching task.

Cortical mapping studies have also been performed in rodent models of stroke. Abo et al., (2001) induced complete infarction of the sensorimotor cortex of rats and demonstrated that at 21 days after stroke, when recovery was apparent, stimulation of the stroke-affected hindlimb elicited activation in the ipsilateral (non-ischaemic) sensorimotor cortex to a greater degree than in normal healthy rats. Dijkuizen et al., (2001) induced a transient occlusion of the MCA in rats and

showed that stimulation of the stroke-affected forepaw at 3 and 14 days after stroke elicited widespread activation in the ipsilateral cortex.

To summarise, human and animal brain mapping studies frequently report over-activation of ipsilateral motor areas during stroke-affected limb movement but the exact function served by increased ipsilateral activation remains to be clarified. It is likely that recovery may rely on different mechanisms depending on the infarct localisation/extent and this may account for some of the above contradictory findings (Stoeckel & Binkofski, 2010).

Insights from anatomical tracing studies

There is evidence from anatomical tracing studies in rodents that the non-ischaemic hemisphere may gain access to the stroke-affected limb through rewiring of its descending axonal projections. Most notably, the CST arising from the non-ischaemic hemisphere may reorganise its arborisation at the level of the spinal cord to replace lost synaptic connections. Following permanent experimental occlusion of the MCA (Liu et al., 2007; Liu et al., 2008), destruction of the primary motor cortex (Bachman et al., 2014; LaPash Daniels et al., 2009; Ueno et al., 2012) and unilateral pyramidotomy (Brus-Ramer et al., 2007; Maier et al., 2008), CST axons originating from the uninjured hemisphere sprout into the denervated (ipsilateral) side of the spinal cord. Manipulating the extent of CST sprouting from the non-ischaemic hemisphere alters the degree of spontaneous motor recovery. For instance, intraspinal delivery of Chondroitinase ABC to degrade growth inhibitory proteoglycans increases sprouting from the non-ischaemic hemisphere and improves performance of sensorimotor tasks (Soleman et al., 2012). Other therapies reported to enhance CST sprouting from the non-ischaemic hemisphere and sensorimotor recovery include: stem cells (Liu et al., 2007; Liu et al., 2008), growth signalling proteins (Zai et al., 2009; Chen et al., 2002), and suppressors of neurite growth inhibitors (Lee et al., 2004; Lindau et al., 2014). Conversely, knockdown of plasminogen, which is implicated in axonal path-finding, reduces CST sprouting from the non-ischaemic hemisphere and impairs motor recovery (Liu et al, 2014).

The precise trajectory by which CST fibres from the non-ischaemic hemisphere reach the denervated (ipsilateral) side of the spinal cord following experimental

stroke is incompletely understood. The "new" fibres may reflect 1) originally crossed fibres re-crossing the midline at the level of the spinal cord, or 2) the sprouting of the pre-existing population of ipsilateral axons (**Figure 1-6**). Studies have reported that CST fibres spontaneously sprout across the midline of the spinal cord, extending across the dorsal and ventral commissure following experimental stroke (Liu et al., 2008; Zai et al., 2009) and unilateral pyramidotomy (Brus-Ramer et al., 2007; Maier et al., 2008). Following transection of the dorsal columns, which contain most of the crossed CST axons, ipsilaterally descending CST axons spontaneously sprout onto motor neuron pools (Weidner et al., 2001). Although, it is yet to be established whether stroke induces the sprouting of ipsilaterally projecting fibres.

Despite the above reports of sprouting, it is yet to be established whether new CST axonal terminals, originating from the non-ischaemic hemisphere, form in the denervated (ipsilateral) half of the spinal cord to replace the synaptic connections lost after stroke. In a transgenic mouse in which CST axons were labelled with yellow fluorescent protein, Liu et al., (2013) investigated terminal remodelling after permanent occlusion of the MCA. An antibody against synaptophysin, an abundant presynaptic vesicle glycoprotein, was used as a marker of synaptogenesis. The number of CST axons containing synaptophysin in the stroke-affected side of the spinal cord was significantly reduced compared with control mice at 14 days after stroke, then significantly increased at 28 days after stroke. Although this is indicative of the formation of new CST terminals, all CST axons were labelled (i.e. from both hemispheres), so the extent to which the CST from the non-ischaemic hemisphere contributes to terminal remodelling remains unclear. Evidence for the formation of new synaptic connections between the non-ischaemic hemisphere and denervated (ipsilateral) limb muscles comes from Liu et al., (2008; 2009); at 4 (or 8) weeks following permanent middle cerebral artery occlusion in the rat, injection of a transsynaptic tracer into affected-forepaw muscles revealed an increased number of labelled cells in the motor cortex of the non-ischaemic (ipsilateral) hemisphere.
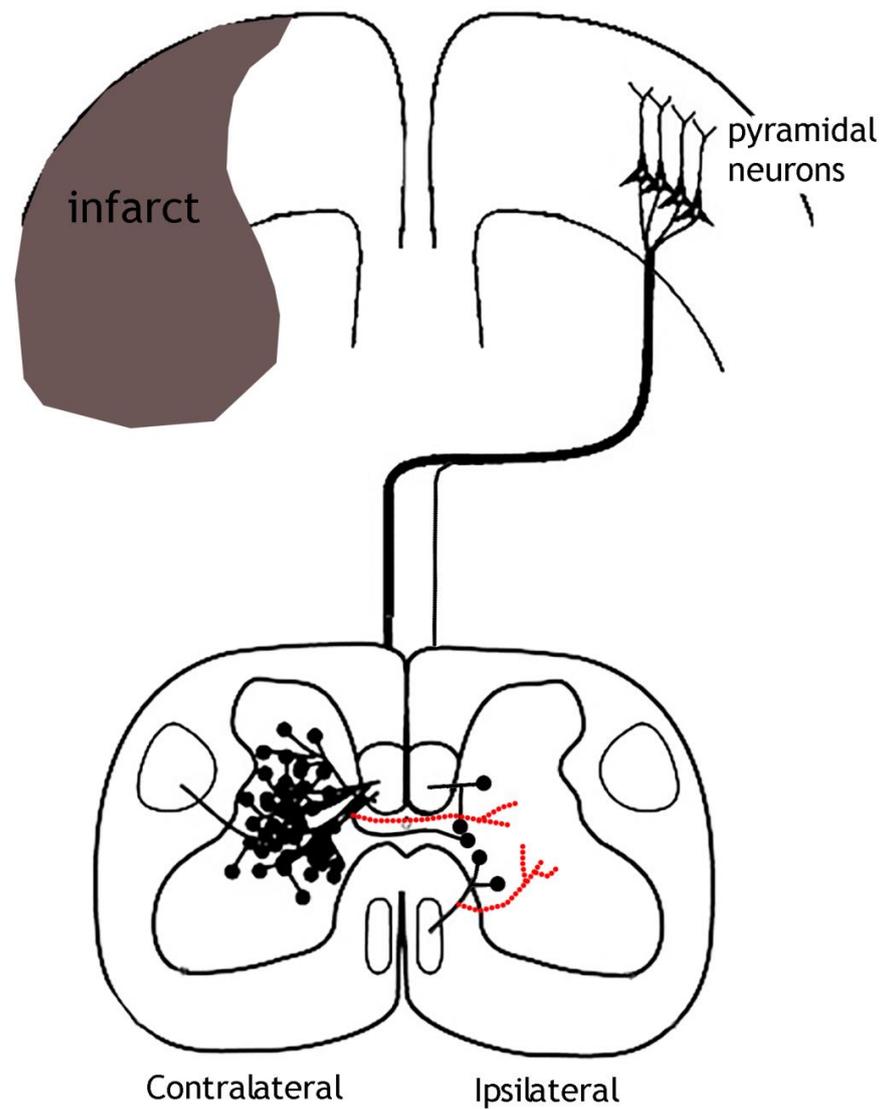
Figure 1-6 Potential patterns of CST sprouting from the non-ischaemic hemisphere

The normal axonal projection patterns are shown in black and the potential patterns of CST sprouting that occur after stroke are shown in red. Fibres from the main contralateral component may sprout collaterals across the midline resulting in a "double crossed" pathway. The small population of pre-existing ipsilateral fibres may also sprout in order to strengthen connections between the non-ischaemic motor cortex and the stroke-affected (ipsilateral) limb. (Modified from Carmel & Martin, 2014).

The CST remodelling studies described above have principally used rodent models involving 1) complete ablation of the pyramidal tract from one hemisphere (Brus-Ramer et al., 2007; Maier et al., 2008); 2) targeted infarction of the entire primary motor cortex (LaPash Daniels et al., 2009; Bachman et al., 2014); 3) or permanent occlusion of the MCA (Liu et al., 2007; 2008; 2009) which typically produces very large infarcts encompassing both subcortical and cortical structures (Garcia et al., 1993). In humans, it has been estimated that less than 15% of all strokes involve cortical infarcts while the majority of strokes are subcortical (Bogousslavsky et al., 1988; Kang et al., 2003; Wessels et al., 2006; Corbetta et al., 2015). Whether subcortical infarcts result in remodelling of the CST from the non-ischaemic hemisphere has yet to be explored.

The vast majority of studies have focussed on CST sprouting directly into the denervated (ipsilateral) side of the spinal cord as a potential mechanism of recovery following stroke. However, it is important to acknowledge that the motor cortex of the non-ischaemic hemisphere could also gain access to the denervated (ipsilateral) side of the spinal cord indirectly via relay neurons located in the brainstem and contralateral spinal cord (**section 1.3)** and the strengthening of these indirect pathways could also contribute to recovery. A small number of studies have alluded to this. For instance, at 4 weeks following cortical infarction in mice, the cortex from the non-ischaemic hemisphere increases its projections to the ipsilateral medullary reticular formation; and in turn, reticular nuclei increase their projections to the denervated (ipsilateral) side of the spinal cord (Bachmann et al., 2014). In primates, following pyramidal tract transection, ReST axons passing through the MLF increase their output to denervated flexor motor neurons (Zaaimi et al., 2012). Additionally, at 4 weeks following permanent occlusion of the MCA in rats, pyramidal neurons in the non-ischaemic hemisphere sprout fibres into the deafferented (contralateral) red nucleus (Liu et al., 2007). Finally, it is also noteworthy that in addition to the adaptive changes described for the non-ischaemic hemisphere, an array of repair-related events have been reported to occur within the ischaemic hemisphere after stroke (reviewed by Benowitz & Carmichael, 2010; Cramer, 2008). Recovery from stroke therefore, likely involves the reorganisation of multiple systems at both the cellular and molecular level.

1.5 Aims of the Thesis

This thesis has two overarching aims:

1) In rodent models of stroke, there is evidence that CST axons originating from the non-ischaemic hemisphere sprout into the denervated (ipsilateral) side of the spinal cord, and the extent of sprouting correlates with the degree of motor recovery (**section 1.4.3**; Liu et al., 2007; Liu et al., 2008; LaPash Daniels et al., 2009; Bachmann et al., 2014). However, it is yet to be confirmed whether the CST from the non-ischaemic hemisphere establishes new terminals in the denervated (ipsilateral) side of the spinal cord after stroke. Hence, the first major aim of this thesis was to assess for CST terminal remodelling between the non-ischaemic hemisphere and denervated (ipsilateral) half of the cervical spinal cord following recovery from experimental stroke in the rat. It was hypothesised that rats subjected to experimental stroke would exhibit an increased number of CST terminals in the denervated (ipsilateral) half of the spinal cord and that the number of terminals would be correlated with the degree of motor recovery.

2) Spinal CINs are a highly heterogeneous population and they play an important role in coordinating inter-limb activity (**section 1.2**). Furthermore, neural pathways involving CINs represent a potential substrate for recovery of function following injury to the CST (e.g. after stroke; **section 1.3**; Jankowska & Edgley, 2006; Edgley et al., 2004). Despite their proposed functional significance, CINs (particularly those of the cervical spinal cord) remain poorly defined and supraspinal input to the various populations of CINs has yet to be fully characterised. Hence, the second major aim of this thesis was to gain a better understanding of how supraspinal pathways engage different populations of CINs within the cervical spinal cord. Specifically, the goal was to characterise CST and ReST contacts onto two different populations of CINs in the rat: i) those that issue long-ranged axonal projections to lumbar segments (commissural LDPNs) and ii) those that have short-range axonal projections confined to a single segment (intrasegmental CINs). It was

hypothesised that CST and ReST axons would establish contacts with both of these cell types.

Chapter 2

General experimental methods

This chapter provides a detailed description of the materials and methods used throughout this project. Any deviations from these procedures or additional techniques carried out to fulfil specific aims will be described in the appropriate results chapters.

2.1 Rodents

All experiments were performed using adult male Sprague-Dawley rats (250-300g, Harlan, Bicester UK). Prior to surgery rats were group housed (12:12, light:dark) with food and water available *ad libitum*. All procedures were approved by the Ethical Review Process Applications Panel of the University of Glasgow and were performed in accordance with the UK Animals (Scientific Procedures) Act, 1986.

2.2 Surgical procedures

2.2.1 Animal preparation

For all surgical procedures anaesthesia was induced in an anaesthetic chamber with 5% isoflurane (Baxter Healthcare Ltd, UK) delivered in 30% oxygen (O_2) and 70% nitrous oxide (N_2O). Absence of the hindlimb withdrawal reflex (assessed by pinching the metacarpal region of the hind-foot) indicated appropriate depth of anaesthesia. During surgery this reflex was assessed at regular intervals (~10 min) to ensure an adequate dose of anaesthesia was maintained. The application of Lacri-Lube (Allergan, Irvine, USA) prevented corneal drying, and body temperature was held stable at 37±2°C by a heated lamp and rectal thermal probe (Physitemp, New Jersey, USA). All surgeries were performed under strict aseptic conditions.

2.2.2 Induction of transient focal cerebral ischaemia

Prior to the induction of transient focal cerebral ischaemia, rats were intubated to allow for mechanical ventilation. This is because the surgical procedure involves manipulation of the vagus nerve, which is implicated in respiration. Firstly, an intubation wedge with a 25° angle made from the barrel of a 3-ml plastic syringe (as outlined by Jou et al., 2000) was inserted into the rat's mouth to expand the oropharyngeal cavity for visualisation of the epiglottis. The rat

was placed in supine position and a flexible fiber-optic light source (Meiji Techno, UK) was shone onto the ventral surface of the neck to gain a clear view of the larynx and trachea. A 16 gauge catheter (MillPledge Veterinary, UK) was inserted through the intubation wedge directly into the tracheal entrance. The wedge was then removed and the catheter connected to a ventilator (Ugo Basile, Linton Instruments, UK) where the stroke volume was set to ~3ml at a frequency of 50 breaths per min. The catheter was sutured to the side of the mouth (4-0 silk) to secure it in place and anaesthesia (reduced to 2-3% isoflurane) was maintained via this method.

Transient MCA occlusion (MCAo) was performed using the intraluminal filament method first described by Koizumi et al., (1986) with subsequent modifications (Longa et al., 1989). Following a ventral midline neck incision (~2 cm), the tracheal strap musculature and submandibular glands were retracted to reveal the left common carotid artery. Using a dissecting microscope (x10 magnification), this vessel was carefully separated from the vagus nerve and surrounding fascia. The external carotid, internal carotid and occipital arteries were then isolated, as shown in **Figure 2-1A**. A loose ligature (4-0 silk) was looped around the carotid artery at the bifurcation and a second tie was placed tightly 1mm below the bifurcation. Loose ties were then placed around the external carotid, internal carotid and occipital vessels and tension was applied to each tie to minimise bleeding. Finally, the pterygopalatine branch of the internal carotid artery was isolated and tied off to prevent accidental intubation of this vessel with the filament. See **Figure 2-1B** for a schematic of the ligated vessels.

The intraluminal filament was constructed from a length of 3-0 nylon monofilament (Covidien, UK) where a small diameter bulb (300-350µm diameter for 250-300g rats) was moulded using a cauterising pen (Aaron Medical, FL, USA). A bend was introduced in the filament at 22mm to ensure the bulb advanced to the proximal origin of the MCA. An arteriotomy was made between the 2 ligatures on the common carotid artery and the filament was inserted and advanced along the internal carotid artery until only the bend of the filament was visible outside the vessel. At this point, resistance indicated that the bulb was lodged at the ostium of the MCA. The loose ligature at the carotid

bifurcation was tied tightly around the filament to secure it in place and the wound was filled with sterile saline and covered with gauze to prevent dehydration. After 60 min, the ligature around the carotid bifurcation was loosened and the filament retracted and removed. The incision point was cauterised with diathermy forceps and all ligatures were removed. The wound was then flushed with sterile saline and stitched using 4-0 silk sutures and 2ml of 0.9% saline was administered subcutaneously (SC) to prevent dehydration.

In animals subjected to sham occlusion as controls, the above surgical procedure was carried out with the exception of the arteriotomy and insertion of the filament. Briefly, the left common carotid artery was exposed and dissected from its bifurcation to the skull base and sterile silk sutures were tied around the common, external, internal, occipital and pterygopalatine vessels. After 60 min, all of the ligatures were removed, the wound was closed and 2mL 0.9% saline injected (SC).

At the end of the MCAo and sham procedures, anaesthesia was withdrawn and 100% O_2 was administered. When the rat began breathing against the ventilator, the O_2 was switched off and the intubation tube was disconnected from the ventilator. Once the rat was breathing unaided, the intubation catheter was removed and the rat was transferred to a recovery cage. Animals were housed individually and their overall health status was closely monitored throughout the survival period. Until the rats fed independently (~3 days), they were hand fed using a 5ml syringe (baby food, Heinz) 3 times daily. Softened rat chow was also provided on the cage floor to encourage feeding for approximately 7 days following surgery.
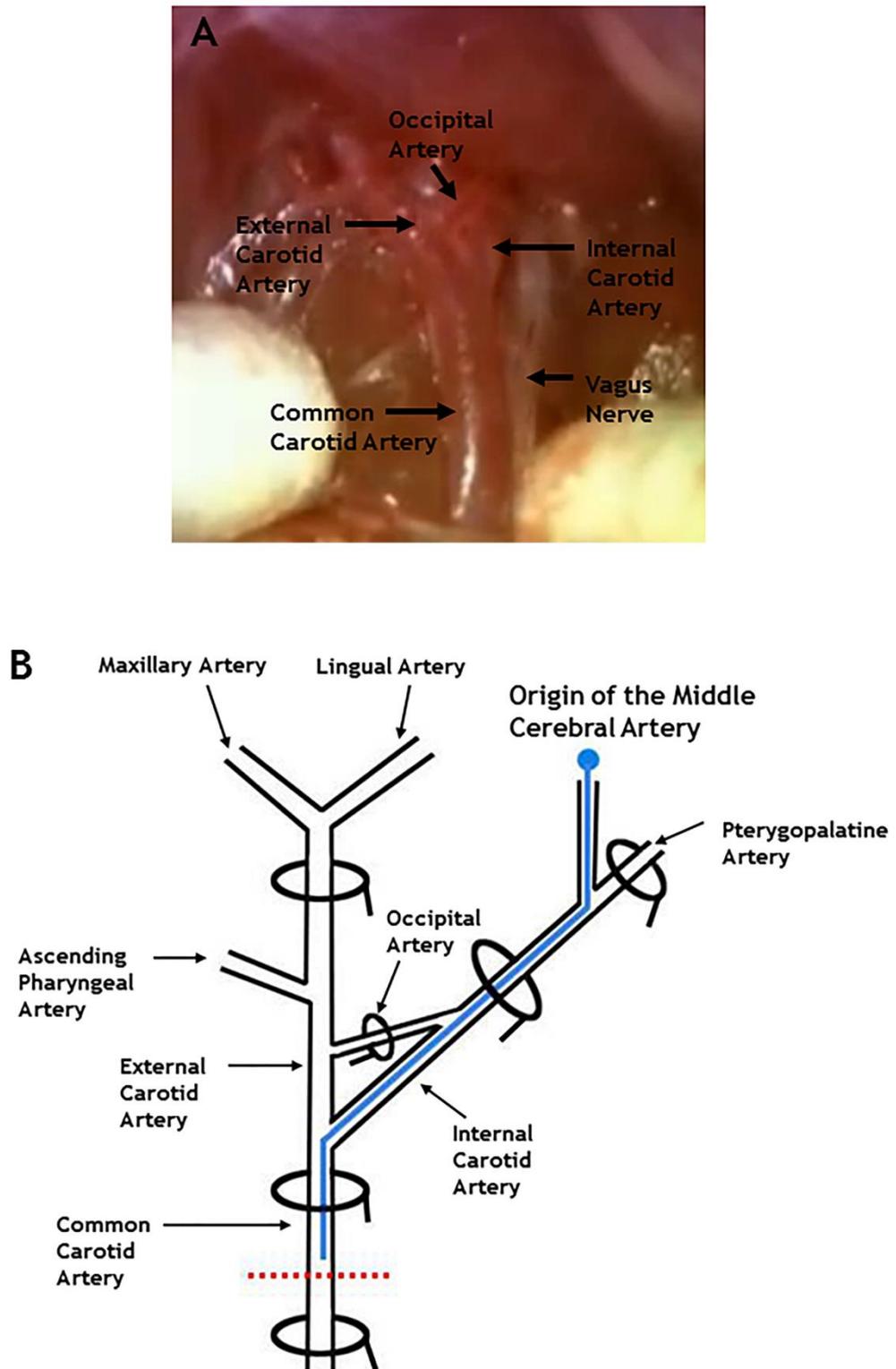
Figure 2-1 MCA occlusion (MCAo) via the intraluminal filament model

A: The common carotid, external carotid, internal carotid and occipital arteries were isolated and particular attention was paid to avoid damaging the vagus nerve. **B:** Once the appropriate vessels were ligated (black circles), an incision was made in the common carotid artery (red dotted line) and a bulbed filament (blue) was inserted and advanced along the lumen of the internal carotid artery until it blocked the origin of the MCA. Note that in this example a left MCAo is depicted but the vessels appear on the right hand side because the rat is in supine position.

2.2.3 Anterograde labelling of axonal terminals

Descending axons were labelled anterogradely by stereotaxic injection of the b-subunit of cholera toxin (CTb) into the forelimb motor cortex or MLF to label CST and ReST axons, respectively. Following induction of anaesthesia (**section 2.2.1**), the fur on the skull was shaved and the rat transferred to a stereotaxic frame (World Precision Instruments, USA), as shown in **Figure 2-2A**. Equidistant ear bars were inserted into each external auditory meatus so that the head could be moved up and down but not laterally and the head was fixed in place by mounting the incisors onto an incisor bar. During the stereotaxic surgery anaesthesia was maintained via face mask (2-3% isoflurane in O_2 and N_2O, 30%:70%). Using a dissecting microscope (x10 magnification), a midline incision was made and the subcutaneous tissue and periosteum were separated to expose the surface of the skull. In rats where the forelimb motor cortex was targeted, Bregma was used as a stereotaxic reference point; whereas in rats where the MLF was targeted the Interaural Line was used as a reference point (**Figure 2.2B**). This is because greater accuracy can be achieved if Bregma is used as landmark for work with rostral structures and the Interaural Line for work with caudal structures (Paxinos et al., 1985). To zero the apparatus for forelimb motor cortex injections, the tip of a glass micropipette (diameter 20μm) was aligned with Bregma and the resultant coordinates in the anterioposterior (AP), mediolateral (ML) and dorsoventral (DV) planes were recorded from the Vernier scale (mm). To zero the apparatus for MLF injections the micropipette tip was aligned with the right ear bar (Interaural Line) for the AP and DV readings and the sagittal suture for the ML reading. To obtain the appropriate injection sites, the known stereotaxic coordinates for each target region were subtracted (or added) from these "zero" coordinates. The stereotaxic coordinates for each target region are listed in **Table 2.1**. The coordinates for the forelimb area were based on those defined by Neafsey et al., (1986) and the coordinates for the MLF were obtained from the stereotaxic atlas of Paxinos & Watson (2005).

Once the micropipette was moved to the designated AP/ML coordinates, a dental drill (World Precision Instruments, USA) was used to expose the surface of the brain. For forelimb area injections, two burr holes were drilled at two different locations, then subsequently connected. For MLF injections, one burr hole was drilled. A 2μl droplet of 1% CTb (Sigma-Aldrich Co., Poole, UK) in

distilled water was placed onto Parafilm (Bemis, USA) then drawn into the micropipette by applying suction with a 20ml syringe. The micropipette was then inserted into the brain at the appropriate depth (DV coordinate) and CTb solution was expelled by using an air pressure device (1-5 pound-force per square inch (psi); Pico-injector, World Precision Instruments, USA). Four 200nl injections were administered for forelimb area labelling and a single 200nl injection was administered for MLF labelling. For each injection the needle remained in place for 5 min to prevent backflow. The exposed surface was then stitched (4-0 silk sutures) and 2mL 0.9% saline was administered (SC) to the animal. The isoflurane was switched off and the animal was allowed to breathe 100% O_2. Once the rat regained the foot-pinch withdrawal reflex, it was transferred to a recovery cage. Health status was recorded daily until termination.

Descending system	Target	Bregma coordinates, mm		
		AP	ML	DV
CST	Forelimb motor cortex	+1.5	-3	-1.5
		-0.5	-2	-1.5
		Interaural coordinates, mm		
		AP	ML	DV
ReST	Medial longitudinal fascicle (MLF)	-3.8	+0.1	+1.0

Table 2-1 Stereotaxic coordinates for labelling of CST and ReST axonal terminals

To target the forelimb area for CST labelling, the coordinates were subtracted (or added) from the position of Bregma. To target the MLF for ReST labelling, the coordinates were subtracted (or added) from the position of the Interaural line (AP and DV) and sagittal suture (ML). AP= anterioposterior; ML= mediolateral; DV= dorsoventral; mm= millimetres
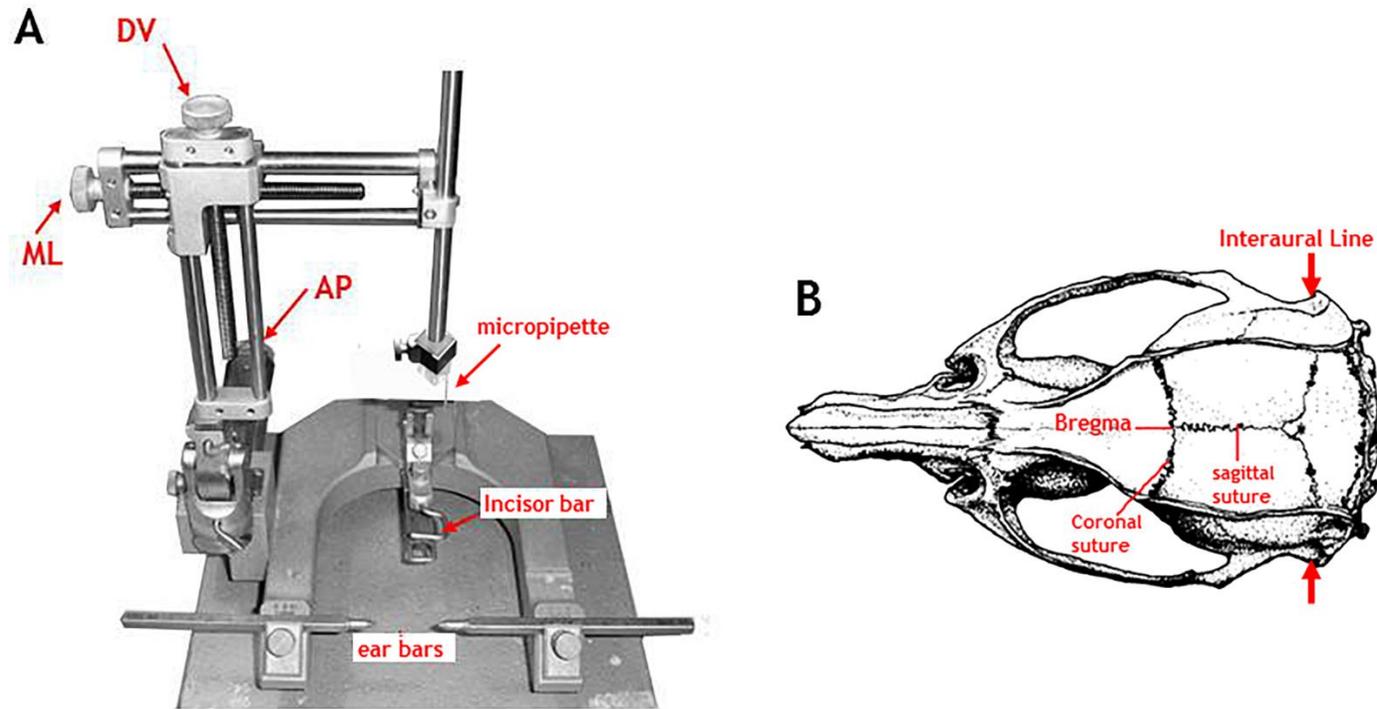
Figure 2-2 Stereotaxic frame and landmarks of the rat skull.

A: The ear and incisor bars were used to fix the rat's head in place and the micropipette was moved to the appropriate coordinates using the anterioposterior (AP), mediolateral (ML) and dorsoventral (DV) stereotaxic arms. **B:** Dorsal view of the rat skull depicting the stereotaxic reference points used in this study. Bregma (the point where the coronal suture is intersected by the sagittal suture) was used as a landmark for targeting the forelimb area whereas the Interaural Line (measured from the position of the ear bars) along with sagittal suture were used as landmarks for targeting the MLF (modified from Paxinos et al.,1985).

2.2.4 Retrograde labelling of LDPNs and intrasegmental CINs

The fluorescent retrograde tracer Fluorogold (FG; Fluorochrome, LLC, USA) was injected into the intermedio-ventral grey matter of the right side of the lumbar (L1/L2) or cervical (C4/C5) spinal to label LDPNs and intrasegmental CINs, respectively. Following induction of anaesthesia (**section 2.2.1**), the rat was placed in a stereotaxic frame and equidistant ear bars were inserted into each external auditory meatus. During this procedure anaesthesia was maintained via face mask (2-3% isoflurane in O_2 and N_2O, 30%:70%). To retrogradely label LDPNs, the L1 segment was targeted by counting down from the point of attachment of the lowest rib at T13; whereas to retrogradely label intrasegmental CINs, the C4 segment was targeted by counting down from the prominent spinous process of the C2 vertebra. Firstly, the fur on the back was shaved and a dorsal midline incision was made extending from ~Th10 to L3 (or ~C1 to C6). The rat was then secured in place by spinal fixators (for L1 injections) or by clamping the C2 spinous process (for C4 injections). A small burr hole (1mm diameter) was then made adjacent to the midline in the laminar surface to expose the dorsal surface of the L1 (or C4) segment of the spinal cord (right side). Using a small syringe needle (Sigma-Aldrich, UK), a break was made in the pia mater to prevent dimpling of the spinal cord during micropipette insertion. A 2µl droplet of 4% FG in distilled water was placed onto Parafilm then drawn into a micropipette. The tip of the micropipette (20µm diameter) was inserted into the spinal cord to a depth of ~1.5mm from the surface at an angle of 15° to target the intermedio-ventral grey matter of the right side of the spinal cord. After waiting 5 min to prevent backflow of the tracer, the micropipette was removed, the wound was sutured and 2mL 0.9% saline was administered (SC). Buprenorphine (0.1mg/100g) and Carprofen (5mg/100g; Reckitt Benkiser Healthcare, Dumfries, UK) were also administered (SC). The animal was allowed to breathe 100% O_2 until it regained the foot-pinch withdrawal reflex and health status was monitored daily until termination.

2.2.5 Perfusion Fixation

All rats were killed by transcardiac perfusion fixation to allow for tissue processing. Following induction of anaesthesia (5% isoflurane in O_2 and N_2O, 30%:70%), the rat received a lethal dose of Pentobarbitone (1ml/200g,

intraperitoneally; Sigma-Aldrich, UK). An incision was made along the midline of the thorax to reflect the skin (~6cm) and the diaphragm was cut. The ribcage was then cut along either side and the tip of the sternum displaced to expose the thoracic cavity. A 16-gauge needle delivering mammalian ringer solution (25-50ml) from a saline bag suspended 2 metres above the operative surface was inserted into the apex of the left ventricle and advanced into the aorta. The needle was clamped in place and the right atrium cut. When the blood was cleared from the liver, fixative (4% formaldehyde in 0.1M phosphate buffer, pH 7.4, ~1L) was perfused through the circulatory system. The brain, cervical and lumbar spinal cord were removed and post-fixed in the same fixative overnight at 4°C. To cryoprotect the brain, sucrose was added to this fixative solution (3g/10ml). If not immediately processed for analysis, tissue was stored in liquid nitrogen which freezes instantly at -210 ℃.

2.3 Sensorimotor testing

In experiments where rats underwent transient MCAo or sham occlusion surgery (Chapters 3 & 4), behavioural testing was employed for the assessment of sensorimotor deficits and recovery. To minimise stress during behavioural experiments, animals were handled daily for 1 week prior to the beginning testing. During a handling session the rat was gently lifted from under the shoulders and placed on the experimenters forearm for 10 min. The rat was then placed back into the home cage and rewarded (Multi-Cheerios, Kellogg's). If a rat displayed obvious signs of stress (e.g. vocalising or freezing) on the seventh day of handling, they were excluded from use in the study. All behavioural testing was conducted at the same time every day (10am).

2.3.1 Neurological score

Global sensorimotor function was assessed using a 33 point neurological scale originally published by Hunter et al., (2000) and subsequently modified by McGill, (2005). The neurological scale is modified from an original scoring system published by Hunter et al., (2000). The scale consists of 11 separate tests which evaluate limb function and motility (**Table 2-2**). The maximum score of 33 denotes normal neurological function; scores lower than 33 are indicative of

neurological dysfunction. This test was performed on the day prior to MCAo (day -1) and postoperatively on days 1, 2, 3, 7 (14, 21 and 28 in Chapter 4).

2.3.2 Adhesive label test

The adhesive label test was used to determine the extent of forelimb-use asymmetry displayed by the animals (Schallert & Whishaw, 1984). During this test, the rat was removed from the home cage and a circular adhesive label (1.3cm diameter, Avery International, USA) was placed on the hairless radial aspect of each wrist as shown in **Figure 2-3**. To prevent order of attachment from biasing motor behaviour, label placement (left paw/right paw) was altered for 4 separate trials and the experimenter touched each forepaw simultaneously immediately after the stimuli were attached. The animal was then placed in an observation cage and behaviour was recorded using a video camera (Sony). If a label fell off without being directly removed, the trial was restarted. Each trial ended when both tabs had been removed, or when 3 min had elapsed and the animal failed to contact/remove each tab. The latency to contact each label with the mouth and the latency to remove each label was subsequently assessed by observing the videos. For each trial, the difference in contact/removal time between the affected (right) and non-affected (left) paw was calculated to prevent the overall activity of the rat from affecting performance (Stroemer et al., 2009). Between each trial the rat was returned to the home cage for 5 min. This test was performed prior to MCAo (day -1) and postoperatively on days 3, 7 (14, 21, and 28 in Chapter 4). A pilot study (Chapter 3) revealed that when MCAo rats were placed in the observation cage at postoperative days 1 and 2, they often exhibited a complete lack of activity, and sometimes remained in the same position for the duration of the trial (3 min). Such freezing behaviour would have confounded experimental results, so the adhesive label test was not performed at those particular time points.

Behaviour	Procedure	Score
Paw placement	Animal held lengthways at edge of table and each paw in turn gently pulled over side of table	1 point for each successful paw placement back onto table (*max 4*)
Righting reflex	Animal placed in supine position	1 point if righted itself
Horizontal bar	Forepaws placed on elevated bar	3: if both hindlimbs raised on bar 2: if one hindlimb raised on bar 1: if animal hangs on 0: if animal falls off (*max 3*)
Inclined platform	Animal placed facing down on 45° incline	4: if animal rotates immediately to face "uphill" 3: if it takes between 15-30s 2: if it takes over 30s 1: if animal remains pointing downwards 0: if animal falls off (*max 4*)
Rotation	Animal held by base of tail and rotated clockwise or anticlockwise. Animal should swivel contralaterally to the direction of rotation	1 point for each side (*max 2*)
Visual fore-paw reaching	Animal held by base of tail and positioned just beneath the table top. The ability of the rat to place both forepaws onto the table was assessed	1 point for each successful placement (*max 2*)
Contralateral reflex	Animal held by tail above table and assessed for reflex (holding of the contralesional limb into the body)	0: for a reflex 1: no reflex
Circling	Rat placed on floor	5: non circling 4: if animal tends to one side 3: large circles >50cm 2: medium circles >15<50cm 1: tight circles <15cm radius 0 spinning (*max 5*)
Grip strength	Animal held by tail and allowed to grip cage lid	3: if both paws grip to cage 2: if both paws grip to cage but let go 1: point if one paw grips to cage 0: if no paws grip (*max 3*)
Motility	Rat placed on floor: maximum score give if animal is active, inquisitive and rearing	4: normal motility 3: if very active 2: if slow but still lively 1: if unsteady 0: if completely immobile (*max 4*)
General condition	Animals assessed for signs of porphyrin around the eyes and nose, weight loss, coat condition, and hunched posture	4 : if normal 3: if good but lack of weight gain 2: fairly good 1. if secretions around eyes/nose 0: if poor (*max 4*)
Maximum score		**33**

Table 2-2 The 33 point neurological score

Limb function, motility and general condition were assessed using a battery of 11 tests originally developed by Hunter et al., (2000) and subsequently modified by McGill (2005).

Figure 2-3 The adhesive label test for the evaluation of forepaw function

An adhesive label was placed on the distal-radial region of each wrist then the rat was returned to the home cage. The latency to contact and latency to remove each label was recorded to determine whether the rat showed bias for the affected or unaffected forelimb

2.4 Tissue preparation

In rats that received CTb injections (into the forelimb motor cortex or MLF), the brain was cut into 100μm coronal sections with a freezing microtome (Leitz, Wetzlar) for histological examination of the injection site. Spinal segments containing anterogradely labelled terminals (and FG injection sites and retrogradely labelled cells) were firstly notched in the right ventral lateral white matter (to aid orientation post-sectioning), then cut into 60μm thick transverse sections using a Vibratome (Leica VT10005, Leica Microsystems, UK). All cut sections were then immediately placed in 50% ethanol (EtOH) for 30 min to enhance antibody penetration. Surplus sections were stored in glycerol (-20°C) and remaining whole blocks of tissue were stored in liquid nitrogen (-210°C). Formulae for common laboratory reagents used throughout this project are provided in **Appendix 1**.

2.5 Identification of brain injection sites and CTb-labelled terminals

Brain injection sites (in the forelimb motor cortex and MLF) and the axon terminals labelled by anterograde transport of CTb were revealed using the chromogen 3, 3'-diaminobenzidine (DAB; Sigma-Aldrich, UK). Brain sections and cervical spinal cord sections were incubated in goat anti-CTb (List Quadratech, USA: 1:50,000) for 48 h followed by 3 x 10 min rinses in phosphate buffered saline (PBS). They were then placed in biotinylated anti-goat immunoglobulin (IgG, Jackson Immunoresearch, USA; 1:500) for 3 h. After additional rinsing, the sections were incubated in avidin-horseradish peroxidase for 1 h (Sigma-Aldrich, UK; 1:1000). All antibodies were diluted with 0.3% Triton X-100 (Sigma-Aldrich, UK) in phosphate buffered saline (PBST). Finally, hydrogen peroxide (H_2O_2) plus DAB was applied for 10 min to reveal immunoreactivity at the injection sites as a brown product. Sections were mounted onto gelatinised slides and stored overnight in formalin vapour. After dehydration in distilled water, 70% EtOH, 90% EtOH and 100% EtOH and clearing in Histoclear (National Diagnostics, USA), the sections were cover-slipped using a mounting medium (Histomount, National Diagnostics, USA). Sections were viewed with transmission light microscopy and digitally photographed with an AxioCam camera (Carl ZEISS, Inc., Germany) using

AxioVision 4.8 software (Carl ZEISS, Inc., Germany). The injection site was then determined using a stereotaxic rat brain atlas (Paxinos & Watson, 2005). The segmental and laminar location of anterogradely labelled terminals was examined by superimposing the photomicrographs onto cervical segmental templates (from Paxinos & Watson, 2005) using Adobe Photoshop 7.0 (1990-2000). Representative photomicrographs are shown in **Figure 2-4.**

2.6 Identification of spinal injection sites and FG-labelled cells

Following spinal segment sectioning (**section 2.5**), FG injection sites and retrogradely labelled LDPNs and intrasegmental CINs could be directly visualised under a fluorescent microscope (ultra violet filter, excitation, 323 nm; emission, 408 nm) without any additional processing. Briefly, sections were washed with PBS (3 x 10 min) then mounted onto glass slides and coverslipped with a glycerol based anti-fade medium (Vectashield: Vector Laboratories, Burlingame, CA, USA). Sections were digitally photographed (AxioCam camera with AxioVision 4.8 software) using an ultraviolet filter and in dark field. The photomicrographs were then superimposed onto spinal templates (taken from Paxinos & Watson, 2005) using Adobe Photoshop in order to examine the segmental location of the injection site as well as the laminar distribution pattern of the retrogradely labelled cells.
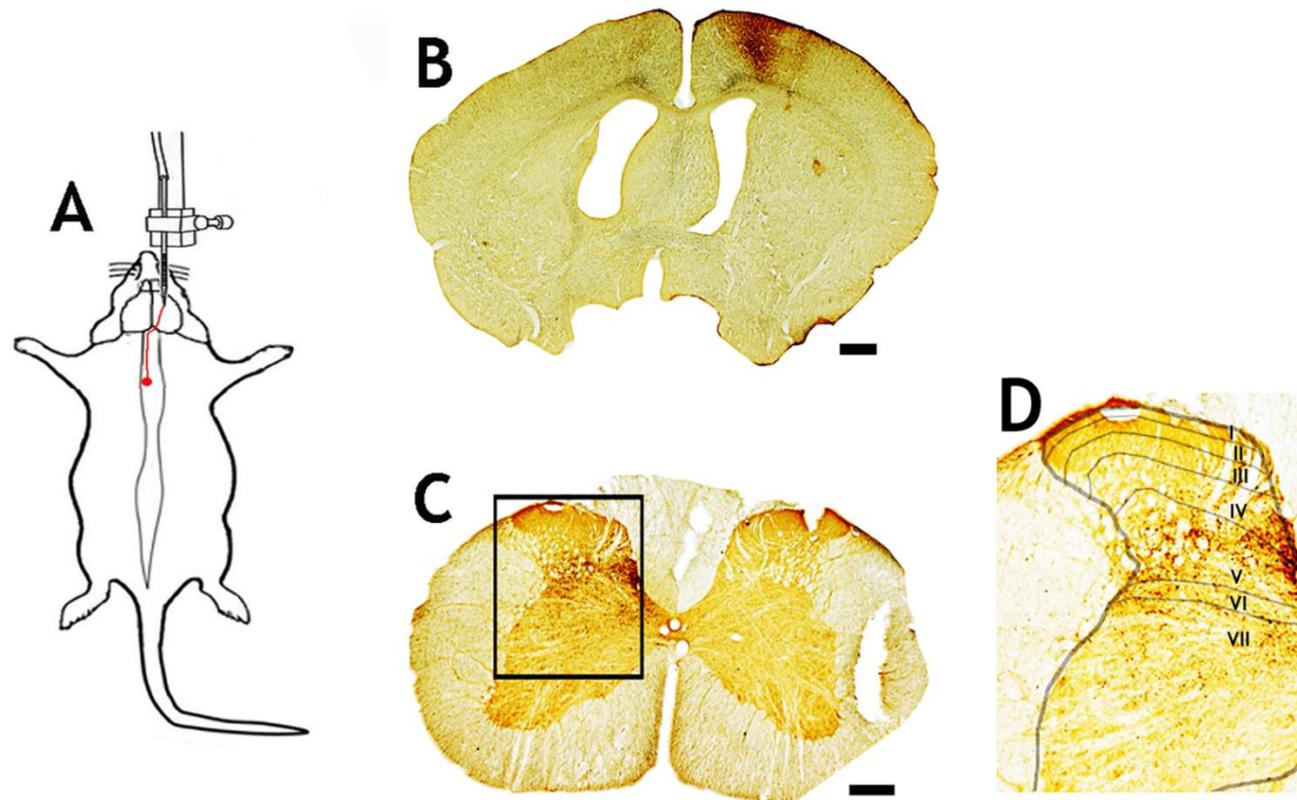
Figure 2-4 Anterograde labelling of terminals in the cervical spinal cord.

In this example, CST terminals in the cervical spinal cord were anterogradely labelled by injecting CTb into the right forelimb motor cortex (**A**). The injection site in the brain (**B**) and the anterogradely labelled terminals in the cervical spinal cord (**C**) were revealed with a DAB reaction. Photomicrographs of spinal sections were superimposed onto cervical maps (obtained from the stereotaxic atlas of Paxinos & Watson, 2005) in order to determine the location of CTb-immunoreactive terminals relative to the various laminae of Rexed (Molander et al., 1989; **D**). In this example, most CTb-immunoreactive terminals were found in laminae IV to VI. **D** is a magnified view of the box outlined in **C**. Scale bar in **B** = 1,000µm; scale bar in **C** = 450µm.

2.7 Multiple immunolabelling of terminals and cells for confocal microscopy

In order to examine the relationship between labelled axonal terminals and specific spinal interneuron populations, cervical sections were processed for confocal microscopy. Immunocytochemistry (ICC) allowed multiple antigens to be detected within a single spinal cord section. The indirect ICC method, which contains two principal steps (**Figure 2-5**), was employed:

1. Sections were incubated with a cocktail of primary antibodies, each with a selective affinity for a target antigen e.g. transporter, neurotransmitter or enzyme. Each primary antibody was derived from a different species.

2. Sections were then incubated with secondary antibodies raised against the primary host species, with each secondary reagent recognising one of those species exclusively. The secondary antibodies were conjugated to fluorophores that emit light at different wavelengths, thus allowing the simultaneous visualisation of multiple antigens within the same section.

The specificity of any given antibody is demonstrated by a negative control e.g. the absence of immunoreactivity in regions of the CNS known not to contain neurons that transport the tracer. For a positive control, the antibody is tested on neurons known to contain the target antigen. Information pertaining to the specificity and application of the primary antibodies utilised in this project (according to supplier product information) is shown in **Appendix 2**.

All ICC experiments in this project followed the same general protocol. Firstly, continuously agitated sections were incubated with the primary antibodies for 72 hr then incubated for 24 hr in secondary antibodies. A secondary antibody was generally an IgG raised in donkey against the IgG belonging to the species of the paired primary antibody. All antibody combinations were diluted with PBST and sections were washed in PBS (3 x 10mins) after each incubation. With notches appropriately aligned, sections were mounted onto glass slides and coverslipped with a glycerol based anti-fade medium (Vectashield: Vector Laboratories, Burlingame, CA, USA).
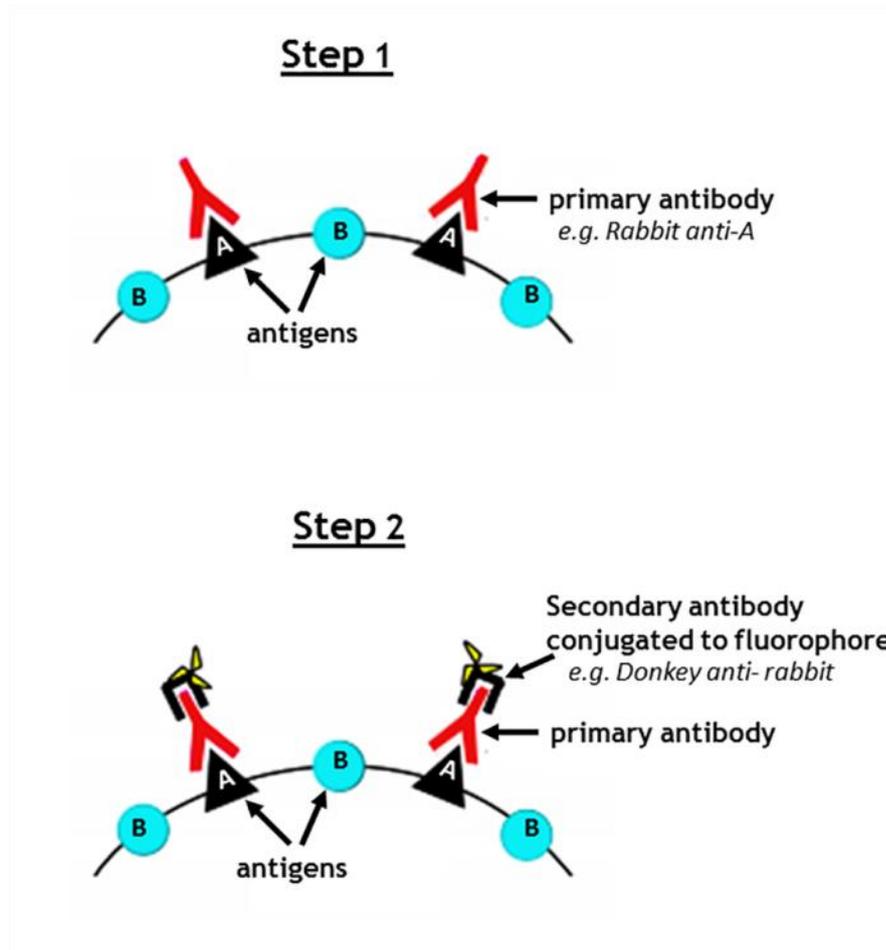
Figure 2-5 The indirect immunocytochemistry (ICC) method

An unconjugated primary antibody binds to a specific antigen and the primary antibody is revealed by a fluorophore-conjugated secondary antibody specific to the IgG of the species providing the primary antibody.

2.8 Confocal microscopy, reconstructions and analyses

Immunoreactive sections containing labelled cells and terminals were scanned with a three-colour channel laser confocal microscope (Radiance 2100, Biorad, UK). Systematic low power scans (x20, zoom factor of 1) were initially performed to assess the laminar location of neurons and to identify neurons with labelled terminals within their vicinity. Selected neurons were then scanned at x40 oil immersion with a zoom factor of 2 at 0.5µm increments (unless otherwise indicated in subsequent chapters). **Table 2-3** shows the excitation-emission wavelengths of the different conjugated fluorophores used in this project.

Neurons were reconstructed three dimensionally using Neurolucida 9.14.3 software (MBF Bioscience, MicroBrightField, Inc.). Firstly, the cell body and dendritic processes were drawn, and then contacts were plotted using a specific marker for each type of contact. Contacts were defined as being in close apposition to neuronal processes in the same focal plane with no intervening black pixels. For a given cell the total dendritic surface area (μm^2) was recorded directly from Neurolucida 9.14.3 software (MBF Bioscience – MicroBrightField, Inc.). The surface area of the soma was calculated by firstly measuring the perimeter from the projected confocal image using ImageJ software (National Institutes of Health, USA) then calculating the surface area of an equivalent sphere (radius (μm) = perimeter/(2π) and surface area (μm^2) = $4\pi r^2$). Data are expressed as the total number of contacts per unit area of neuronal surface ($100\mu m^2$).

Fluorophore	Excitation(λ)	Emission(λ)
Rhodamine-red	543	591
Alexa-Fluor 488	488	517
Dylight 649	652	670

Table 2-3 Excitation-emission wavelengths of the fluorophores used in this project

2.9 Statistical analysis

A common problem identified in scientific literature is "pseudoreplication" which involves taking multiple observations per individual subject and treating each observation as an independent data point (Lazic, 2010). Pseudoreplication should be carefully avoided because it artificially inflates the sample size which falsely raises the statistical power and devalues the conclusions drawn about a specific population. Therefore, in experiments where multiple observations were taken per rat, all of the observations for an individual rat were averaged. For example, in the adhesive label test each rat received 4 trials on a given day (see **section 2.3.2**) and these 4 data points were averaged so that each rat only contributed one value to the analysis.

Statistically analysed data are presented graphically using Graphpad Prism statistical software (Graphpad Software, Inc. version 5, USA). Data from all experiments are expressed as mean ± standard deviation (SD). The following symbols were used to indicate varying levels of significance:

Symbol	Significance level
*	$p < 0.05$
**	$P < 0.01$
***	$P < 0.001$
****	$P < 0.0001$

Prior to applying statistical analysis, raw data were visually inspected in a frequency histogram to assess for normal (bell shaped) distribution. Supplementary to the graphical assessment of normality the Shapiro-Wilk test was applied, which compares the actual data to a normally distributed data set with the same mean and standard deviation. The null hypothesis is that the sampled data are from a normally distributed population, thus if the test was significant ($p<0.05$) the distribution was assumed to be non-normal and a nonparametric test was applied e.g. Mann-Whitney or Kruskal-Wallis. Otherwise data were analysed using parametric t-tests and analysis of variance (ANOVA). Accompanying *post hoc* tests are described in the corresponding chapters.

Chapter 3

Establishing a suitable experimental stroke model: assessment of final infarct and sensorimotor outcome following transient MCAo

3.1 Introduction

Mimicking all of the characteristics of human stroke using a single animal model is not possible as ischaemic stroke is a highly complex and heterogeneous disorder. The strengths and weaknesses of the available stroke models must therefore be considered in relation to the research question. Ideally, an appropriate model should adhere to the following criteria: 1) the surgical technique for the induction of ischaemia should be minimally invasive; 2) the ischaemic process should be relevant to human stroke; 3) the size and distribution of the infarct should be reproducible; 4) the model should replicate the anatomical, physiological or functional features of stroke most pertinent to the research question (Durukan & Tatlisumak, 2007; Carmichael, 2005). The current project is concerned with the neuroanatomical correlates of sensorimotor function after stroke. As such, the animal model should exhibit ischaemic damage in the motor system and measurable sensorimotor deficits.

For this project, the intraluminal filament model (Koizumi et al., 1986), which involves blocking the ostium of the MCA with a bulbed monofilament (see **Figure 2-1**), was selected. Unlike other available rodent stroke models (Tamura et al., 1981; Robinson et al., 1990; Frost et al., 2006), the intraluminal filament model enables the occlusion of the MCA without the use of a craniectomy. This is advantageous given that a craniectomy is invasive and does not mimic human stroke very closely. The major advantage of this model however, is that the filament can be withdrawn at any time to permit restoration of blood flow. Stroke models allowing for transient vessel occlusion are preferable given that human stroke generally involves a degree of reperfusion, either spontaneously or following thrombolysis therapy using recombinant tissue plasminogen activator (Carmichael, 2005).

Using the intraluminal filament model to block the origin of the MCA in the rat produces infarcts in two general vascular territories: the deep lenticulostriate arteries (involving the basal ganglia and internal capsule) and the superficial branches (involving the lateral surface of the cortex and underlying white matter) (Uluç et al., 2011). A similar pattern occurs in humans, whereby depending on the occlusion site, MCA territory infarcts can be superficial, deep or both (Geyer & Gomez, 2009; see Chapter 1 **section 1.4.1**). In rats, the

intraluminal filament model induces contralateral limb deficits which have been well characterised using an array of behavioural tests. Examples of contralateral limb deficits include impaired reaching and grasping of food pellets, impaired detection and removal of adhesive labels placed on the forepaw, reduced grip strength and increased fore- and hindlimb faults during grid walking (reviewed by Kleim et al., 2007 and Hunter et al., 1998). Furthermore, in rats, the intraluminal filament model has been shown to induce axonal damage in the internal capsule (Valeriani et al., 2000). This is of particular relevance to the current project, given that the aim is to model the sensorimotor dysfunction of human stroke, which has been correlated with corticofugal axonal injury at the level of the internal capsule (Schiemanck et al., 2007; Puig et al., 2010). Targeted destruction of the internal capsule in rats leads to contralateral limb deficits such as impaired reaching and grasping (Kim et al., 2014), suggesting that the internal capsule of the rat serves a similar function to that of humans. Taken together, MCAo via the intraluminal filament method can be used to model the pathophysiological and functional aspects of human stroke.

With the intraluminal filament model, consistent ischaemic infarcts have been reported following arterial occlusion times ranging from 20 min to 2 h (reviewed by Liu et al., 2009). However, there are various confounders that can limit the reproducibility of this model. For instance, subtle changes in filament insertion length (Zarow et al., 1999), bulb diameter (Abraham et al., 2002), temperature (Busto et al., 1987; Noor et al., 2003) and surgical technique (Chen et al., 2008; Tsuchiya et al., 2003) can significantly alter the degree of ischaemic injury. It was therefore important to conduct a pilot study to ensure an optimal setting for the induction of reproducible infarcts. A 60 min occlusion time was selected and depending on success rate, mortality rate and outcome variation, this occlusion period could be altered for future experiments if necessary. Based on previous reports, it was anticipated that MCAo for 60 min using the intraluminal filament model would produce infarcts encompassing the striatum and lateral cortex (Memezawa et al., 1992; Modo et al., 2000; Gharbawie et al., 2008).

As well as infarct reproducibility, it was important to ensure that the experimental stroke model induced detectable sensorimotor deficits. Therefore, the sensorimotor outcome of MCAo for 60 min was examined using a neurological

scoring system and the adhesive label test. As described previously (Chapter 2 **section 2.3**), a neurological score provides a global sensorimotor assessment and the adhesive label test can be used to detect forelimb use asymmetries. Based on previous reports, (Modo et al., 2000; Gharbawie et al., 2008), it was anticipated that MCAo for 60 min would be sufficient for the induction of sensorimotor deficits.

Study aims:

- To determine the degree of tissue loss in the brain at 7 days following 60 min MCAo and to characterise the anatomical distribution of tissue loss throughout the MCA territory

- To characterise sensorimotor function over 7 days following 60 min MCAo

Hypothesis

MCAo for 60 min will result in reproducible infarcts and impairments in both neurological score and the adhesive label test

3.2 Methods

3.2.1 Experimental design

Eight adult male Sprague-Dawley rats (250-300g) were used in this study. A timeline of the experimental design is shown in **Figure 3-1**. All rats underwent left MCAo for 60 min. Behavioural testing was conducted before MCAo (day -1) and post-MCAo for 7 days to examine sensorimotor outcome. Rats were perfused with fixative on post-MCAo day 7 for histological examination of tissue loss in the brain.

3.2.2 Induction of transient focal cerebral ischaemia

Anaesthesia was induced in a chamber with 5% isoflurane delivered in O_2 and N_2O (30%: 70%. See Chapter 2, **section 2.2.1**). The rat was then intubated for mechanical ventilation and the MCA was occluded as described in Chapter 2, **section 2.2.2**. Briefly, the left common carotid artery was exposed from the

bifurcation to the base of the skull. Following an arteriotomy in the common carotid artery, a 3-0 monofilament with a bulbed tip (~0.3mm diameter) was advanced along the lumen of the internal carotid artery until it blocked the origin of the MCA (~22mm). The filament was withdrawn after 60min to allow for reperfusion. Anaesthesia was withdrawn and rats were transferred to recovery cages and health status was monitored throughout the survival period.

3.2.3 Sensorimotor testing

Rats were assessed prior to MCAo surgery (day -1) and at 1, 2, 3, 5 and 7 days post-MCAo using a battery of 10 tests to provide an overall neurological score (maximum score of 33 indicates normal neurological function, see Chapter 2 **section 2.3.1**). The adhesive label test (detailed in Chapter 2 **section 2.3.2**), which measures latency to contact and remove an adhesive label from the ventral surface of each forepaw, was also performed prior to MCAo (day -1) and at days 1, 2 3 and 7 post-MCAo. Each rat received 4 trials on a given day and these 4 data points were averaged so that each rat contributed only one value to the statistical analysis (see Chapter 2 **section 2.9**).
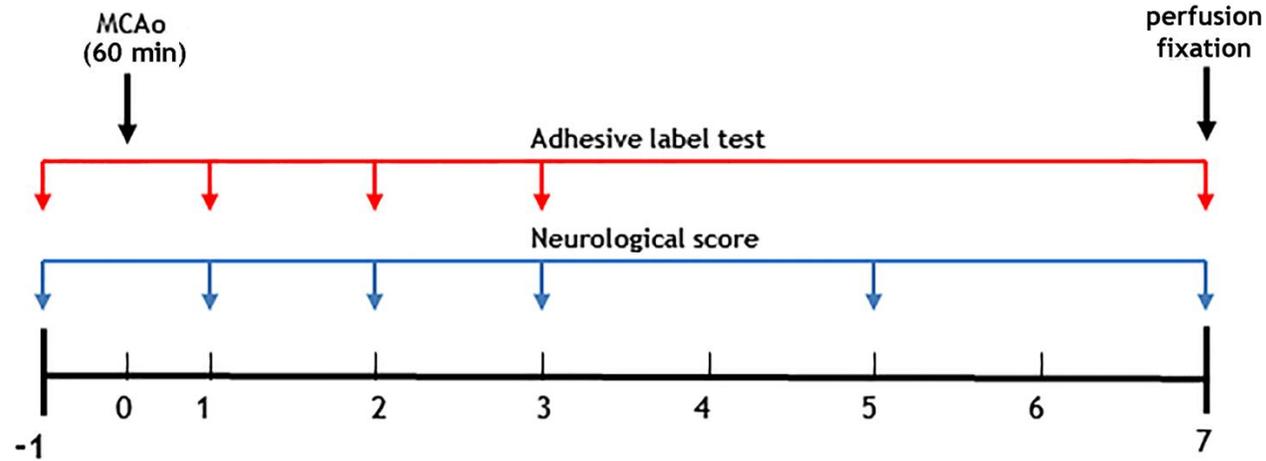
Figure 3-1 Timeline of experimental procedures

All rats underwent MCAo for 60 min (day 0). Neurological scoring was performed prior to surgery (day -1) and on post-MCAo days 1, 2, 3, 5 and 7. The adhesive label test was performed prior to MCAo (day -1) and on post-MCAo days 1, 2, 3 and 7. Rats were perfused with fixative on post-MCAo day 7 for histological examination of tissue loss in the brain.

3.2.4 Assessment of final infarct

For this pilot study, final infarcts were assessed using haematoxylin and eosin (H&E) staining. Following transcardial perfusion fixation (see Chapter 2 **section 2.2.5**) at day 7 post-MCAo, the brain was processed and embedded in paraffin wax in an automatic processor (Miles Scientific, see **Appendix 3** for the paraffin processing steps). The embedded brain was then cut into 6µm thick sections using a microtome (Leica RM2135) and mounted onto poly-L-lysine glass slides. Brain sections from eight pre-determined coronal levels of the forebrain (described by Osborne et al., 1987) were stained with H&E (**Appendix 4**). Briefly, sections were immersed in a series of graded alcohols followed by haematoxylin (Surgipath, UK) staining. Then sections were washed, differentiated in acid alcohol, and dehydrated before eosin (Surgipath, UK) staining. Further dehydration was followed by immersion in histoclear prior to mounting the slides using DPX mounting medium (Raymond Lamb Laboratory supplies, Thermo Scientific, USA).

Infarcted tissue exhibits characteristic changes in cellular morphology and neuropil such that it can be clearly distinguished from normal non-infarcted tissue using H&E staining (detailed by Garcia et al., 1993). At 3-7 days following ischaemia, the injured region adopts a homogeneously pale appearance that can be delineated (**Figure 3-2A**). When viewed under high magnification (x20) the pallor area exhibits early cavitation due to the reabsorption of necrotic debris by macrophages. See **Figures 3-2B & C** for a comparison of normal versus infarcted tissue, respectively. For each of the eight sections, a tiled photomicrograph was obtained (x10 magnification, Image-Pro, MediaCybernetics, USA). For a given section, ImageJ was used to directly delineate the contralesional hemisphere and the intact ipsilesional hemisphere (minus the region of pallor) and the area of each delineated region was calculated. The total volume of each hemisphere was determined by plotting areas against the known stereotaxic location of each section relative to Bregma (+3.24mm to 6.36mm) and calculating the area under the curve. To correct for any shrinkage that may have resulted from tissue dehydration and processing, the following equation was applied (based on Swanson et al., 1990):

Corrected lesion volume	=	Volume of contralesional hemisphere	-	Volume of intact ipsilesional hemisphere

The resultant value was expressed as a percentage of the contralesional hemisphere to show the extent of tissue loss. To examine the location and distribution of the infarct throughout the rostrocaudal extent of the MCA territory, the pallor region on each section was superimposed onto a coronal brain template (taken from Paxinos and Watson, 2005) of the corresponding stereotaxic level (Adobe Photoshop).

3.2.5 Statistical analysis

For all results shown in this chapter, statistical analysis is based on the number of animals (not the number of behavioural trials) in order to avoid pseudoreplication (see Chapter 2 **section 2.9**). In accordance with the Shapiro-Wilk normality test, behavioural data were analysed using repeated measures (RM) 1-way analysis of variance (ANOVA) with day as the independent variable and neurological score or contact/removal difference as the dependent variable. The Dunnett's *post hoc* test was applied to compare data at each post-MCAo time point with day -1 (pre- MCAo) to assess for behavioural deficits. Each post-MCAo time point was also compared with the post-MCAo day 1 to assess for recovery. Pearson's correlation was used to examine associations between tissue loss and behavioural outcome. Data are expressed as means ± SD and differences are considered significant at $p < 0.05$.
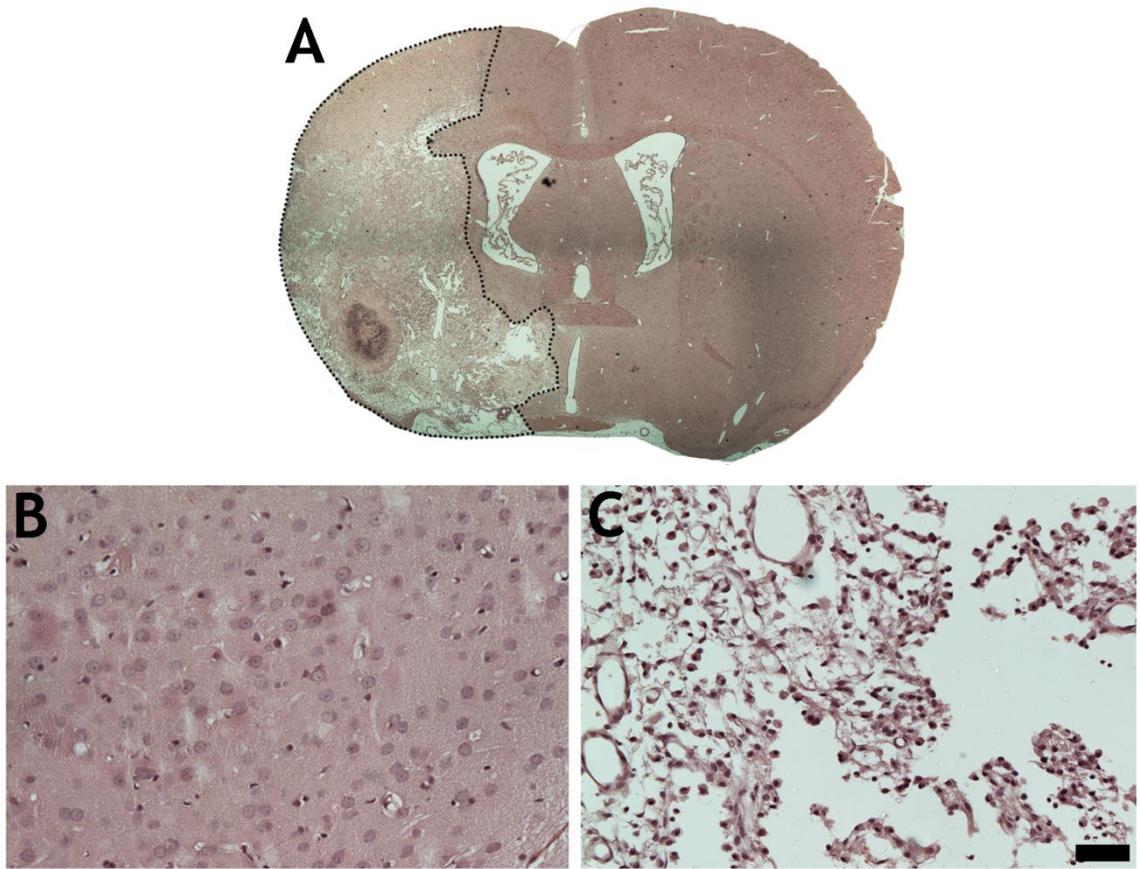
Figure 3-2 H&E defined infarct at 7 days following 60 min MCAo

A: A light microscope (x10) image of an H&E stained section displaying the boundary between infarcted (area of pallor outline by dotted line) and non-infarcted tissue. **B**: A high power (x20) image of healthy non-infarcted tissue where neuronal cell bodies are pale stained and round. **C**: Image depicting infarcted tissue. Note neuronal loss and the appearance of early cavitation (scale bar = 100µm)

3.3 Results

3.3.1 Excluded animals and data

One, out of the eight animals used in this study died at 24 hours following MCAo surgery and assessment of the brain revealed signs of cerebral haemorrhage. Data for this rat were excluded from statistical analysis. All other animals began feeding within 48 hours and survived for the 7 day duration of the study.

3.3.2 Ischaemic damage in the brain

Total tissue loss was 18.9 ± 12.5% (ranging from 8.6 to 37.4%). With a coefficient of variation of 66%, total tissue loss was very variable between rats. Two rats exhibited very large infarcts encompassing both cortical and subcortical structures; whereas 5 rats exhibited smaller infarcts confined to subcortical structures (**Figure 3-3**). In the 2 rats with cortical damage, tissue loss was mainly in lateral cortical structures. The primary and secondary motor cortices along with the fore- and hindlimb regions of the primary sensory cortex were mainly spared, apart from a small degree of tissue loss within the rostral aspects of these structures. Irrespective of cortical involvement, all 7 rats exhibited tissue loss within large portions of the striatum. Tissue loss within the ventral location of the internal capsule was also apparent in all rats. Examples of H&E stained sections showing tissue loss relative to the location of the internal capsule, from the rat with the largest infarct and rat with the smallest infarct are shown in **Figures 3-4A** and **3-4B**, respectively.

Figure 3-5 shows area of tissue loss across the 8 coronal sections for all rats. A similar pattern of tissue loss was observed for all animals, whereby the sections with the highest degree of tissue loss were within end artery MCA territory (between 1.68 and -2.40 mm, relative to Bregma) and the sections with the lowest degree of tissue loss were within rostro-caudal regions that receive more collateral supply.
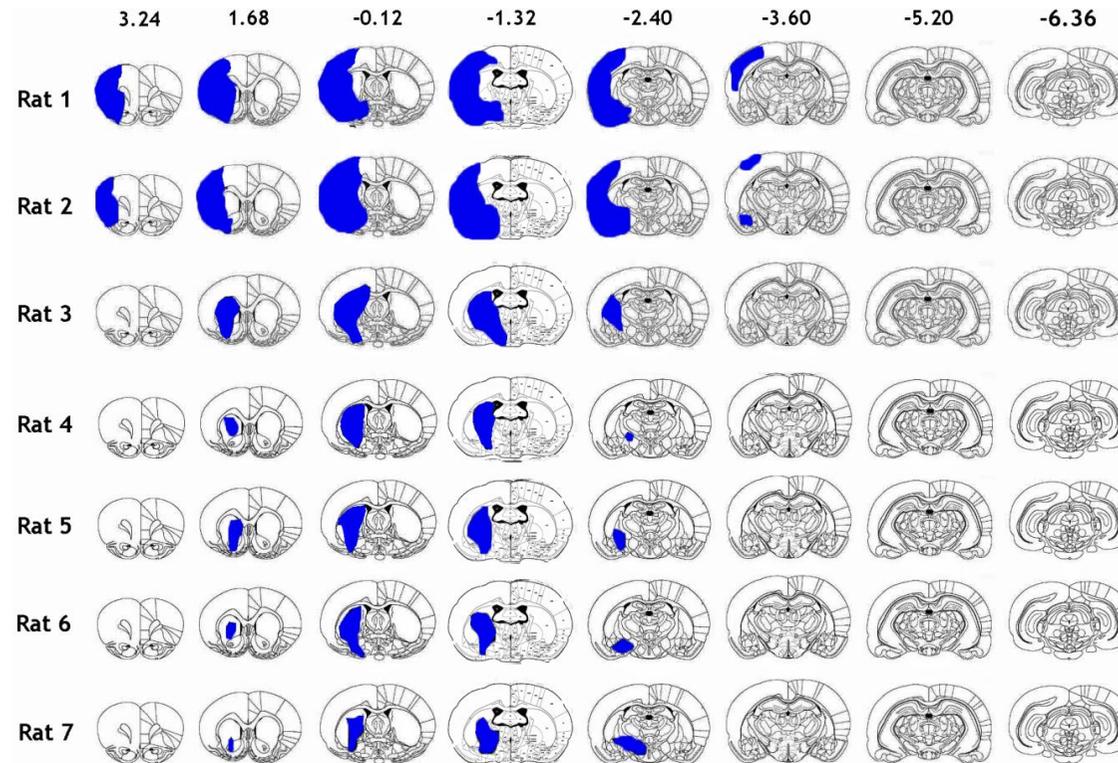
Figure 3-3 Tissue loss across the territory of the MCA at 7 days following 60 min MCAo

For each rat, the infarct (blue) is shown over eight coronal levels, with the distance from Bregma (mm) defined at each level. Two rats exhibited large infarcts that encompassed both cortical and subcortical structures whereas 5 rats exhibited infarcts confined to subcortical structures, mainly the striatum. Reconstructions were obtained by delineating infarcted areas onto line diagrams (Paxinos and Watson, 2005) from light microscope images (x10) of H&E stained sections.
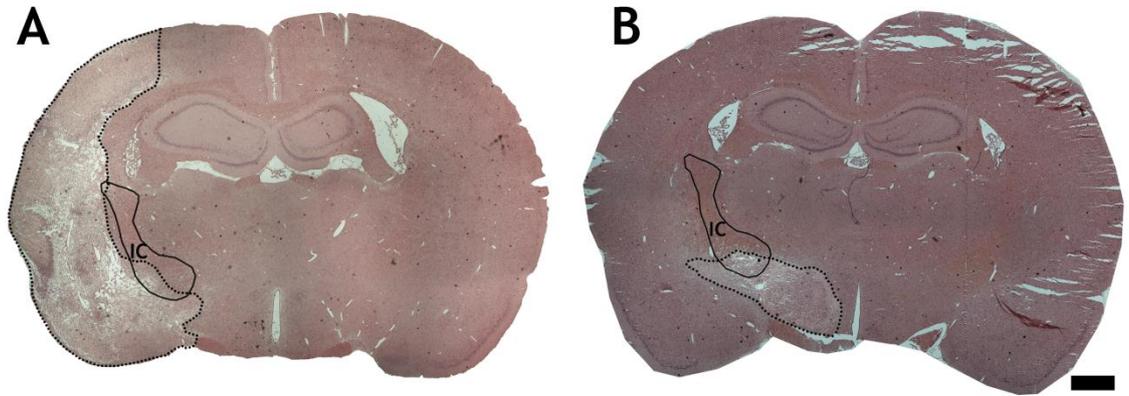
Figure 3-4 Tissue loss relative to the location of the internal capsule

Low power (10x) light microscope images of H&E stained sections (-2.40mm from Bregma) from the rat with the largest infarct (**A**) and rat with the smallest infarct (**B**). The approximate anatomical location (taken from the atlas of Paxinos & Watson, 2005) of the internal capsule (IC) is shown. Note that for both rats, the infarct (area of pallor outlined by dotted line) appears to impinge upon the ventral location of the IC. Scale bar = 1000µm
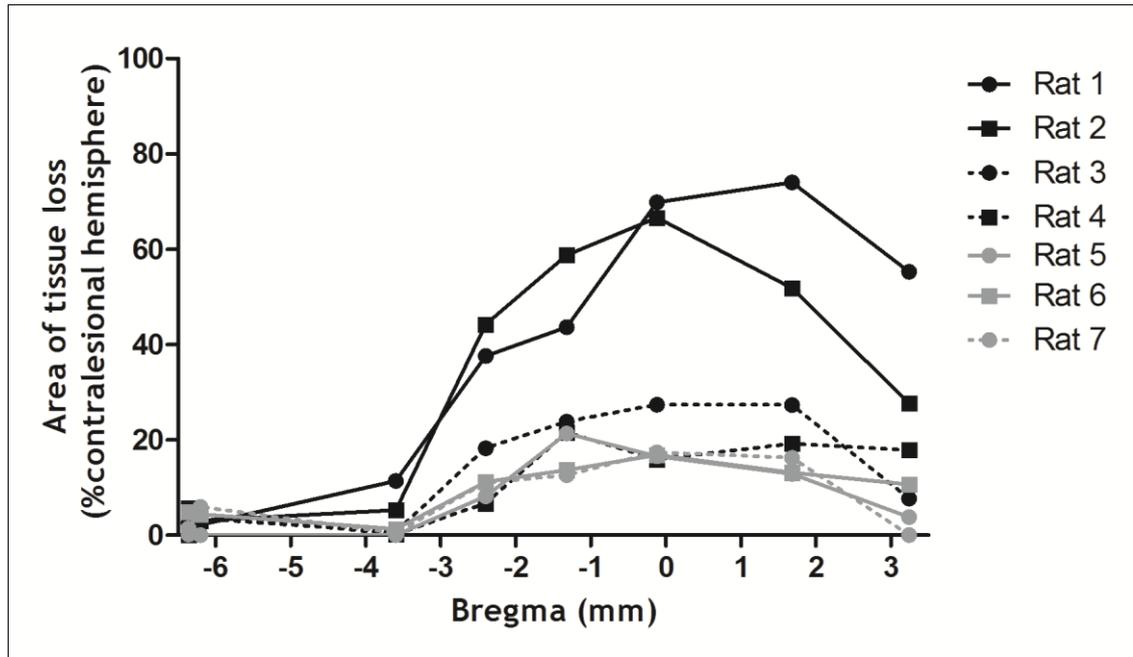
Figure 3-5 Distribution of tissue loss at 7 days following 60 min MCAo

Tissue loss is shown for 8 stereotaxic coordinates relative to the location of Bregma (mm) for each rat. Although the extent of tissue loss varied between rats, each rat exhibited a similar pattern of damage, whereby regions within end artery MCA territory (from 1.68 to -2.40 mm) showed the highest degree of tissue loss.

3.3.3 Sensorimotor outcome

Figure 3-6A shows the mean neurological scores. A RM 1 way ANOVA revealed a significant effect of day on score (p<0.0001) and *post hoc* comparisons revealed that the mean score for each post-MCAo day (days 1 to 7) was significantly reduced compared to the mean score achieved prior to MCAo (day -1). Although the deficit in score lasted 7 days, the mean score at post-MCAo day 7 was significantly higher than that of post-MCAo day 1, suggestive of a degree of recovery. Individual scores for all seven rats are shown in **Figure 3-6B.** All rats received the maximum score of 33 before MCAo (day -1), indicative of normal neurological function. MCAo resulted in a marked reduction in score in all rats, followed by a gradual improvement. Despite the gradual improvement, none of the rats reached baseline score by day 7, suggestive of a persistent deficit. **Table 3-1** shows the number of rats that exhibited impairments in each of the 11 subtests, across different time points. Note that all 7 rats were impaired in the paw placement, horizontal bar, visual forepaw reaching and grip strength tests and that the rats were still impaired in these tests by day 7. All 7 rats were also impaired in the rotation, motility and general condition tests, but for some animals these impairments were absent by day 7. The inclined platform and circling tests were less susceptible to MCAo impairments, with 5 and 3 rats exhibiting deficits, respectively. Righting reflex was unaffected by MCAo and only 1 rat exhibited a contralateral reflex after MCAo which resolved after a day.
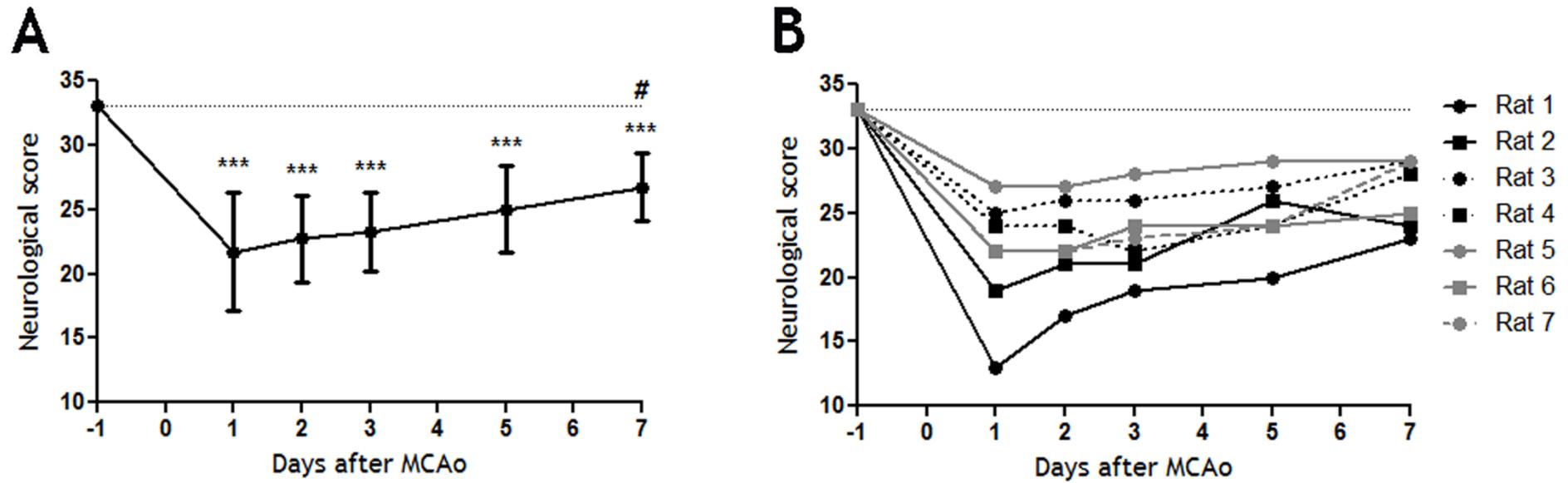
Figure 3-6 Effect of 60 min MCAo on neurological score over 7 days

A: A RM 1 way ANOVA revealed a significant effect of day on score ($F_{(5, 30)} = 28.14$, $p<0.0001$). *Post hoc* comparisons using the Dunnett's test indicated that neurological score was significantly reduced at post-MCAo days 1, 2, 3, 5 and 7 compared to the pre-MCAo score (day -1). The score at day 7 was significantly higher than the initial deficit on day 1, thereby indicating a degree of recovery. Data represent mean ± SD. **B:** Individual scores for all 7 rats. Prior to MCAo (day -1) all rats received the maximum score of 33, after which, all scores were reduced. Although a gradual improvement was observed over time, none of the rats had returned to baseline score by day 7. The dotted horizontal line indicates the maximum score of 33, which denotes normal neurological function.

*** $p<0.001$ versus day -1; # $p<0.001$ versus day 1.

	No. of rats with impairments					
	Day -1	Day 1	Day 2	Day 3	Day 5	Day 7
Paw placement	0	7	7	7	7	7
Righting reflex	0	0	0	0	0	0
Horizontal bar	0	7	7	7	7	7
Inclined platform	0	5	5	5	4	2
Rotation	0	7	7	3	3	3
Visual fore-paw reaching	0	7	7	7	7	6
Contralateral reflex	0	1	0	0	0	0
Circling	0	3	3	3	2	2
Grip strength	0	7	7	7	7	7
Motility	0	7	4	3	1	1
General condition	0	7	3	4	1	1

Table 3-1 No. of rats with impairments in each of the 11 subtests of the neurological score

All rats were impaired in the paw placement, horizontal bar, visual forepaw-reaching and grip strength tests, and the deficit tended to persist for 7 days. Deficits in the inclined platform, rotation, circling, motility tests were also apparent for some rats, with performance tending to improve over the 7 days. Righting reflex and contralateral reflex were not affected by MCAo.

For the adhesive label test, when the rats were placed in the observation cage at postoperative days 1 and 2, they exhibited freezing behaviour. Three of the rats in particular did not move position for the entire duration of each trial (3 min). Five rats exhibited porphyrin around the eyes, which is consistent with stress. To prevent such freezing behaviour from confounding the experimental data, contact/removal latencies for days 1 and 2 were not analysed. No evidence of freezing was observed from postoperative day 3 onwards.

The mean differences in contact time between the affected and unaffected paws are shown in **Figure 3-7A**. A RM 1 way ANOVA revealed a significant effect of day on contact difference time (p = 0.005) and *post hoc* comparisons revealed that contact difference time was significantly increased at post-MCAo day 3 but not at post-MCAo day 7. This is indicative of a bias for detecting stimuli on the unaffected paw that resolved after 7 days. **Figure 3-7B** shows the mean contact difference times for each individual rat (out of the 4 trials for each day). Following MCAo, all 7 rats exhibited an increased contact difference time that was then lessened by day 7. However, 2 rats exhibited much higher contact difference times than the other 5 rats at post-MCAo days 3 and 7. There was also a significant effect of day on removal difference time (p<0.0001; **Figure 3-7C**), and *post hoc* comparisons revealed that removal difference time was significantly increased at post-MCAo days 3 and 7. This indicates a bias for removing stimuli from the unaffected paw that persisted for 7 days. **Figure 3-7D** shows the mean removal difference times for each individual rat. Following MCAo, all 7 rats exhibited an increased removal difference time that was then lessened by day 7. However, 2 rats exhibited much higher removal difference times than the other 5 rats at both post-MCAo days 3 and 7. Although the removal difference time was lessened by day 7, there was still a marked deficit at this time point, with none of the rats reaching baseline performance.
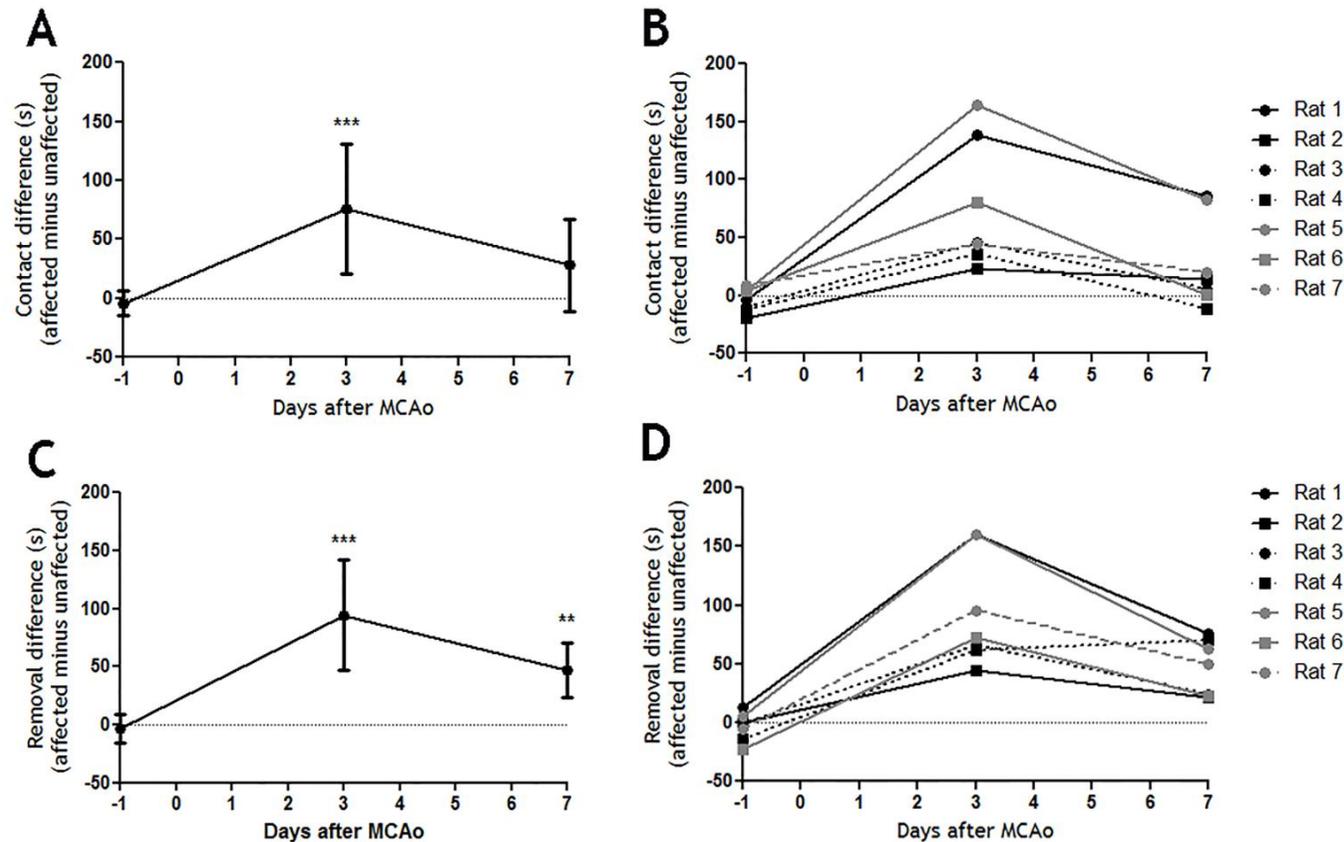
Figure 3-7 Effect of 60 min MCAo on contact (and removal) difference times over 7 days

A: A RM 1 way ANOVA revealed a significant effect of day on contact difference time ($F_{(2, 20)}$ = 14.61, p= 0.0006). Compared to day -1 (pre-MCAo), the contact difference time was significantly increased at post-MCAo day 3 but not 7 (Dunnett's *post hoc* test). Data represent mean ± SD **B:** The mean contact difference times for all 7 rats. Note that 2 rats exhibited particularly high contact difference times at both post-MCAo days 3 and 7. **C:** There was a significant effect of day on removal difference time ($F_{(2, 20)}$ = 25.08, p< 0.0001). Compared to day -1 (pre-MCAo), the removal difference time was significantly increased at post-MCAo days 3 and 7. **D:** The mean removal difference times for all 7 rats. Note that 2 rats exhibited particularly high removal difference times and that all rats still exhibited asymmetries at post-MCAo day 7. The dotted horizontal line indicates zero, which denotes symmetrical limb contact (and removal) latencies.

*** p< 0.001 versus day 0. **p<0.01 versus day 0.

Pearson's correlation was performed for post-MCAo days 3 and 7 in order to explore associations between total tissue loss and sensorimotor function. There was an inverse correlation between total tissue loss and neurological score i.e. as tissue loss increased, neurological score decreased. This trend was strong but non-significant for post-MCAo day 3 (r = -0.75; p = 0.053; **Figure 3-8A**) and significant for post-MCAo day 7 (r = -0.78; p = 0.04; **Figure 3-8B**). There was no correlation between contact difference time and total tissue loss on post-MCAo day 3 (r = -0.04; p>0.05; **Figure 3-8C**) or post-MCAo day 7 (r = 0.26; p>0.05; **Figure 3-8D**). Similarly, there was no correlation between removal difference time and total tissue loss on post-MCAo day 3 (r = 0.02; p>0.05; **Figure 3-8E**) or post-MCAo day 7 (r = 0.07; p>0.05; **Figure 3-8F**).
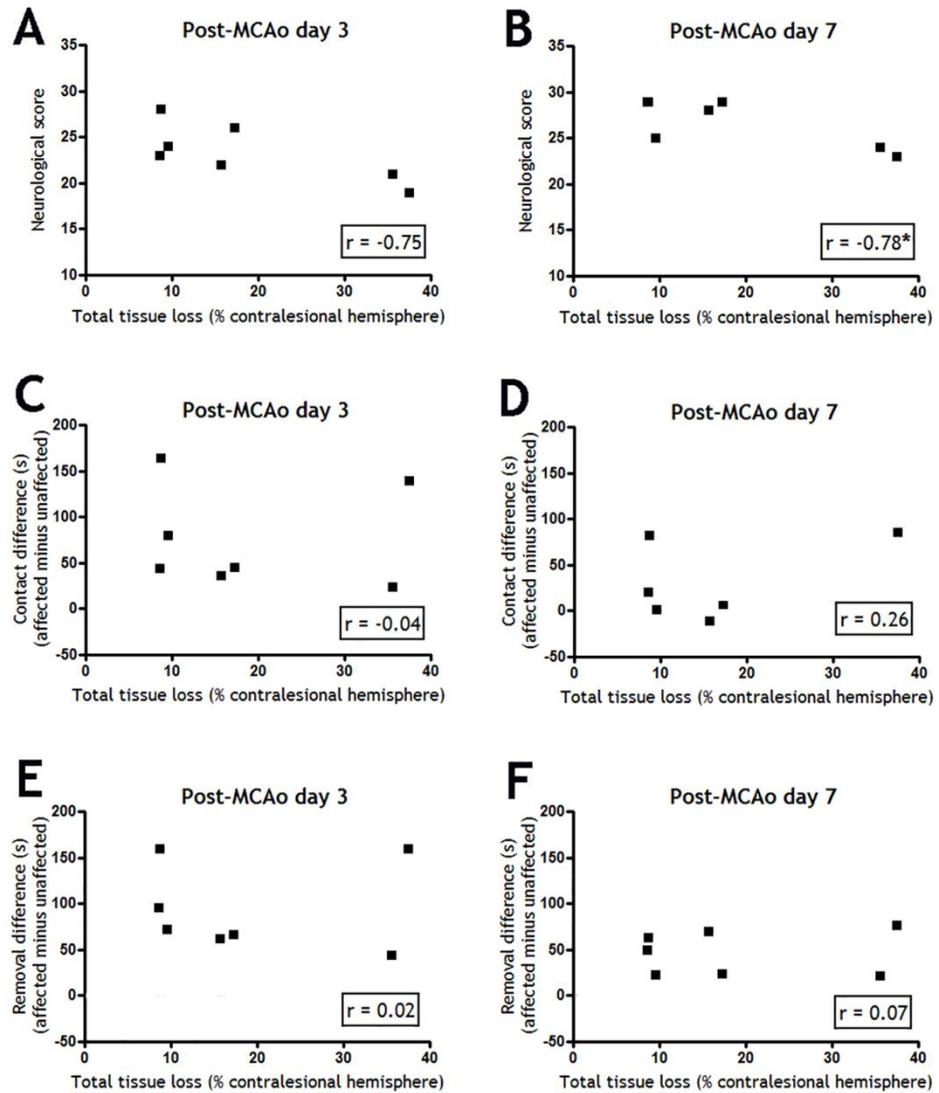
Figure 3-8 Associations between tissue loss and sensorimotor outcome after 60 min MCAo

There was an inverse correlation between total tissue loss and neurological score on post-MCAo days 3 (**A**) and 7 (**B**). There was no obvious trend between contact difference time and total tissue loss on post-MCAo days 3 (**C**) and 7 (**D**). Similarly, there was no obvious trend between removal difference time and total tissue loss on post-MCAo days 3 (**E**) and 7 (**F**). Pearson's correlation.

*p<0.05

3.4 Discussion

This pilot study has yielded two important results in the selection of an appropriate stroke model for subsequent studies in this thesis: 1) MCAo for 60 min using the intraluminal filament model produced lesions that encompassed subcortical regions alone, or cortical plus subcortical regions; 2) MCAo for 60 min induced impairments in neurological score and the adhesive label test that persisted for 7 days.

Ischaemic damage in the brain

Reproducibility of experimentally induced ischaemic injury is crucial for the utility of any animal stroke model. Following 60 min MCAo all rats exhibited tissue loss in subcortical brain regions, particularly the striatum and internal capsule. Cortical damage was less frequent however, with only 2 out of 7 rats exhibiting tissue loss within lateral cortical structures. This is in agreement with a study performed by Gharbawie et al., (2008) who reported that following 60 min MCAo, all rats exhibited infarcts in subcortical structures, with the infarct encroaching into lateral cortical structures in some of the more severe cases. The unpredictable cortical involvement is likely due to Heubner anastomoses in the cortex having the ability to compensate for reductions in blood flow, unlike striatal tissue which is supplied by end arteries (Carmichael, 2005). In the current study, the primary and sensory motor cortices along with the fore- and hindlimb regions of the primary sensory cortex were spared, apart from in the 2 rats with the largest lesions that exhibited a small degree of damage within the rostral portions of these structures. Predominant sparing of these structures following 60 min MCAo was also reported by Gharbawie et al., (2008). Interestingly, using intracortical microstimulation to elicit forelimb movements, Gharbawie and colleagues (2008) demonstrated a diminished forelimb map in the ipsilesional hemisphere of rats subjected to 60 min MCAo, even when the lesions were very small and subcortical. Thus, MCAo for 60 min disrupts pathways between the motor cortex and limb motor neurons, even when the motor cortex is not directly encompassed within the infarct. An animal stroke model that predominantly disrupts subcortical structures reflects the clinical situation well, given that most human strokes involve subcortical infarcts, while cortical infarcts account for less than 15% of the total number of cases (Bogousslavsky

et al., 1988; Kang et al., 2003; Wessels et al., 2006). Furthermore, (see Chapter 1 **section 1.4.1**), axonal damage in the internal capsule plays a key role in motor outcome in human stroke (Schiemanck et al., 2007; Puig et al., 2010; Pendlebury et al., 1999) and there appeared to be tissue loss within the internal capsule in rats following 60 min MCAo in the current study.

Sensorimotor outcome

MCAo for 60 min resulted in a marked reduction in neurological score that persistent for 7 days. Although a deficit in neurological score was still present at post-MCAo day 7, the mean score was significantly higher than that of the initial deficit at post-MCAo day 1, thereby indicating a degree of recovery. Such results are in agreement with Hunter et al., (2000) who employed a 21 point neurological score comprised of the same subtests used in the current study (except for grip strength), and reported a significant reduction in neurological score followed by partial recovery over 7 days after transient (90 min) MCAo. Modo et al., (2000) also demonstrated a reduction in neurological score after 60 min MCAo using a slightly different scoring system. On examining the results for each separate subtest, it appeared that the partial recovery observed at day 7 was mainly due to improvements in the inclined platform, rotation, circling, motility and general condition. Impairments in the forelimb placing, horizontal bar, visual- forepaw reaching and grip strength tests were still apparent at day 7. This suggests that 60 min MCAo produced persistent forelimb deficits. The partial recovery in some of the tests at this acute time point is likely attributed to the resolution of tissue oedema and the cessation of inflammation (Wieloch & Nikolich, 2006).

In the adhesive label test, following 60 min MCAo, rats were impaired at contacting and removing labels attached to the affected (contralesional) forepaw, and the contact deficit recovered by post-MCAo day 7 while the removal deficit persisted. Following transient MCAo (90 min), Hunter et al. (2000) also reported impairments in contacting/removing labels attached to the affected forepaw that partially recovered over 7 days. Similar results were obtained by Modo et al., (2000) who noted that, following 60 min MCAo, rats were impaired in removing labels attached to the affected forepaw and although this deficit lessened over time, it was still present 12 weeks later. Unlike

neurological score which was inversely correlated with total tissue loss, there was no relationship between the extent of the contact/removal asymmetry and total tissue loss in the current study. Intriguingly, the rat with the smallest contact/removal asymmetry exhibited an extensive lesion affecting both cortical and subcortical structures whereas the rat with the largest contact/removal asymmetry exhibited a small lesion confined to subcortical structures. This result contradicts reports from Wegener et al., (2005) who found that following 60 min MCAo, rats were only deficient in the adhesive label test if they exhibited infarcts encompassing both cortical and subcortical structures; whereas if rats exhibited infarcts confined to subcortical structures they performed no differently to sham-operated rats. A possible explanation for this discrepancy is that the subcortical infarcts reported by Wegener and collegues appear to be within the lateral striatal region, whereas the subcortical infarcts in the current study were more medial, potentially affecting axons of the internal capsule to a greater extent. The fact that use of a similar ischaemic duration and MCAo approach may lead to several different lesion types with varying sensorimotor outcomes highlights the impact of variables such as surgical technique, physiological parameters, housing environment and test conditions on the stroke model in the individual laboratory. It also emphasises the importance of performing pilot studies to establish the optical parameters for any new study (Liu et al., 2009). Finally, Virley et al., (2000) demonstrated a close correlation between impairments in the adhesive label test and pathological changes in the striatum, parietal cortex and forelimb motor cortex following transient (90 min) MCAo as depicted by fMRI, suggesting that damage to a range of brain regions can contribute to the functional impairments in this task.

To summarise, MCAo for 60 min resulted in a 100% lesion success rate, a low mortality rate and tissue loss affecting either subcortical regions alone, or cortical plus subcortical regions. Despite variation in the extent of tissue loss between rats, all rats exhibited tissue loss within portions of the striatum and there also appeared to be tissue loss relative to the location of the internal capsule. Moreover, all rats exhibited impairments in neurological score and the adhesive label test. Based on such findings, MCAo for 60 min via the intraluminal filament model was selected in order to examine the neuroanatomical correlates of sensorimotor motor function after stroke (Chapter 4).

Chapter 4

Quantification of corticospinal tract terminals originating from the non-ischaemic hemisphere at 28 days following transient MCAo

4.1 Introduction

In Chapter 3, MCAo for 60 min was found to induce a measurable sensorimotor deficit that partially recovered over 7 days. The recovery detected at this early stage is attributed to the resolution of oedema, reperfusion of the ischaemic penumbra and cessation of inflammation (Wieloch & Nikolich, 2006). Any recovery occurring beyond the first week is thought to involve reorganisation of networks that have been spared by the infarct. These reorganisation processes are poorly understood but may involve 1) the unmasking/strengthening of existing but functionally weak pathways 2) sprouting of fibres from surviving neurons to form new synaptic connections 3) redundancy of pathways to allow for alternative circuits to take over function (Nudo, 2006).

There is great interest in the possibility that the motor cortex of the non-ischaemic hemisphere is involved in control of the spontaneously recovered (ipsilateral) limb after stroke. Evidence for this comes from imaging studies of stroke survivors showing that movement of the affected hand elicits abnormally enhanced activity in the motor cortex of the non-ischaemic hemisphere (Grefkes & Fink, 2011; Ward & Frackwiak, 2006; Rehme et al., 2011; Chollet et al., 1999; Grefkes et al., 2008; see Chapter 1 **section 1.4.3** for more detail).

According to anatomical tracing studies performed in rodents, the non-ischaemic hemisphere may gain control of the affected limb through rewiring of its CST projections at the level of the spinal cord. After permanent MCAo (Liu et al., 2007; Liu et al., 2008), destruction of the primary motor cortex (Bachman et al., 2014; LaPash Daniels et al., 2009; Ueno et al.,2012) and unilateral pyramidotomy (Brus-Ramer et al., 2007; Maier et al., 2008), CST axons originating from the uninjured hemisphere sprout into the denervated (ipsilateral) side of the spinal cord. Moreover, therapies that increase the extent of CST sprouting from the non-ischaemic hemisphere have been shown to enhance sensorimotor recovery (Soleman et al., 2012; Liu et al., 2007; Liu et al., 2008; Zai et al., 2009; Chen et al., 2002; Lee et al., 2004; Lindau et al., 2014; see Chapter 1 **section 1.4.3**).

Despite the above reports of fibre sprouting, it is yet to be confirmed whether the CST from the non-ischaemic hemisphere establishes new axonal terminals in

the denervated (ipsilateral) side of the spinal cord in association with recovery from stroke. Although increased staining of the synaptic-specific protein synaptophysin in the spinal cord after permanent MCAo is indicative of the formation of new terminals (Liu et al., 2007; Liu et al., 2013), the extent to which the CST from the non-ischaemic hemisphere contributes to terminal remodelling remains unclear. Hence, the goal of the current study was to characterise the termination patterns of the CST arising from the non-ischaemic hemisphere in the cervical spinal cord following MCAo. Specifically, the objective was to determine whether the number of CST terminals in the denervated (ipsilateral) side of the spinal cord changed in association with sensorimotor recovery.

To test for terminal remodelling, CST axonal terminals arising from the non-ischaemic hemisphere were anterogradely labelled using CTb at 28 days after MCAo. Although biotinylated dextran amine (BDA) is more commonly used to trace the CST system, CTb is transported much faster and it has been shown to label terminal structures more robustly (Hagg et al., 2005). Terminals were examined at 28 days post-MCAo because previous studies of experimental stroke have reported CST axonal sprouting (Liu et al., 2007; LaPash Daniels et al., 2009; Bachman et al., 2014) and increased synaptophysin staining (Liu et al., 2007; Liu et al., 2013) in the denervated side of the spinal cord at this stage. A model of transient (60 min) MCAo was selected because human stroke typically involves a degree of reperfusion (Carmichael, 2005). Furthermore, as established in Chapter 3, MCAo for 60 min predominantly disrupts subcortical structures and this reflects the clinical situation well given that the large majority of human strokes are subcortical (Bogousslavsky et al., 1988; Kang et al., 2003; Wessels et al., 2006). Sensorimotor testing was employed to explore associations between CST terminal remodelling and functional outcome.

Study aims:

- To characterise the laminar termination pattern of the CST originating from the non-ischaemic hemisphere in the cervical spinal cord at 28 days following 60 min MCAo or sham surgery

- To quantify CST terminals originating from the non-ischaemic hemisphere in the cervical spinal cord at 28 days following 60 min MCAo or sham surgery

<u>Hypothesis</u>

Rats subjected to 60 min MCAo will exhibit an increased number of labelled CST terminals in the denervated (ipsilateral) side of the spinal cord compared with sham operated rats, and the number of terminals will be correlated with the degree of spontaneous sensorimotor recovery

4.2 Methods

4.2.1 Power Calculation

For ethical and economic reasons, it is important to use the minimum number of animals necessary to achieve scientific goals – but not so few as to miss biologically important effects (Festing & Altman, 2002). The current study is concerned with the neuroanatomical correlates of sensorimotor function after MCAo. A power analysis calculator (http://www.graphpad.com/scientific-software/statmate) was used to determine the minimum group sizes necessary to detect a significant reduction in neurological score in MCAo rats (versus sham rats). The means and SDs were estimated based on data obtained in Chapter 3 (neurological scores at post- MCAo day 7; **Figure 3-6**). It was assumed that sham-occlusion surgery would not alter baseline measures of neurological score. To detect a mean difference in neurological score of 7 with a significance of 0.05 and a power of 0.8, a total of 6 rats per group would be required assuming a SD of 3.5. Therefore, 12 male Sprague-Dawley rats (250-300g) were used in this experiment, where 6 rats underwent MCAo and 6 rats underwent sham-occlusion surgery.

4.2.2 Experimental design

A timeline of the experimental design is shown in **Figure 4-1**. Six rats underwent left MCAo for 60 min and 6 rats underwent sham occlusion surgery. Sensorimotor testing was conducted prior to surgery (day-1) and after surgery for 28 days for the assessment of functional deficit and recovery. A T_2 weighted MRI scan was

performed at post-MCAo day 7 for assessment of the infarct in the brain. At day 28, all rats received a stereotaxic CTb injection into the right forelimb motor cortex for the visualisation of axonal terminals arising from this region. At day 32 (4 days post-CTb injection), rats were perfused with fixative for the examination of CTb-labelled terminals in the cervical spinal cord. All image analysis and terminal counting was performed with the experimenter blinded to the identity of the rat.

4.2.3 Induction of transient focal cerebral ischaemia

Anaesthesia was induced in a chamber with 5% isoflurane delivered in O_2 and N_2O (30%: 70%. See Chapter 2 **section 2.2.1**). The rat was then intubated for mechanical ventilation and the MCAo was performed as described in Chapter 2, **section 2.2.2**. Following exposure of the left common carotid artery bifurcation, a filament with a bulbed tip was advanced along the lumen of the internal carotid artery until it blocked the origin of the MCA. The filament was withdrawn after 60 min to allow for tissue reperfusion. Sham operated rats underwent the same procedures with the exception of the insertion and advancement of the filament. Animals were transferred to recovery cages and health status was closely monitored throughout the survival period.

4.2.4 Sensorimotor testing

Neurological scoring was performed on the day prior to MCAo/sham surgery (day -1) and on postoperative days 1, 2, 3, 7, 14, 21 and 28 (as described in Chapter 2 **section 2.3.1**). The adhesive label test (detailed in Chapter 2 **section 2.3.2**) was also performed prior to MCAo/sham surgery (day -1) and postoperatively on days 3, 7, 14, 21 and 28. Each rat received 4 trials on a given day and these 4 data points were averaged so that each rat contributed only one value to the statistical analysis (see Chapter 2 **section 2.9**).
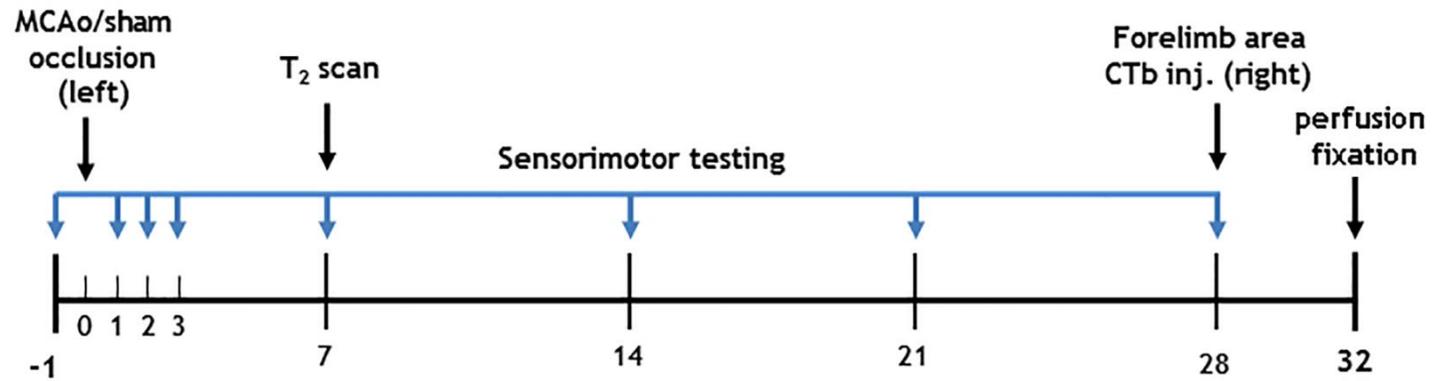
Figure 4-1 Timeline of experimental procedures

Rats underwent left MCAo for 60 min or sham occlusion surgery (day 0). Sensorimotor testing was conducted at days -1, 1, 2, 3, 7, 14, 21, and 28. A T_2 weighted MRI scan was performed at day 7 to examine infarcted tissue in the brain. At day 28, terminals originating from the right forelimb motor cortex were anterogradely labelled with CTb. Rats were perfused with fixative on day 32 for examination of the labelled terminals.

4.2.5 Assessment of final infarct

MRI RARE T_2 weighted imaging was used to determine the anatomical distribution and size of the infarct. After induction of anaesthesia (**section 2.2.1**), the animal was transferred to a Bruker Biospin Avance 7T (300 MHz) MRI scanner with a gradient coil (121 mmID, 400mT/m) and a 72 mm birdcage resonator. The head was secured in place using ear and incisor bars and a linear surface receiver coil was placed onto the head. Anaesthesia was maintained via face mask (2-3% isoflurane in O_2 and N_2O, 30%:70%). A 4-channel phased array surface receiver coil was placed on the head and a RARE T_2 weighted sequence was acquired (TE=72.7ms, TR=5086.1ms, matrix=256x256, 16 coronal slices; 0.75mm thick). The rat was then allowed to breathe 100% O_2 until it regained the foot-pinch withdrawal reflex before being placed in a recovery cage. Final infarct was defined as the hyperintense areas on the T_2 weighted images (see **Figure 4-4**). These areas were manually delineated on each of the 16 T_2 slices spanning the territory of the MCA using ImageJ software (National Institutes of Health, USA). The infarct volume was calculated by multiplying the total area across the 16 slices by the slice thickness (0.75mm).

4.2.6 Anterograde labelling of CST terminals originating from the non-ischaemic hemisphere

At 28 days post-MCAo/sham surgery, all rats received a stereotaxic injection of CTb into the forelimb motor cortex of the non-ischaemic (right) hemisphere, (see Chapter 2, **section 2.2.3**). Briefly, following induction of anaesthesia (Chapter 2 **section 2.2.1**), the 2 burr holes were made in the skull and a micropipette containing 1% CTb was inserted into the brain at 4 standardised points. At each point, 200nl of CTb was injected using a Pico Injector (World Precision Instruments, USA). See **Table 2.1** for the stereotaxic coordinates used for targeting the right forelimb motor cortex. The scalp was sutured and health status of the animal was monitored until termination.

4.2.7 Tissue preparation

Four days following CTb injection (32 days after MCAo/sham surgery), rats were transcardially perfused with fixative (as described in Chapter 2 **section 2.2.5**). The brain and spinal cord were removed and post-fixed over night at 4°C. To

cryoprotect the brain, sucrose was added to the fixative (3g/10ml). The brain was then sectioned coronally (100μm) with a freezing microtome and segments C3-C8 of the cervical spinal cord were cut into transverse sections (60μm) with a Vibratome. All cut sections were immediately placed in 50% EtOH (30 min) to enhance antibody penetration.

4.2.8 Identification of cortical CTb injection sites

CTb injection sites in the cortex of the non-ischaemic hemisphere were revealed using DAB as a chromagen (see Chapter 2 **section 2.5**). Brain sections were incubated in goat anti-CTb for (48 h), and then biotinylated anti-goat IgG (3 h) followed by avidin-horseradish peroxidase (1 h). Finally H_2O_2 plus DAB was applied (10 min) for visualisation of CTb immunoreactivity. Sections were viewed under transmission light microscopy and digitally photographed (x5; Axiovision software). To confirm the anatomical location, injection sites were reconstructed onto coronal maps taken from a stereotaxic atlas (Paxinos & Watson, 2005) using Adobe Photoshop.

4.2.9 Assessment of CST axonal loss from the ischaemic hemisphere

To test whether MCAo led to the loss of CST axons originating from the ischaemic hemisphere, the intensity of protein kinase C gamma (PKC-γ) immunoreactivity in the dorsal columns was measured. PKC-γ is an important intracellular signalling kinase found in a specific subset of excitatory interneurons in lamina II and in axons of the dorsal CST (Mori et al., 1990). It has therefore been employed as a marker of CST axonal loss following pyramidotomy and stroke (Tan et al., 2012; Lindau et al., 2014; Bradbury et al., 2002). For each rat, PKC-γ immunoreactivity was examined in 2 transverse sections from segment C8 of the cervical spinal cord. Sections were incubated with anti- PKC-γ for 72 h (**Table 4.1**) followed by donkey anti-rabbit Alexa 488 secondary antibody (24 h). They were then rinsed in PBS (3 x 10 min) and mounted with anti-fade (Vectashield). The dorsal columns were imaged using a BioRad radiance 2100 confocal microscope at x20 magnification (zoom factor of 0.9 at 0.5μm intervals), whereby the entire thickness of the section was scanned. PKC-γ labelling intensity was then measured on the projected confocal microscope

image using ImageJ software. The software detected the brightness intensity of each pixel in a selected "region of interest" (ROI). A value of 0 indicated "no" brightness in pixels measured (i.e. black), and a value of 255 indicated the maximum brightness value the software could measure (i.e. white). As shown in **Figure 4-2**, the unaffected (left) side was delineated and the mean brightness intensity calculated. The image was then flipped horizontally so the same ROI could be applied to the affected (right) side. The absolute values of brightness intensity were subsequently expressed as a ratio of the affected (right) side versus unaffected (left) side to control for variation in immunolabelling between sections and animals. A value of 1 indicated no difference in PKC-γ immunoreactivity between the affected and unaffected side. For every rat, brightness intensity ratio was averaged (out of the 2 sections) so that each rat contributed only one value to the statistical analysis (see Chapter 2 **section 2.9**).
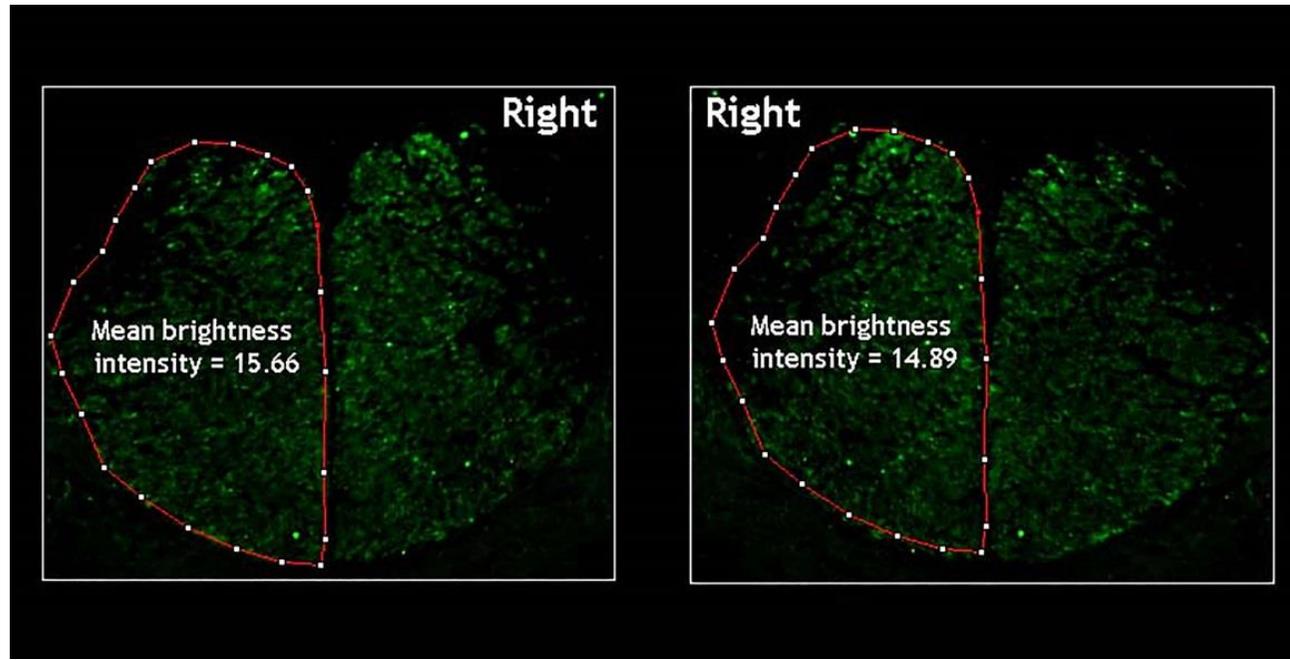
Figure 4-2 Method for measuring PKC-γ immunoreactivity in the dorsal columns

On the projected confocal microscope image, the unaffected (left) side was delineated (red) and the mean brightness intensity calculated. The image was then flipped horizontally to measure the mean brightness intensity of the affected (right) side. A ratio of affected (right) side/ unaffected (left) side was used to express the degree of symmetry of PKC-γ immunoreactivity. In this particular example the brightness intensity ratio was 0.95. Image taken from a randomly selected sham occluded rat.

4.2.10 Examination of VGLUT-1 immunoreactivity in CTb-labelled axonal swellings

CST axonal terminals are enriched with VGLUT-1 (Du Beau et al., 2012) therefore co-expression of VGLUT-1 and CTb was used to verify that CTb-labelled axonal swellings in the spinal cord were terminals. Three sham and three MCAo rats were randomly selected. Sections (3-4 per rat) from cervical segment C4 were incubated with anti- CTb and anti-VGLUT-1 (72 h) followed by secondary antibodies coupled to Alexa 488 and Dylight 649, respectively (24 h; **Table 4-1**). They were then rinsed in PBS (3 x 10 min) and mounted with anti-fade (Vectashield). Using confocal microscopy (BioRad radiance 2100), fields containing CTb-labelled terminals were scanned using a x40 oil-immersion lens (zoom factor of 2 at 0.5µm intervals). For each section 4 fields were obtained: 3 fields from the unaffected (left) side (contralateral to the injection site) encompassing the medial dorsal horn and medial intermediate grey matter, which is where previous studies have reported the majority of CST terminals to be distributed (Gribnau & Dederen, 1989; Liang, 1991; Du Beau et al., 2012); and 1 field from the affected (right) side (ipsilateral to the injection site) encompassing the intermediate grey matter which is where uncrossed CST axons have been reported to terminate (Brösamle & Schwab, 1997). Using Neurolucida software, stacks were initially viewed in a grid (10 x10 µm^2) so that only CTb-immunoreactivity (green channel) was visible. For each square, a CTb-labelled terminal closest to the bottom right corner was marked, and then the marked terminals were examined in the blue channel to assess for co-expression of VGLUT-1. The percentage of double-labelled CTb terminals as a proportion of the total number of CTb terminals was calculated for each rat.

4.2.11 Assessment of the laminar distribution of CTb-labelled terminals in the cervical spinal cord

For each rat, 1 section from segments C3, C5 and C7 was processed for D1AB (Chapter 2 **section 2.6**). A tiled image (x40 magnification) of each section was acquired using Image-Pro software. To make laminar distribution comparisons between rats, the terminals were mapped onto spinal templates (taken from Paxinos & Watson, 2005). This was achieved by thresholding the image so that only the dark coloured pixels (i.e. the DAB positive regions) were visible, then

transposing the dark coloured pixels onto corresponding spinal templates using Adobe Photoshop.

4.2.12   Quantification of CTb-labelled terminals in the cervical spinal cord

For each rat, 3 sections from segments C3, C5 and C7 were processed for DAB (Chapter 2 **section 2.5**) and a tiled image (x40 magnification) of each section was acquired using Image-Pro software. A ROI (0.9mm x 1mm) was then applied to each side of the grey matter. Each ROI was aligned with the ventromedian fissure (the midline) and the base of the grey commissure (as shown in **Figure 4-3A**). This particular area of the grey matter was selected based on previous reports that fibres spontaneously sprout across the midline extending across the dorsal and ventral commissure following stroke and unilateral pyramidotomy (Liu et al., 2008; Maier et al., 2008; Brus-Ramer et al., 2007). An automatic counting technique was employed for calculating the numbers of terminals. Image-pro software allows for the automatic detection of "objects" based on pixel colour variations from the background. DAB-positive terminals appear as dark spots on a light background, so the software was calibrated to recognize dark areas on the image. On a given image, a few representative "objects" (or terminals) were selected and a region of background was defined. Only darkly labelled terminals that were fully in focus were selected (**Figure 4-3B**). Due to the thick vibratome sections images contained terminals that were partially in focus (**Figure 4-3C**); however, such terminals were not quantified because on initial testing the software could not accurately segment them from the background. The software automatically detected and counted all "objects" within the image that had the same colour disparity from the background as the representative "objects". See **Figure 4-3D** for a x40 magnified image of DAB-positive terminals and **Figure 4-3E** for the same terminals detected with the software.

On assessment of the data from the first few sections, a potential source of error was identified: when examining the resultant area (μm^2) for all of the individually detected "objects", the majority were less than 4 μm^2; however, occasionally objects ranging from 5 to 10 μm^2 were detected, which were deemed too large to be single terminals. On visual inspection of the images, this appeared to be attributed to the software counting several clustered or

overlapping terminals (**Figure 4-3F**) as one single dark "object" (**Figure 4-3G**). To resolve this clustering issue, the software was calibrated to detect concavity created by an overlap. The intersection of two overlapping terminals was identified by the presence of two concave points (like a "figure of eight"). Instead of erroneously grouping the terminals as a single "object", the software split the terminals at the point of overlap (i.e. at the narrowest part of the "figure of eight"). In case the software still failed to segment individual terminals, particularly in regions where they were densely distributed (e.g. the medial base of the dorsal horn, see **Figure 4-3A**), the total "object" surface area (mm^2) within each ROI was also calculated.

In the C5 sections for all rats, manual counting was performed specifically within the grey matter immediately surrounding the central canal. This was to assess for any changes that may have been too subtle for the automatic counting software. A 200μm x 300μm ROI was applied to each side of the grey matter, and aligned with the ventromedian fissure and base of the grey commissure, as above. Because of the relatively low density of terminals within this region compared to the dorsal horn, manual counting was deemed feasible. Using ImageJ, a marker was placed on each individual terminal, and then the total number of markers within the ROI was recorded. Again, only dark terminals in full focus were selected.

Initially terminal counts (or CTb-positive surface areas) were compared in sham versus MCAo rats for each side of the cervical spinal cord separately. However, it was important to control for variation in CTb-immunoreactivity between rats that may have occurred due to subtle differences in the CTb injection volume or location. Therefore, terminal counts (or CTb-positive surface areas) were also expressed as ratios: affected/unaffected (ipsilateral to injection/contralateral) and the ratios in sham and MCAo rats were compared. Data were averaged (out of the 3 sections) for each rat so that an individual rat contributed only one value to the statistical analysis (Chapter 2, **section 2.9**).
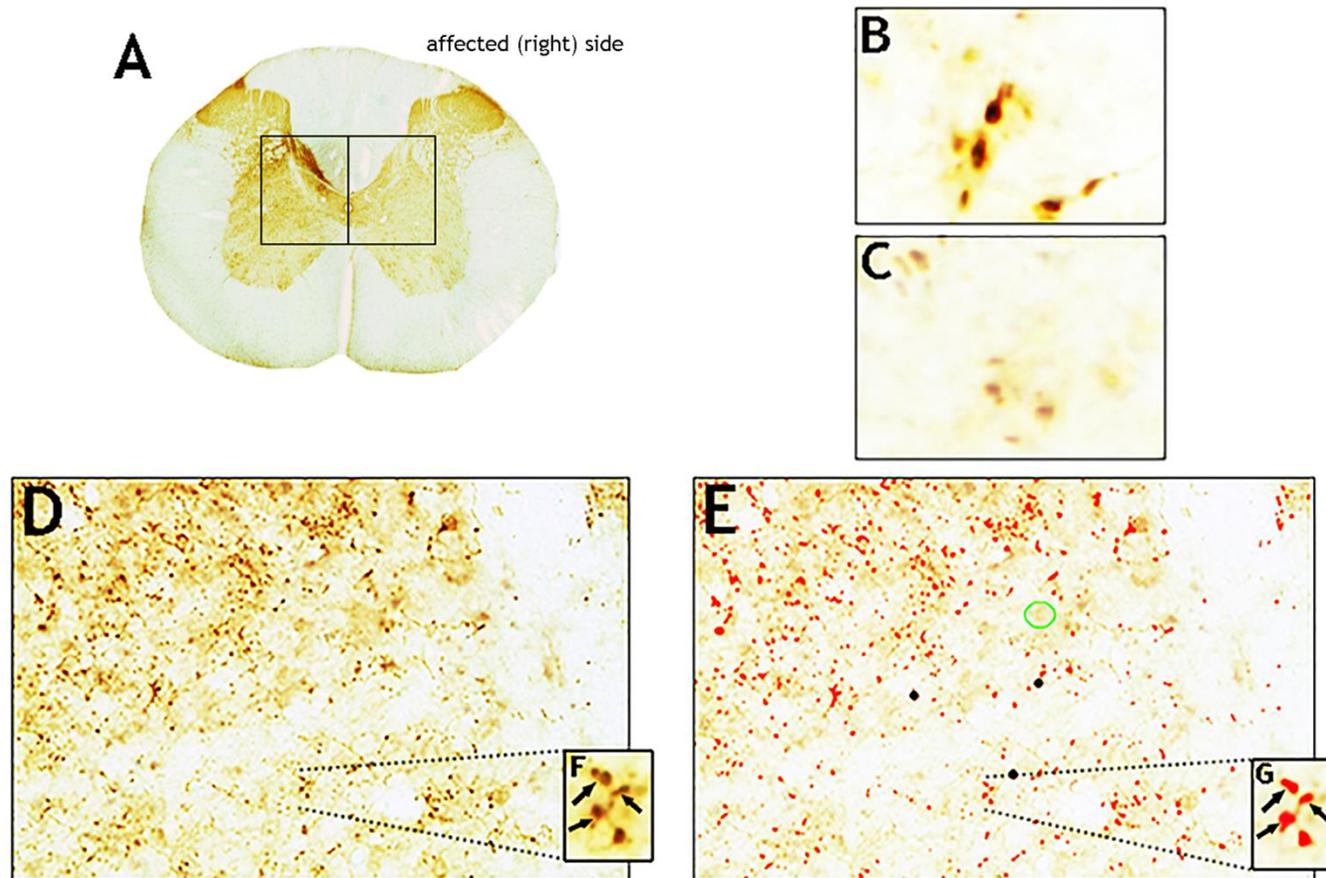
Figure 4-3 Automatic detection of CTb-labelled terminals

A: Photomicrograph showing CTb-immunoreactivity and the ROI (0.9mm x 1mm) on each side of the grey matter. **B:** An example of darkly labelled terminals that were fully in focus. **C:** An example of partially in focus terminals that were not quantified because they could not be segmented from the background by the detection software. A raw image of DAB labelled terminals is shown (**D**) and then the same image is presented whereby the terminals have been automatically detected (**E:** red). This was achieved by selecting a few representative "objects" (or terminals; black markers) and defining a region of background (green circle). In this example 893 "objects" were counted. **F:** Examples of overlapping terminals (arrows). **G:** In this case the software failed to separate single terminals and counted each "cluster" as a single "object."

4.2.13   Statistical analysis

For all results shown in this chapter, statistical analysis is based on the number of animals (not the number of spinal sections or number of behavioural trials) in order to avoid pseudoreplication (see Chapter 2 **section 2.9**). Based on results from the Shapiro-Wilk normality test, all statistical analysis was conducted using parametric statistics. Neurological score and adhesive label test data were analysed by RM 2 way ANOVA with surgery (MCAo or sham) as the independent variable and time and neurological score/contact difference/removal difference as the dependant variables. The Bonferroni's *post hoc* test was applied to compare sham vs MCAo at each time point. Two sample *t* test was used to analyse group differences in PKC-γ immunoreactivity and labelled terminals. Pearson's correlation was used to examine associations between anatomical changes and behavioural outcome. Data are expressed as means ± SD and differences are considered significant at $p < 0.05$.

	Primary antibody combination	Concentration	Supplier	Secondary antibody combination	Concentration	Sequential reaction
1	rb. PKC-γ	1:500	List Biological Laboratories, Campell, CA	Alexa 488	1:500	
2	gt. CTb	1:5000	List Biological Laboratories, Campell, CA	Biotinylated IgG	1:500	Avidin HRP (1:1000) + DAB
3	gp. VGLUT1	1:5000	Millipore, Harlow, UK	Dylight 649	1:500	
	gt. CTb	1:5000	List Biological Laboratories, Campell, CA	Alexa 488	1:500	

Table 4-1 Summary of primary and secondary antibody combinations and concentrations used in the current experiment

1. For the examination of PKC-γ labelling in the dorsal columns (segment C8). **2.** For the visualisation of the CTb injection site in the cortex of the non-ischaemic hemisphere and for the quantification of labelled terminals (segments C3, C5 & C7). **3.** For the assessment of the co-localisation of VGLUT1 and CTb as a marker of CST terminals (segment C4).

rb = rabbit; gt = goat; gp = guinea pig

4.3 Results

4.3.1 Excluded animals and data

One sham rat and two MCAo rats were excluded from all analysis because there were no labelled terminals detected in the spinal cord for these animals. On examination of the MRI T_2-weighted images, it was noted that the excluded MCAo rats exhibited very large infarcts encompassing both cortical and subcortical areas. Interestingly, bilateral ventricular expansion was also evident in these two rats (**see Figure 4-4A**) which is an indicator of brain atrophy (Ding et al., 2010). Brain atrophy, therefore, may have distorted the stereotaxic location of the forelimb motor cortex in the rats with particularly extensive infarcts. Accordingly, the CTb injection site in these two rats was located lateral to the primary and secondary motor cortices (see **Appendix 7A** for an example). In total, 9 rats were used for analysis (5 sham and 4 MCAo rats).

4.3.2 Ischaemic damage in the brain and CST

Infarct volume defined by MRI T_2-weighted imaging at day 7 after MCAo was 45.1 ± 17.6mm^3 (ranging from 33.0 to 70.9 mm^3). In all 4 rats, infarcted tissue was confined to subcortical structures, particularly the striatal region which is supplied by end arteries (see **Figure 4-4B** for an example).

The extent of injury was also determined at the spinal cord level using immunoreactivity for PKC-γ to examine whether MCAo led to loss of CST axons arising from the ischaemic hemisphere. In sham-occluded rats, PKC-γ was visualised bilaterally in the dorsal columns (**Figure 4-5A**). In MCAo rats, partial loss of PKC-γ contralateral to the ischaemic hemisphere (affected/right side) was observed (**Figure 4-5B**). The mean PKC-γ brightness intensity ratio (affected versus unaffected side) for the sham group was 0.98 ± 0.08; whereas the mean PKC-γ brightness intensity ratio for the MCAo group was 0.66 ± 0.12, and the difference between the two groups was statistically significant (p = 0.012; **Figure 4-5C**). The CST axonal loss was likely due to ischaemic damage in the internal capsule, the ventral location of which appeared to be encompassed within the infarct (based on examination of the atlas of Paxinos & Watson, 2005). Residual PKC-γ immunoreactivity was still present in the affected side of

MCAo rats, with the mean loss of axons from the ischaemic hemisphere being 34 ± 14%. This suggests that MCAo for 60 min only partially disrupted the CST from the ischaemic hemisphere. There was a negative, but not significant correlation between infarct volume and PKC-γ brightness intensity ratio, whereby the rat with the largest infarct volume had the lowest brightness intensity ratio (Pearson's r: -0.74, p = 0.26).
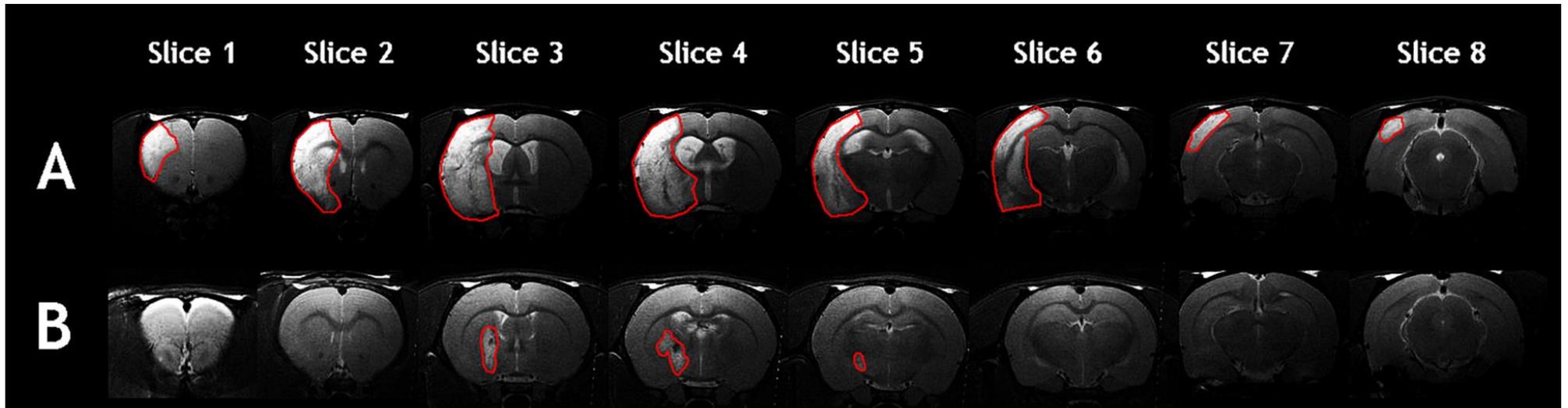
Figure 4-4 Ischaemic damage in the brain at 7 days following 60 min MCAo

A: MRI T$_2$-weighted images from an excluded MCAo rat. The infarct (the hyperintense region outlined in red) is extensive, encompassing both cortical and subcortical structures and the ventricles of both hemispheres appear enlarged. **B:** MRI T$_2$-weighted images from a representative MCAo rat included in all analysis. Note that the infarct is subcortical, mainly affecting the striatal region. The 8 coronal slices represent every second slice from the 16 images acquired during the T$_2$ scan and show the rostro-caudal extent of the territory supplied by the MCA.
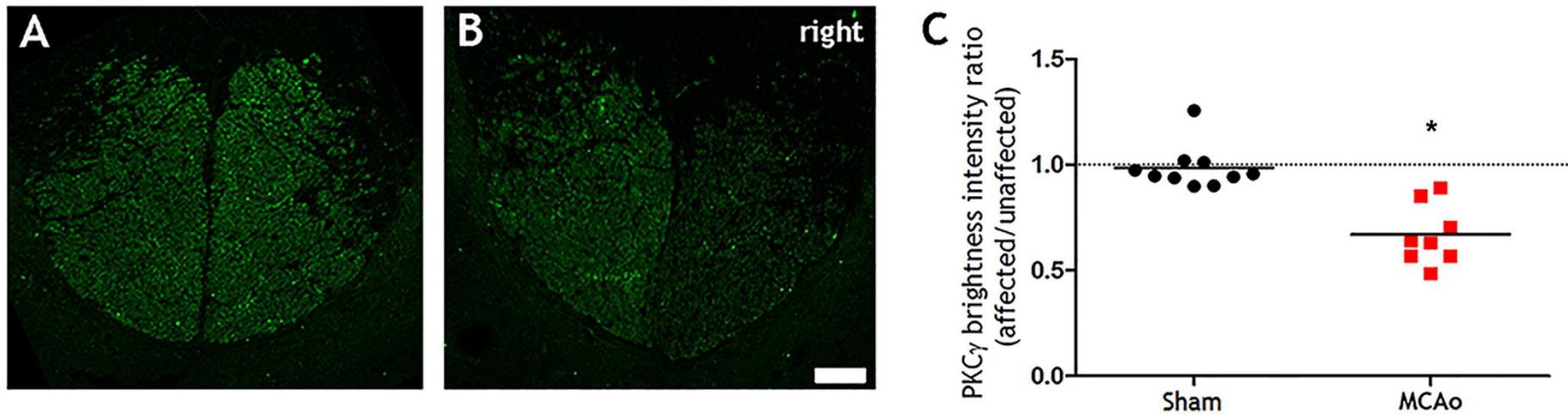
Figure 4-5 PKC-γ immunoreactivity in the dorsal columns at 28 days after 60 min MCAo

A: Projected confocal microscope image of the dorsal columns (C8) from a sham rat labelled for PKC-γ. Note symmetrical labelling. **B:** The dorsal columns from a MCAo rat labelled for PKC-γ. Note the reduced PKC-γ immunoreactivity in the affected (right) side, indicative of CST fibre loss (Scale bar = 50μm). **C:** PKC-γ brightness intensity, expressed as a ratio of affected (right) side/unaffected (left) side, was significantly reduced in the MCAo group compared with the sham group. Each data point represents a spinal section (2 sections per rat; n=5 sham rats and 4 MCAo rats). The dashed horizontal line indicates 1, which denotes symmetrical PKC-γ immunoreactivity between the affected and unaffected sides.

*p<0.05, unpaired t test (analysis based on number of animals, not number of sections)

4.3.3 Sensorimotor outcome

Figure 4-6A shows the mean neurological scores. A RM 2 way ANOVA showed a significant effect of MCAo on score (p<0.001); *post hoc* comparisons revealed that MCAo rats exhibited significantly reduced mean scores compared to the sham rats on post-MCAo days 1 to 21. Individual scores for the 5 sham rats are shown in **Figure 4-6B**. All rats received the maximum score of 33 prior to surgery (day -1). Although a slight reduction in score occurred on post-MCAo days 1 and 2, most rats exhibited the baseline score throughout the 28 days of testing. Individual scores for the 4 MCAo rats are shown in **Figure 4-6C**. As with the sham rats, all MCAo rats received the maximum score of 33 prior to surgery (day -1). All rats then exhibited a marked reduction in score after surgery followed by a gradual improvement over the 28 days of testing. By day 28, two rats had almost reached baseline score (score = 32). Taken together, MCAo resulted in a neurological deficit that gradually recovered over 28 days. On examination of the scores for each of the 11 subtests, it was noted that most rats, including sham operated rats, were impaired in the horizontal bar, inclined platform and general conditions tests following surgery. By day 3, no sham rats exhibited impairments in these tests, while the MCAo rats were still impaired. This suggests that the anaesthesia or vessel manipulation may have caused transient deficits in balance or grip strength. The number of sham and MCAo rats exhibiting impairments in each of the 11 subtests across time can be seen in **Appendix 5** and **Appendix 6**, respectively.
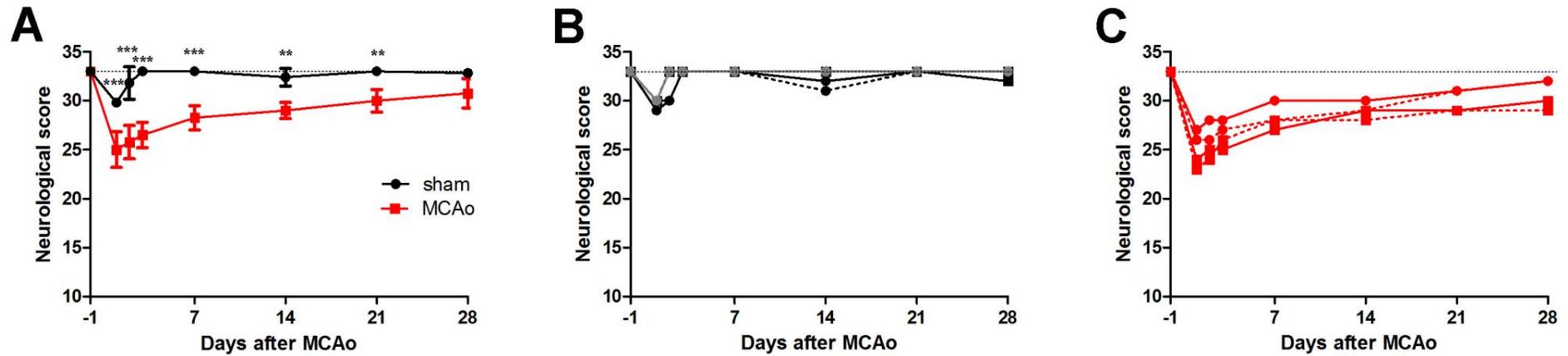
Figure 4-6 Effect of 60 min MCAo on neurological score over 28 days

A: A RM 2 way ANOVA revealed a significant group effect ($F_{(1, 71)}= 20.10$, $p<0.001$). Bonferroni *post hoc* analyses showed that the MCAo rats exhibited significantly reduced scores compared to sham rats at post-MCAo days 1 to 21. Data represent mean ± SD. **B:** Individual scores for all 5 sham rats. Prior to surgery (day -1), all rats received the maximum score of 33 followed by a slight reduction in score that had returned to baseline by day 3. **C:** Individual scores for all 4 MCAo rats. Prior to surgery, all rats received the maximum score of 33, after which, all scores were markedly reduced. A gradual improvement was observed over 28 days. The dotted horizontal line indicates the maximum score of 33, which denotes normal neurological function.

***$p<0.001$, **$p <0.01$

The mean differences in contact time between the affected and unaffected paws are shown in **Figure 4-7A**. A RM 2 way ANOVA revealed a significant effect of MCAo on contact difference time ($p < 0.0001$); *post hoc* analysis showed that the contact difference time was significantly increased in the MCAo group versus the sham group on post-MCAo days 3 to 7. This indicates that MCAo induced a bias for detecting stimuli on the unaffected paw that resolved after 14 days. The mean contact difference times for each sham rat (out of the 4 trials for each day) are depicted in **Figure 4-7B**. For all 5 rats, the contact difference times remained relatively close to zero throughout the duration of testing, which indicates symmetry in the detection of forepaw stimulation. The mean contact difference values for each MCAo rat are shown in **Figure 4-7C**. Prior to MCAo, all 4 rats exhibited contact difference times close to zero, after which the contact difference times for all 4 rats increased. This asymmetry had resolved in 2 rats by post-MCAo day 14 and in all rats by post-MCAo day 28.

The mean removal difference times are shown in **Figure 4-8A**. A RM-2 way ANOVA revealed a significant effect of MCAo ($p < 0.0001$): *post hoc* comparisons showed that MCAo rats exhibited a significantly increased removal difference time versus sham rats on post-MCAo days 3 to 21. This indicates that MCAo resulted in a bias for removing stimuli from the unaffected paw that resolved after 21 days. The mean removal differences for each sham rat are depicted in **Figure 4-8B**. For all 5 rats, the removal difference time remained relatively close to zero throughout the duration of testing, indicating that there were no biases for either paw. **Figure 4-8C** shows the mean removal difference times for each individual MCAo rat. Prior to MCAo, the removal difference time for all rats was close to zero, after which the removal difference time increased in all rats. The degree of this asymmetry gradually decreased over the 28 days of testing. Although at day 28, the removal difference time for all rats was still above zero, suggesting that there was still a slight bias for the unaffected paw at this time point.
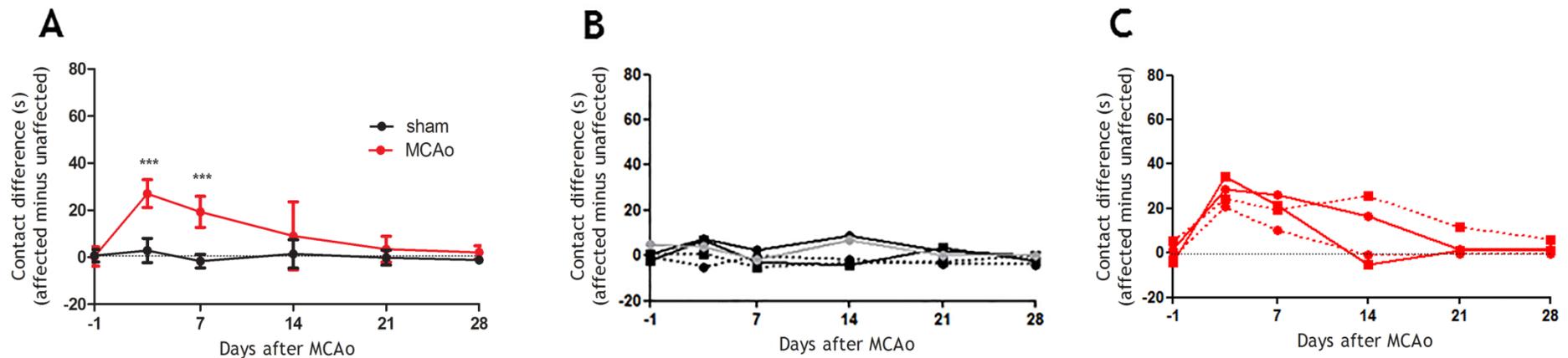
Figure 4-7 Effect of 60 min MCAo on contact difference times over 28 days

A: A RM 2 way ANOVA revealed a significant group effect on contact difference ($F_{(1, 71)}= 23.19$, $p<0.001$). Bonferroni *post hoc* analyses showed that the MCAo group exhibited an increased contact difference times versus the sham group on post-MCAo days 3 to 7. Data represent mean ± SD (n = 5 sham rats and 4 MCAo rats). **B:** The mean contact difference values for all sham rats. Note the contact difference time was close to zero throughout the testing period. **C:** The mean contact difference times for all MCAo rats. Note the increased contact different time for all rats after MCAo, followed by a gradual return to zero. The dotted horizontal line indicates zero, which denotes symmetrical limb contact latencies.
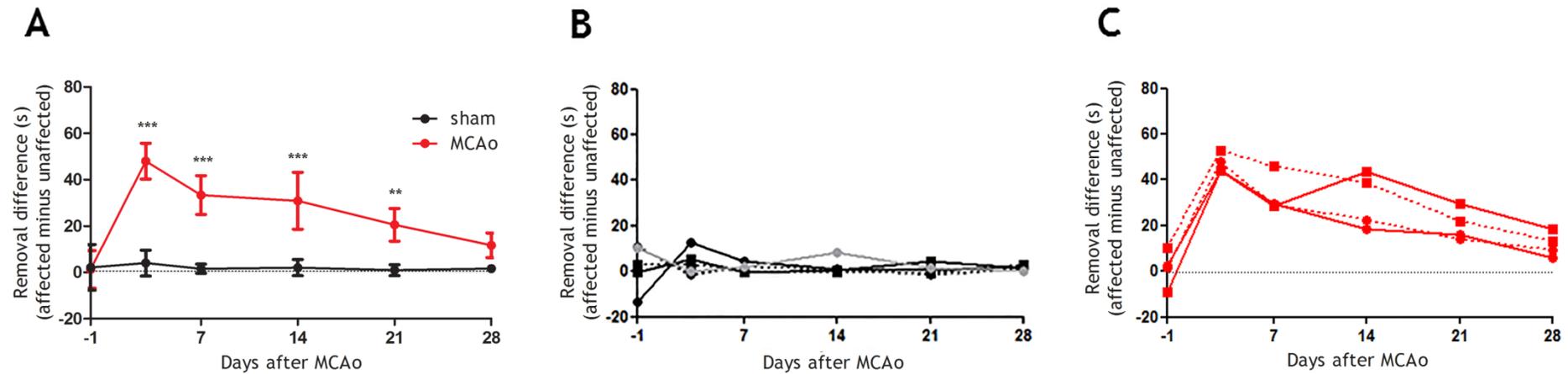
***$p<0.001$

Figure 4-8 Effect of 60 min MCAo on removal difference times over 28 days

A: A significant group effect was yielded for removal difference (F(1,34) = 125.2, p<0.0001) where the removal difference time was significantly higher in the MCAo group versus the sham group at post-MCAo days 3 to 21. Data represent mean ± SD (n = 5 sham rats and 4 MCAo rats). **B:** The mean removal difference values for all sham rats. Note that the removal difference time was close to zero throughout the testing period. **C**: The mean removal difference times for all MCAo rats. Note the increased removal difference time for all rats after MCAo, followed by a gradual reduction over 28 days. However by day 28, all rats still exhibited removal difference times above zero. The dotted horizontal line indicates zero, which denotes symmetrical limb contact latencies.

***p<0.001, **p <0.01.

4.3.4 CTb injection sites in the non-ischaemic hemisphere

In all rats, the CTb injection site was confined to the cortex of the non-ischaemic (right) hemisphere, as revealed with an immunoperoxidase reaction. In all rats, the injection sites incorporated aspects of the primary motor cortex, secondary motor cortex and primary somatosensory cortex. Photomicrographs of injections and reconstructions from a representative sham and MCAo rat are shown in **Figure 4-9A** and **Figure 4-9B**, respectively. Reconstructed injection sites for all rats used in this experiment are shown in **Appendix 7B.**

4.3.5 VGLUT-1 immunoreactivity of CTb-labelled axonal swellings

VGLUT-1 immunolabelled varicosities were present throughout the cervical spinal grey matter, with the highest density in the dorsal horn and a moderate density in the intermediate and ventral grey matter. Confocal microscopy revealed that in both sham (**Figures 4-10A to C**) and MCAo rats (**Figures 4-10D to F**), CTb-labelled axonal swellings originating from the non-ischaemic hemisphere almost universally contained VGLUT-1, suggesting they are glutamatergic terminals. **Table 4-2** summarises the percentages of CTb-labelled terminals that contained VGLUT-1 in both sham and MCAo rats. In the unaffected/left side (contralateral to the injection site) 95 ± 1% of CTb-labelled terminals in the sham group and 97 ± 1% of CTb-labelled terminals in the MCAo group contained VGLUT-1. In the affected/right side (ipsilateral to the injection site) 87 ± 13% of CTb-labelled terminals in the sham group and 83 ± 5% of CTb-labelled terminals in the MCAo group contained VGLUT-1. The lower percentage of double labelled terminals in the affected (right) side for both groups appeared to be due to the very small number of CTb-immunoreactive varicosities in this side. This meant that the presence of a single CTb-immunoreactive varicosity that did not contain VGLUT-1 dramatically affected the overall proportion of double labelled terminals within this side.
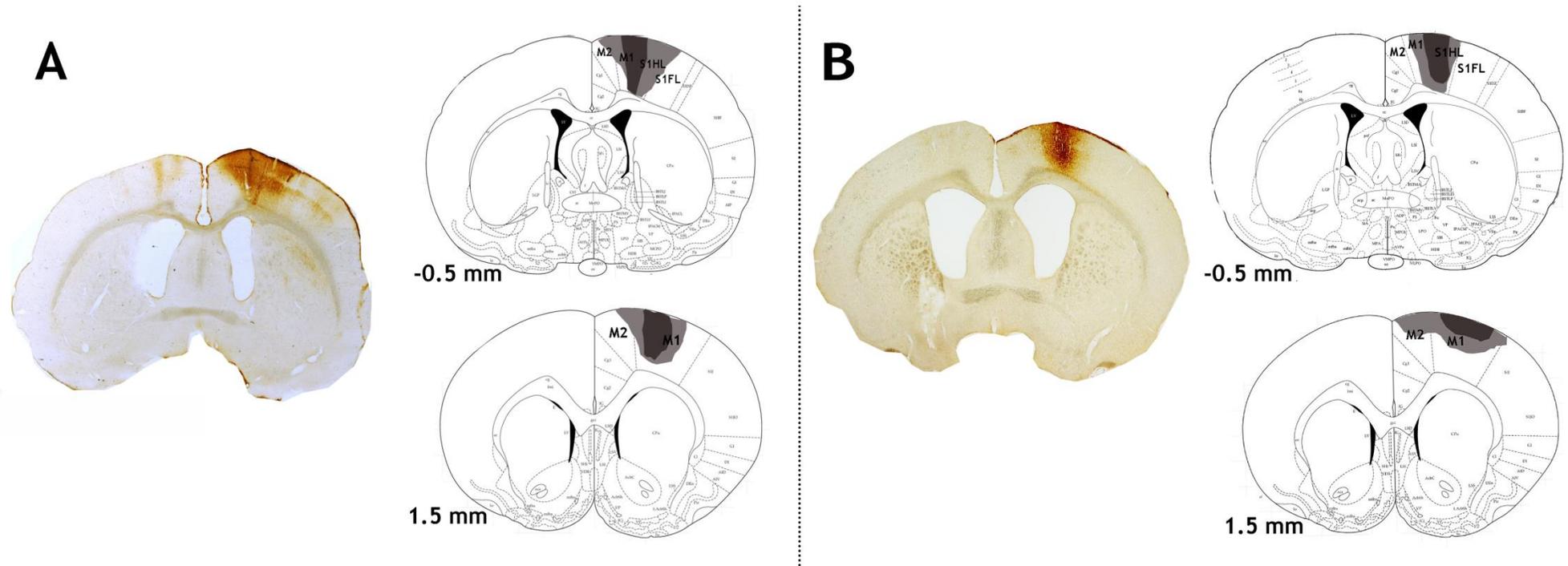
Figure 4-9 CTb tracer injection sites in the non-ischaemic (right) hemisphere

Photomicrographs show CTb injection sites revealed with an immunoperoxidase reaction taken from a sham (**A**) and a MCAo rat (**B**). The drawings (based on the atlas of Paxinos & Watson, 2005) indicate the location and extent of reaction product relative to the location of the forelimb motor cortex (defined by Neafsey et al., 1986) and the distance from Bregma (mm) is defined. The dark shading shows the core of the injection site and the light shading shows the spread surrounding the injection site.

M1 = primary motor cortex; M2 = secondary motor cortex; S1HL= primary somatosensory-hindlimb region; S1FL = primary somatosensory-forelimb region
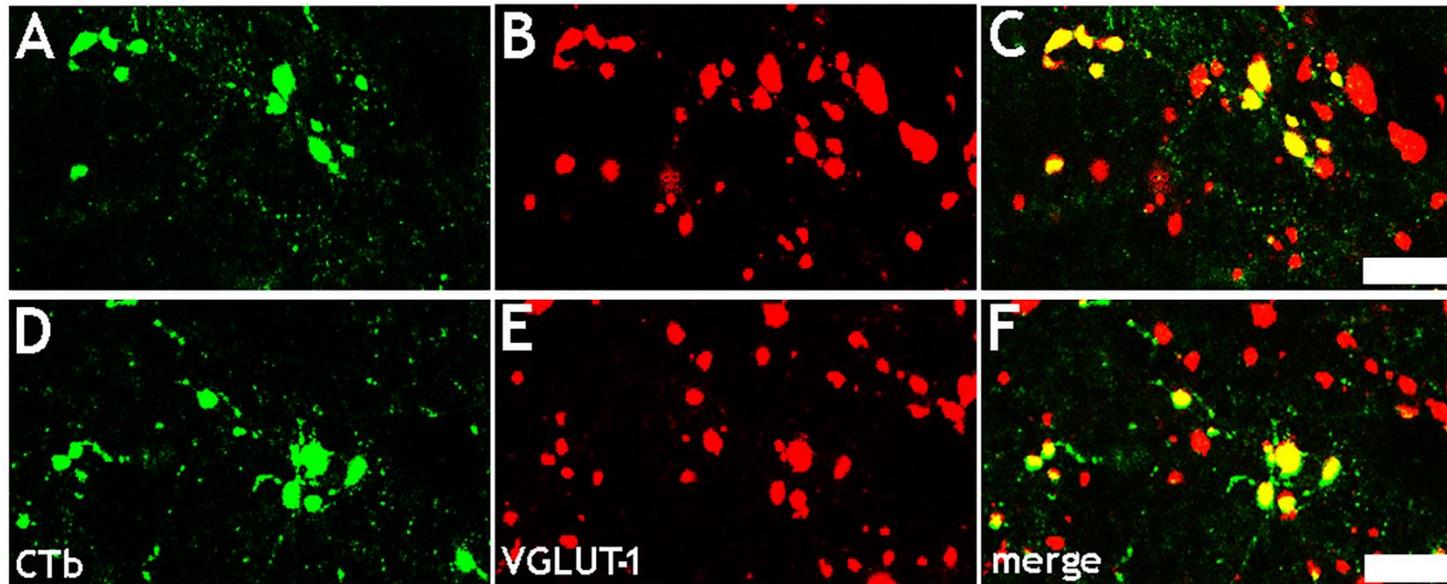
Figure 4-10 Co-expression of VGLUT-1 with CTb-labelled axonal swellings from the non-ischaemic (right) hemisphere

A: Single optical section (from segment C4) showing CTb-labelled axonal swellings (green) in a sham rat. **B:** immunoreactivity in the same plane for VGLUT-1 (red). **C:** Merged image. A similar series is also shown for a MCAo rat (**D-F**). Note that CTb-labelled axonal varicosities are immunoreactive for VGLUT-1, suggesting they are glutamatergic terminals. Scale bar = 5μm.

		Unaffected (left) side		Affected (right) side	
		Total no. CTb terminals	% VGLUT-1	Total no. CTb terminals	% VGLUT-1
Sham	rat 1	375	96.3	23	73.9
	rat 2	267	95.1	22	86.4
	rat 3	305	94.9	9	100
	mean ± SD		**95 ± 1**		**87 ± 13**
MCAo	rat 1	647	95.3	16	87.5
	rat 2	856	96.2	49	77.6
	rat 3	601	98	20	85
			97 ± 1		**83 ± 5**

Table 4-2 Percentages of CTb-immunoreactive axonal swellings in the cervical spinal cord (segment C4) that contained VGLUT-1

Note that for all rats the vast majority of CTb- immunoreactive terminals contained VGLUT-1. Terminals quantified in 3-4 cervical sections per rat.

4.3.6 Laminar distribution of CTb-labelled terminals originating from the non-ischaemic hemisphere

CTb-immunoreactive terminals were similarly distributed in all rats at each of the cervical segments examined (C3, C5 and C7). See **Figures 4-11A** and **4-11B** for examples of mapped out terminals from a sham and MCAo rat, respectively. Terminals were primarily located in the grey matter contralateral to the injection site (unaffected/left side). They were most numerous in the medial part of the base of the dorsal horn (lamina IV to VI) but they were also present in laminae III to X. Occasionally terminals were observed ipsilateral to the injection site (affected/right side), scattered diffusely mainly throughout the intermediate grey matter. Within this side of the grey matter, a very small number of terminals and fibres immediately adjacent to the central canal were detected. Because of the proximity of these structures to the midline, they may represent ramifications of axons that have re-crossed segmentally. However they were very rare in both sham and MCAo rats. They were present in 5 out of the 15 sections examined in the sham group, and 3 out of the 12 sections examined in the MCAo group. See **Figures 4-12A** and **4-12B** for example images of terminals from a sham and MCAo rat, respectively.
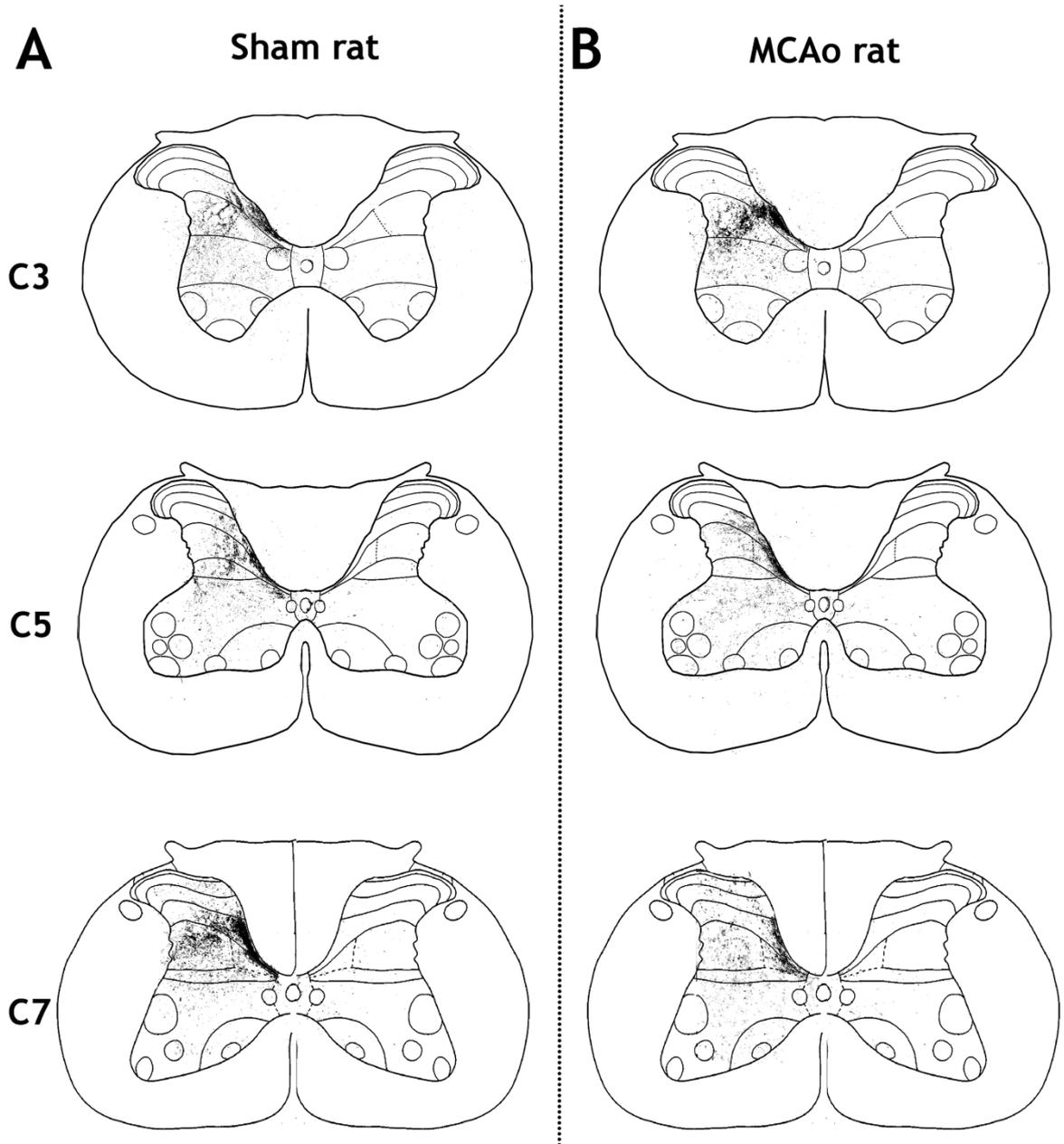
Figure 4-11 Laminar distribution pattern of CTb-labelled terminals originating from the non-ischaemic (right) hemisphere

A: Distribution of CTb-labelled terminals for C3, C5 and C7 segments taken from a sham rat. Each representation was made from a single 60µm section reacted with DAB. The DAB immunoreactivity was transposed onto spinal templates (based on Paxinos & Watson, 2005) using Adobe Photoshop. Note that the vast majority of terminals were contralateral to the injection site (unaffected/left side), particularly in the medial base of the dorsal horn. However a small number of terminals were found in the side ipsilateral to the injection site (affected/right side) mainly scattered diffusely in the intermediate region. **B:** A similar series of images taken from a MCAo rat
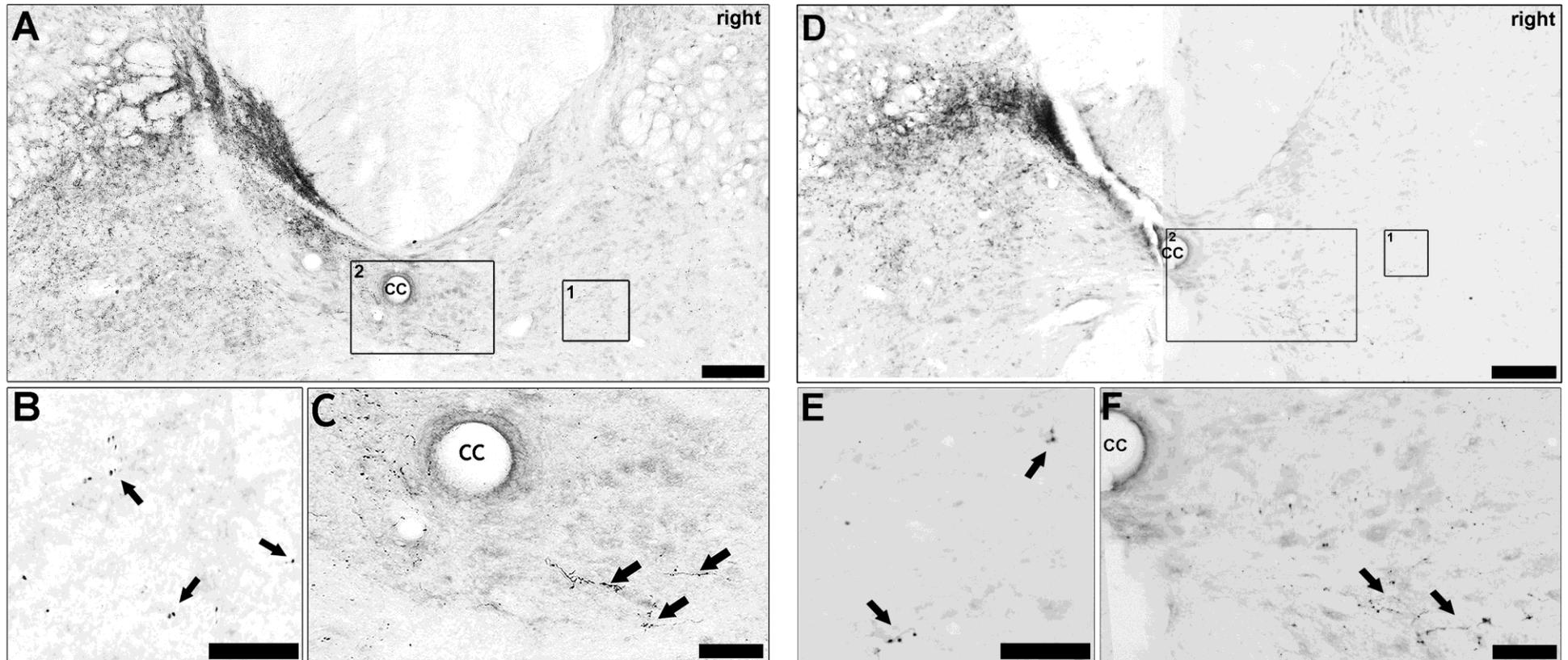
Figure 4-12 Photomicrographs of CTb-labelled terminals originating from the non-ischaemic (right) hemisphere

A: CTb-labelled terminals in a C3 section from a sham rat revealed with a DAB reaction. Note the majority of terminals are located in the side contralateral to the injection site (unaffected/left side) at the medial base of the dorsal horn. Terminals were also scattered diffusely throughout the intermediate grey matter of the side ipsilateral to the injection site (affected/right side; **B**). Occasionally, fibres and terminals were detected adjacent to the central canal, potentially representing ramifications of midline crossing fibres (**C**). **B** & **C** are magnified views of boxes 1 & 2 of plate **A**. A similar series of images are shown for MCAo rat (**D**, **E**, **F**). Scale bar in **A** & **D** = 150µm; Scale bar in **B**, **C**, **E** & **F** = 50µm

4.3.7 CTb-labelled terminal counts in the cervical spinal cord

CTb-labelled terminals originating from the non-ischaemic (right) hemisphere were quantified in the cervical spinal cord using three different counting methods (as detailed in **section 4.2.11**). The results for each of the three counting methods are as follows:

Automatic CTb-labelled terminal counts

For each cervical segment examined (C3, C5 and C7), the mean number of terminals counted in the unaffected (left) side was not significantly different between sham and MCAo rats (**Figure 4-13A**, p>0.05). Similarly, for all analysed segments, the mean number of terminals in the affected (right) side was not significantly different between sham and MCAo rats (**Figure 4-13B**, p>0.05). Within both sham and MCAo groups the terminal counts varied between individual rats. This was likely due to subtle differences in the location/volume of the CTb injection. To compensate for variable terminal labelling between rats, the automatic terminal counts were also expressed as a ratio: affected (right)/unaffected (left). However, mean terminal counts expressed as a ratio were not significantly different between sham and MCAo rats, for all three segments examined (**Figure 4-13C**, p>0.05).

CTb-positive surface area (mm^2)

In case the automatic counting software failed to segment individual terminals in regions where terminals were densely distributed, the CTb-positive surface area (mm^2) within each side of the cervical grey matter was also measured. For each cervical segment analysed (C3, C5 and C7), the mean CTb-positive surface area in the unaffected (left) side was not significantly different between sham and MCAo rats (**Figure 4-14A**, p>0.05). Similarly, for all segments analysed, the mean CTb-positive surface area in the affected (right) side was not significantly different between sham and MCAo rats (**Figure 4-14B**, p>0.05). To control for variable labelling (as described above), the CTb-positive surface area was also presented as a ratio: (affected (right)/unaffected (left). However, the mean CTb-positive surface ratio was not significantly different between sham and MCAo rats, for all segments analysed (**Figure 4-14C**; p>0.05). The CTb-positive

surface area ratios tended to be slightly lower than the ratios obtained for the automatic terminal counts. This suggests that the automatic counting software may have underestimated the number of terminals in the unaffected (left) side, presumably by erroneously detecting clusters of overlapping terminals as a single "object" as discussed previously (**section 4.2.11**).

Manual CTb-labelled terminal counts

To assess for potential changes that may have been too subtle for the automatic counting software to detect, terminals were quantified manually with the region of the grey matter immediately adjacent to the central canal on the C5 sections. The mean number of terminals counted in the unaffected (left) side was not significantly different between sham and MCAo rats (**Figure 4-15A**, p>0.05). Similarly, the mean number of terminals in the affected (right) side was not significantly different between sham and MCAo rats (**Figure 4-15B**, p>0.05). To control for variable terminal labelling (as above) the manual terminal counts were presented as ratios: affected (right)/unaffected (left). However, the mean terminal ratio was not significantly different between sham and MCAo rats (**Figure 4-15C**, p>0.05). The mean ± SDs acquired using all three counting methods are listed in **Appendix 8**.
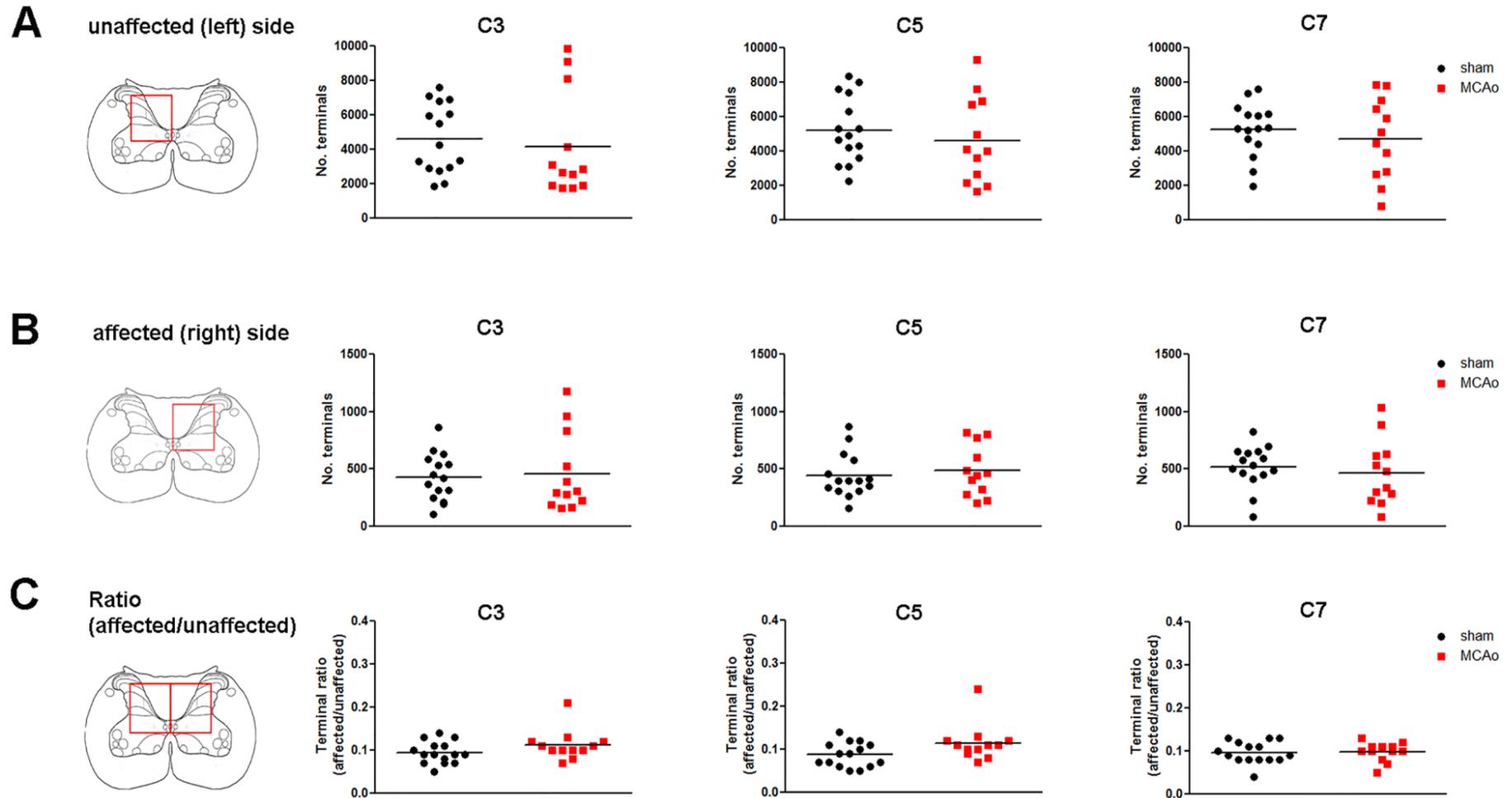
Figure 4-13 Automatic counts of CTb-labelled terminals in the cervical spinal cord

A: CTb-immunoreactive terminal counts for the unaffected (left) side shown for cervical segments C3, C5 and C7. Each data point represents a single section (4 sections per rat; n= 5 sham rats and 4 MCAo rats). Inset diagram shows the laminar location where counting was performed (red box). A similar series of images are shown for the affected (right) side (**B**) and the terminal ratio (affected/unaffected; **C**). There were no significant differences between sham and MCAo groups.

p>0.05, unpaired t test (analysis based on number of animals, not number of sections)
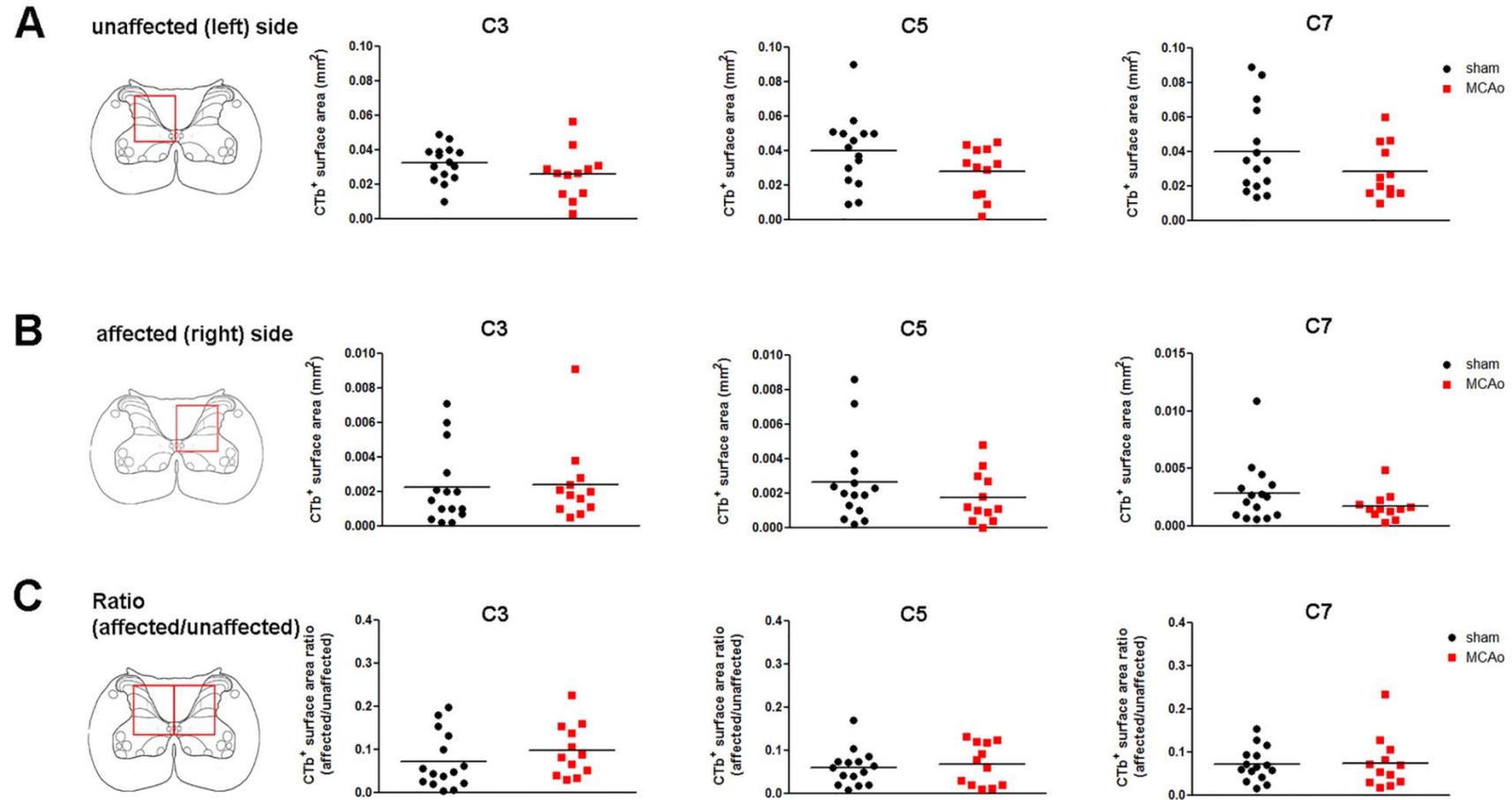
Figure 4-14 CTb-positive surface area (mm^2) in the cervical spinal cord

A: CTb-positive surface areas for the unaffected (left) side shown for cervical segments C3, C5 and C7. Each data point represents a single section (4 sections per rat; n = 5 sham rats and 4 MCAo rats). Inset diagram shows the laminar location where counting was performed (red box). A similar series of images are shown for the affected (right) side (**B**) and the terminal ratio (affected/unaffected; **C**). There were no significant differences between sham and MCAo groups.

p>0.05, unpaired t test (analysis based on number of animals, not number of sections)

Figure 4-15 Manual counts of CTb-labelled terminals in the cervical spinal cord

A: CTb-immunoreactive terminal counts for the unaffected (left) side shown for cervical segment C5. Each data point represents a single section (4 sections per rat; n = 5 sham rats and 4 MCAo rats). Inset diagram shows the laminar location where counting was performed (red box). A similar series of images are shown for the affected (right) side (**B**) and the terminal ratio (affected/unaffected; **C**). There were no significant differences between sham and MCAo groups.

p>0.05, unpaired t test (analysis based on number of animals, not number of sections)

4.4 Discussion

In this study, 60 min MCAo was associated with loss of approximately 35% of CST axons originating from the ischaemic hemisphere. Rats exhibited sensorimotor deficits in the early phase after MCAo but recovered over time such that there were no significant differences in sensorimotor performances between sham-operated and MCAo rats at post-operative day 28. Despite the functional recovery demonstrated by MCAo rats, the number of CST axon terminals in the cervical spinal cord originating from the non-ischaemic hemisphere was not altered compared to shams.

Sensorimotor outcome

MCAo for 60 min resulted in a sensorimotor deficit, as detected by neurological scoring and the adhesive label test. However, by post-operative day 28, there were no significant differences between sham and MCAo rats in both tests, suggestive of spontaneous sensorimotor recovery. Similar results were obtained by Modo et al., (2000) who noted that, following 60 min MCAo, rats were impaired in removing labels attached to the affected forepaw. However, in contrast to the current study, Modo and colleagues reported this deficit to still be present at 12 weeks after MCAo, with rats only exhibiting partial recovery at this stage. A potential explanation for this discrepancy is that the adhesive labels used by Modo and colleagues were much larger (6cm long strips) and likely more difficult to remove compared to the labels used in the current study (1.3cm circular dots) and as such, the test used by Modo and colleagues may have been more sensitive to residual sensorimotor deficits compared to the test used in the current study. Another possibility is that the procedure used by Modo and co-workers to transiently occlude the MCA may have disrupted the sensorimotor system to a greater extent than in the current study, thereby producing a larger and more longer-lasting deficit. Accordingly, Modo and colleagues reported very large lesions encompassing both cortical and subcortical structures, while the lesions produced in the current study were confined to subcortical structures only. In agreement with the current study, Trueman et al., (2011) reported an impairment in contacting/removing labels (0.7cm dots) attached to the affected forepaw after 60 min MCAo, followed by

gradual recovery, whereby the MCAo rats approached sham levels of performance by post-MCAo week 4.

CTb-labelled terminals in the cervical spinal cord

In all rats, CTb-immunoreactive terminals were mainly located within the grey matter contralateral to the injection site (unaffected/left side), particularly within the medial base of the dorsal horn (lamina III to VI), as described previously (Gribnau & Dederen, 1989; Liang, 1991; Du Beau et al., 2012). A much smaller number of diffusely scattered labelled terminals were also present ipsilateral to the injection site (affected/right side), mainly in the intermediate grey matter. These terminals are likely to be components of the uncrossed CST described by Brösamle and Schwab (1997; see Chapter 1 **section 1.1.1**). It is probable that most of these terminals are sites of synaptic interaction as they were almost universally immunoreactive for VGLUT-1 which is present in some types of glutamatergic presynaptic boutons, including those of the CST (Du Beau et al., 2012). Quantitative analysis revealed that the number of CTb-immunoreactive terminals (and CTb^+ surface area (mm^2)) within the affected (right) and unaffected (left) sides of the cervical spinal cord of MCAo rats was not significantly different to that of shams. Therefore, the data from the current study do not support the hypothesis that the density of CST synaptic terminals in the denervated side of the spinal cord increases at a time when rats have achieved functional recovery.

Nevertheless, it is possible that there may have been subtle changes in terminal reorganisation in response to transient MCAo that were of insufficient magnitude to be detected by the methodology employed in the current study. For instance, the formation of new or enhanced CST synaptic connections with CINs located in the unaffected side of the spinal cord could provide an alternative route for information to be transmitted from the non-ischaemic hemisphere to the denervated (ipsilateral) side of the spinal cord (as discussed in Chapter 1 **section 1.3**), in a similar way to the synaptic remodelling that occurs after spinal damage to the CST (Bareyre et al., 2004; see Chapter 1 **section 1.2.2**).

An increased number of CST terminals in the denervated side of the cervical spinal cord following 60 min MCAo might have been predicted, based on previous

reports of CST fibre sprouting from the uninjured hemisphere to the denervated half of the spinal cord after permanent MCAo (Liu et al., 2007; Liu et al., 2008), destruction of the primary motor cortex (Bachman et al., 2014; LaPash Daniels et al., 2009; Ueno et al., 2012) and unilateral pyramidotomy (Brus-Ramer et al., 2007; Maier et al., 2008). The data from the current study may indicate that although CST axonal sprouting occurs, new terminals are not formed. Liu et al., (2013) reported enhanced staining of the presynaptic protein, synaptophysin, in CST axons located in the denervated half of the spinal cord following MCAo, and this change occurred in relation to sensorimotor recovery. The finding from the current study – that the number of CST terminals in the cervical spinal cord originating from the non-ischaemic hemisphere in recovered MCAo rats was not altered compared to shams - suggests that the synaptic remodelling reported by Liu and colleagues might have involved CST axons arising from the ischaemic hemisphere, rather than the non-ischaemic hemisphere. An alternative explanation is that the extent of CST terminal reorganisation from the non-ischaemic hemisphere depends on the size and location of the infarct. Liu et al., (2007) reported sprouting of CST axons from the non-ischaemic hemisphere after permanent MCAo, an arterial occlusion method that typically produces infarcts encompassing large areas of the cortex and subcortical structures (Garcia et al., 1995). A subsequent study from the same laboratory reported evidence of CST synaptic remodelling after permanent MCAo (Liu et al., 2013, as mentioned above). In both of these previous studies animals were examined at 28 days post-MCAo, a similar time-point to that of the current study. Thus, it seems unlikely that the current study did not detect changes because the timeframe was markedly difference from these other studies. However, the location and severity of the infarcts in the current study were different from those studies. The infarcts produced in the current study were relatively small and located subcortically. This contrasts with the size and distribution of the infarcts in the aforementioned studies (Liu et al., 2007; 2008; 2013). The results of the current study also contrast with previous reports of sprouting after the entire primary motor cortex was infarcted by means of photothrombosis (LaPash Daniels et al., 2009; Bachmann et al., 2014) or the entire pyramidal tract transected (Brus-Ramer et al., 2007; Maier et al., 2008). In the current study, 65% of the CST, as measured by PKC-γ immunoreactivity at the level of the dorsal columns, was preserved. Taken together, the evidence raises the possibility than in cases

where there is sparing of a relatively large proportion of the CST (as in the current study), fibres from the ischaemic hemisphere might principally mediate recovery; whereas, in cases of severe stroke, when ipsilesional plasticity is limited, networks of the non-ischaemic hemisphere might be recruited (Nudo, 2006). Accordingly, deactivation of the motor cortex of non-ischaemic hemisphere with lidocaine following recovery from MCAo was found to reinstate the original deficits only in rats with large infarcts (Biernaskie et al., 2005). To explore this hypothesis further, Pearson's correlation was performed in order to assess whether there was an association between the loss of CST axons (as measured by PKC-γ immunostaining) and the number of labelled terminals/CTb-positive surface area (mm^3) in the affected side of the spinal cord, but there was no relationship or trend. It would be interesting to compare the numbers of CST terminals in the spinal cord after recovery following different durations of MCAo. Understanding the effect of the size/location of the infarct on plasticity processes would be important for determining which patient groups might benefit from interventions aimed at strengthening these processes.

With a non-significant finding, it is important to consider the possibility that the study was underpowered i.e. the sample sizes may not have been large enough to detect a statistically significant difference in terminal numbers between sham and MCAo rats, particularly if the difference is small. Because the current study was novel, there was no pre-existing terminal count data available that could have been utilised to calculate appropriate sample sizes prior to the study. Using the standard deviation of automatic terminal counts in the affected (right) side (segment C5), a sample size calculation for a hypothetical future study was performed (StatMate, http://www.graphpad.com/scientific-software/statmate). It is difficult to predict what a biologically significant effect size would be, but 370, 80 and 35 rats per group would be required to detect hypothetical mean differences of 10%, 20% and 30%, respectively (with power set at 0.8 and α set at 0.05). Therefore, if a 10% (20% or 30%) difference in terminal counts exists between sham and MCAo rats, then an unrealistically large number of rats would be necessary to detect it.

Recovery from stroke, whether involving large or small infarcts, is unlikely to be solely attributed to CST terminal reorganisation in the denervated

(contralesional) side of the spinal cord. As discussed previously (Chapter 1 **section 1.3**), the motor cortex from the non-ischaemic hemisphere may have access to the denervated (ipsilateral) side of the spinal cord via relay neurons located in the brainstem and contralateral spinal cord and the strengthening of these indirect pathways could also underlie recovery. Evidence to support this notion comes from Bachmann et al., (2014) who reported that after cortical infarction in mice, the motor cortex from the non-ischaemic hemisphere increases its projections to ipsilateral reticular nuclei and the reticular nuclei in turn, increase their projections to the denervated (ipsilateral) side of the spinal cord (Bachman et al., 2014). Strengthening of ReST output to affected motor neurons has also been reported in the primate after pyramidal tract transection (Zaaimi et al., 2012). Additionally, sprouting of corticorubral fibres from the non-ischaemic hemisphere has also been reported in rats after MCAo (Liu et al., 2007). Finally, it is important to acknowledge that in addition to adaptive process described for the non-ischaemic hemisphere, a range of repair related events have also been reported to occur within the ischaemic hemisphere after stroke (reviewed by Benowitz & Carmichael, 2010; Cramer, 2008).

To summarise, despite functional recovery demonstrated by MCAo rats, the number of CST terminals originating from the non-ischaemic hemisphere in the cervical spinal cord was not altered compared to shams. This observation suggests that, following stroke, the motor cortex from the non-ischaemic hemisphere may not take over control of the impaired limb by increasing its direct projections to the denervated (ipsilateral) side of the spinal cord. However, involvement of the motor cortex of the non-ischaemic hemisphere in recovery cannot be excluded based on the results of this study because there are several indirect routes via which the motor cortex from the non-ischaemic hemisphere could gain access to the denervated (ipsilateral) side of the spinal cord (see Chapter **1 section 1.3**). These indirect routes require further investigation but may involve neurons located in the brainstem and contralateral (unaffected) side of the spinal cord (Jankowska & Edgley, 2006).

Chapter 5

Examination of corticospinal contacts from the non-ischaemic hemisphere to spinal interneuron populations at 28 days following transient MCAo

5.1 Introduction

In Chapter 4, following 60 min MCAo, rats exhibited a sensorimotor deficit that spontaneously recovered over 28 days. This recovery was not associated with the formation of new CST terminals from the non-ischaemic hemisphere to the denervated (ipsilateral) side of the spinal cord. However (as mentioned in Chapter 1 **section 1.3**), the motor cortex from the non-ischaemic hemisphere may have the capacity to take over control of the impaired limb via strengthening of indirect routes involving relay neurons located in the brainstem and contralateral (unaffected) side of the spinal cord (Jankowska & Edgley, 2006). For instance, the formation of new/enhanced CST connections with CINs located in the contralateral (unaffected) side of the spinal cord would allow for information to be conveyed from the non-ischaemic hemisphere to the denervated (ipsilateral) side of the spinal cord without the need for long-distance CST sprouting. CST input to spinal CINs is poorly characterised, even in intact animals (see Chapter 1 **section 1.3**). However, given that a moderate proportion of contralaterally descending CST axons terminate in laminae VI to VII, a region containing many CIN populations (Jankowska, 1992), it is probable that the CST establishes connections with CINs under normal circumstances. Hence, a short exploratory study was performed in order to examine whether recovery following 60 min MCAo was associated with new/enhanced CST contacts from the non-ischaemic hemisphere to spinal interneuron populations with known commissural components that have their somata in the contralateral (unaffected) side of the spinal cord. The spinal interneurons with commissural components were identified based on their neurochemical phenotypes.

The first spinal interneuron population of interest were cholinergic partition cells located in lamina X and medial lamina VII. These interneurons directly influence motor neuron excitability during locomotion via large "C-bouton" synapses (Miles et al., 2007; Zagoraiou et al., 2009). Injection of a transsynaptic tracer unilaterally into the quadriceps of mice has revealed that medial cholinergic partition cells monosynaptically connected with motor neurons fall into two categories; those that project exclusively ipsilaterally and those that project both ipsi- and contralaterally (Stepien et al., 2010). Thus, medial cholinergic partition cells directly influence motor neurons and they have a well-defined commissural component. Although most studies have focused on lumbar

circuitry, cholinergic partition cells are also present in cervical segments (Phelps et al., 1984) and likely have similar projection patterns and functions as those located in lumbar segments. In the cervical spinal cord of the cat, contralaterally projecting CST axons terminate within the immediate vicinity of cholinergic cells located in medial lamina VII (Chakrabarty et al., 2009), suggesting that the CST may establish connections with this cell population in the intact animal.

The second spinal interneuron population of interest were those expressing the calcium binding proteins calbindin and calretinin. In the rat, unilateral injection of a retrograde tracer into L1/L3 was found to label LDPNs in all cervical segments and approximately half of the labelled cells were commissural i.e. they were located in the grey matter contralateral to the tracer injection site (Brockett et al., 2013; see Chapter 1 **section 1.2.2**). These cells were mainly found in medial laminae VII/VIII and some were found to express calbindin and calretinin. Transsynaptic tracing in mice has revealed that LDPNs have monosynaptic connections with hindlimb motor neurons (Ni et al., 2014). Evidence on CST input to commissural LDPNs is conflicting, with electrophysiological data from cats suggesting that commissural LDPNs are directly influenced by the CST (Alstermark et al., 1987) and anatomical data from mice suggesting that commissural LDPNs are rarely contacted by CST axons (Ni et al., 2014).

Spinal cord tissue from MCAo and sham rats produced in Chapter 4 was used for this short exploratory study. A combination of immunofluorescence and confocal microscopy was employed in order to explore associations between anterogradely labelled CST terminals from the non-ischaemic hemisphere and different spinal interneuron populations. Antibodies against CTb were utilised to identify anterogradely labelled terminals and antibodies against choline acetyltransferase (ChAT; the enzyme responsible for the biosynthesis of acetylcholine; Oda, 1999), calbindin and calretinin were used to identify spinal interneuron populations.

<u>Study aim:</u>

- To characterise CST contacts from the non-ischaemic hemisphere to ChAT, calbindin and calretinin- expressing interneurons with somata located in the contralateral (unaffected) side of the cervical spinal cord at 28 days following 60 min MCAo or sham surgery

<u>Hypothesis</u>

Rats subjected to 60 min MCAo will exhibit new or increased CST contacts to ChAT/calbindin/calretinin- expressing cells in the contralateral (unaffected) side of the cervical spinal cord compared to sham-operated rats

5.2 Methods

5.2.1 Immunolabelling of terminals and cells

Three MCAo rats and three sham-occluded rats produced in Chapter 4 were randomly selected for use in this study. For the identification of CTb-labelled terminals and spinal interneurons, 60μm thick transverse sections from segment C5 (4 per rat) were incubated for 72 h with primary antibody combinations: (a) anti-CTb and anti-ChAT or (b) anti-CTb, anti-calbindin and anti-calretinin. Sections were then incubated for 24 h with secondary antibodies coupled to (a) Rhodamine red, Alexa 488, or (b) Rhodamine red, Dylight 649 and Alexa 488 (as shown in **Table 5-1**). Finally, sections were rinsed with PBS (3 x 10 min) and mounted with anti-fade (Vectashield; see Chapter 2 **section 2.7** for detailed ICC steps.

5.2.2 Confocal microscopy, reconstructions, and analyses

Confocal microscopy and image analysis was conducted with the experimenter blinded to the identity of the rat. Immunoreactive spinal sections containing labelled cells and terminals were scanned with a three-colour channel laser confocal microscope (Biorad Radiance 2100). Scanning was performed on the unaffected side of the grey matter (contralateral to the CTb injection site). For ChAT- immunoreactive interneurons, imaging was focused within lamina X and medial lamina VII, which is where cholinergic partition cells with monosynaptic

connections to contralateral (and ipsilateral) motor neurons are located (Stepien et al., 2010); and for calbindin and calretinin- immunoreactive interneurons, imaging was focussed within medial laminae VII and VIII, which is where commissural LDPNs expressing these calcium binding proteins are located (Brockett et al., 2013). Firstly, systematic low power scans (x20, zoom factor of 1) were performed to locate regions where CST terminals were in the immediate vicinity of interneurons. Selected neurons were then scanned using a x40 oil-immersion lens (zoom factor of 2 at 0.5µm increments). If CTb-labelled terminals established contacts with a cell, the cell was reconstructed using Neurolucida Software (as described in Chapter 2 **section 2.8**) and contact density was expressed as the number of contacts per 1000 µm^2 of neuronal surface. Contact densities were averaged for each rat so that an individual rat contributed only one value to the statistical analysis (see Chapter 2 **section 2.9**).

5.2.3 Statistical analysis

For all results shown in this chapter, statistical analysis is based on the number of animals (not the number of spinal sections or number of cells) in order to avoid pseudoreplication (see Chapter 2 **section 2.9**). Contact densities in sham and MCAo groups were compared using the non-parametric Mann-Whitney test, because the data were skewed and failed the Shapiro-Wilk normality test. Data are expressed as means ± SD and differences are considered significant at $p < 0.05$.

	Primary antibody combination	Concentration	Supplier	Secondary antibody combination
1	mo. CTb	1:250	A. Wikström, University of Gothenburg	Rh.Red
	gt. ChAT	1:100	Millipore, Harlow, UK	Alexa488
2	mo.CTb	1:250	A. Wikström, University of Gothenburg	Rh.Red
	rb.Calbindin	1;1000	Swant, Bellizona, Switzerland	Dylight649
	gt. Calretinin	1:1000	Swant, Bellizona, Switzerland	Alexa488

Table 5-1 Summary of primary and secondary antibody combinations used in the current experiment

1. For the examination of CTb-labelled contacts to ChAT- expressing interneurons. **2.** For the examination of CTb- labelled contacts to calbindin and calretinin-expressing interneurons (segment C5)

gt=goat; gp=guinea pig; mo=mouse; rb=rabbit; Rh.Red=Rhodamine red

5.3 Results

5.3.1 CST contacts to ChAT- expressing interneurons

Figure 5-1 shows the distribution pattern of ChAT- immunoreactive cells in the cervical spinal cord. There were 4 major groups of ChAT-positive neurons: 1) motor neurons with large somata in the medial and lateral motor columns; 2) cells with small somata scattered very diffusely through laminae III to V of the dorsal horn; 3) cells with very small somata clustered around the central canal; 4) a prominent group of partition cells with medium sized soma in lamina X and VII, forming a dividing line between the dorsal and ventral horn. For each group (sham and MCAo), a total of 23 ChAT- expressing partition cells (7-8 per rat) located in lamina X/medial lamina VII of the unaffected side (contralateral to the CTb injection site) were imaged and CTb-labelled contacts to these cells were quantified. In all rats, CTb-labelled terminals were distributed within the immediate vicinity of ChAT- immunoreactive cells. However, the terminals rarely established contacts with the cells, with the majority of the cells receiving no contacts. See **Figures 5-2A** and **5-2B** for examples of ChAT-immunoreactive cells with no CTb-labelled contacts, taken from a sham and MCAo rat, respectively. A small proportion of cells did receive CTb-labelled contacts (35% in the sham group; 39% in the MCAo group), and these cells tended to be located in lamina X, however they only received a very limited number of contacts (1-2 per cell). See **Figures 5-3A** and **5-3B** for examples of ChAT-immunoreactive cells that received contacts, taken from a sham and MCAo rat, respectively. For the sham group, the number of contacts per 1000 μm^2 of neuronal surface was 0.04 ± 0.05 for somata and 0.13 ± 0.07 for dendritic processes; for the MCAo group the contact density was 0.11 ± 0.13 for somata and 0.20 ± 0.11 for dendritic processes, and there were no significant difference between the two groups (p>0.05; **Figure 5-4**).
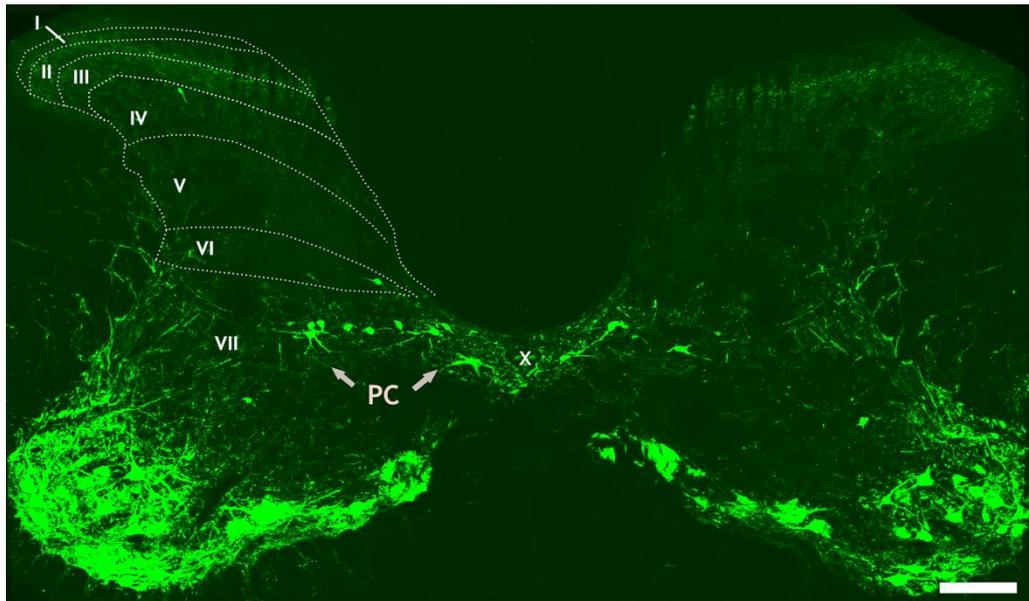
Figure 5-1 Distribution pattern of ChAT- expressing neurons in the cervical spinal cord

Projected confocal microscope image (100μm thick) showing ChAT- expressing cells in a transverse cervical section (C5). A spinal template (taken from Paxinos & Watson, 2005) demarcating laminae I-VII and X is superimposed onto the image. Arrows indicate lamina X/VII partition cells (PC) that span across the grey matter, dividing the dorsal horn from the ventral horn. Scale bar = 100μm
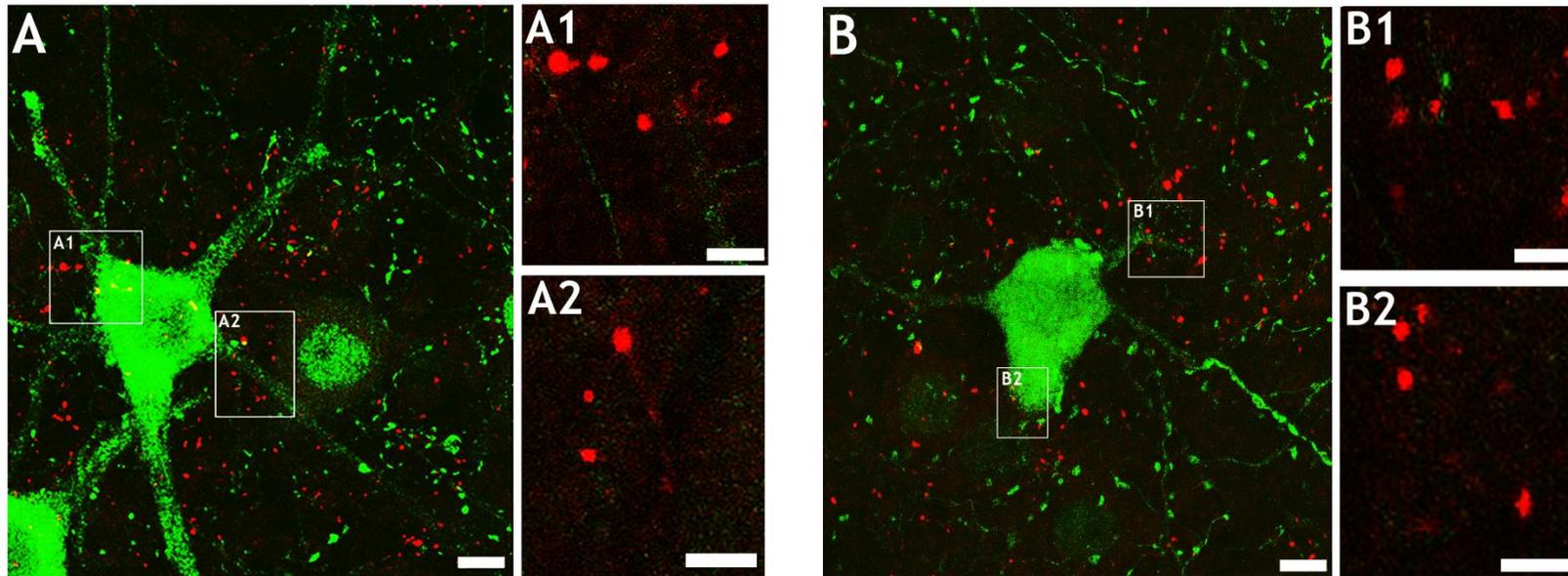
Figure 5-2 Examples of ChAT- expressing cells with no contacts from CTb-labelled terminals

A: A projected confocal microscope image (57 optical sections, 0.5µm increments) from a sham rat showing numerous terminals (red) within the vicinity of a ChAT-expressing cell (green). However, single optical images of the terminals (insets **A1** & **A2**) show that the terminals do not establish contacts with the cell. **B:** A similar example is shown from a MCAo rat (64 optical sections, 0.5µm increments) whereby CTb-labelled terminals are within the vicinity of the cell but do not establish contacts (insets **B1** & **B2**). Both images are taken from medial lamina VII. Scale bar in **A** & **B** = 20µm. Scale bar in insets =10µm
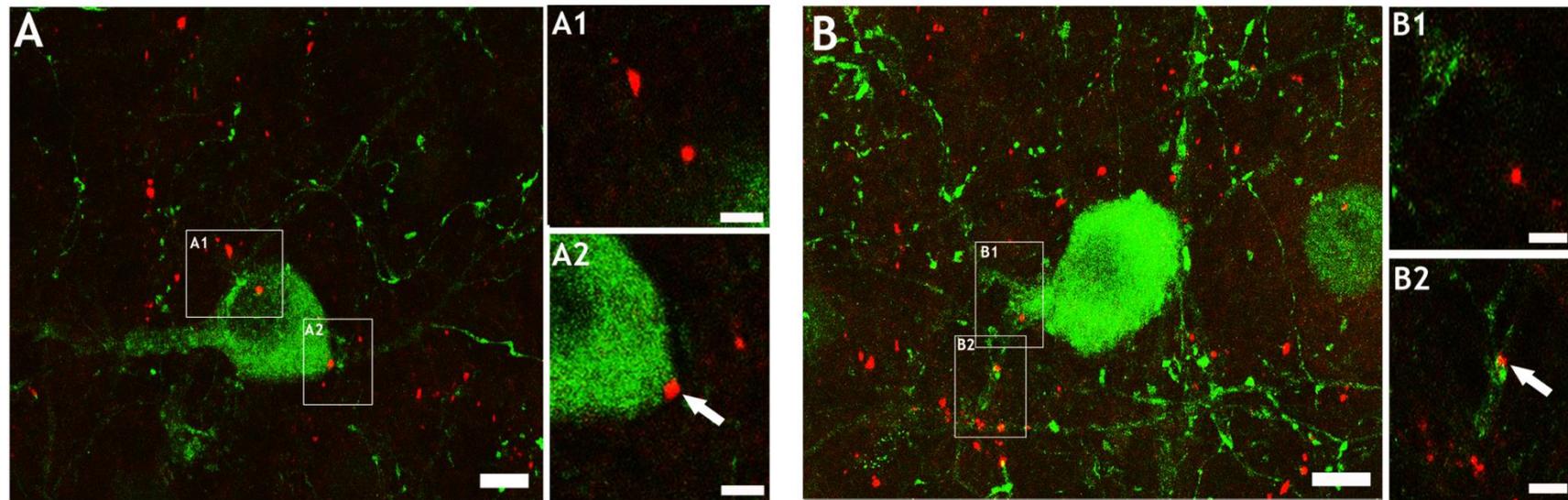
Figure 5-3 Example of ChAT-expressing cells with contacts from CTb-labelled terminals

A: A projected confocal microscope image (32 optical sections, 0.5µm increments) from a sham rat showing numerous terminals (red) within the vicinity of a ChAT-expressing cell (green). The majority of the terminals within the vicinity of the cell did not establish contact with the cell (inset **A1**), however one terminal made contact with the soma (inset **A2**). **B:** A similar example is shown from a MCAo rat (41 optical sections, 0.5µm increments), whereby most CTb-labelled terminals within the territory of the cell did not make contact (inset **B1**). However, one terminal made contact with a dendritic process (inset **B2**). Both images are taken from lamina X. Arrows indicate terminals that established contacts with the cells. Scale bar in **A** & **B**= 20µm. Scale bar in insets =10µm

Figure 5-4 Density of CTb-labelled contacts to lamina X/VII ChAT- expressing cells

Each data point represents a cell (7-8 cells per rat; n = 3 sham and 3 MCAo rats). For both somata and dendritic processes, the mean density of contacts was not significantly different between sham (black) and MCAo (red) groups.

p>0.05, Mann-Whitney test (analysis based on number of animals, not number of cells/sections)

5.3.2 CST contacts to calbindin and calretinin- expressing interneurons

Figure 5-5A shows the distribution pattern of calbindin and calretinin-immunoreactive cells in the cervical spinal cord. For both groups, immunoreactivity was densest within the superficial laminae. Calbindin and calretinin-positive cells were much more dispersed throughout the grey matter than ChAT-positive cells. Calbindin-expressing cells (**Figure 5-5B**) were less abundant than calretinin-expressing cells (**Figure 5-5C**).

For each group (sham and MCAo), a total of 14 calbindin-positive cells (4-5 cells per rat) located in medial laminae VII and VIII of the unaffected side (contralateral to the CTb injection site) were imaged and CTb-labelled contacts to these cells were quantified. In all rats, CTb-labelled terminals tended to be located outside the territory of calbindin-positive cells. Although a small proportion of the more medially located cells did have terminals within the immediate vicinity of their somata and dendritic processes and some of the terminals established contacts with these cells. The proportion of cells that received contacts was 35% in the sham group and 15% in the MCAo group, but each cell only received 1 contact (see **Figures 5-6A** and **5-6B** for examples taken from a sham and MCAo rat, respectively). For the sham group the density of contacts per 1000μm^2 of neuronal surface was 0.41 ± 0.22 for somata and 0.25 ± 0.45 for dendritic processes; for the MCAo group the density of contacts for somata was 0.08 ± 0.08 and 0 for dendritic processes, and there was no significant difference between the two groups (p>0.05**; Figure 5-7**).

For each group (sham and MCAo), a total of 14 calretinin-positive cells (4-5 cells per rat) located in medial laminae VII and VIII of the unaffected side (contralateral to the CTb injection site) were imaged and CTb-labelled contacts to these cells were quantified. In all rats, CTb-labelled terminals tended to be located outside the territory of calretinin-positive cells. Although a small proportion of the more medially located cells did have terminals within the immediate vicinity of their somata and dendritic processes and some of the terminals established contacts with these cells. The proportion of cells that received contacts was 21% in the sham group and 21% in the MCAo group, however each cell only received 1 contact (see **Figures 5-8A** and **5-8B** for

examples taken from a sham and MCAo rat). For the sham group the density of contacts per 1000µm^2 of neuronal surface was 0.05 ± 0.08 for somata and 0.09 ± 0.13 for dendritic processes; for the MCAo group the density of contacts was 0 for somata and 0.18 ± 0.31 for dendritic processes, and there was no significant difference between the two groups (p>0.05; **Figure 5-9**).
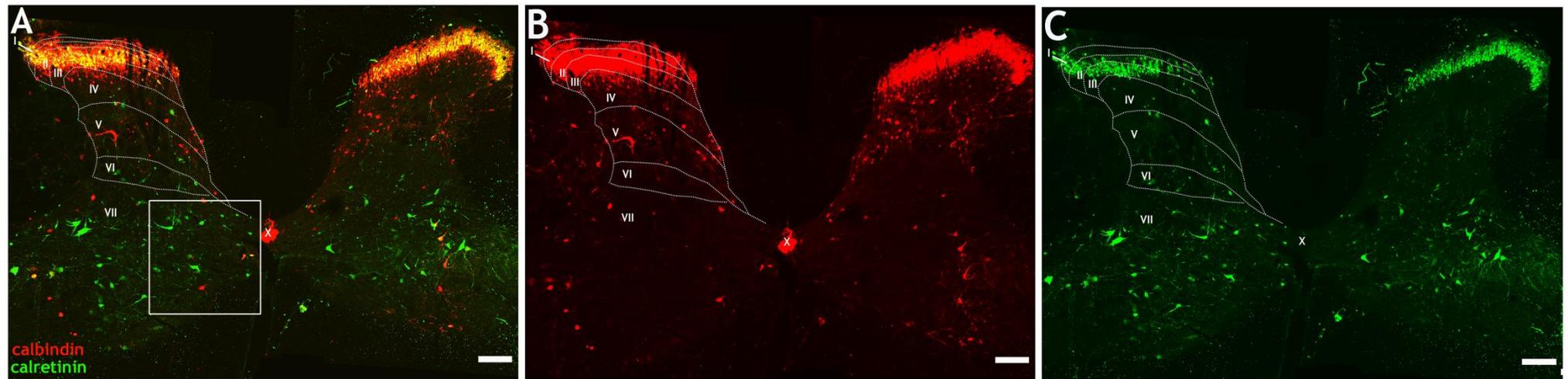
Figure 5-5 Distribution pattern of calbindin and calretinin-expressing cells in the cervical spinal cord

A: Projected confocal microscope image (100μm thick) of calbindin (red) and calretinin (green) - expressing cells in a transverse cervical section (segment C5). A template (taken from Paxinos & Watson, 2005) demarcating laminae I-VII and X is superimposed onto the image. Calbindin and calretinin immunoreactivity are also shown separately (**B** & **C**). Box in **A** depicts the region where scanning was performed for the assessment of CTb- labelled contacts to cells. Scale bar = 100μm
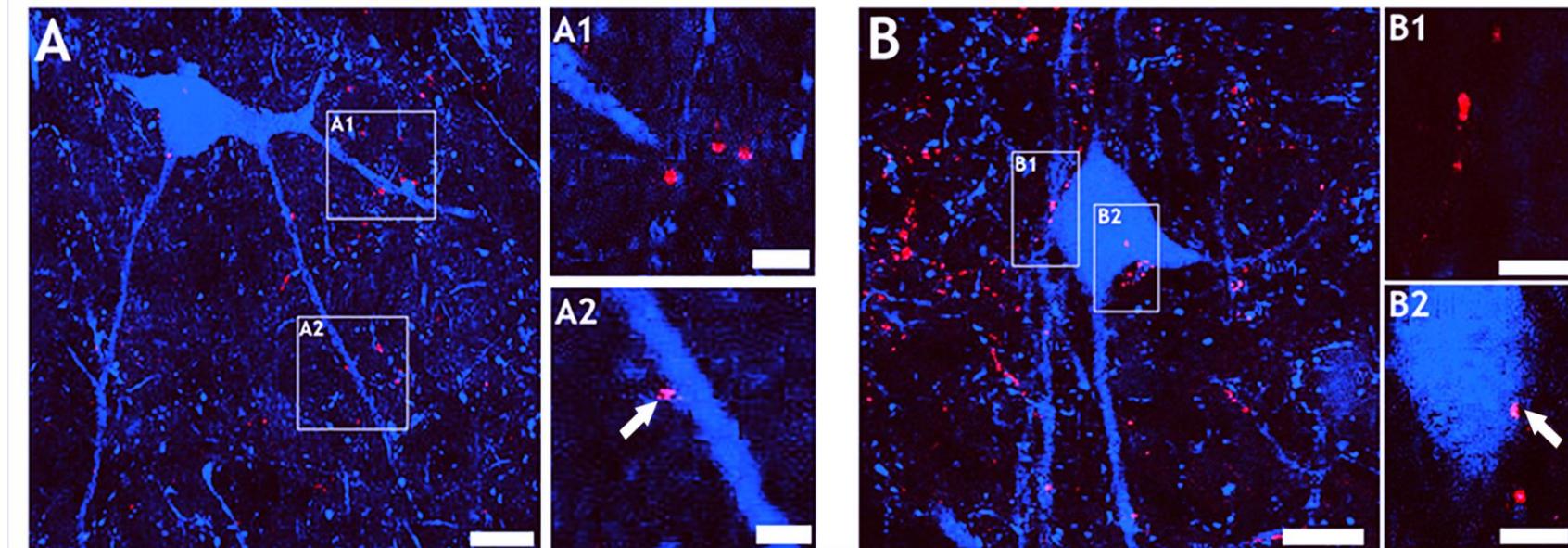
Figure 5-6 Examples of calbindin- expressing cells with contacts from CTb- labelled terminals

A: Projected confocal microscope image (72 optical sections, 0.5µm increments) from a sham rat showing terminals (red) within the vicinity of a calbindin- expressing cell (blue). The majority of the terminals within the vicinity of the cell did not establish contact with the cell (inset **A1**), however one terminal established contact with a dendritic process (inset **A2**). **B:** A similar example is shown from a MCAo rat (56 optical sections, 0.5µm increments) whereby most CTb- labelled terminals within the cell territory did not make contact (**B1**), but a single terminal was found to make contact with the soma (**B2**). Both images are taken from the medial lamina VII. Arrows indicate terminals that established contacts with the cells. Scale bar in **A** & **B**= 20µm. Scale bar in insets =10µm
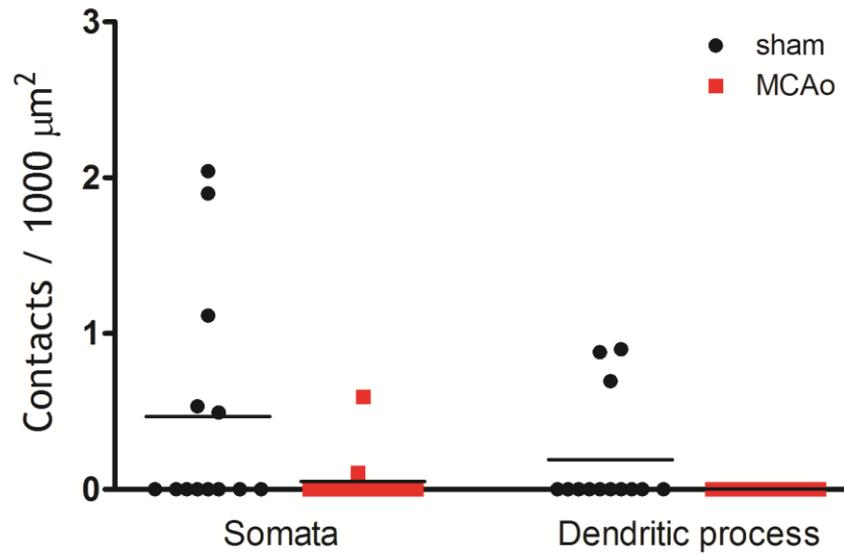
Figure 5-7 Density of CTb-labelled contacts to lamina VII/VIII calbindin-expressing cells

Each data point represents a cell (4-5 cells per rat; n = 3 sham and 3 MCAo rats). For both somata and dendritic processes, the mean density of contacts was not significantly different between sham (black) and MCAo (red) groups.

p>0.05, Mann-Whitney test (analysis based on number of animals, not number of cells/sections)
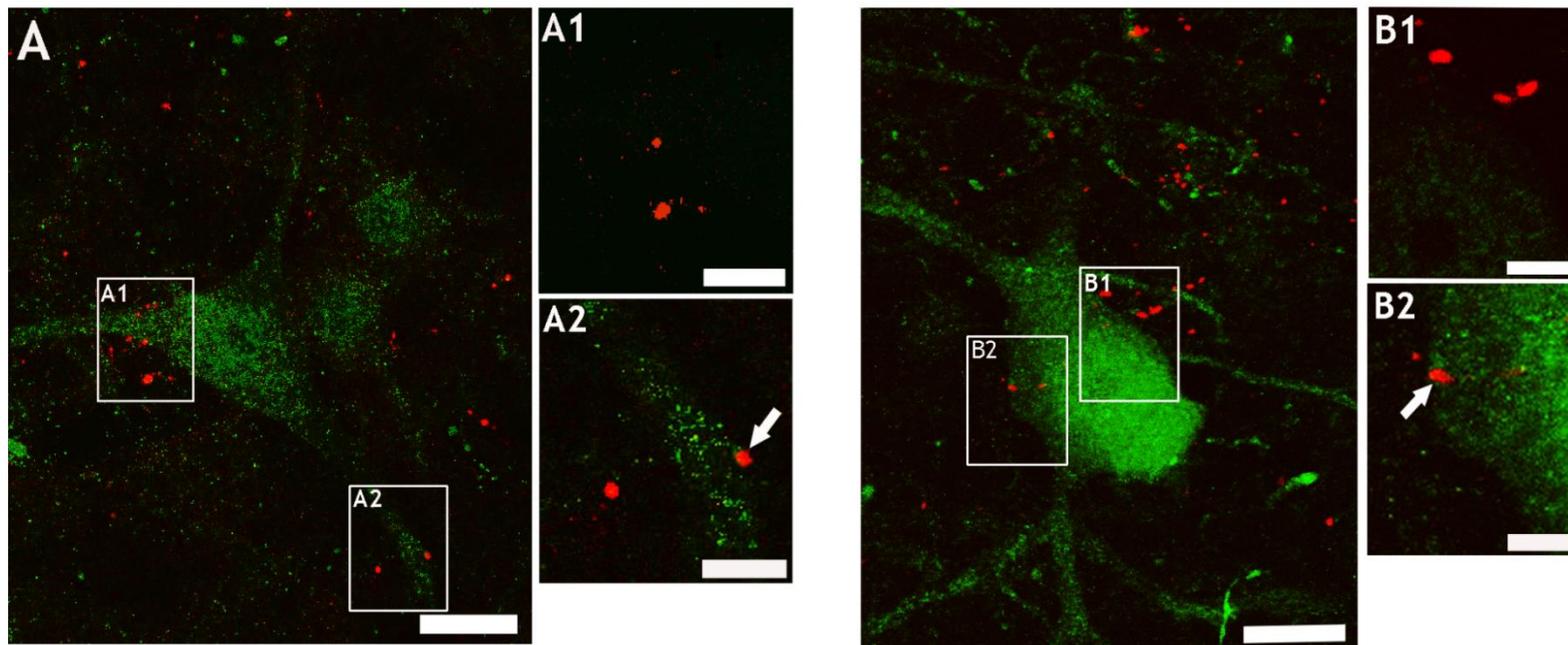
Figure 5-8 Examples of calretinin- expressing cells with contacts from CTb- labelled terminals

A: Projected confocal microscope image (35 optical sections, 0.5µm increments) from a sham rat showing terminals (red) within the vicinity of a calretinin- expressing cell (green). The majority of the terminals within the vicinity of the cell did not establish contact with the cell (inset **A1**), however one terminal made contact with a dendritic process (inset **A2**). **B:** A similar example is shown from a MCAo rat (56 optical sections, 0.5µm increments) whereby most CTb- labelled terminals within the cell territory did not make contact with the cell (**B1**), but a single terminal was found to make contact with the cell soma (**B2**). Both images are taken from the medial lamina VII. Arrows indicate terminals that established contacts with the cells. Scale bar in **A** & **B**= 20µm. Scale bar in insets =10µm
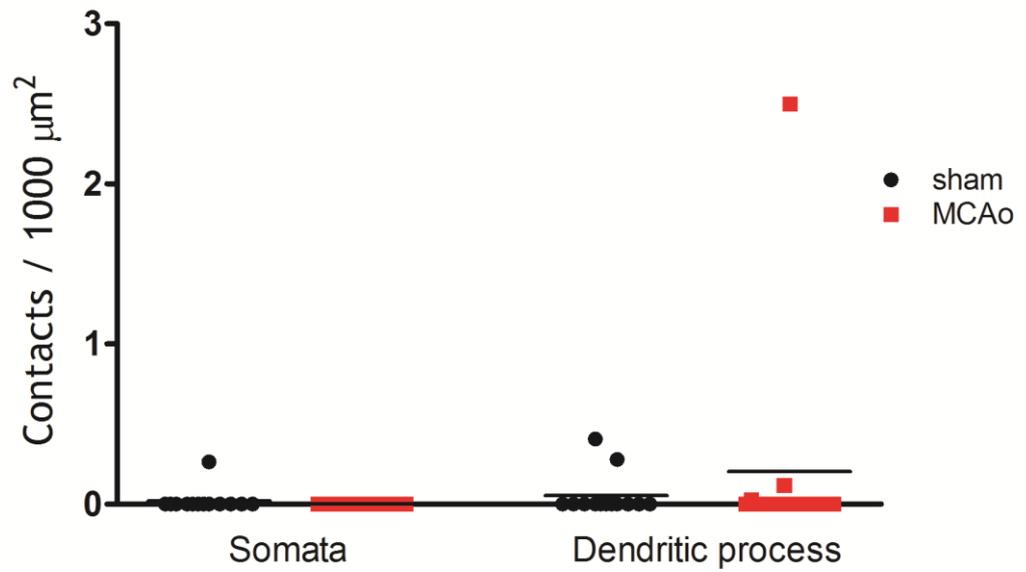
Figure 5-9 Density of CTb-labelled contacts to lamina VII/VIII calretinin-expressing cells

Each dot represents a cell (4-5 cells per rat; n = 3 sham and 3 MCAo rats). For both somata and dendritic processes, the mean density of contacts was not significantly different between sham (black) and MCAo (red) groups.

$p > 0.05$, Mann-Whitney test (analysis based on number of animals, not number of cells/sections)

5.4 Discussion

In this short exploratory study, the contact densities of CST terminals originating from the non-ischaemic hemisphere to ChAT, calbindin and calretinin-expressing cells located in the contralateral (unaffected) side of the cervical spinal cord of MCAo rats were not significantly different to that of shams.

It is likely that the rare number of contacts between CST axons and interneurons detected in this study were sites of synaptic interactions because (as reported in Chapter 4 **section 4.3.5**) the terminals expressed VGLUT-1 which is present in glutamatergic presynaptic boutons (Persson et al., 2006; Fremeau et al., 2001). To confirm that these contacts were synapses however, a combination of confocal and electron microscopy would have been required (Todd, 1997) because there is currently no reliable neurochemical marker for the identification of excitatory synapses. Nonetheless, the contact densities were not significantly different between sham and MCAo rats, thus the data from the current study do not support the hypothesis that the CST from the non-ischaemic hemisphere increases its connections with these three interneuron types at a time point associated with sensorimotor recovery after MCAo (28 days).

In accordance with Chakrabarty et al., (2009), a large number of terminals were found within the immediate vicinity of the somata and dendritic processes of ChAT- expressing partition cells in lamina X/medial lamina VII. However, in both sham and MCAo rats, the terminals rarely established contacts with these cells. This suggests that cholinergic partition cells are not major targets of the CST and that CST terminals must establish contacts with non-cholinergic cells in lamina X/medial lamina VII. This region of the grey matter is composed of a diverse population of interneurons important in motor coordination (Jankowska, 1992).

In both sham and MCAo groups, terminals were typically located outside the territory of calbindin and calretinin- expressing cells of medial lamina VII/VIII apart from a small proportion of cells in close proximity to the midline that received a very limited number of contacts. Cells that express these calcium-binding proteins are widely distributed throughout the spinal grey matter (Ren & Rudo, 1994; **Figure 5-5**) but the current study only focused on those located in medial laminae VII/VIII because a proportion of these cells are likely to be

commissural LDPNs (Brockett et al., 2012). Thus, it is possible that the CST targets calbindin and calretinin- expressing cells located in other spinal laminae, particularly the more dorsal areas.

An increased density of CST contacts onto ChAT/calbindin/calretinin- expressing cells after MCAo might have been predicted, because subpopulations of these cells are known to have commissural projections (Stepien et al., 2010; Brockett et al., 2012), and cells with commissural projections are postulated to provide an indirect route for information to be conveyed from the non-ischaemic hemisphere to the denervated (ipsilateral) side of the spinal cord after stroke (see Chapter 1 **section 1.3**). However, the ChAT, calbindin and calretinin-expressing cells examined in the current study make up a relatively small proportion of the total population of CINs and therefore, the possibility that the CST formed new/enhanced contacts with other types of CINs after MCAo cannot be excluded. Further experiments combining MCAo and anterograde CST terminal labelling with retrograde CIN labelling would allow for a more specific characterisation of CST termination patterns to such cell types. One way of testing for the formation of new intraspinal circuits involving CINs would be to inject forelimb muscles with a transsynaptic tracer then determine whether the tracer labelled the CINs of interest along with neurons in the motor cortex of the non-ischaemic hemisphere. This strategy has already been used to establish the presence of new intraspinal circuits after spinal cord injury (Bareyre et al., 2004; see Chapter 1 **section 1.2.2**).

To summarise, the numbers of CST contacts from the non-ischaemic hemisphere onto ChAT/calbindin/calretinin- expressing cells located in the contralateral (unaffected) side of the spinal cord in MCAo rats were not significantly altered compared to shams. However, because these cells only make up a small proportion of the total number of CINs, the possibility that the CST formed new/enhanced contacts with other types of CINs after MCAo cannot be ruled out. It would be useful to have a better understanding of how the CST and other supraspinal systems engage CIN populations in the intact animal, as this would provide a better insight into the systems that could be strengthened after MCAo so that the non-ischaemic hemisphere can gain control of the denervated (ipsilateral) limb.

Chapter 6

Characterisation of corticospinal and reticulospinal inputs to long descending propriospinal and intrasegmental commissural interneurons in the cervical spinal cord

6.1 Introduction

As discussed in Chapter 1 (**section 1.2.1**), numerous subpopulations of CINs have been characterised within the lumbar spinal cord (Matsuyama et al., 2004; Jankowska et al., 2003; Stokke et al., 2002; Bannatyne et al., 2003) but there is little information available on CINs located within the cervical spinal cord. In the rat, retrograde tracing has revealed that there are commissural (and uncrossed) LDPNs present in all cervical segments that project to rostral lumbar segments (L1-L3; Brockett et al., 2013; Reed et al., 2009; Chapter 1 **section 1.2.2**). These cells are implicated in the coordination of fore- and hindlimb function (Ballion et al., 2001; Juvin et al., 2005; Zaporozhets et al., 2006). Transsynaptic tracing in mice has shown that commissural (and uncrossed) LDPNs establish monosynaptic connections with hindlimb motor neurons (Ni et al., 2014). In the same study, Ni and colleagues reported commissural (and uncrossed) LDPNs to receive contacts from CST axons and brain-stem derived serotonergic axons, but the bouton numbers were very limited (0 to 2 per cell), so the authors concluded that these supraspinal pathways are not chief regulators of LDPNs in mice. However, in cats, commissural (and uncrossed) LDPNs were monosynaptically excited by stimulation of the contralateral medullary pyramid (and stimulation of the MLF and vestibular nuclei; Alstermark et al., 1987), suggesting that these cells are under direct influence from the CST (as well as the ReST and VST). The disagreement in the available literature warrants further examination of CST inputs to commissural LDPNs.

Intrasegmental CINs with axons confined to a single segment are postulated to be directly involved in the coordination of left-right homonymous muscles (Stokke et al., 2002; Quinlan & Kiehn, 2007; Kjaerulff & Kiehn, 1997; Chapter 1 **section 1.2.1**). Despite the proposed functional importance of intrasegmental CINs, information on these cells at the cervical level is currently lacking.

As discussed in Chapter 1 (**section 1.3 & 1.4.3**), neural pathways involving CINs might contribute to recovery following injury of the CST (e.g. after stroke), by providing indirect routes for information to be conveyed from the motor cortex of the uninjured hemisphere to the denervated (ipsilateral) side of the spinal cord (Jankowska & Edgley, 2006; Edgley et al., 2006). It is therefore important to have detailed maps of CINs and their inputs from different supraspinal

sources. The hypothetical neural pathways between the motor cortex and ipsilateral motor neurons examined in the current study are summarised in **Figure 6-1**.

The goal of the current study was to characterise CST and ReST contacts onto commissural LDPNs and intrasegmental CINs in the cervical spinal cord of the intact rat using anatomical tracing techniques. Descending axons were labelled anterogradely by injecting CTb into the right forelimb motor cortex and MLF to label CST and ReST axons, respectively. There are several components of the ReST (**Chapter 1 section 1.1.3**); this study focused upon axons projecting via the MLF because in electrophysiological studies it is possible to activate many ReST fibres via stimulation within this region which produces profound effects on networks involved in motor control (Jankowska et al., 2003; Edgley et al., 2004). Commissural LDPNs and intrasegmental CINs were labelled retrogradely by injecting FG into the right side of the intermediate grey matter of segments L1/L2 and C4/C5, respectively. The ReST is a complex pathway, whereby a single axon can innervate both sides of the grey matter (see Chapter 1 **section 1.1.2**; Matsuyama et al., 1999; Jankowska et al., 2003). Furthermore, because of the proximity of the MLF to the midline, tracer injection spreads to both sides of the MLF, thereby labelling ipsilateral and contralateral axonal projections from both the left and right sides of the MLF (Du Beau et al., 2012). This bilateral labelling of ReST terminals provided an opportunity to characterise ReST contacts to LDPNs located on both sides of the grey matter in order to examine whether the ReST differentially targets commissural versus uncrossed LDPNs. As discussed previously (Chapter 1 sections **1.1.1** & **1.1.2**), the CST is purely excitatory with all of its axons containing VGLUT-1; whereas ReST axons passing through the MLF are a heterogeneous population of excitatory and inhibitory axons with 59% of axons containing VGLUT-2 and 20% containing VGAT (Du Beau et al., 2012). Thus, the neurotransmitter phenotypes of contacts onto cells were investigated using antibodies against VGLUT-1 (CST) as well as VGLUT-2 and VGAT (ReST).
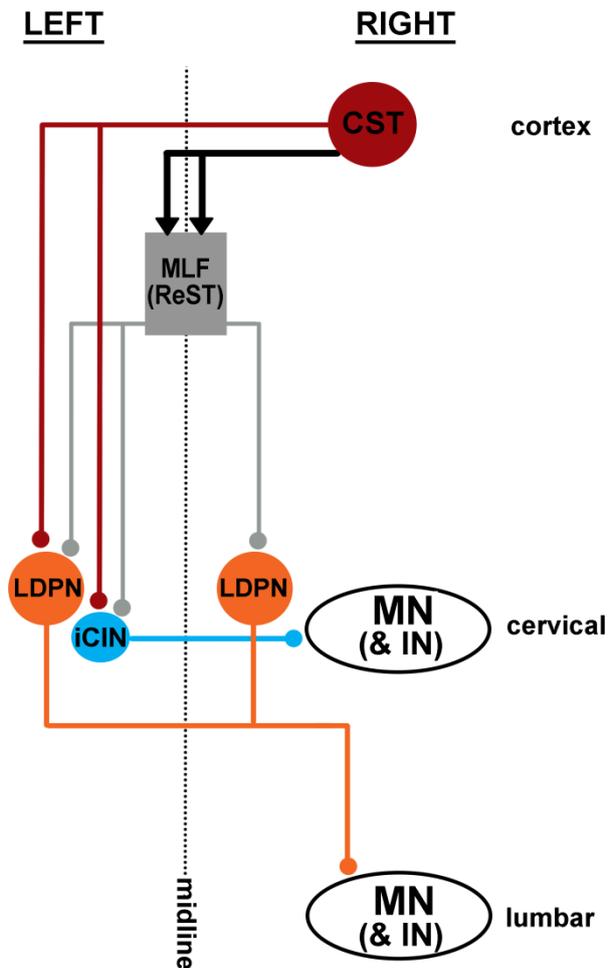
Figure 6-1 Hypothetical neural pathways between the motor cortex and ipsilateral motor neurons examined in the current study

One potential mechanism is via contralaterally projecting CST axons (red) influencing LDPNs (orange) and iCINs (blue), which in turn, project across to MNs and INs in the opposite side of the spinal cord. An alternative mechanism may involve corticobulbar axons (represented by black arrows) that influence ReST neurons (grey), which in turn, activate LDPNs or iCINs.

CST = corticospinal tract; ReST = reticulospinal tract; MLF = medial longitudinal fasciculus; LDPN = long descending propriospinal interneuron; iCIN = intrasegmental commissural interneuron; MN = motor neuron; IN = interneuron

Aims:

- To investigate whether LDPNs in the cervical spinal cord receive contacts from the CST and ReST and to examine the neurotransmitter phenotypes of these contacts

  - CST contacts were examined onto commissural LDPNs only

  - ReST contacts were examined onto both commissural and uncrossed LDPNs

- To investigate whether intrasegmental CINs in the cervical cord receive contacts from the CST and ReST and to examine the neurotransmitter phenotypes of these contacts

Hypotheses:

The CST will establish contacts with commissural LDPNs; and the ReST will establish contacts with both commissural and uncrossed LDPNs

Both the CST and ReST will establish contacts with intrasegmental CINs

6.2 Methods

6.2.1 Animals

A total of 12 male Sprague Dawley rats (250-300g) were used in this experiment. Six rats received FG injections into the right intermediate grey matter of the lumbar cord (L1/L2; to retrogradely label LDPNs) and CTb was injected either into the right forelimb motor cortex or the MLF (3 rats in each group). Six rats received FG injections into the right intermediate grey matter of the cervical cord (C4/C5; to retrogradely label intrasegmental CINs) and CTb was injected either into the right forelimb motor cortex or the MLF (3 rats in each group).

6.2.2 Anterograde labelling of CST and ReST axonal terminals

Following induction of anaesthesia (Chapter 2 **section 2.2.1**), the skull was drilled to expose the right forelimb motor cortex or MLF. Bregma was used as a stereotaxic reference point for cortical injections and the Interaural Line was used to target the MLF; see **Table 2-1** for the stereotaxic coordinates used for targeting each injection site. A micropipette containing 1% CTb was inserted into the brain at 4 standardised points (or 1 point for the MLF). At each point, 200nl of CTb was injected using a Pico Injector (World Precision Instruments, USA; see **Chapter 2 section 2.2.3**). The scalp was sutured and health status of the animal was closely monitored until termination.

6.2.3 Retrograde labelling of LDPNs and intrasegmental CINs

At 48 h after the brain injections, rats received a unilateral injection of FG into the intermedio-ventral grey matter of the right side of the lumbar (L1/L2) or cervical (C4/C5) spinal cord. The procedure is described in detail in Chapter 2 **section 2.2.4**. To retrogradely label LDPNs, the L1/L2 segment was targeted by counting down from the point of attachment of the lowest rib at T13; to retrogradely label intrasegmental CINs, the C4/C5 segment was targeted by counting down from the prominent spinous process of the C2 vertebra. A small burr hole (1mm diameter) was then made adjacent to the midline in the laminar surface to expose the dorsal surface of the L1/L2 (or C4/C5) segments of the spinal cord (right side). A unilateral spinal injection of 50nl was made with a micropipette containing 4% FG in distilled water. The tip was inserted at a depth of 1.5mm from the surface at an angle of 15° to target the intermediate grey matter of the right side of the spinal cord. The wound was sutured and animals closely monitored until termination.

6.2.4 Tissue processing

Four days following FG injection, rats were transcardially perfused with fixative (as described in Chapter **2 section 2.2.5**). The brain and spinal cord were removed and post-fixed over night at 4°C. To cryoprotect the brain, sucrose was added to the fixative (3g/10ml). The brain was then sectioned coronally (100μm) with a freezing microtome and spinal segments C4/C5 (and L1/L2 in rats with labelled LDPNs) were cut into transverse sections (60μm) with a Vibratome. All

cut sections were immediately placed in 50% EtOH (30 min) to enhanced antibody penetration.

6.2.5 Identification of brain and spinal injection sites

CTb injections sites in the cortex and MLF were revealed using DAB as a chromagen (see Chapter 2 **section 2.5**). Brain sections were incubated in goat anti-CTb for (48 h), and then biotinylated anti-goat IgG (3 h) followed by avidin-horsradish peroxidase (1 h). Finally H_2O_2 plus DAB was applied (10 min) for visualisation of CTb immunoreactivity. Sections were viewed under transmission light microscopy and digitally photographed (x5; AxioVision software). To confirm the anatomical location, injection sites were reconstructed onto coronal maps taken from a stereotaxic atlas (Paxinos & Watson, 2005) using Adobe Photoshop.

FG injection sites in L1/L2 (or C4/C5) could be directly visualised under a fluorescent microscope without any additional processing (as described in Chapter 2 **section 2.6**). Sections were digitally photographed (x5; AxioVision software) using an ultraviolet filter and in dark field. Photomicrographs were then superimposed onto spinal templates (based on Paxinos & Watson, 2005) using Adobe Photoshop in order to examine the segmental location of the injection site and spread of FG.

6.2.6 Immunolabelling of terminals and cells

Sections (60µm) from cervical segments C4/C5 were reacted for 72 h with the following primary antibody combinations: (a) anti- CTb, anti- FG and anti-VGLUT-1 for rats with CST labelling; (b) anti- CTb, anti- FG and ant- VGLUT-2 or anti- CTb, anti- FG, and anti- VGAT for rats with ReST labelling. Sections were then incubated in secondary antibodies coupled to Rhodamine red, Alexa 488 and Dylight 649 for 48h (**See Table 6-1**). Finally, sections were rinsed with PBS (3 x 10 min) and mounted with anti-face (Vectashield; see Chapter 2 **section 2.7** for detailed ICC steps.

6.2.7 Assessment of the laminar distribution pattern of labelled cells and terminals in the cervical spinal cord

For each rat, 2 transverse sections (60µm) from segment C4/C5 containing immunolabelled terminals (CTb) and cells (FG; above) were imaged (x10; AxioVision software) and the photomicrographs were superimposed onto spinal templates (taken from Paxinos & Watson, 2005). FG-labelled cells were recorded on the corresponding site on the template as a dot. CTb-labelled terminals were also mapped onto the templates to assess whether CST and ReST terminations were within the territory of the labelled LDPNs and intrasegmental CINs.

6.2.8 Confocal microscopy, reconstructions and analyses

Cells were scanned using a x40 oil-immersion lens (zoom factor of 2 at 0.5µm increments). If CTb-labelled terminals established contacts with a cell, the cell was reconstructed using Neurolucida Software (as described in Chapter 2 **section 2.8**) and contact density was expressed as the number of contacts per 100 µm^2 of neuronal surface. Contact densities were averaged for each rat so that an individual rat contributed only one value to the statistical analysis (see Chapter 2 **section 2.9**).

6.2.9 Statistical analysis

For all results shown in this chapter, statistical analysis is based on the number of animals (not the number of cells or number of sections) in order to avoid pseudoreplication (see Chapter 2 **section 2.9**). The data were analysed using non-parametric tests because the raw contact densities were skewed and failed the Shapiro-Wilk normality test. The Mann-Whitney test was used for individual comparisons of contact densities. The Kruskal-Wallis test was used to compare contact densities between cells located across different laminar boundaries. Data are expressed as means ± SD and differences are considered significant at $p < 0.05$.

	Primary antibody combination	Concentration	Supplier	Secondary antibody combination	Concentration	Sequential reaction
1	gt. CTb	1:5000	List Biological Laboratories, Campell, CA	Biotinylated IgG	1:500	Avidin HRP (1:1000) + DAB
2	gt. CTb	1:5000	List Biological Laboratories, Campell, CA	Rh. Red	1:100	
	rb. FG	1:5000	Chemicon/Millipore, CA, USA	Alexa 488	1:500	
	gp. VGLUT-1	1:5000	Millipore, Harlow, UK	Dylight 649	1:500	
3	gt. CTb	1:5000	List Biological Laboratories, Campell, CA	Rh. Red	1:100	
	rb. FG	1:5000	Chemicon/Millipore, CA, USA	Alexa 488	1:500	
	gp. VGLUT-2	1:5000	Chemicon/Millipore, CA, USA	Dylight 649	1:500	
4	gt. CTb	1:5000	List Biological Laboratories, Campell, CA	Rh. Red	1:100	
	rb. FG	1:5000	Chemicon/Millipore, CA, USA	Alexa 488	1:500	
	mo. VGAT	1:1000	Chemicon/Millipore, CA, USA	Dylight 649	1:500	

Table 6-1 Summary of primary and secondary antibody combinations and concentrations used in the current experiment

1. For the visualisation of the CTb injection site in the brain. **2.** For the assessment of CST contacts to cells. **3.** For the assessment of excitatory ReST contacts to cells. **4.** For the assessment of inhibitory ReST contacts to cells.

rb = rabbit; gt = goat; gp = guinea pig; mo = mouse; Rh.Red= Rhodamine red

6.3 Results

6.3.1 CST and ReST contacts to LDPNs

6.3.1.1 *Injection sites*

Figure 6-2 shows the CTb injection sites in the cortex and corresponding FG injection sites in the lumbar cord (L1/L2) for each rat. The CTb injection sites were focussed within the primary and secondary motor cortex and the adjacent primary sensory cortex and they were confined to the right hemisphere (**Figure 6-2A**). The FG injections were confined to L1/L2, and injection sites were present in the grey matter in all three rats, although the precise location varied with the core of the injection being in the intermediate grey matter for 1 rat, and slightly more dorsal 2 rats (**Figure 6-2B**). In all rats, there was considerable spread of FG within the grey matter ipsilateral to the injection sites but there was no spread to the contralateral grey matter.

Figure 6-3 shows the CTb injection sites into the MLF and corresponding FG injection sites into the lumbar cord (L1/L2) of each rat. The micropipette for the MLF injections was placed in the right side (**Table 2-1**) but due to the proximity of the MLF to midline, CTb labelling was visualised in both sides of the MLF (**Figure 6-3A**). There was some spread of CTb into the raphe obscurus and tectospinal tract. The FG injections into the lumbar spinal cord were confined to L1/L2, with core of the injection site being in the intermedio-ventral grey matter for all three rats, and spread confined to the grey matter ipsilateral to the injection sites (**Figure 6-3B).**
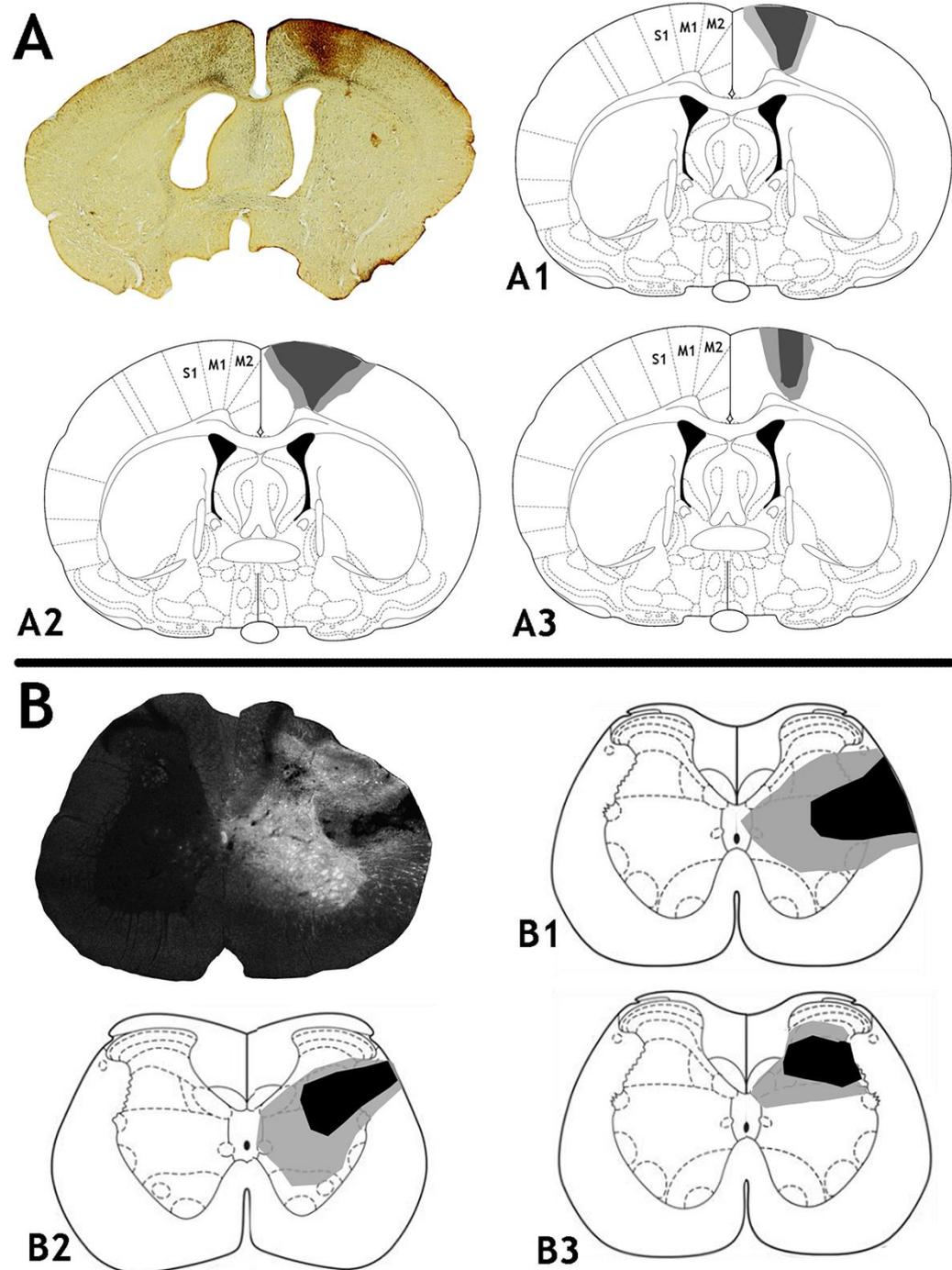
Figure 6-2 CTb tracer injection sites in the cortex (right) and FG tracer injection sites in the lumbar spinal cord (right) of each rat

 A: A representative CTb injection site revealed with an immunoperoxidase reaction. **A1**, **A2**, **A3** are reconstructions of injection sites for each rat on brain templates (taken from Paxinos & Watson, 2005; -0.5mm relative to Bregma). The darkest shading represents the core of the injection and lighter shading represents spread beyond the core. **B:** A representative fluorescence/dark field micrograph showing a FG injection site within a transverse section of the lumbar spinal cord (L2). **B1**, **B2**, **B3** are reconstructions of injection sites for each rat on spinal templates (based on Paxinos & Watson, 2005). The core of the injection is shown in black and the spread shown in grey.
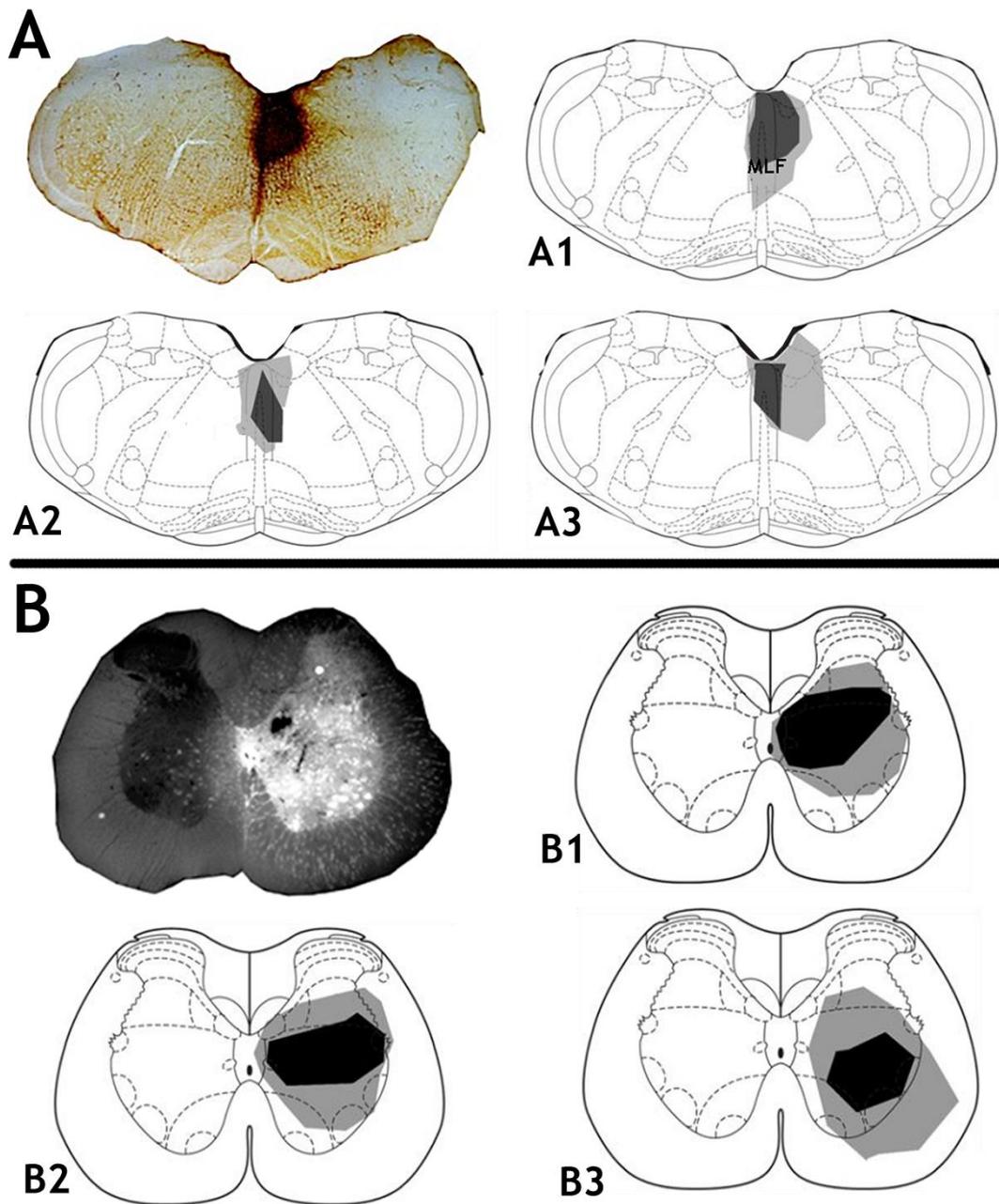
FIgure 6-3 CTb tracer injection sites in the MLF and FG injection sites in the lumbar spinal cord (right) of each rat

A: A representative CTb injection site revealed with an immunoperoxidase reaction. **A1**, **A2**, **A3** are reconstructions of injection sites for each rat on brain templates (taken from Paxinos & Watson, 2005; -12.6mm from Bregma). The darkest shading represents the core of the injection and lighter shading represents spread beyond the core. **B:** A representative fluorescence/dark field micrograph showing a FG injection site within a transverse section of the lumbar spinal cord (L2). **B1**, **B2**, **B3** are reconstructions of injection sites for each rat on spinal templates (based on Paxinos & Watson, 2005). The core of the injection is shown in black and the spread shown in grey.

6.3.1.2 Laminar distribution pattern of LDPNs in relation to CST and ReST terminals in the cervical cord

Figure 6-4 shows the laminar distribution pattern of LDPNs in relation to CST and ReST terminals in segment C5 for all rats. The distribution of FG-labelled LDPNs within the grey matter was similar for all rats despite some variation in the location of the FG-injection sites (see above). The largest numbers of cells were found in laminae VII and VIII both contralateral and ipsilateral to the L1/L2 injection site; however the contralateral cells tended to be concentrated in the medial region of laminae VII unlike the ipsilateral cells which were more evenly distributed throughout the intermediate grey matter. LDPNs were relatively large cells, with a mean surface area (μm^2) of 1313 ± 720 and 6337 ± 3200 for the somata and dendritic processes, respectively. CTb-labelled CST terminals were mainly found in the side of the grey matter contralateral to the cortical injection site (and contralateral to the L1/L2 FG injection site). As shown in **Figures 6-4A to 4D**, CST terminals were concentrated medially in laminae IV to VI which is dorsal to most LDPNs. However, a moderate number of CST terminals were also found in laminae VI to VII, within the same territory as LDPNs. CTb-labelled ReST terminals were distributed bilaterally and were numerous through the deep dorsal horn, intermediate grey matter and ventral horn (**Figure 6-4E to H**); thus, on examination of the overall laminar distribution of cells and terminals, there were more ReST than CST terminals within the vicinity of LDPNs.
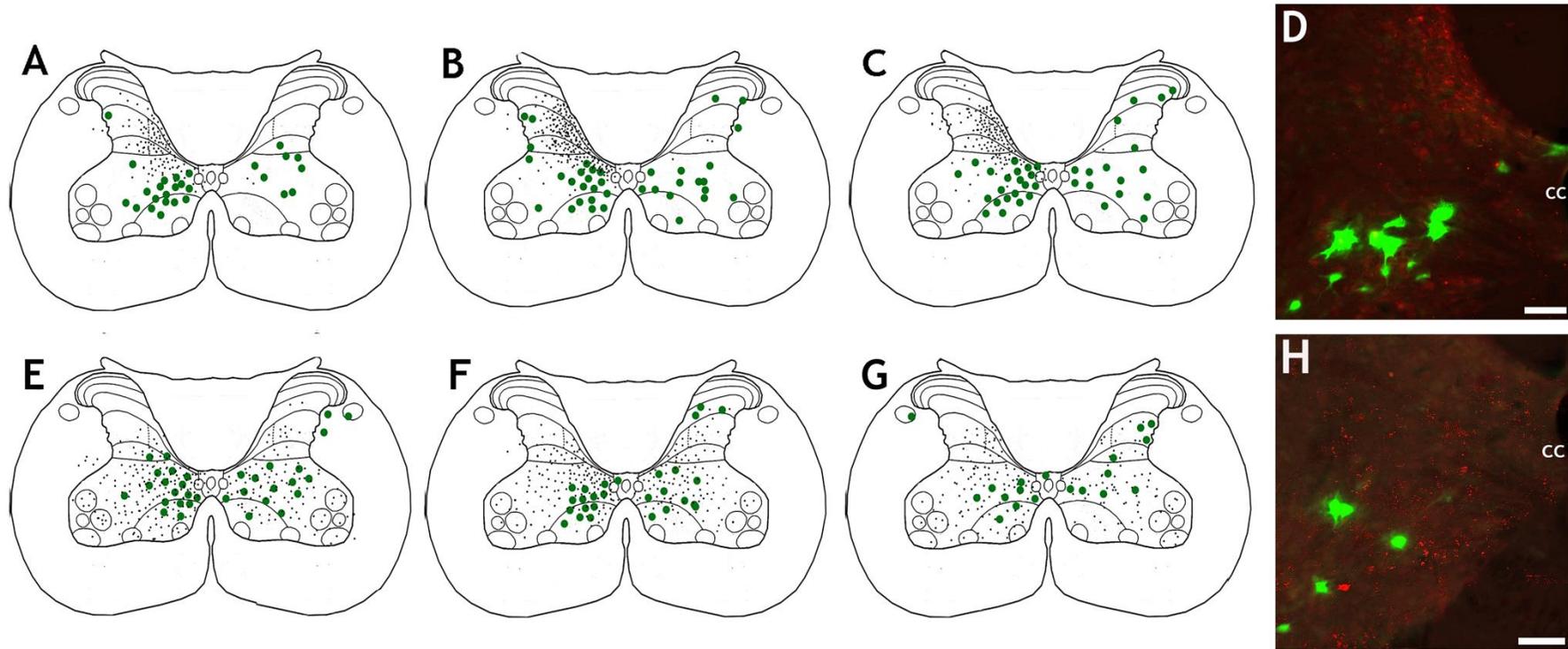
Figure 6-4 Distribution of LDPNs and axonal terminals in the cervical spinal cord (C5)

A, B, C: Laminar distribution of FG-labelled LDPNs (green) in association with CTb-labelled CST terminals (black) for each rat. Note that most CST terminals were located in medial laminae IV to VI, but a moderate number were also located in deeper laminae, within the territory occupied by LDPNs. Each representation was made from two 60μm spinal sections. **D**: Photomicrograph of LDPNs (green) and CST terminals (red) taken from the grey matter contralateral to the lumbar injection site. **E, F, G**: Laminar distribution of FG-labelled LDPNs (green) in association with CTb-labelled ReST terminals (black) for each rat. Note that ReST terminals were much more evenly distributed throughout the grey matter in comparison to CST terminals and many ReST terminals were located within the territory of LDPNs. **H:** Photomicrograph of LDPNs (green) and ReST terminals (red) taken from the grey matter contralateral to the lumbar injection site (Scale bar = 50μm). CC = central canal

6.3.1.3 Density of CST and ReST contacts onto LDPNs

To examine CST inputs to commissural LDPNs, a total of 32 retrogradely labelled cells (9-12 cells per rat) were imaged. A moderate number of CTb-labelled CST terminals were found within the immediate vicinity of commissural LDPNs, particularly for those cells located in medial lamina VII; however, a very limited number of these terminals were found to establish contacts with the cells. **Figure 6-5** shows an example of a commissural LDPN with numerous CTb-labelled terminals within its immediate territory, but only 2 of the terminals were found to establish contacts with the cell. As shown in **Table 6-2**, all of the detected CTb-labelled contacts to commissural LDPNs were immunoreactive for VGLUT-1.

	No. cells reconstructed	CTb contacts (total)	VGLUT-1^{+CTb} contacts	% VGLUT-1
Rat 1	12	5	5	100
Rat 2	11	5	5	100
Rat 3	9	7	7	100

Table 6-2 Immunoreactive contacts from the sensorimotor cortex to commissural LDPNs in cervical segment C5

Note that for each rat, all of the CTb-labelled contacts were immunoreactive for VGLUT-1.

The mean number of CTb-labelled CST contacts per 100μm^2 of neuronal surface was higher for the dendritic processes (0.02 ± 0.03) compared to the somata (0.005 ± 0.01) (**Figure 6-6A**) but this difference was not statistically significant (p>0.05). In order to examine whether the CST targets commissural LDPNs located within specific regions of the grey matter, the CTb-labelled contact densities onto cells located within different laminar boundaries were compared. There were no significant differences in the density of contacts to cells located in different laminae for both the somata (**Figure 6-6B**) and dendritic processes (**Figure 6-6C**) (p>0.05).
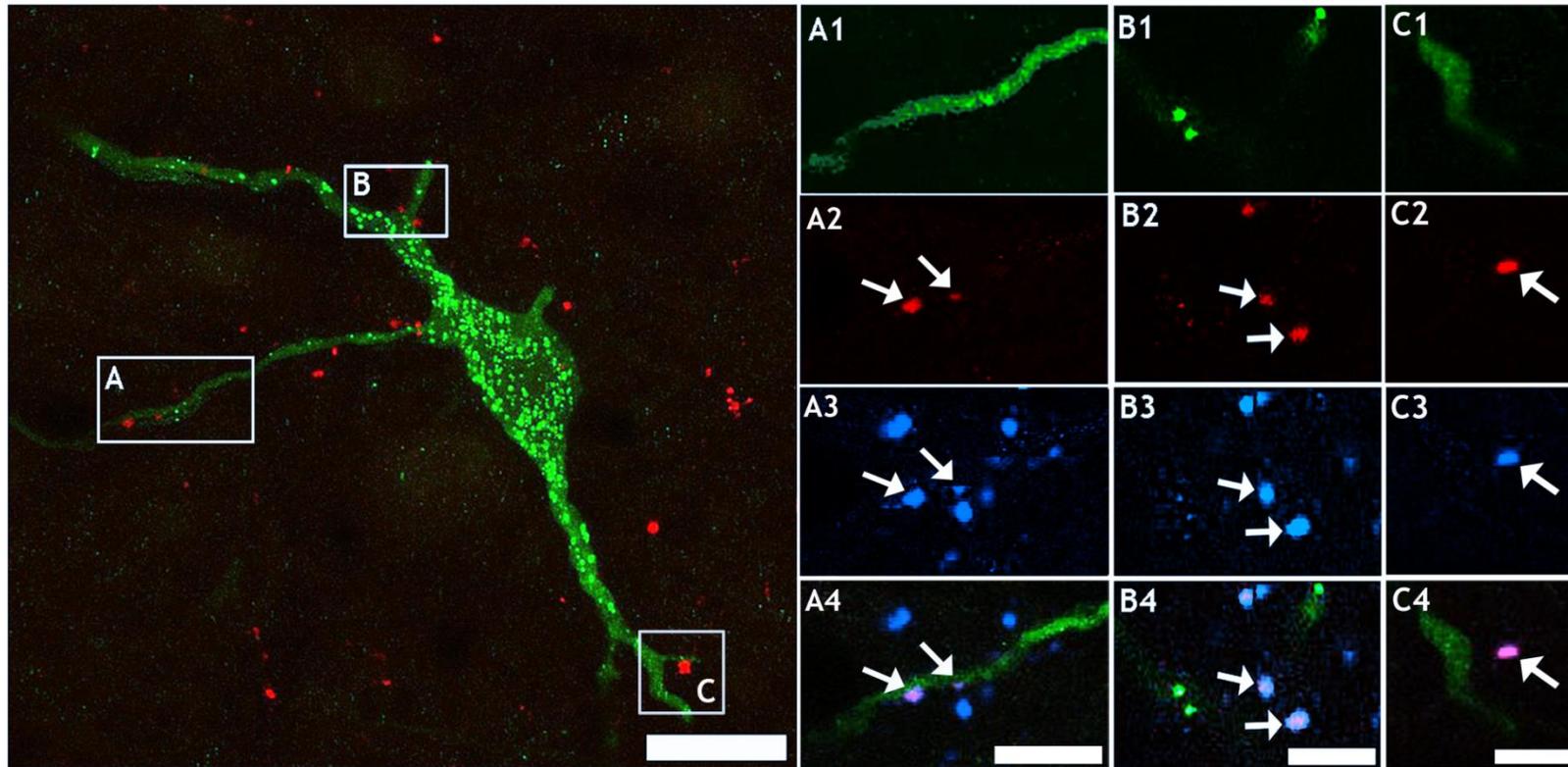
Figure 6-5 CST contacts onto a commissural LDPN in cervical segment C5

A projected confocal microscope image (44 optical sections, 0.5µm increments) of a FG-labelled LDPN (green) and CTb-labelled CST terminals (red) taken from the medial region of lamina VII (contralateral to the L1/L2 injection site). Scale bar = 20µm. Insets are single optical sections: **A1** to **A4** correspond to the region demarcated in **A**; insets **B1** to **B4** correspond to the region demarcated in **B**; insets **C1** to **C4** correspond to the region demarcated in **C**. **A1**, **B1**, **C1** show immunoreactivity for FG; **A2**, **B2**, **C2** show immunoreactivity for CTb; **A3**, **B3**, **C3** show immunoreactivity for VGLUT-1; **A4**, **B4**, **C4** are merged images. This LDPN was found to have a total of two CST contacts, shown in **A**. The remaining terminals found within the immediate vicinity of the cell did not establish contacts with the cell and examples are shown in **B** and **C**. CTb-labelled terminals are indicated by arrows. Scale bar = 5µm.
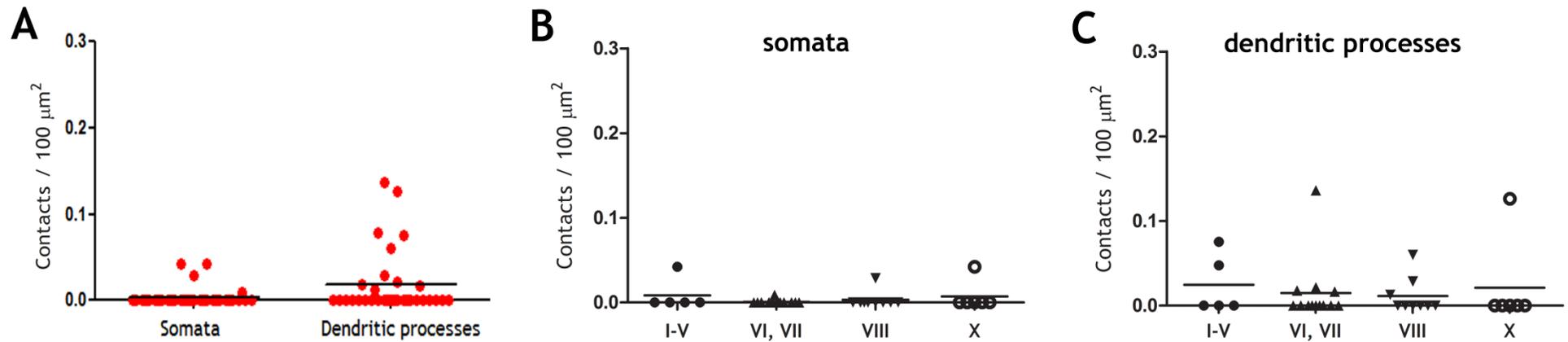
Figure 6-6 Density of CTb-labelled CST contacts to commissural LDPNs in cervical segment C5

A: Density of CTb-labelled CST contacts to commissural LDPNs. Each data point represents a cell (9-12 cells per rat; n = 3 rats). The contact densities tended to be higher for dendritic processes compared to the somata but this difference was not statistically significant (p>0.05, Mann-Whitney test). **B**, **C**: The Kruskal-Wallis test compared contact densities to cells located in different laminae of Rexed (based on Molander, 1989). For both somata (**B**) and dendritic processes (**C**), there were no significant differences in contact densities between cells located in different laminar boundaries (p > 0.05).

(All analysis based on number of animals, not number of cells/ sections)

To examine excitatory ReST contacts to LDPNs, a total of 36 cells (18 contralateral and 18 ipsilateral to the L1/L2 injection site) were imaged. An extensive number of CTb-labelled ReST terminals were detected within the immediate vicinity of both commissural and uncrossed LDPNs and many of these terminals were found to establish excitatory (VGLUT-2 immunoreactive) contacts with the cells. **Figure 6-7** shows an example of a cell with numerous excitatory (VGLUT-2 immunoreactive) ReST contacts. As summarised in **Table 6-3**, the majority of ReST contacts to both commissural (78.9 ±4.7%) and uncrossed (73.4 ± 8%) LDPNs were immunoreactive for VGLUT-2.

		No. cells reconstructed	CTb contacts (total)	VGLUT-2^{+CTb}	% VGLUT-2
Commissural LDPNs	Rat 1	7	356	283	79.49
	Rat 2	6	81	60	74.07
	Rat 3	5	84	70	83.33
Mean					**78.9**
SD					**4.7**
Uncrossed LDPNs	Rat 1	5	262	171	65.27
	Rat 2	7	102	75	73.53
	Rat 3	6	299	243	81.27
Mean					**73.4**
SD					**8**

Table 6-3 Excitatory immunoreactive contacts from the MLF to commissural and uncrossed LDPNs in cervical segment C5

Note that for both commissural and uncrossed LDPNs, the majority of CTb-labelled contacts were immunoreactive for VGLUT-2.

The contact densities for all of the 36 reconstructed LDPNs are shown in **Figure 6-8A**; for the somata, the mean overall number of CTb-labelled terminals per 100µm^2 of neuronal surface was 0.75 ± 0.83 and the mean number of CTb-labelled terminals that contained VGLUT-2 (VGLUT-2^{+CTb}) was 0.53 ± 0.64; for the dendritic processes, the mean total number of CTb-labelled terminals per 100µm^2 of neuronal surface was 0.42 ± 0.34 and the mean number of CTb-labelled terminals that contained VGLUT-2 (VGLUT-2^{+CTb}) was 0.30 ± 0.27. The mean contact densities were higher for the somata versus dendritic processes but these differences were not statistically significant (p>0.05). In order to examine whether excitatory ReST axons target LDPNs located within specific areas of the grey matter, the VGLUT-2^{+CTb} contact densities onto cells located

within different laminar boundaries were compared. However there were no significant differences in the density of contacts to cells of different laminae for both the somata (**Figure 6-8B**) and dendritic processes (**Figure 6-8C**) (p>0.05). To assess whether the excitatory ReST axons differentially target commissural versus uncrossed LDPNs, VGLUT-2^{+CTb} contact densities onto cells located on the either side of the spinal cord were compared. However, the density of contacts onto somata (**Figure 6-9A**) and dendritic processes (**Figure 6-9B**) did not vary between neurons located contralateral versus ipsilateral to the L1/L2 injection site (p>0.05).
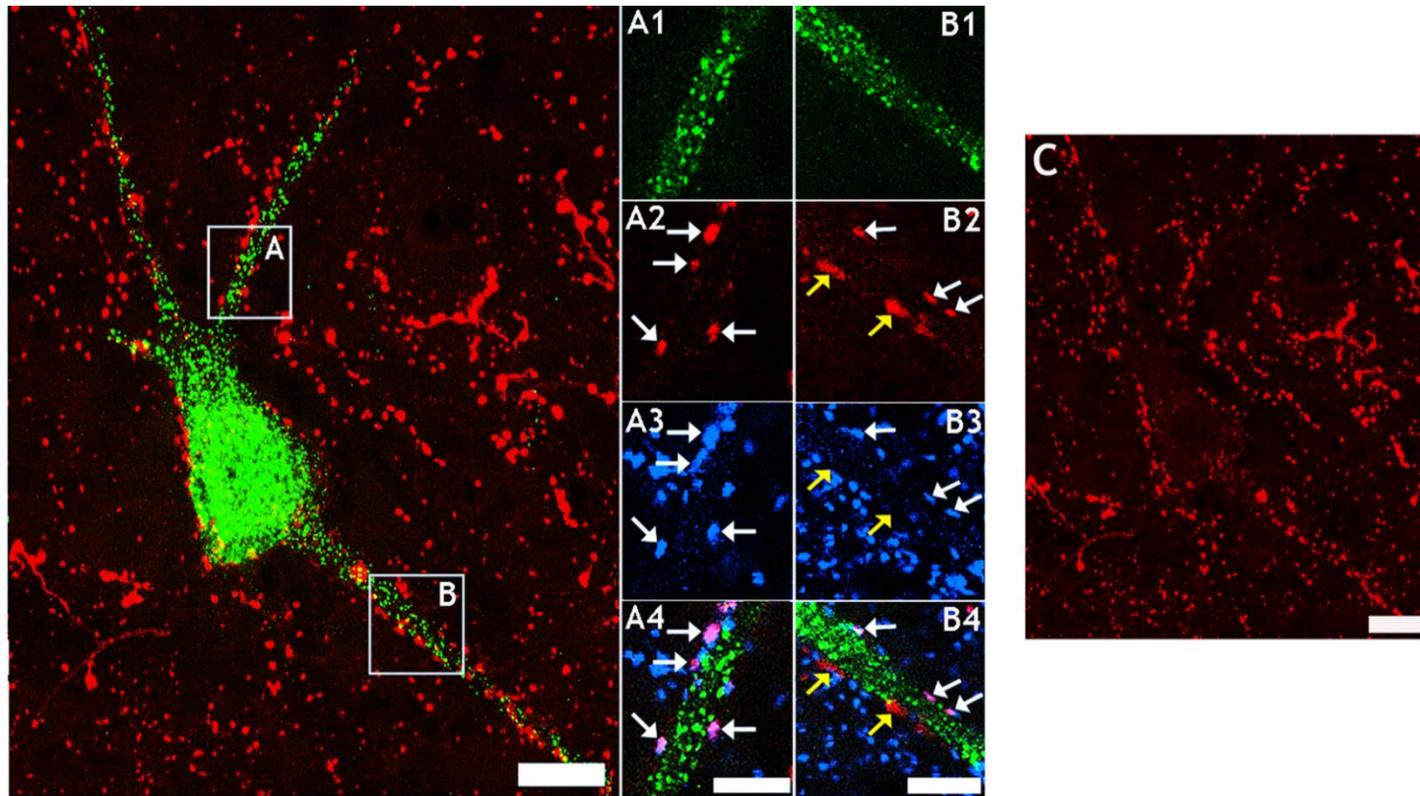
Figure 6-7 Excitatory ReST inputs onto a LDPN in cervical segment C5

A projected confocal microscope image (39 optical sections, 0.5μm increments) of a FG-labelled cell (green) and CTb-labelled ReST terminals (red) taken from the medial region of lamina VII (contralateral to the L1/L2 injection site). Scale bar = 20μm. Insets are single optical sections: **A1** to **A4** correspond to the region demarcated in **A**. **B1** to **B4** correspond to the region demarcated in **B**. **A1**, **B1** show immunoreactivity for FG; **A2**, **B2** show immunoreactivity for CTb; **A3**, **B3** show immunoreactivity for VGLUT-2; **A4**, **B4** are merged images. This LDPN has 123 ReST contacts in total and 103 of these contacts were immunoreactive for VGLUT-2. White arrows indicate CTb-labelled contacts that are immunoreactive for VGLUT-2. Yellow arrows indicate CTb-labelled contacts that are negative for VGLUT-2. Scale bar = 10μm. The projected confocal microscope image for the CTb-labelled ReST terminals only is shown in panel **C**. This image highlights the extensive number of contacts to the cell, because even though the cell (FG-immunoreactivity) is absent, the outline of the cell can still be seen as it is demarcated by terminals. Scale bar = 20μm
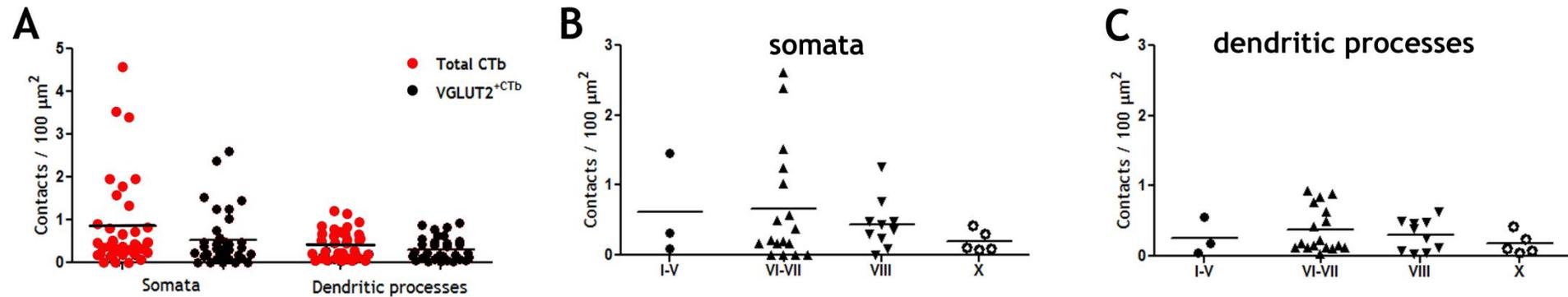
Figure 6-8 Density of excitatory ReST contacts to LDPNs in cervical segment C5

A: Density of ReST contacts to LDPNs reported as total CTb-labelled contacts (red) and CTb-labelled contacts immunoreactive for VGLUT-2 (VGLUT2[+CTb]; black). Each data point represents a cell (10-12 per rat; n = 3 rats). Contact densities tended to be higher for somata compared to dendritic processes but these differences were not statistically significant (p>0.05, Mann-Whitney test). **B**, **C**: The Kruskal-Wallis test compared VGLUT2[+CTb] contact densities on cells located in different laminae of Rexed (based on Molander, 1989). For both somata (**B**) and dendritic processes (**C**), there were no significant differences in contact densities between cells located in different laminar boundaries (p > 0.05).

(All analysis based on number of animals, not number of cells/ sections)
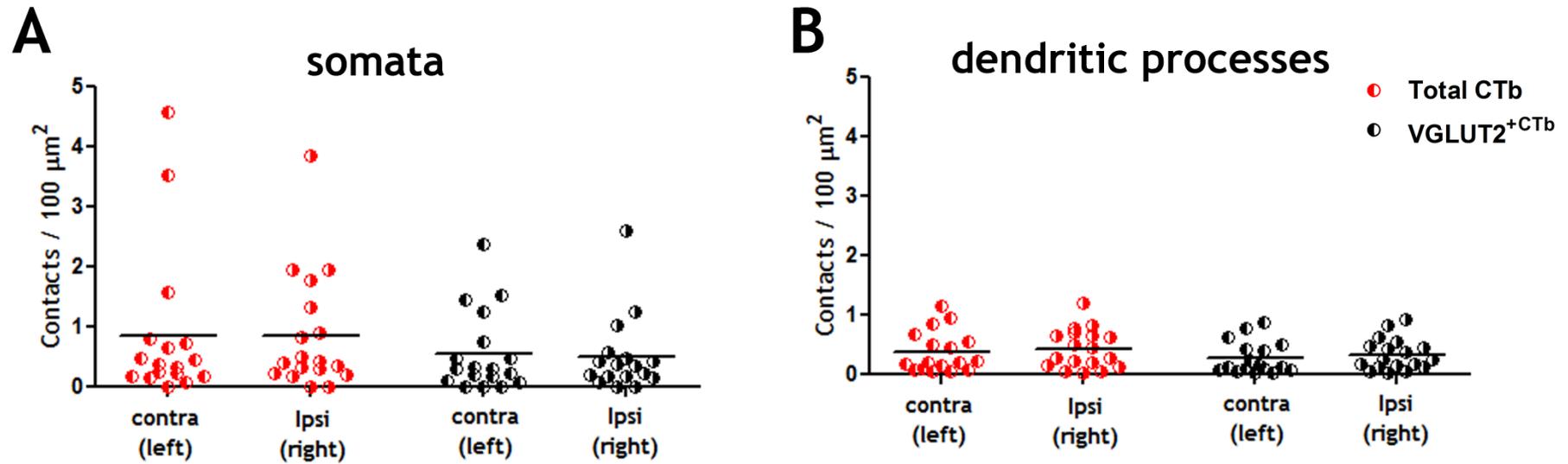
Figure 6-9 Densities of excitatory ReST contacts onto commissural (contralateral to the L1/L2 injection site) versus uncrossed (ipsilateral to the L1/L2 injection site) LDPNs in cervical segment C5

The densities of contacts onto somata **(A)** and dendritic processes (**B**) did not vary between LDPNs located contralateral or ipsilateral to the FG-L1/L2 injection site (p>0.05, Mann-Whitney). Each dot represents a cell (5-7 cells per rat; n = 3 rats)

(All analysis based on number of animals, not number of cells/ sections)

To examine inhibitory ReST contacts to LDPNs, a total of 33 cells (20 contralateral and 13 ipsilateral to the L1/L2 injection site) were imaged. An extensive number of CTb-labelled ReST terminals were detected within the immediate vicinity of both contralateral and ipsilateral LDPNs and some of these terminals were found to establish inhibitory (VGAT immunoreactive) contacts with the cells. **Figure 6-10** shows an example of a cell with inhibitory (VGAT immunoreactive) ReST contacts. As summarised in **Table 6-4**, a small proportion of ReST contacts to both commissural (20.1 ± 2.7%) and uncrossed (19.7 ± 2.3%) LDPNs were immunoreactive for VGAT.

		No. cells reconstructed	CTb contacts (total)	VGAT $^{+CTb}$	% VGAT
Commissural LDPNs	Rat 1	8	733	169	23.06
	Rat 2	5	72	14	19.44
	Rat 3	7	427	76	17.80
Mean					**20.1**
SD					**2.7**
Uncrossed LDPN	Rat 1	4	32	8	22.22
	Rat 2	5	62	12	19.35
	Rat 3	4	91	16	17.58
Mean					**19.7**
SD					**2.3**

Table 6-4 Inhibitory immunoreactive contacts from the MLF to commissural and uncrossed LDPNs in cervical segment C5

Note that for both commissural and uncrossed LDPNs, a sizeable minority of CTb-labelled contacts were immunoreactive for VGAT

The contact densities for all of the 33 reconstructed LDPNs are shown in **Figure 6-11A**; for the somata, the mean total number of CTb-labelled terminals per $100\mu m^2$ of neuronal surface was 0.99 ± 1.1 and the mean number of CTb-labelled terminals that contained VGAT (VGAT^{+CTb}) was 0.24 ± 0.33; for the dendritic processes, the mean total number of CTb-labelled terminals per $100\mu m^2$ of neuronal surface was 0.48 ± 0.64 and the mean number of CTb-labelled terminals that contained VGAT (VGAT^{+CTb}) was 0.08 ± 0.10. The mean contact densities were higher for the somata versus dendritic processes and these differences were not statistically significant (p>0.05). In order to examine whether inhibitory ReST axons target LDPNs located within specific areas of the grey matter, the CTb-labelled contact densities onto cells located within

different laminar boundaries were compared. However there were no significant differences in the density of contacts to cells of different laminae for both the somata (**Figure 6-11B**) and dendritic processes (**Figure 6-11C**) (p>0.05). To assess whether the inhibitory ReST axons differentially target contralaterally (commissural) versus ipsilaterally projecting LDPNs, VGAT^{+CTb} contact densities onto cells located on the either side of the spinal cord were compared. However, the density of contacts onto somata (**Figure 6-12A**) and dendritic processes (**Figure 6-12B**) did not vary between neurons located contralateral or ipsilateral to the L1/L2 injection site (p>0.05).
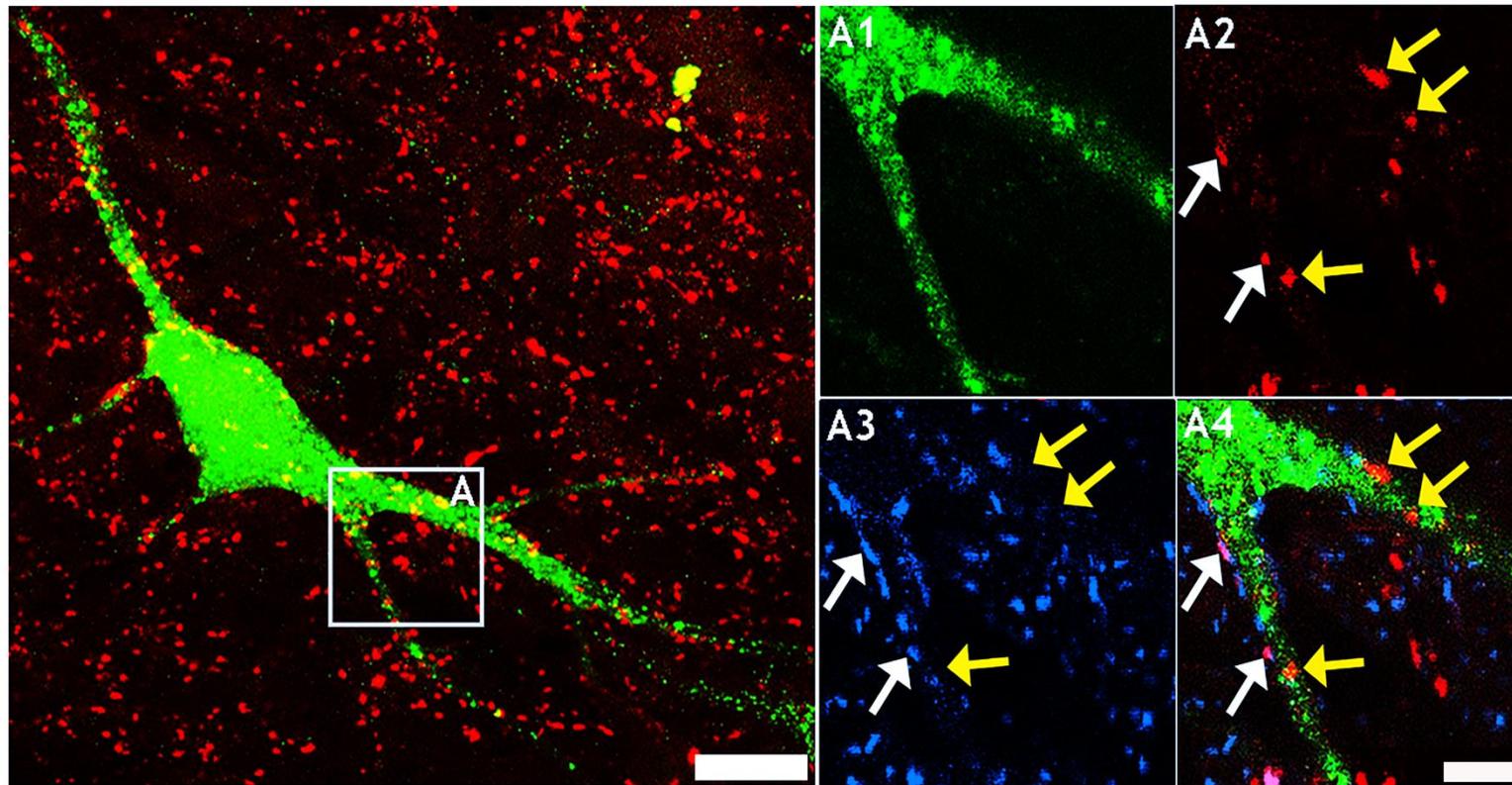
Figure 6-10 Inhibitory ReST contacts onto a LDPN in cervical segment C5

A projected confocal microscope image (54 optical sections, 0.5µm increments) of a FG-labelled cell (green) and CTb-labelled ReST terminals (red) taken from the medial region of lamina VII (contralateral to the L1/L2 injection site). Scale bar = 20µm. Insets **A1** to **A4** are single optical sections and correspond to the region demarcated in **A.** **A1** shows immunoreactivity for FG; **A2** shows immunoreactivity for CTb; **A3** shows immunoreactivity for VGAT; **A4** is a merged image. This LDPN has 117 ReST contacts in total and 28 of these contacts were immunoreactive for VGAT. White arrows indicate CTb-labelled contacts immunoreactive for VGAT; yellow arrows indicate CTb-labelled contacts negative for VGAT. Scale bar = 5µm.
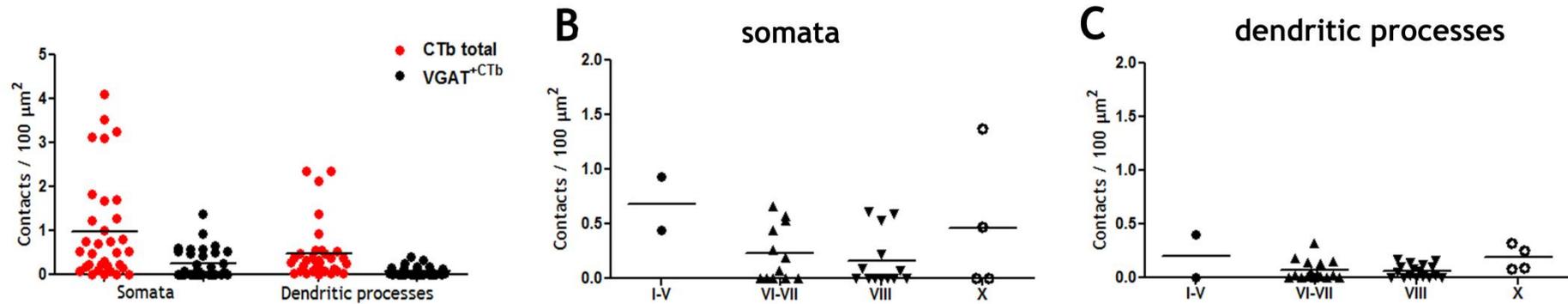
Figure 6-11 Density of inhibitory ReST contacts to LDPNs in cervical segment C5

A: Density of ReST contacts to LDPNs reported as total CTb-labelled contacts (red) and CTb-labelled contacts immunoreactive for VGAT (VGAT[+CTb]; black). Each data point represents a cell (10-12 cells per rat; n = 3). Contact densities tended to be higher for somata compared to dendritic processes but these differences were not statistically significant (p>0.05, Mann-Whitney test). **B**, **C**: The Kruskal-Wallis test compared VGAT[+CTb] contact densities on cells located in different laminae of Rexed (based on Molander, 1989). For both somata (**B**) and dendritic processes (**C**), there were no significant differences in contact densities between cells located in different laminar boundaries (p > 0.05).

(All analysis based on number of animals, not number of cells/ sections)
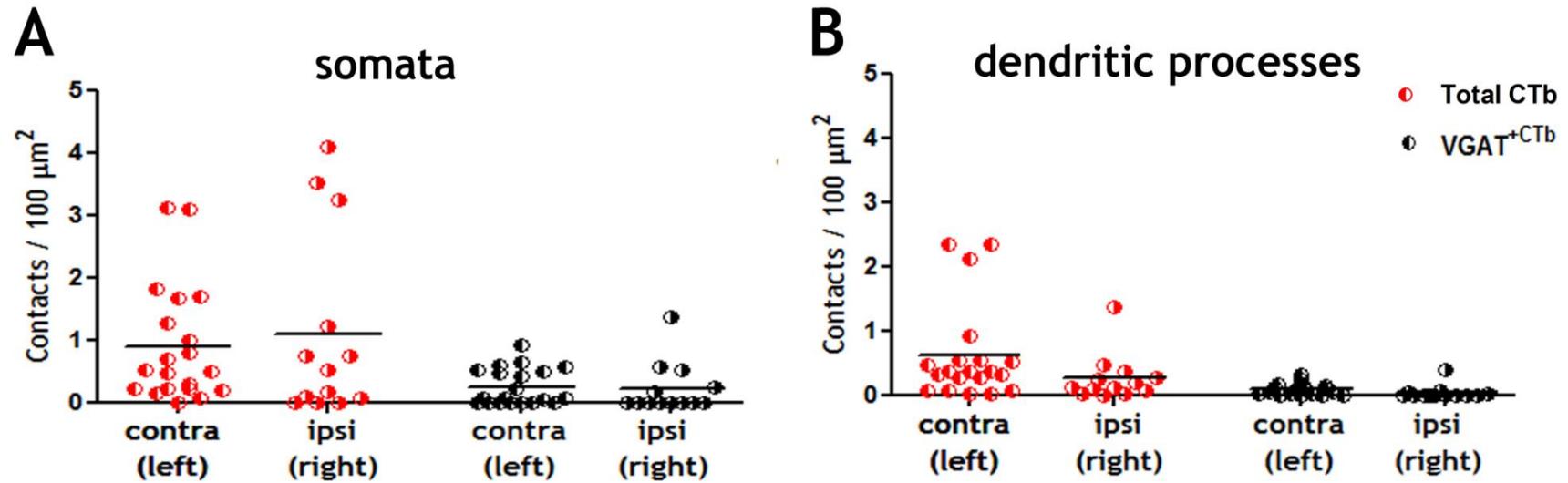
Figure 6-12 Densities of inhibitory ReST contacts onto commissural (contralateral to the L1/L2 injection site) versus uncrossed (ipsilateral to the L1/L2 injection site) LDPNs in cervical segment C5

The densities of contacts onto somata **(A)** and dendritic processes (**B**) did not vary between LDPNs located contralateral or ipsilateral to the FG-L1/L2 injection site (p>0.05, Mann-Whitney). Each dot represents a cell (4-8 per rat; n = 3 rats).

(All analysis based on number of animals, not number of cells/ sections)

6.3.2 CST and ReST contacts to intrasegmental CINs

6.3.2.1 Injection sites

Figure 6-13 shows the CTb injection sites into the cortex and the corresponding FG injection sites into the cervical cord (C4/C5) for each rat. The CTb injection sites were focussed within the primary and secondary motor cortex and the adjacent primary sensory cortex and were confined to the cortex of the right hemisphere (**Figure 6-13A**). The FG injections were confined to C4/C5. Although there was some variation in the location of the injection site, the injection site was present in the grey matter of all three rats with considerable spread of FG within the grey matter ipsilateral to the injection site and no spread into the contralateral grey matter (**Figure 6-13B**).

Figure 6-14 shows the CTb injection sites into the MLF and corresponding FG injection sites into the cervical cord (C4/C5) of each rat. In the MLF CTb labelling was visualised bilaterally (**Figure 6-14A**) and there was some spread of CTb into the raphe obscurus and tectospinal tract. The FG injections were confined to C4/C5; for all three rats, the core of the FG injection site was within the grey matter and there was considerable spread of FG within the grey matter ipsilateral to the injection site but there was no spread of FG into the contralateral grey matter (**Figure 6-14B).**
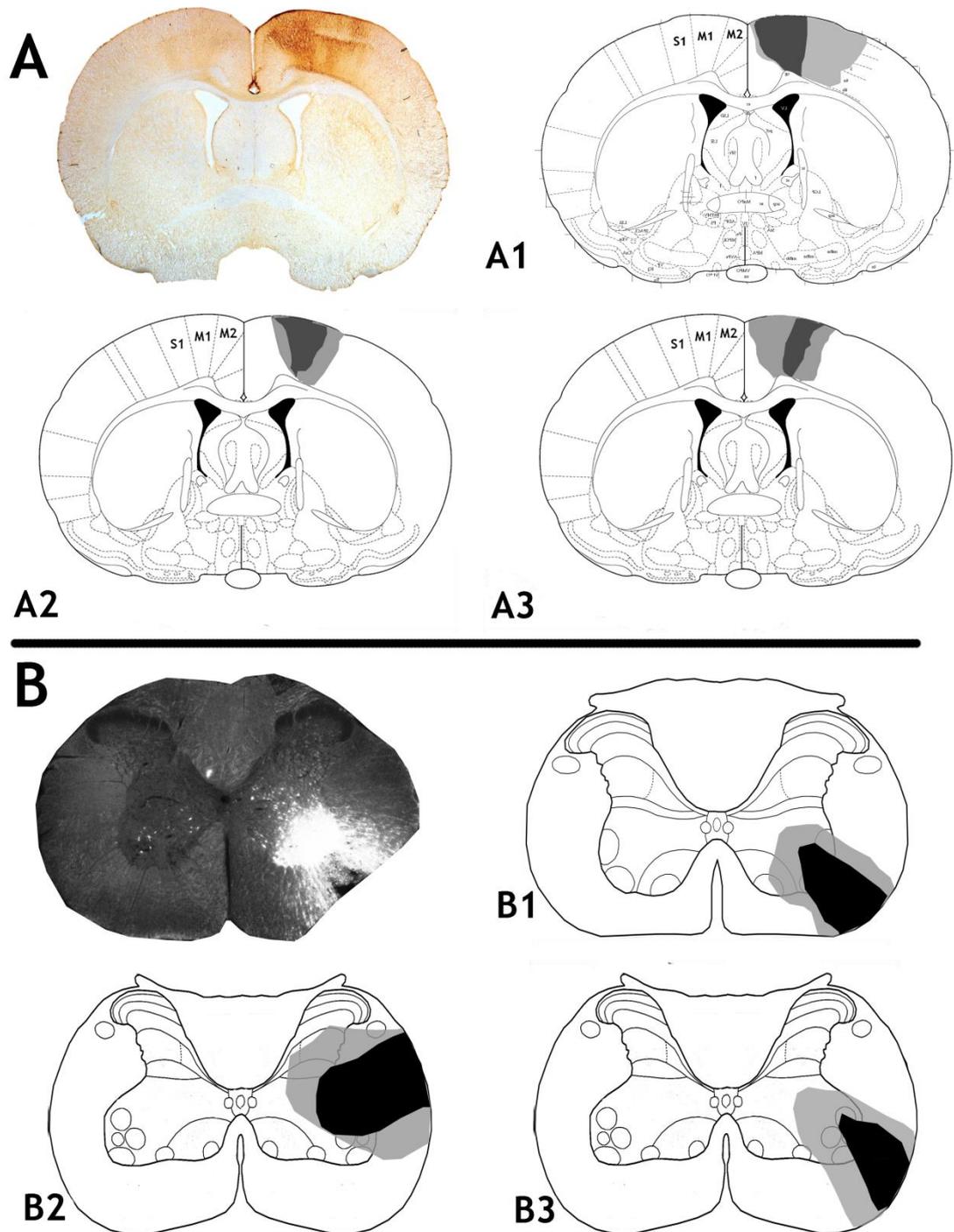
Figure 6-13 CTb injections into the sensorimotor cortex and FG injections into the cervical spinal cord (right) of each rat

A: A representative CTb injection site revealed with an immunoperoxidase reaction. **A1**, **A2**, **A3** are reconstructions of injection sites for each rat on brain templates (taken from Paxinos & Watson, 2005; -0.5mm from Bregma). The darkest shading represents the core of the injection and lighter shading represents spread beyond the core. **B:** A representative fluorescence/dark field micrograph showing a FG injection site within a transverse section of the lumbar spinal cord (C4). **B1**, **B2**, **B3** are reconstructions of injection sites for each rat on spinal templates (based on Paxinos & Watson, 2005). The core of the injection is shown in black and the spread shown in grey.
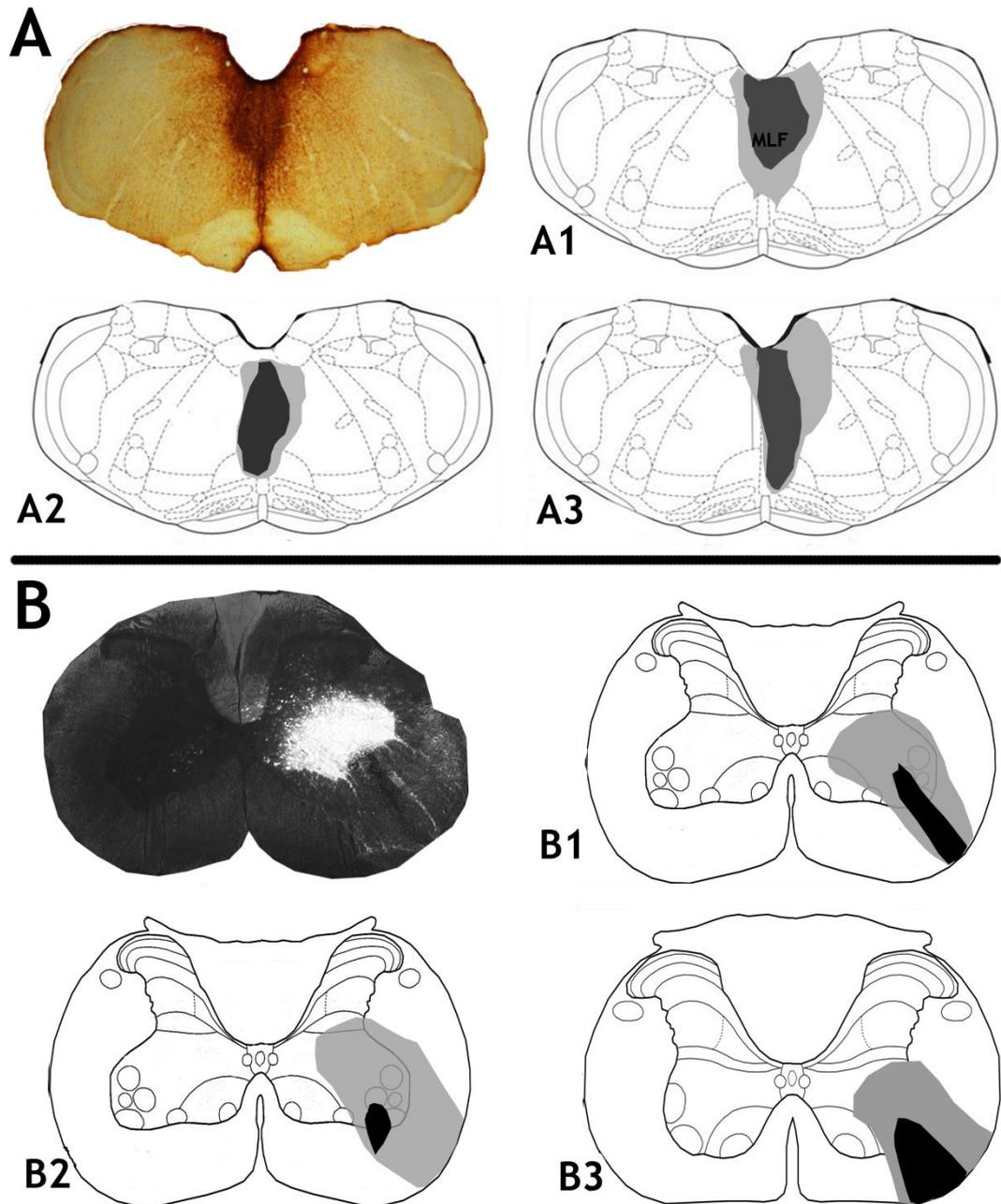
Figure 6-14 CTb injections into the MLF and FG injections into the cervical spinal cord (right) of each rat

A: A representative CTb injection site revealed with an immunoperoxidase reaction. **A1**, **A2**, **A3** are reconstructions of injection sites for each rat on brain templates (taken from Paxinos & Watson, 2005; -12.6mm from Bregma). The darkest shading represents the core of the injection and lighter shading represents spread beyond the core.**B:** A representative fluorescence/dark field micrograph showing a FG injection site within a transverse section of the lumbar spinal cord (C5). **B1**, **B2**, **B3** are reconstructions of injection sites for each rat on spinal templates (based on Paxinos & Watson, 2005). The core of the injection is shown in black and the spread shown in grey.

6.3.2.2 Laminar distribution pattern of intrasegmental CINs in relation to CST and ReST terminals in the cervical cord

Figure 6-15 shows the laminar distribution pattern of intrasegmental CINs in relation to CST and terminals in segment C4/C5 for all rats. The distribution of FG-labelled intrasegmental CINs within the grey matter was similar for all rats, despite some variation in the locations of the injection sites (see above). In comparison to the LDPNs characterised above (**section 6.3.1**), intrasegmental CINs were more numerous and they were more evenly distributed throughout laminae VI to VIII and X. Intrasegmental CINs tended to be smaller than LDPNs, with a mean surface area (μm^2) of 1008 ± 590 and 2156 ± 1236 for the somata and dendritic processes, respectively. CTb labelled CST terminals were located in the grey matter contralateral to the cortical injection site (contralateral to the C4/C5 FG injection) (**Figures 6-15A to D**). Although the majority of CST terminals were dorsal to the intrasegmental CINs (in laminae IV to VI), a moderate number of CST terminals were visible in laminae VI to VII, within the same territory as the LDPNs. CTb-labelled ReST terminals were distributed bilaterally and were numerous through the deep dorsal horn, intermediate grey matter and ventral horn (**Figure 6-15E to H**); thus, on examination of the overall laminar distribution of cells and terminals, there were more ReST than CST terminals within the vicinity of intrasegmental CINs.
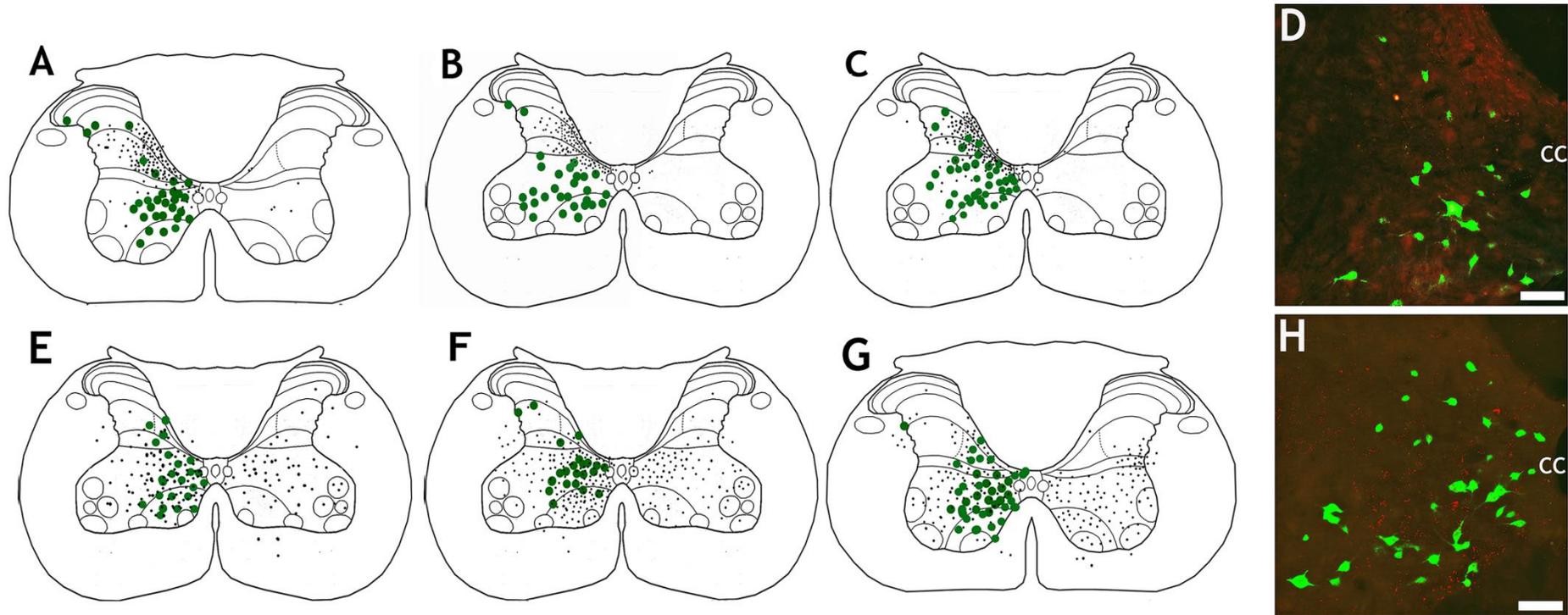
Figure 6-15 Distribution of intrasegmental CINs and axonal terminals in the cervical spinal cord (C5)

A, B, C: Laminar distribution of FG-labelled CINs (green) in association with CTb-labelled CST terminals (black) for each rat. Note that most CST terminals were dorsal to CINs. Each representation was taken from 2 60µm thick spinal sections. **D**: Photomicrograph of CINs (green) and CST terminals (red) taken from the grey matter contralateral to the lumbar injection site**. E, F, G**: Laminar distribution of FG-labelled CINs (green) in association with CTb-labelled ReST terminals (black) for each rat. Note that ReST terminals were much more evenly distributed throughout the grey matter in comparison to CST terminals and many ReST terminals were located within the territory of CINs. **H:** Photomicrograph of CINs (green) and ReST terminals (red) taken from the grey matter contralateral to the lumbar injection site (Scale bar = 50µm). CC= central canal

6.3.2.3 Density of CST and ReST contacts onto intrasegmental CINs

To examine CST contacts to intrasegmental CINs (cervical segment C4/C5), a total of 39 retrogradely labelled cells (9-12 per rat) were imaged. On inspection of the first few cells, it was found that although CTb-labelled terminals were present within the vicinity of the cells, they very rarely established contacts with the cells. Thus, for the remaining cells, confocal imaging was performed using the green and red channels only. However, 4 cells with detected contacts were re-scanned using the blue channel in order to confirm that the contacts were terminals i.e. that they contained VGLUT-1; and all of those contacts contained VGLUT-1. **Figure 6-16** shows a rare example of an intrasegmental CIN with a CTb-labelled contact that was immunoreactive for VGLUT-1. The mean number of CTb-labelled CST contacts per 100µm^2 of neuronal surface was higher for the dendritic processes (0.019 ± 0.05) compared to the somata (0.005 ± 0.02) (**Figure 6-17A**) but this difference was not statistically significant (p>0.05). In order to examine whether the CST targets intrasegmental CINs located within specific regions of the grey matter, the CTb-labelled contact densities onto cells located within different laminar boundaries were compared. However there were no significant differences in the density of contacts to cells of different laminae for both the somata (**Figure 6-17B**) and dendritic processes (**Figure 6-17C**) (p>0.05).
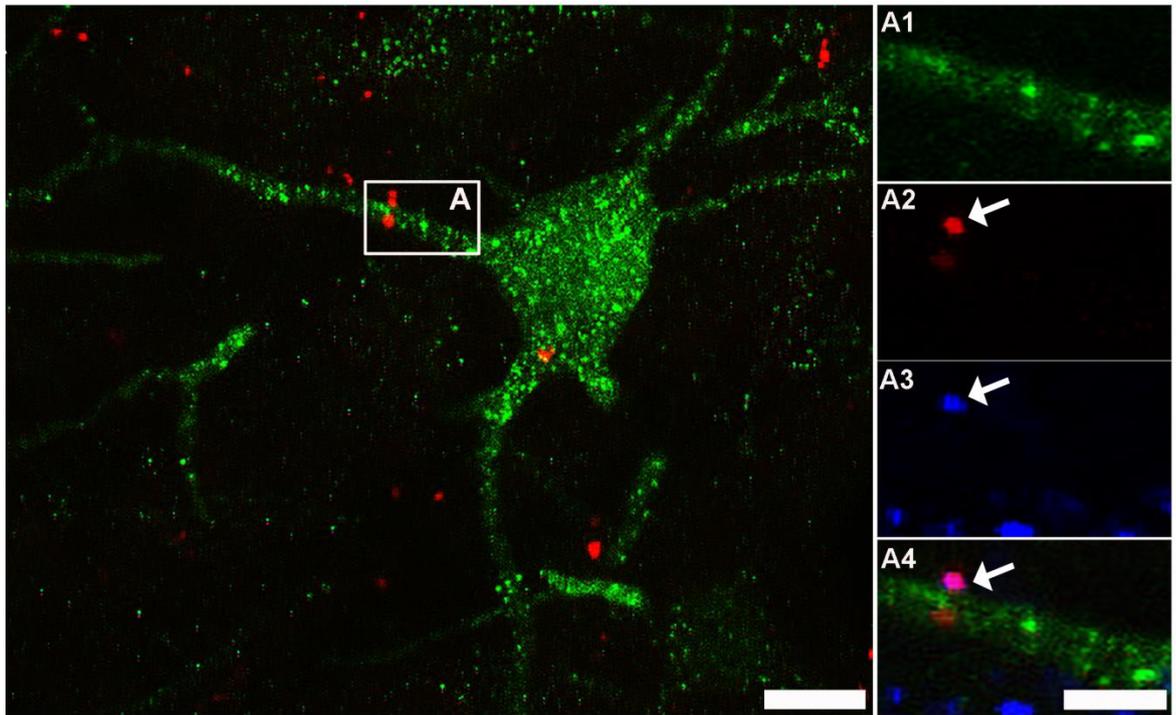
Figure 6-16 CST contacts onto a segmental CIN in the cervical spinal cord

A projected confocal microscope image (36 optical sections, 0.5µm increments) of a FG-labelled LDPN (green) and CTb-labelled CST terminals (red) taken from the medial region of lamina VII (contralateral to the C5 injection site). Scale bar = 20µm. Insets are single optical sections: **A1** to **A4** correspond to the region demarcated in **A**. **A1** shows immunoreactivity for FG; **A2** shows immunoreactivity for CTb; **A3** shows immunoreactivity for VGLUT-1; **A4** is a merged image. This CIN was found to have a total of 1 CST contact. CTb-labelled terminals are indicated by arrows. Scale bar = 5µm.
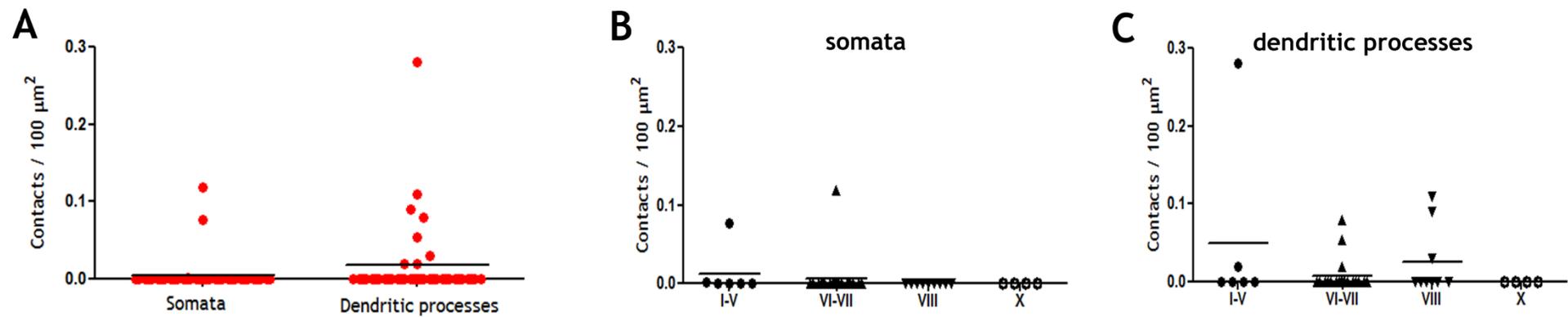
Figure 6-17 Density of CST contacts to intrasegmental CINs in the cervical segments C4/C5

A: Density of CTb-labelled CST contacts onto intrasegmental CINs. Each data point represents a cell (9-12 cells per rat; n = 3 rats). Contact densities were higher onto dendritic processes compared to somata but this difference was not statistically significant (p>0.05, Man-Whitney). **B, C**: The Kruskal-Wallis test compared CST contact densities on cells located in different laminae of Rexed (based on Molander, 1989). For both somata (**B**) and dendritic processes (**C**), there were no significant differences in contact densities between cells located in different laminar boundaries (p > 0.05).

(All analysis based on number of animals, not number of cells/ sections)

To examine excitatory ReST contacts to intrasegmental CINs, a total of 31 cells (10-11 per rat) were imaged. An extensive number of CTb-labelled ReST terminals were detected within the immediate vicinity of intrasegmental CINs and many of these terminals were found to establish excitatory (VGLUT-2 immunoreactive) contacts with the cells. **Figure 6-18** shows an example of a cell with numerous excitatory (VGLUT-2 immunoreactive) ReST contacts. As summarised in **Table 6-5**, the majority of ReST contacts to intrasegmental CINs (78.8 ± 4%) were immunoreactive for VGLUT-2.

	No. cells reconstructed	CTb contacts (total)	VGLUT-2^{+CTb}	% VGLUT-2
Rat 1	11	136	108	79.41
Rat 2	10	97	80	82.47
Rat 3	10	196	146	74.49
Mean				**78.8**
SD				**4**

Table 6-5 Immunoreactive excitatory contacts from the MLF to intrasegmental CINs
Note that the majority of CTb-labelled contacts were immunoreactive for VGLUT-2.

The contact densities for all of the 31 reconstructed intrasegmental CINs are shown in **Figure 6-19A**; for the somata, the mean overall number of CTb-labelled terminals per 100μm^2 of neuronal surface was 0.62 ± 0.63 and the mean number of CTb-labelled terminals that contained VGLUT-2 (VGLUT-2^{+CTb}) was 0.47 ± 0.60; for the dendritic processes, the mean total number of CTb-labelled terminals per 100μm^2 of neuronal surface was 0.46 ± 0.43 and the mean number of CTb-labelled terminals that contained VGLUT-2 (VGLUT-2^{+CTb}) was 0.40 ± 0.4. The mean contact densities were higher for the somata versus dendritic processes but this different was not statistically significant ($p > 0.05$). In order to examine whether excitatory ReST axons target intrasegmental CINs located within specific areas of the grey matter, the CTb-labelled contact densities onto cells located within different laminar boundaries were compared. Quantitative analysis revealed no significant differences in the density of contacts to cells of different laminae for both the somata (**Figure 6-19B**) and dendritic processes (**Figure 6-19C**) ($p>0.05$).
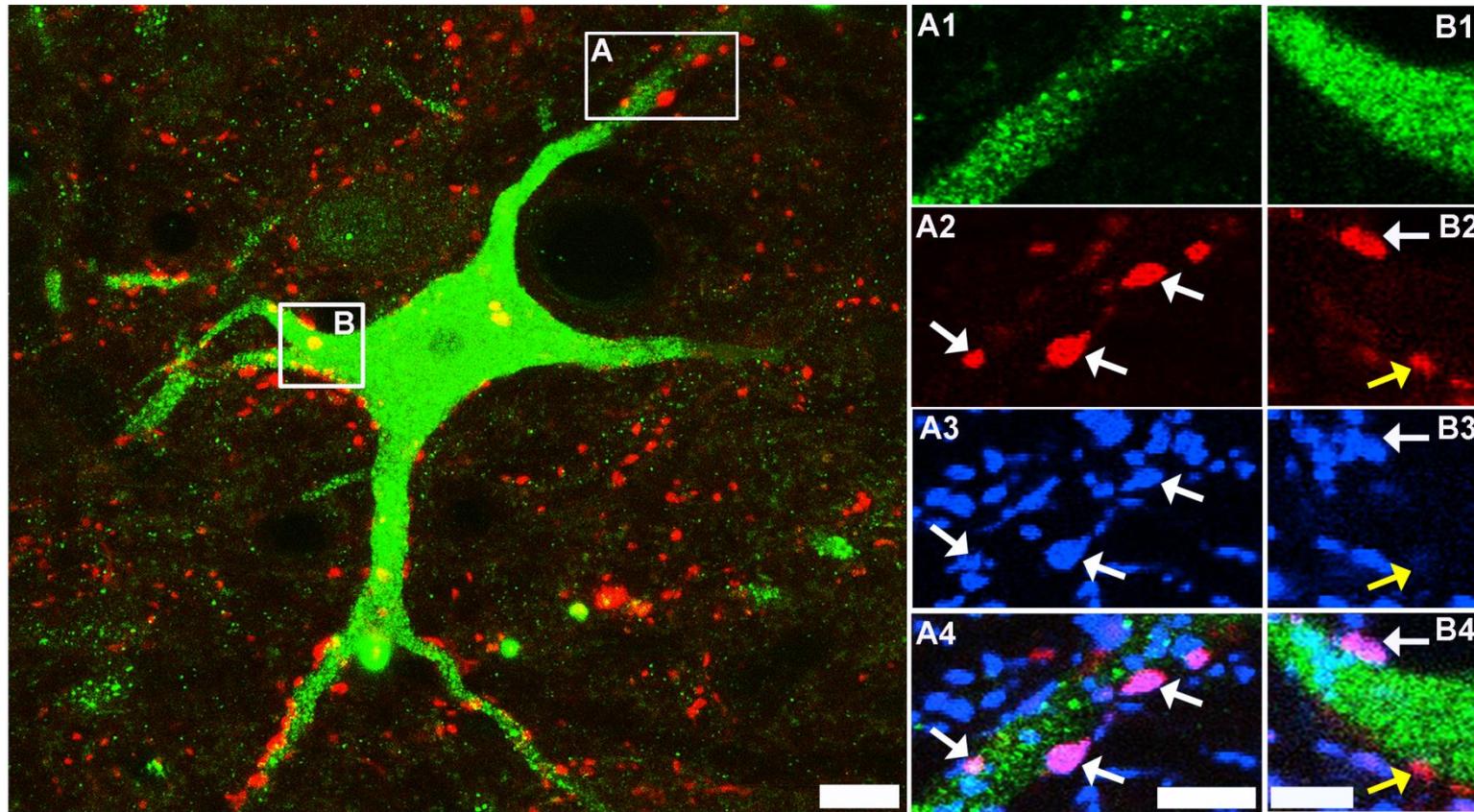
Figure 6-18 Excitatory ReST inputs onto an intrasegmental CIN in the cervical spinal cord

A projected confocal microscope image (47 optical sections, 0.5μm increments) of a FG-labelled cell (green) and CTb-labelled ReST terminals (red) taken from the medial region of lamina VII (contralateral to the C5 injection site). Scale bar = 20μm. Insets **A1** to **A4** are single optical sections and correspond to the region demarcated in **A**. **B1** to **B4** are single optical sections and correspond to the region demarcated in **B**. **A1** and **B1** show immunoreactivity for FG; **A2** and **B2** show immunoreactivity for CTb; **A3** and **B3** show immunoreactivity for VGLUT-2; **A4** and **B4** are merged images. This cell has 19 ReST contacts in total and 17 of these contacts were immunoreactive for VGLUT-2. White arrows indicate CTb-labelled contacts that are immunoreactive for VGLUT-2. Yellow arrows indicate CTb-labelled contacts that are negative for VGLUT-2. Scale bar = 5μm.
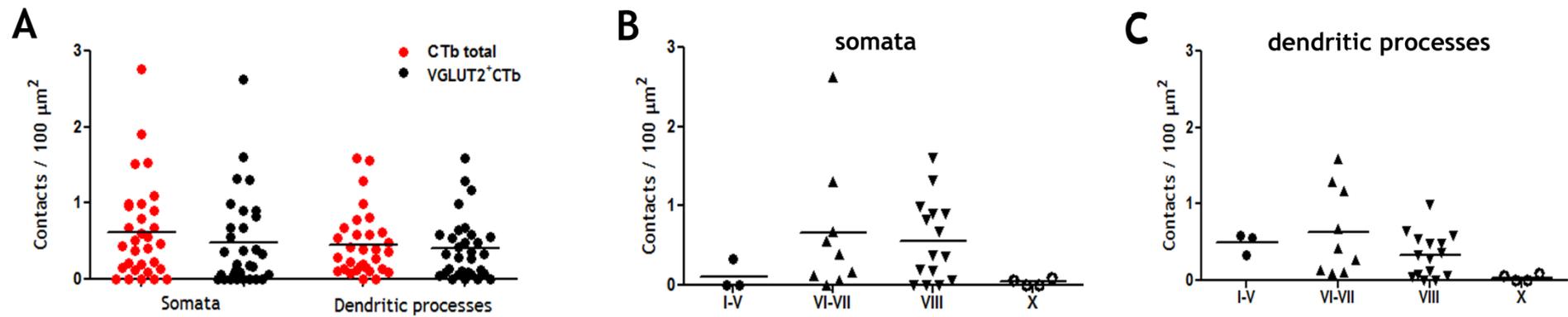
Figure 6-19 Density of excitatory ReST contacts to intrasegmental CINs in the cervical segments C4/C5

A: Density of ReST contacts to intrasegmental CINs reported as total CTb-labelled contacts (red) and CTb-labelled contacts immunoreactive for VGLUT-2 (VGLUT2^{+CTb}; black). Each data point represents a cell (10-11 per rat). Contact densities tended to be higher for somata compared to dendritic processes but this difference was not statistically significant ($p > 0.05$, Mann-Whitney). **B**, **C**: The Kruskal-Wallis test compared VGLUT2^{+CTb} contact densities on cells located in different laminae of Rexed (based on Molander, 1989). For both somata (**B**) and dendritic processes (**C**), there were no significant differences in contact densities between cells located in different laminar boundaries ($p > 0.05$).

(All analysis based on number of animals, not number of cells/ sections)

To examine inhibitory ReST contacts to intrasegmental CINs, a total of 21 cells (5-8 per rat) were reconstructed. An extensive number of CTb-labelled ReST terminals were detected within the immediate vicinity of intrasegmental CINs and a proportion of these terminals were found to establish inhibitory (VGAT immunoreactive) contacts with the cells. **Figure 6-20** shows an example of a cell with inhibitory (VGAT immunoreactive) ReST contacts. As summarised in **Table 6-5**, a sizeable minority of ReST contacts to intrasegmental CINs (19.8 ± 2.4%) immunoreactive for VGAT.

		No. cells reconstructed	CTb contacts (total)	VGAT $^{+CTb}$	% VGAT
	Rat 1	8	72	13	18.06
	Rat 2	5	96	18	18.75
	Rat 3	7	133	30	22.56
Mean					**19.8**
SD					**2.44**

Table 6-6 Immunoreactive inhibitory contacts from the MLF to intrasegmental CINs

Note that a sizeable minority of CTb-labelled contacts were immunoreactive for VGAT

The contact densities for all of the 21 reconstructed intrasegmental CINs are shown in **Figure 6-21A**; for the somata, the mean total number of CTb-labelled terminals per 100µm^2 of neuronal surface was 0.76 ± 1.32 and the mean number of CTb-labelled terminals that contained VGAT (VGAT^{+CTb}) was 0.23 ± 0.59; for the dendritic processes, the mean total number of CTb-labelled terminals per 100µm^2 of neuronal surface was 0.29 ± 0.35 and the mean number of CTb-labelled terminals that contained VGAT (VGAT^{+CTb}) was 0.06 ± 0.07. The mean contact densities were higher for the somata versus dendritic processes but this difference was not statistically significant (p>0.05). In order to examine whether inhibitory ReST axons target intrasegmental CINs located within specific areas of the grey matter, the CTb-labelled contact densities onto cells located within different laminar boundaries were compared. However there were no significant differences in the density of contacts to cells of different laminae for both the somata (**Figure 6-21B**) and dendritic processes (**Figure 6-21C**) (p>0.05).
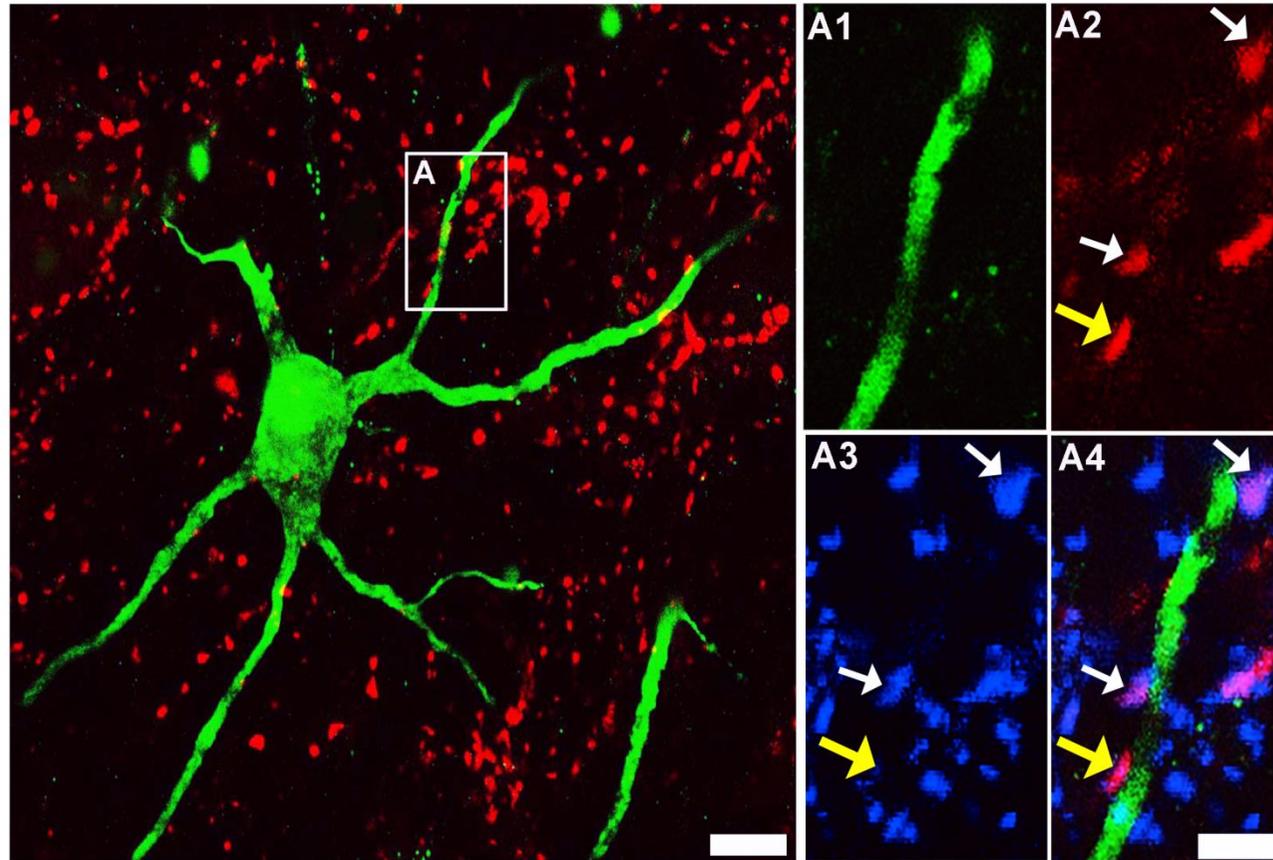
Figure 6-20 Inhibitory ReST inputs onto an intrasegmental CIN in the cervical spinal cord

A projected confocal microscope image (39 optical sections, 0.5µm increments) of a FG-labelled cell (green) and CTb-labelled ReST terminals (red) taken from the medial region of lamina VII (contralateral to the C5 injection site). Scale bar = 20µm. Insets **A1** to **A4** are single optical sections and correspond to the region demarcated in **A**. **A1** shows immunoreactivity for FG; **A2** shows immunoreactivity for CTb; **A3** shows immunoreactivity for VGAT; **A4** is a merged image. This cell has 12 ReST contacts in total and 3 of these contacts were immunoreactive for VGAT. White arrows indicate CTb-labelled contacts that are immunoreactive for VGAT. Yellow arrows indicate CTb-labelled contacts that are negative for VGLUT-2. Scale bar = 5µm.
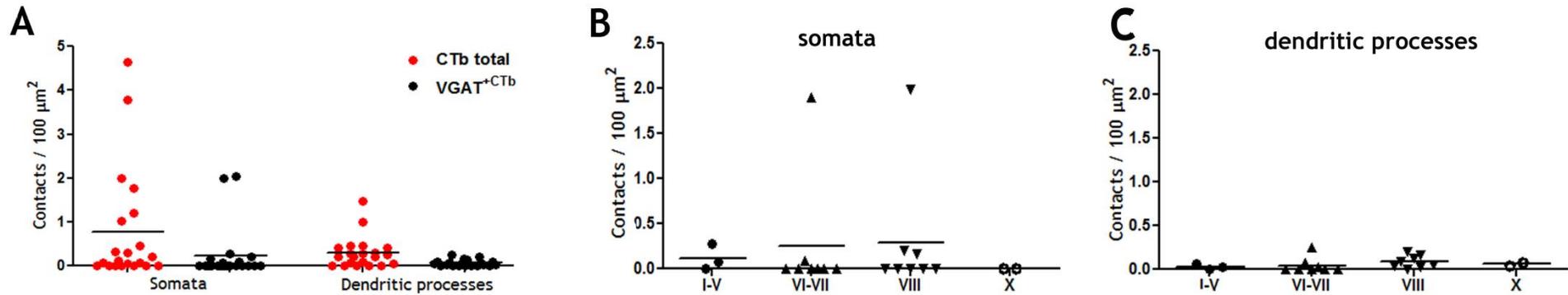
Figure 6-21 Density of inhibitory ReST contacts to intrasegmental CINs in the cervical segments C4/C5

A: Density of ReST contacts to intrasegmental CINs reported as total CTb-labelled contacts (red) and CTb-labelled contacts immunoreactive for VGAT (VGAT^{+CTb}; black). Each data point represents a cell (5-8 per rat; n = 3 rats). Contact densities tended to be higher for somata compared to dendritic processes but this difference was not statistically significant (p > 0.05, Mann-Whitney). **B**, **C**: The Kruskal-Wallis test compared VGAT^{+CTb} contact densities on cells located in different laminae of Rexed (based on Molander, 1989). For both somata (**B**) and dendritic processes (**C**), there were no significant differences in contact densities between cells located in different laminar boundaries (p > 0.05).

(All analysis based on number of animals, not number of cells/ sections)

6.4 Discussion

In this study, LDPNs (both commissural and uncrossed) and intrasegmental CINs in the rat cervical spinal cord were found to receive a sparse number of contacts from the CST and an extensive number of contacts from the ReST. Use of VGLUT-2 and VGAT revealed that both types of cell received about 80% of excitatory and 20% of inhibitory RST contacts. In normal rats therefore the CST has a minimal influence on LCINs and LDPNs but the RST has a powerful influence. Therefore following loss of CST axons, the cortico-reticulospinal-commissural pathway has the capacity to convey information from the intact hemisphere to the denervated spinal cord.

Technical considerations

CTb is a highly sensitive tracer that may be transported in the anterograde as well as the retrograde direction (Ericson & Blomqvist, 1988), but it is taken up by undamaged axons of passage in the CNS (Chen & Aston-Jones, 1995). On this basis, the possibility that the tracer contaminated axons derived from cell sources beyond the intended area of injection cannot be excluded. This is especially likely to be the case with MLF injections as fibres of the medial VST (Nyberg-Hansen & Mascitti, 1964; Wilson & Peterson, 1978) and the tectospinal tract (Petras, 1967) also descend within this region; although the medial VST of the rat terminates predominantly in the dorsal horn (Bankoul & Neuhuber, 1992) and tectospinal fibres are mainly found in upper cervical segments (C1 to C3; Yasui et al., 1998) so it is unlikely that the terminals analysed in the current study originated from these tracts. Another potential complication with MLF injections is that in addition to ReST axons, spinoreticular cells are also labelled and therefore the collateral axons of these cells may have contaminated the sample. However, a previous study using a sensitive method for revealing CTb reported that retrogradely transported CTb is detected in cell bodies and dendrites but not axons or fibre bundles (Angelucci et al., 1996).

FG is taken up by axon terminals or through injured axons, and retrogradely transported to neuronal cell bodies, thereby specifically labelling neurons that project to the region of application (Catapano et al., 2008). A limitation of the study is that the FG does not label the most distal parts of dendritic trees and

therefore the numbers of contacts on LCINs and LDPNs may have been underestimated. Although the estimates of contact densities may not represent absolute values the difference in the relative values of contact densities between CST and RST terminals is striking.

It is likely that the contacts reported in the this study were sites of synaptic interaction because they expressed VGLUT-1 (for the CST) and VGLUT-2 (for the ReST) which are present in glutamatergic presynaptic boutons (Persson et al., 2006; Fremeau et al., 2001) and VGAT (for the ReST) which is present in both GABAergic and glycinergic boutons (Chaudhry et al., 1998). To confirm that inhibitory sites of contact were synapses, antibodies against the glycinergic receptor anchoring protein gephyrin could have been used whereby VGAT terminals in contact with gephyrin puncta on the cell indicates a synaptic interaction (Puskár et al., 2001). Due to the absence of a reliable neurochemical marker for the identification of excitatory synapses however, a combination of confocal and electron microscopy would have been required to determine synapses at sites of glutamatergic contacts (Todd, 1997).

CST and ReST contacts to LDPNs

Following unilateral FG injections into segments L1/L2, retrogradely labelled LDPNs were found in both sides of the grey matter of segment C5, with the majority of cells concentrated in laminae VII and VIII. This observation is consistent with findings from Brockett et al., (2010) who injected CTb into segments L1/L2 and described bilaterally labelled cells to be present in all cervical segments. Similarly, Reed et al., (2009) reported dense bilateral descending projections from cervical to lumbar segments following unilateral injection of BDA into the ventrolateral funiculus at T9.

Both commissural and uncrossed LDPNs were found to receive a very limited number of CST contacts, suggesting that the CST may not be a chief regulator of these cells. This finding is consistent with Ni et al., (2014) who demonstrated that in mice, 35% of LDPNs are contacted by CST axons but the number of contacts per cell was very limited (< 2). However, according to Alstermark et al., (1987), LDPNs (mostly commissural but some uncrossed) in the cat are directly excited by stimulation of the contralateral medullary pyramid. Taking

this anatomical and electrophysiological evidence together, this might reflect the existence of highly potent synaptic contacts between CST axons and LDPNs such that a small number of synapses are sufficient for inducing strong depolarisations. An alternative explanation is that the CST directly influences LDPNs in cats, but not in rodents. Accordingly, the cat CST terminates most extensively in the deep dorsal horn and intermediate zone (Scheibel & Scheibel, 1966; Chakrabarty et al., 2009); whereas the rat CST terminates most extensively in the deep dorsal horn, with lesser terminations in the intermediate zone (see Chapter 4 of this thesis; Gribnau & Dederen, 1989; Casale et al., 1988). Thus, in the cat, the region of the grey matter occupied by LDPNs receives more CST projections compared to the rat. At this point it is worth briefly referring to the well-studied C3/C4 propriospinal system, which consists of shorter-axoned interneurons that project to caudal forelimb segments. Unlike in cats and primates, the C3/C4 propriospinal system of rodents does not receive monosynaptic excitation from the CST, only disynaptic excitation (Alstermark et al., 2004); but the C3/C4 propriospinal system of rodents can be monosynaptically activated by stimulation of the MLF (Azim et al., 2014). Taking all of these findings into account, it could be possible that in rodents the motor cortex accesses propriospinal systems via a cortico-reticulo-propriospinal pathway rather than via a cortico-propriospinal pathway. However a better comparison of these systems between different species is required. Strong ReST control of LDPNs appears to be conserved in rats and cats because stimulation of the MLF in the cat evokes monosynaptic excitation and/or inhibition in the large majority of cells (both commissural and uncrossed; Alstermark et al., 1987); and the current study has demonstrated a very high number ReST contacts (both excitatory and inhibitory) to these cells in the rat.

The large majority of ReST contacts to LDPNs contained VGLUT-2 (~75%) but a sizeable proportion contained VGAT (~20%). This is consistent with previous reports that the ReST of the rat is a heterogeneous system of excitatory and inhibitory axons (Du Beau et al., 2013).

CST and ReST contacts to intrasegmental CINs

Following unilateral FG injections into segments C4/C5, a large number of retrogradely labelled cells were found in the grey matter contralateral to the

injection site and these cells were particularly concentrated within laminae VI to VIII and X. This is consistent with data obtained from the lumbar spinal cord of mice, showing that cells located in laminae VI to VIII and X have axonal projections spanning < 1.5 segments and excite or inhibit motor neurons and interneurons in the contralateral grey matter (Quilan & Kiehn, 2007).

Intrasegmental CINs in segments C4/C5 were found to receive a very sparse number of contacts from the CST, with the CST contact densities being similar to those obtained for the commissural (and uncrossed) LDPNs. In contrast, the intrasegmental CINs received extensive contacts from ReST axons, with the ReST contact densities being similar to those obtained for the commissural (and uncrossed) LDPNs. Also in accordance with the data obtained for the commissural (and uncrossed LDPNs), the large majority of ReST contacts to intrasegmental CINs were excitatory (79% expressing VGLUT-2) and a sizeable proportion were inhibitory (20% expressing VGAT). This anatomical finding is consistent with an electrophysiological study performed in the lumbar spinal cord of cats, showing that CINs with short axons projecting in and around the somata's segmental level are excited monosynaptically by ReST pathways (Matsuyama et al., 2004).

Taken together, the data from the current study support the hypothesis that the ReST establishes contacts onto commissural (and uncrossed) LDPNs and intrasegmental CINs. However, CST contacts onto both of these cell types were very rare, suggesting that the CST has minimal influence on these cells.

Implications for functional recovery

The findings of this study have various implications relating to neural pathways that might underlie recovery of function following damage to the CST after stroke. As discussed previously (Chapter 1 **section 1.4.3**), there is evidence that recovery of the impaired limb may be mediated by the non-ischaemic hemisphere and there are various potential routes via which the non-ischaemic hemisphere may gain access to denervated motor neurons (Chapter 1 **sections 1.3 & 1.4.3**). A potential route is via CST axons from the non-ischaemic hemisphere acting on spinal CINs; if contralaterally descending CST fibres target CINs, the CINs would in turn either monosynaptically or polysynaptically affect

motor neurons on the opposite (denervated) side of the spinal cord. The findings from the current study suggest that if direct CST-CIN connections contribute to recovery of function after injury, this must occur through the formation of new connections, since CST connections to CINs were very sparse in the intact rat. Evidence from studies of spinal lesions suggest that LDPNs that bridge the lesion acquire new CST connections (Bareyre et al., 2004), thus the possibility still remains that the CST-commissural system contributes to recovery via the formation of *de novo* contacts with CINs. However it seems highly probable given the finding that CINs receive extensive input from RST axons that this pathway is a more readily available source of "detour circuits" after injury. Accordingly, studies have already identified that the motor cortex can gain access to ipsilateral motor neurons indirectly via a "double-crossed" pathway, involving contralaterally descending ReST neurons, which in turn, activate spinal CINs that project back across to the opposite spinal grey matter (Jankowska & Edgley, 2006; **Figure 1-3**).

To summarise, the results of this study suggest that in normal rats, the CST has minimal influence over CINs, while the ReST has a powerful influence over these cells. This finding has implications pertaining to the neural pathways underlying recovery of function following damage to the CST after stroke. The cortico-reticulospinal-commissural system represents a pre-existing pathway that could become strengthened in order to convey signals from the non-ischaemic hemisphere to denervated motor neurons. However the CST-commissural system is weak in normal rats; for this system to contribute to recovery it would require the formation of *de novo* contacts.

Chapter 7

Concluding remarks

The motor cortex exerts strong control over contralateral limb function via the CST. A growing body of evidence however, suggests that the motor cortex may also contribute to ipsilateral limb function, through currently ill-defined pathways (Jankowska & Edgley, 2006). It is important to ascertain which neural pathways might mediate ipsilateral actions of the motor cortex because these pathways could become strengthened after damage to the crossed CST (e.g. after stroke) so that the undamaged hemisphere can take over control of the denervated limb. The overarching aim of this thesis was to extend the knowledge of neural systems that may underlie ipsilateral actions of the motor cortex, both under normal circumstances and after stroke. The studies detailed within this thesis have generated two main novel findings:

Despite functional recovery of MCAo rats, the number of CST axonal terminals in the cervical spinal cord originating from the non-ischaemic hemisphere was not altered compared to shams

This finding suggests that, after stroke, the motor cortex from the non-ischaemic hemisphere may not contribute to recovery of the affected limb via increasing its direct CST connections to the denervated (ipsilateral) side of the spinal cord. If the motor cortex from the non-ischaemic hemisphere does take over control of denervated (ipsilateral) spinal circuitry after stroke, then it may utilise indirect routes. Indirect routes could involve brainstem relay systems as proposed by Jankowska & Edgley (2006; see Chapter 1 **section 1.3**). Accordingly, in mice, a recent study demonstrated that recovery from motor cortex infarction is accompanied by corticoreticular and ReST sprouting in addition to CST sprouting from the non-ischaemic hemisphere (Bachmann et al., 2014). Moreover, the ReST sprouts in the cervical spinal cord were more numerous than the CST sprouts (Bachmann et al., 2014). This suggests that strengthening of indirect routes involving brainstem systems might be particularly important for recovery of function. Further investigations are required to determine whether sprouted brainstem fibres form new synaptic connections with cells in the denervated side of the spinal cord in association with functional recovery. There is already evidence that ReST axons passing through the MLF increase their motor output to denervated motor neurons after pyramidal tract transection in primates

(Zaaimi et al., 2012). It would be interesting to perform similar experiments in a rodent model of stroke.

In intact rats, LDPNs and intrasegmental CINs were found to receive few contacts from CST terminals but significant numbers of contacts from ReST terminals

Therefore, in normal rats the CST has minimal influence on CINs but the ReST has a powerful influence on these cells. This finding has implications relating to the neural pathways that might underlie recovery of function following damage to the CST (e.g. after stroke). The cortico-reticulospinal-commissural system represents a pre-existing pathway that may have the capacity to convey information from the non-ischaemic hemisphere to denervated motor neurons. However the CST-commissural system is weak in normal rats; if this system does contribute to recovery processes it would require the formation of new synaptic connections between CST axons and CINs. According to spinal lesioning studies performed in rats, LDPNs that bridge the injury site acquire new connections from CST axons (Bareyre et al., 2004). Therefore, the possibility still remains that the CST-commissural system contributes to recovery via the formation of *de novo* contacts with CINs. A potential future experiment would be to quantify CST contacts onto CINs following MCAo in rats in order to examine whether contact density increases in association with functional recovery.

With regards to potential strategies for enhancing ipsilateral actions of the motor cortex to improve recovery after injury, the large majority of studies have focussed on applying therapies that promote large-scale structural rearrangements, particularly CST sprouting into the denervated side of the spinal cord (Liu et al., 2007; Liu et al., 2008; Zai et al., 2009; Chen et al., 2002; Lee et al., 2004; Lindau et al., 2014). An alternative intervention, however, could be to increase the effectiveness of synaptic transmission of pre-existing pathways. For instance, in the cat, Edgley et al., (2004) identified the presence of a "double-crossed" pathway between the motor cortex and ipsilateral motor neurons, involving contralateral ReST neurons which in turn activate CINs that project back across the spinal cord to motor neurons and interneurons (see **Figure 1-3**). In a subsequent study (Jankowska et al., 2005), application of the K^+ channel blocker 4-aminopyridine (4-AP) was shown to enhance synaptic

transmission between cortical neurons and ReST neurons, and synaptic transmission between ReST neurons and ipsilateral motor neurons via CINs (Jankowska et al., 2005). Therefore, the development of pharmacological therapies for potentiating the actions of pre-existing but normally weak synaptic connections may represent a better opportunity for promoting recovery after injury to the CST.

References

ABO, M., CHEN, Z., LAI, L. J., REESE, T. & BJELKE, B. 2001. Functional recovery after brain lesion--contralateral neuromodulation: an fMRI study. *Neuroreport,* 12, 1543-7.

ABRAHAM, H., SOMOGYVARI-VIGH, A., MADERDRUT, J. L., VIGH, S. & ARIMURA, A. 2002. Filament size influences temperature changes and brain damage following middle cerebral artery occlusion in rats. *Exp Brain Res,* 142, 131-8.

AL-IZKI, S., KIRKWOOD, P. A., LEMON, R. N. & ENRÍQUEZ DENTON, M. 2008. Electrophysiological actions of the rubrospinal tract in the anaesthetised rat. *Experimental Neurology,* 212, 118-131.

ALSTERMARK, B. & EKEROT, C.-F. 2013. The lateral reticular nucleus: a precerebellar centre providing the cerebellum with overview and integration of motor functions at systems level. A new hypothesis. *The Journal of Physiology,* 591, 5453-5458.

ALSTERMARK, B., ISA, T. & TANTISIRA, B. 1991. Pyramidal excitation in long propriospinal neurones in the cervical segments of the cat. *Exp Brain Res,* 84, 569-82.

ALSTERMARK, B. & KÜMMEL, H. 1990. Transneuronal transport of wheat germ agglutinin conjugated horseradish peroxidase into last order spinal interneurones projecting to acromio- and spinodeltoideus motoneurones in the cat. *Experimental Brain Research,* 80, 96-103.

ALSTERMARK, B. & PETTERSSON, L.-G. 2014. Skilled Reaching and Grasping in the Rat: Lacking Effect of Corticospinal Lesion. *Frontiers in Neurology,* 5, 103.

ALSTERMARK, B., LUNDBERG, A., NORRSELL, U. & SYBIRSKA, E. 1981. Integration in descending motor pathways controlling the forelimb in the cat. 9. Differential behavioural defects after spinal cord lesions interrupting defined pathways from higher centres to motoneurones. *Exp Brain Res,* 42, 299-318.

ALSTERMARK, B., LUNDBERG, A., PINTER, M. & SASAKI, S. 1987. Subpopulations and functions of long C3-C5 propriospinal neurones. *Brain Res,* 404, 395-400.

ALSTERMARK, B., OGAWA, J. & ISA, T. 2004. Lack of monosynaptic corticomotoneuronal EPSPs in rats: disynaptic EPSPs mediated via reticulospinal neurons and polysynaptic EPSPs via segmental interneurons. *J Neurophysiol,* 91, 1832-9.

ALSTERMARK, B. & SASAKI, S. 1985. Integration in descending motor pathways controlling the forelimb in the cat. 13. Corticospinal effects in shoulder, elbow, wrist, and digit motoneurones. *Exp Brain Res,* 59, 353-64.

ANTAL, M. 1984. Termination areas of corticobulbar and corticospinal fibres in the rat. *Journal für Hirnforschung,* 25, 12.

ANTAL, M., SHOLOMENKO, G. N., MOSCHOVAKIS, A. K., STORM-MATHISEN, J., HEIZMANN, C. W. & HUNZIKER, W. 1992. The termination pattern and postsynaptic targets of rubrospinal fibers in the rat spinal cord: a light and electron microscopic study. *J Comp Neurol,* 325, 22-37.

ARMAND, J. 1982. The origin, course and terminations of corticospinal fibers in various mammals. *Prog Brain Res,* 57, 329-60.

ARMAND, J., HOLSTEGE, G. & KUYPERS, H. G. 1985. Differential corticospinal projections in the cat. An autoradiographic tracing study. *Brain Res,* 343, 351-5.

ARMAND J, KUYPERS HG. 1980. Cells of origin of crossed and uncrossed corticospinal fibers in the cat: a quantitative horseradish peroxidase study. Exp Brain Res 40:23–34

ARVIN, B., NEVILLE, L. F., BARONE, F. C. & FEUERSTEIN, G. Z. 1996. The Role of Inflammation and Cytokines in Brain Injury. *Neuroscience & Biobehavioral Reviews,* 20**,** 445-452.

AZIM, E., JIANG, J., ALSTERMARK, B. & JESSELL, T. M. 2014. Skilled reaching relies on a V2a propriospinal internal copy circuit. *Nature,* 508**,** 357-63.

BACHMANN, L. C., LINDAU, N. T., FELDER, P. & SCHWAB, M. E. 2014. Sprouting of brainstem-spinal tracts in response to unilateral motor cortex stroke in mice. *J Neurosci,* 34**,** 3378-89.

BALLION, B., MORIN, D. & VIALA, D. 2001. Forelimb locomotor generators and quadrupedal locomotion in the neonatal rat. *Eur J Neurosci,* 14**,** 1727-38.

BANKOUL, S. & NEUHUBER, W. L. 1992. A direct projection from the medial vestibular nucleus to the cervical spinal dorsal horn of the rat, as demonstrated by anterograde and retrograde tracing. *Anat Embryol,* 185**,** 77-85.

BANNATYNE, B. A., EDGLEY, S. A., HAMMAR, I., JANKOWSKA, E. & MAXWELL, D. J. 2003. Networks of inhibitory and excitatory commissural interneurons mediating crossed reticulospinal actions. *The European journal of neuroscience,* 18**,** 2273-2284.

BANNATYNE, B. A., EDGLEY, S. A., HAMMAR, I., JANKOWSKA, E. &
MAXWELL, D. J. 2006. Differential projections of excitatory and inhibitory dorsal horn interneurons relaying information from group II muscle afferents in the cat spinal cord. *J Neurosci,* 26**,** 2871-80.

BAREYRE, F. M., KERSCHENSTEINER, M., RAINETEAU, O., METTENLEITER, T. C., WEINMANN, O. & SCHWAB, M. E. 2004. The injured spinal cord spontaneously forms a new intraspinal circuit in adult rats. *Nat Neurosci,* 7**,** 269-77.

BELHAJ-SAIF, A. & CHENEY, P. D. 2000. Plasticity in the distribution of the red nucleus output to forearm muscles after unilateral lesions of the pyramidal tract. *J Neurophysiol,* 83**,** 3147-53.

BENOWITZ, L. I. & CARMICHAEL, S. T. 2010. Promoting axonal rewiring to improve outcome after stroke. *Neurobiol Dis,* 37**,** 259-66.

BERKHEMER, O. A., FRANSEN, P. S. S., BEUMER, D., VAN DEN BERG, L. A., LINGSMA, H. F., YOO, A. J., et al., 2015. A Randomized Trial of Intraarterial Treatment for Acute Ischemic Stroke. *New England Journal of Medicine,* 372**,** 11-20.

BIERNASKIE, J., SZYMANSKA, A., WINDLE, V. & CORBETT, D. 2005. Bi-hemispheric contribution to functional motor recovery of the affected forelimb following focal ischemic brain injury in rats. *European Journal of Neuroscience,* 21**,** 989-999.

BOGOUSSLAVSKY, J. & CAPLAN, L. R. 2001. Stroke Syndromes. *(2nd Ed), Cambridge. Cambridge University Press.*

BOLTON, P. S., GOTO, T. & WILSON, V. J. 1991. Commissural neurons in the cat upper cervical spinal cord. *Neuroreport,* 2**,** 743-6.

BOWKER, R. M., WESTLUND, K. N. & COULTER, J. D. 1981. Origins of serotonergic projections to the spinal cord in rat: an immunocytochemical-retrograde transport study. *Brain Res,* 226**,** 187-99.

BRADBURY, E. J., MOON, L. D. F., POPAT, R. J., KING, V. R., BENNETT, G. S., PATEL, P. N., FAWCETT, J. W. & MCMAHON, S. B. 2002. Chondroitinase ABC promotes functional recovery after spinal cord injury. *Nature,* 416**,** 636-640.

BROCKETT, E. G., SEENAN, P. G., BANNATYNE, B. A. & MAXWELL, D. J. 2013. Ascending and descending propriospinal pathways between lumbar and cervical segments in the rat: evidence for a substantial ascending

BRÖSAMLE, C. & SCHWAB, M. E. 1997. Cells of origin, course, and termination patterns of the ventral, uncrossed component of the mature rat corticospinal tract. *J Comp Neurol,* 386**,** 293-303.

BRÖSAMLE, C. & SCHWAB, M. 2000. Ipsilateral, ventral corticospinal tract of the adult rat: Ultrastructure, myelination and synaptic connections. *Journal of Neurocytology,* 29**,** 499-507.

BROUNS, R. & DE DEYN, P. P. 2009. The complexity of neurobiological processes in acute ischemic stroke. *Clin Neurol Neurosurg,* 111**,** 483-95.

BROWN, L. T. 1974. Corticorubral projections in the rat. *The Journal of Comparative Neurology,* 154**,** 149-167.

BRUS-RAMER, M., CARMEL, J. B., CHAKRABARTY, S. & MARTIN, J. H. 2007. Electrical stimulation of spared corticospinal axons augments connections with ipsilateral spinal motor circuits after injury. *J Neurosci,* 27**,** 13793-801.

BUSTO, R., DIETRICH, W., GLOBUS, M., VALDES, I., SCHEINBERG, P. & GINSBERG, M. 1987. Small differences in intraischemic brain temperature critically determine the extent of ischemic neuronal injury. *J Cereb Blood Flow Metab,* 7**,** 729 - 38.

BUTT, S. J., HARRIS-WARRICK, R. M. & KIEHN, O. 2002a. Firing properties of identified interneuron populations in the mammalian hindlimb central pattern generator. *J Neurosci,* 22**,** 9961-71.

BUTT, S. J. B. & KIEHN, O. 2003. Functional Identification of Interneurons Responsible for Left-Right Coordination of Hindlimbs in Mammals. *Neuron,* 38**,** 953-963.

BUTT, S. J. B., LEBRET, J. M. & KIEHN, O. 2002b. Organization of left–right coordination in the mammalian locomotor network. *Brain Research Reviews,* 40**,** 107-117.

CAMPBELL, B. C. V., MITCHELL, P. J., KLEINIG, T. J., DEWEY, H. M., CHURILOV, L., YASSI, N., YAN, B., DOWLING, R. J., PARSONS, M. W., OXLEY, T. J., WU, T. Y., et al. 2015. Endovascular Therapy for Ischemic Stroke with Perfusion-Imaging Selection. *New England Journal of Medicine,* 372**,** 1009-1018.

CANEDO, A. & LAMAS, J. A. 1993. Pyramidal and corticospinal synaptic effects over reticulospinal neurones in the cat. *The Journal of Physiology,* 463**,** 475-489.

CARMEL, J. B. & MARTIN, J. H. 2014. Motor cortex electrical stimulation augments sprouting of the corticospinal tract and promotes recovery of motor function. *Front Integr Neurosci,* 8.

CARMICHAEL, S. T. 2003. Plasticity of cortical projections after stroke. *Neuroscientist,* 9**,** 64-75.

CARMICHAEL, S. 2005. Rodent Models of Focal Stroke: Size, Mechanism, and Purpose. *NeuroRx,* 2**,** 396 - 409.

CASALE, E. J., LIGHT, A. R. & RUSTIONI, A. 1988. Direct projection of the corticospinal tract to the superficial laminae of the spinal cord in the rat. *J Comp Neurol,* 278**,** 275-86.

CHAKRABARTY, S., SHULMAN, B. & MARTIN, J. H. 2009. Activity-dependent codevelopment of the corticospinal system and target interneurons in the cervical spinal cord. *J Neurosci,* 29**,** 8816-27.

CHAN, S. L. & MATTSON, M. P. 1999. Caspase and calpain substrates: Roles in synaptic plasticity and cell death. *Journal of Neuroscience Research,* 58, 167-190.

CHAVEZ JC, HURKO O, BARONE FC, FEUERSTEIN GZ.2009. Pharmacologic interventions for stroke. Looking beyond the thrombolysis time window into the penumbra with biomarkers, not a stopwatch. *Stroke,* 40:e558-e563.

Chen S, Aston-Jones G (1995) Evidence that cholera toxin B subunit (CTb) can be avidly taken up and transported by fibers of passage. Brain Res 674:107111.

CHEN, P., GOLDBERG, D. E., KOLB, B., LANSER, M. & BENOWITZ, L. I. 2002. Inosine induces axonal rewiring and improves behavioral outcome after stroke. *Proc Natl Acad Sci U S A,* 99, 9031-6.

CHEN, R. L., BALAMI, J. S., ESIRI, M. M., CHEN, L. K. & BUCHAN, A. M. 2010. Ischemic stroke in the elderly: an overview of evidence. *Nat Rev Neurol,* 6, 256-65.

CHEN, Y., ITO, A., TAKAI, K. & SAITO, N. 2008. Blocking pterygopalatine arterial blood flow decreases infarct volume variability in a mouse model of intraluminal suture middle cerebral artery occlusion. *J Neurosci Methods,* 174, 18-24.

CHOLLET, F., DIPIERO, V., WISE, R. J., BROOKS, D. J., DOLAN, R. J. & FRACKOWIAK, R. S. 1991. The functional anatomy of motor recovery after stroke in humans: a study with positron emission tomography. *Ann Neurol,* 29, 63-71.

CORBETTA M, RAMSEY L, CALLEJAS A, BALDASSARRE A, HACKER CD, SIEGEL JS. 2015. Common behavioral clusters and subcortical anatomy in stroke. *Neuron,* 85, 927-41.

COURTINE, G., BUNGE, M. B., FAWCETT, J. W., GROSSMAN, R. G., KAAS, J. H., LEMON, R., MAIER, I., MARTIN, J., NUDO, R. J., RAMON-CUETO, A., ROUILLER, E. M., SCHNELL, L., WANNIER, T., SCHWAB, M. E. & EDGERTON, V. R. 2007. Can experiments in nonhuman primates expedite the translation of treatments for spinal cord injury in humans? *Nat Med,* 13, 561-566.

CRAMER, S. C. 2008. Repairing the human brain after stroke: I. Mechanisms of spontaneous recovery. *Ann Neurol,* 63, 272-87.

CRONIN, C. A. 2010. Intravenous Tissue Plasminogen Activator for Stroke: A Review of the ECASS III Results in Relation to Prior Clinical Trials. *The Journal of Emergency Medicine,* 38, 99-105.

DANCAUSE, N. 2006. Vicarious function of remote cortex following stroke: recent evidence from human and animal studies. *Neuroscientist,* 12, 489-99.

DAVIS, M. F., LAY, C. & FROSTIG, R. D. 2013. Permanent cerebral vessel occlusion via double ligature and transection. *J Vis Exp,* 21, 50418.

DECAVEL, P., VUILLIER, F. & MOULIN, T. 2012. Lenticulostriate infarction. *Front Neurol Neurosci,* 30, 115-9.

DEKKER, J. J. 1981. Anatomical evidence for direct fiber projections from the cerebellar nucleus interpositus to rubrospinal neurons. A quantitative EM study in the rat combining anterograde and retrograde intra-axonal tracing methods. *Brain Research,* 205, 229-244.

DIJKHUIZEN, R. M., REN, J., MANDEVILLE, J. B., WU, O., OZDAG, F. M., MOSKOWITZ, M. A., ROSEN, B. R. & FINKLESTEIN, S. P. 2001. Functional magnetic resonance imaging of reorganization in rat brain after stroke. *Proc Natl Acad Sci U S A,* 98, 12766-71

DING, G., JIANG, Q., LI, L., ZHANG, L., WANG, Y., ZHANG, Z. G., LU, M., PANDA, S., LI, Q., EWING, J. R. & CHOPP, M. 2010. Cerebral tissue repair

and atrophy after embolic stroke in rat: a magnetic resonance imaging study of erythropoietin therapy. *J Neurosci Res,* 88**,** 3206-14.

.DIRNAGL, U., IADECOLA, C. & MOSKOWITZ, M. A. 1999. Pathobiology of ischaemic stroke: an integrated view. *Trends Neurosci,* 22**,** 391-7.

DOBKIN, B. H. 2005. Rehabilitation after Stroke. *New England Journal of Medicine,* 352**,** 1677-1684.

DU BEAU, A., SHAKYA SHRESTHA, S., BANNATYNE, B. A., JALICY, S. M., LINNEN, S. & MAXWELL, D. J. 2012. Neurotransmitter phenotypes of descending systems in the rat lumbar spinal cord. *Neuroscience,* 227**,** 67-79.

DURUKAN, A. & TATLISUMAK, T. 2007. Acute ischemic stroke: Overview of major experimental rodent models, pathophysiology, and therapy of focal cerebral ischemia. *Pharmacology Biochemistry and Behavior,* 87**,** 179-197.

DUTTON, R. C., CARSTENS, M. I., ANTOGNINI, J. F. & CARSTENS, E. 2006. Long ascending propriospinal projections from lumbosacral to upper cervical spinal cord in the rat. *Brain Research,* 1119**,** 76-85.

EDGLEY, S. A., JANKOWSKA, E. & HAMMAR, I. 2004. Ipsilateral Actions of Feline Corticospinal Tract Neurons on Limb Motoneurons. *The Journal of neuroscience : the official journal of the Society for Neuroscience,* 24**,** 7804-7813.

ERICSON, H. & BLOMQVIST, A. 1988. Tracing of neuronal connections with cholera toxin subunit B: light and electron microscopic immunohistochemistry using monoclonal antibodies. *J Neurosci Methods,* 24**,** 225-35.

ESPOSITO, M. S., CAPELLI, P. & ARBER, S. 2014. Brainstem nucleus MdV mediates skilled forelimb motor tasks. *Nature,* 508**,** 351-356.

FANARDJIAN, V. V. & GORODNOV, V. L. 1988. Complex composition of synaptic potentials of the rubrospinal neurons to corticofugal impulses. *Behavioural Brain Research,* 28**,** 131-137.

FESTING, M. F. & ALTMAN, D. G. 2002. Guidelines for the design and statistical analysis of experiments using laboratory animals. *ILAR J,* 43**,** 244-58.

FLOETER, M. K., SHOLOMENKO, G. N., GOSSARD, J. P. & BURKE, R. E. 1993. Disynaptic excitation from the medial longitudinal fasciculus to lumbosacral motoneurons: modulation by repetitive activation, descending pathways, and locomotion. *Exp Brain Res,* 92**,** 407-19.

FREMEAU RT, TROYER MD, PAHNER I, NYGAARD GO, TRAN CH, REIMER RJ, BELLOCCHIO EE, FORTIN D, STORM-MATHISEN J, EDWARDS RH .2001. The expression of vesicular glutamate transporters defines two classes of excitatory synapse. *Neuron* 31:247–260.

FROST, S. B., BARBAY, S., MUMERT, M. L., STOWE, A. M. & NUDO, R. J. 2006. An animal model of capsular infarct: Endothelin-1 injections in the rat. *Behavioural Brain Research,* 169**,** 206-211.

GARCIA, J. H., LIU, K.-F. & HO, K.-L. 1995. Neuronal Necrosis After Middle Cerebral Artery Occlusion in Wistar Rats Progresses at Different Time Intervals in the Caudoputamen and the Cortex. *Stroke,* 26**,** 636-643.

GARCIA, J. H., WAGNER, S., LIU, K.-F. & HU, X.-J. 1995. Neurological Deficit and Extent of Neuronal Necrosis Attributable to Middle Cerebral Artery Occlusion in Rats: Statistical Validation. *Stroke,* 26**,** 627-635.

GARCIA, J. H., YOSHIDA, Y., CHEN, H., LI, Y., ZHANG, Z. G., LIAN, J., CHEN, S. & CHOPP, M. 1993. Progression from ischemic injury to infarct following middle cerebral artery occlusion in the rat. *The American Journal of Pathology,* 142**,** 623-635.

GARTHWAITE, J. & BOULTON, C. L. 1995. Nitric oxide signaling in the central nervous system. *Annu Rev Physiol,* 57, 683-706.

GEYER, J. D. & GOMEZ, C. R. 2009. *Stroke: A practical approach,* Philadelphia, PA, Wolters Kluwer Health/Lippincott Williams and Wilkins.

GHARBAWIE, O. A., WILLIAMS, P. T., KOLB, B. & WHISHAW, I. Q. 2008. Transient middle cerebral artery occlusion disrupts the forelimb movement representations of rat motor cortex. *Eur J Neurosci,* 28, 951-63.

GINSBERG, M. D. 2009. Current Status of Neuroprotection for Cerebral Ischemia Synoptic Overview. *Stroke; a journal of cerebral circulation,* 40, S111-S114.

GIUFFRIDA, R., AICARDI, G. & RAPISARDA, C. 1991a. Projections from the Cerebral Cortex to the Red Nucleus of the Guinea-pig. A Retrograde Tracing Study. *Eur J Neurosci,* 3, 866-875.

GIUFFRIDA, R., VOLSI, G. L. & PERCIAVALLE, V. 1988. Influences of cerebral cortex and cerebellum on the red nucleus of the rat. *Behavioural Brain Research,* 28, 109-111.

GOYAL, M., DEMCHUK, A. M., MENON, B. K., EESA, M., REMPEL, J. L., THORNTON, J., ROY, D., JOVIN, T. G., WILLINSKY, R. A., SAPKOTA, B. L., et al. 2015. Randomized Assessment of Rapid Endovascular Treatment of Ischemic Stroke. *New England Journal of Medicine,* 372, 1019-1030.

GREFKES, C. & FINK, G. R. 2011. Reorganization of cerebral networks after stroke: new insights from neuroimaging with connectivity approaches. *Brain,* 134, 1264-1276.

GREFKES, C., NOWAK, D. A., EICKHOFF, S. B., DAFOTAKIS, M., KUST, J., KARBE, H. & FINK, G. R. 2008. Cortical connectivity after subcortical stroke assessed with functional magnetic resonance imaging. *Ann Neurol,* 63, 236-46.

GRIBNAU, A.A.., DEDEREN, P.J. 1989. Collateralization of the cervical corticospinal tract in the rat. *Neuroscience Letters,* 105, 47-51

GWYN, D. G. & FLUMERFELT, B. A. 1974. A comparison of the distribution of cortical and cerebellar afferents in the red nucleus of the rat. *Brain Research,* 69, 130-135.

HAGG, T., BAKER, K. A., EMSLEY, J. G. & TETZLAFF, W. 2005. Prolonged local neurotrophin-3 infusion reduces ipsilateral collateral sprouting of spared corticospinal axons in adult rats. *Neuroscience,* 130, 875-87.

HOLSTEGE, J. C. & KUYPERS, H. G. J. M. 1987. Brainstem projections to lumbar motoneurons in rat—I. An ultrastructural study using autoradiography and the combination of autoradiography and horseradish peroxidase histochemistry. *Neuroscience,* 21, 345-367.

HOLSTEGE, G. & KUYPERS, H. G. J. M. 1982. The Anatomy of Brain Stem Pathways to the Spinal Cord in Cat. A Labeled Amino Acid Tracing Study. *In:* KUYPERS, H. G. J. M. & MARTIN, G. F. (eds.) *Progress in Brain Research*. Elsevier.

HOLSTEGE, J. C. 1991. Ultrastructural evidence for GABAergic brain stem projections to spinal motoneurons in the rat. *J Neurosci,* 11, 159-67.

HOLSTEGE, J. C. & BONGERS, C. M. 1991. A glycinergic projection from the ventromedial lower brainstem to spinal motoneurons. An ultrastructural double labeling study in rat. *Brain Res,* 566, 308-15.

HONGO, T., JANKOWSKA, E. & LUNDBERG, A. 1972. The rubrospinal tract. IV. Effects on interneurones. *Experimental Brain Research,* 15, 54-78.

Houk JC, Gibson AR, Harvey CF, Kennedy PR., & Van Kan PLE. *(1988)* Activity of primate magnocellular red nucleus related to hand and finger movements. *Behav Brain Res 28:201-206*

HUMPHREY, D. R., GOLD, R. & REED, D. J. 1984. Sizes, laminar and topographic origins of cortical projections to the major divisions of the red nucleus in the monkey. *The Journal of Comparative Neurology,* 225**,** 75-94.

HUNTER, A. J., HATCHER, J., VIRLEY, D., NELSON, P., IRVING, E., HADINGHAM, S. J. & PARSONS, A. A. 2000. Functional assessments in mice and rats after focal stroke. *Neuropharmacology,* 39**,** 806-16.

ILLERT, M., LUNDBERG, A. & TANAKA, R. 1976. Integration in descending motor pathways controlling the forelimb in the cat. 1. Pyramidal effects on motoneurones. *Exp Brain Res,* 26**,** 509-19.

ISA, T., KINOSHITA, M. & NISHIMURA, Y. 2013. Role of Direct vs. Indirect Pathways from the Motor Cortex to Spinal Motoneurons in the Control of Hand Dexterity. *Frontiers in Neurology,* 4**,** 191.

IVANCO, T. L., PELLIS, S. M. & WHISHAW, I. Q. 1996. Skilled forelimb movements in prey catching and in reaching by rats (Rattus norvegicus) and opossums (Monodelphis domestica): relations to anatomical differences in motor systems. *Behavioural Brain Research,* 79**,** 163-181.

JANKOWSKA, E. 2008. Spinal interneuronal networks in the cat: elementary components. *Brain Res Rev,* 57**,** 46-55.

JANKOWSKA, E. 1988. Target cells of rubrospinal tract fibres within the lumbar spinal cord. *Behav Brain Res,* 28**,** 91-6.

JANKOWSKA, E. 1992. Interneuronal relay in spinal pathways from proprioceptors. *Prog Neurobiol,* 38**,** 335-78.

JANKOWSKA, E. & EDGLEY, S. A. 2006. How Can Corticospinal Tract Neurons Contribute to Ipsilateral Movements? A Question With Implications for Recovery of Motor Functions. *The Neuroscientist : a review journal bringing neurobiology, neurology and psychiatry,* 12**,** 67-79.

JANKOWSKA, E., EDGLEY, S. A., KRUTKI, P. & HAMMAR, I. 2005. Functional d ifferentiation and organization of feline midlumbar commissural interneurones. *The Journal of Physiology,* 565**,** 645-658.

JANKOWSKA, E., HAMMAR, I., SLAWINSKA, U., MALESZAK, K. & EDGLEY, S. A. 2003. Neuronal basis of crossed actions from the reticular formation on feline hindlimb motoneurons. *J Neurosci,* 23**,** 1867-78.

JANKOWSKA, E., CABAJ, A. & PETTERSSON, L. G. 2005. How to Enhance Ipsilateral Actions of Pyramidal Tract Neurons. *The Journal of neuroscience: the official journal of the Society for Neuroscience,* 25**,** 7401-7405.

JANKOWSKA, E. & STECINA, K. 2007. Uncrossed actions of feline corticospinal tract neurones on lumbar interneurones evoked via ipsilaterally descending pathways. *The Journal of Physiology,* 580**,** 133-147.

JOHANSEN-BERG, H., RUSHWORTH, M. F. S., BOGDANOVIC, M. D., KISCHKA, U., WIMALARATNA, S. & MATTHEWS, P. M. 2002. The role of ipsilateral premotor cortex in hand movement after stroke. *Proceedings of the National Academy of Sciences of the United States of America,* 99**,** 14518-14523.

JOU, I.-M., TSAI, Y.-T., TSAI, C.-L., WU, M.-H., CHANG, H.-Y. & WANG, N.-S. 2000. Simplified rat intubation using a new oropharyngeal intubation wedge. *Journal of Applied Physiology,* 89**,** 1766-1770.

JUVIN, L., SIMMERS, J. & MORIN, D. 2005. Propriospinal circuitry underlying interlimb coordination in mammalian quadrupedal locomotion. *J Neurosci,* 25**,** 6025-35.

KANG DW, CHALELA JA, EZZEDDINE MA, WARACH S. 2003. Association of ischemic lesion patterns on early diffusion-weighted imaging with TOAST stroke subtypes. *Arch Neurol,* 60:1730-4.

KEIZER, K. & KUYPERS, H. G. 1984. Distribution of corticospinal neurons with collaterals to lower brain stem reticular formation in cat. *Exp Brain Res,* 54**,** 107-20.

KEIZER, K. & KUYPERS, H. G. 1989. Distribution of corticospinal neurons with collaterals to the lower brain stem reticular formation in monkey (Macaca fascicularis). *Exp Brain Res,* 74**,** 311-8.

KIEHN, O. 2006. Locomotor circuits in the mammalian spinal cord. *Annu Rev Neurosci,* 29**,** 279-306.

KIEHN, O. & BUTT, S. J. 2003. Physiological, anatomical and genetic identification of CPG neurons in the developing mammalian spinal cord. *Prog Neurobiol,* 70**,** 347-61.

KIM, H.-S., KIM, D., KIM, R. G., KIM, J.-M., CHUNG, E., NETO, P. R., LEE, M.-C. & KIM, H.-I. 2014. A rat model of photothrombotic capsular infarct with a marked motor deficit: a behavioral, histologic, and microPET study. *J Cereb Blood Flow Metab,* 34**,** 683-689.

KJAERULFF, O. & KIEHN, O. 1997. Crossed rhythmic synaptic input to motoneurons during selective activation of the contralateral spinal locomotor network. *J Neurosci,* 17**,** 9433-47.

KLEIM, J. A., BOYCHUK, J. A. & ADKINS, D. L. 2007. Rat Models of Upper Extremity Impairment in Stroke. *ILAR Journal,* 48**,** 374-385.

KOIZUMI, J., YOSHIDA, Y., NAZAKAWA, T. & OONEDA, G. 1986. Experimental studies of ischemic brain edema: a new experimental model of cerebral embolism in rats in which re circulation can be introduced in the ischemic area. *Jpn J Stroke,* 8**,** 1 - 8.

KUYPERS, H. G. 1960. Central cortical projections to motor and somato-sensory cell groups. An experimental study in the rhesus monkey. *Brain,* 83**,** 161-84.

LACROIX, S., HAVTON, L. A., MCKAY, H., YANG, H., BRANT, A., ROBERTS, J. & TUSZYNSKI, M. H. 2004. Bilateral corticospinal projections arise from each motor cortex in the macaque monkey: a quantitative study. *J Comp Neurol,* 473**,** 147-61.

LAPASH DANIELS, C. M., AYERS, K. L., FINLEY, A. M., CULVER, J. P. & GOLDBERG, M. P. 2009. Axon sprouting in adult mouse spinal cord after motor cortex stroke. *Neurosci Lett,* 450**,** 191-5.

LAWRENCE, D. G. & KUYPERS, H. G. 1968. The functional organization of the motor system in the monkey. I. The effects of bilateral pyramidal lesions. *Brain,* 91**,** 1-14.

LAWRENCE, E. S., COSHALL, C., DUNDAS, R., STEWART, J., RUDD, A. G., HOWARD, R. & WOLFE, C. D. 2001. Estimates of the prevalence of acute stroke impairments and disability in a multiethnic population. *Stroke,* 32**,** 1279-84.

LAZIC, E.S. 2010. The problem of pseudoreplication in neuroscientific studies: is it affecting your analysis? *BMC Neuroscience,* 11, 1-17

LEE, J. K., KIM, J. E., SIVULA, M. & STRITTMATTER, S. M. 2004. Nogo receptor antagonism promotes stroke recovery by enhancing axonal plasticity. *J Neurosci,* 24**,** 6209-17.

LEMON, R. N. 2008. Descending pathways in motor control. *Annu Rev Neurosci,* 31**,** 195-218.

LEMON, R. N., KIRKWOOD, P. A., MAIER, M. A., NAKAJIMA, K. & NATHAN, P. 2004. Direct and indirect pathways for corticospinal control of upper limb motoneurons in the primate. *In:* SHIGEMI MORI, D. G. S. & MARIO, W. (eds.) *Progress in Brain Research.* Elsevier.

LI, X. G., FLORENCE, S. L. & KAAS, J. H. 1990. Areal distributions of cortical neurons projecting to different levels of the caudal brain stem and spinal cord in rats. *Somatosens Mot Res,* 7, 315-35.

LIANG, D., BHATTA, S., GERZANICH, V. & SIMARD, J. M. 2007. Cytotoxic edema: mechanisms of pathological cell swelling. *Neurosurgical focus,* 22, E2-E2.

LIANG, P., MORET, V., WIESENDANGER, M. & ROUILLER, E. M. 1991. Corticomotoneuronal connections in the rat: Evidence from double-labeling of motoneurons and corticospinal axon arborizations. *The Journal of Comparative Neurology,* 311, 356-366.

LINDAU, N. T., BANNINGER, B. J., GULLO, M., GOOD, N. A., BACHMANN, L. C., STARKEY, M. L. & SCHWAB, M. E. 2014. Rewiring of the corticospinal tract in the adult rat after unilateral stroke and anti-Nogo-A therapy. *Brain,* 137, 739-56.

LIU, S., ZHEN, G., MELONI, B. P., CAMPBELL, K. & WINN, H. R. 2009. Rodent Stroke Model Guidelines for Preclinical Stroke Trials (1st Edition). *J Exp Stroke Transl Med,* 2, 2-27.

LIU Z, CHOPP M, DING X, CUI Y, LI Y. 2013. Axonal remodeling of the corticospinal tract in the spinal cord contributes to voluntary motor recovery after stroke in adult mice. *Stroke,* 44(7), 1951-6.

LIU, Z., LI, Y., QIAN, J., CUI, Y. & CHOPP, M. 2014. Plasminogen deficiency causes reduced corticospinal axonal plasticity and functional recovery after stroke in mice. *PLoS ONE,* 9.

LIU, Z., LI, Y., QU, R., SHEN, L., GAO, Q., ZHANG, X., LU, M., SAVANT-BHONSALE, S., BORNEMAN, J. & CHOPP, M. 2007. Axonal Sprouting into the Denervated Spinal Cord and Synaptic and Postsynaptic Protein Expression in the Spinal Cord after Transplantation of Bone Marrow Stromal Cell in Stroke Rats. *Brain Research,* 1149, 172-180.

LIU, Z., LI, Y., ZHANG, X., SAVANT-BHONSALE, S. & CHOPP, M. 2008. Contralesional Axonal Remodeling of the Corticospinal System in Adult Rats After Stroke and Bone Marrow Stromal Cell Treatment. *Stroke; a journal of cerebral circulation,* 39, 2571-2577.

LONGA, E., WEINSTEIN, P., CARLSON, S. & CUMMINS, R. 1989. Reversible middle cerebral artery occlusion Without craniectomy in rats. *Stroke,* 20, 84 - 91.

LOTZE, M., MARKERT, J., SAUSENG, P., HOPPE, J., PLEWNIA, C. & GERLOFF, C. 2006. The role of multiple contralesional motor areas for complex hand movements after internal capsular lesion. *J Neurosci,* 26, 6096-102.

MACRAE, I. M. 1992. New models of focal cerebral ischaemia. *British Journal of Clinical Pharmacology,* 34, 302-308.

MACRAE, I. M. 2011. Preclinical stroke research – advantages and disadvantages of the most common rodent models of focal ischaemia. *British Journal of Pharmacology,* 164, 1062-1078.

MAIER, I. C., BAUMANN, K., THALLMAIR, M., WEINMANN, O., SCHOLL, J. & SCHWAB, M. E. 2008. Constraint-induced movement therapy in the adult rat after unilateral corticospinal tract injury. *J Neurosci,* 28, 9386-403.

MARKUS, H. 2004. Cerebral perfusion and stroke. *Journal of Neurology, Neurosurgery, and Psychiatry,* 75, 353-361.

MATSUYAMA, K. & DREW, T. 1997. Organization of the projections from the pericruciate cortex to the pontomedullary brainstem of the cat: a study using the anterograde tracer Phaseolus vulgaris-leucoagglutinin. *J Comp Neurol,* 389, 617-41.

MATSUYAMA, K., MORI, F., KUZE, B. & MORI, S. 1999. Morphology of single pontine reticulospinal axons in the lumbar enlargement of the cat: a study using the anterograde tracer PHA-L. *J Comp Neurol,* 410, 413-30.

MATSUYAMA, K., NAKAJIMA, K., MORI, F., AOKI, M. & MORI, S. 2004. Lumbar commissural interneurons with reticulospinal inputs in the cat: morphology and discharge patterns during fictive locomotion. *J Comp Neurol,* 474, 546-61.

MEMEZAWA, H., SMITH, M. L. & SIESJO, B. K. 1992. Penumbral tissues salvaged by reperfusion following middle cerebral artery occlusion in rats. *Stroke,* 23, 552-9.

MCGILL, J. 2005. Functional recovery after stroke in the stroke-prone spontaneously hypertensive rat (SHRSP) and Wistar Kyoto rat (WKY) (PhD thesis, University of Glasgow).

MILES, G. B., HARTLEY, R., TODD, A. J. & BROWNSTONE, R. M. 2007. Spinal cholinergic interneurons regulate the excitability of motoneurons during locomotion. *Proceedings of the National Academy of Sciences,* 104, 2448-2453.

MILLER, M. W. 1987. The origin of corticospinal projection neurons in rat. *Exp Brain Res,* 67, 339-51.

MODO, M., STROEMER, R. P., TANG, E., VEIZOVIC, T., SOWNISKI, P. & HODGES, H. 2000. Neurological sequelae and long-term behavioural assessment of rats with transient middle cerebral artery occlusion. *J Neurosci Methods,* 104, 99-109.

MOLANDER, C., XU, Q., RIVERO-MELIAN, C. & GRANT, G. 1989. Cytoarchitectonic organization of the spinal cord in the rat: II. The cervical and upper thoracic cord. *J Comp Neurol,* 289, 375-85.

MONTGOMERY, L. R., HERBERT, W. J. & BUFORD, J. A. 2013. Recruitment of ipsilateral and contralateral upper limb muscles following stimulation of the cortical motor areas in the monkey. *Experimental Brain Research,* 230, 153-164.

MORI, M., KOSE, A., TSUJINO, T. & TANAKA, C. 1990. Immunocytochemical localization of protein kinase C subspecies in the rat spinal cord: Light and electron microscopic study. *The Journal of Comparative Neurology,* 299, 167-177.

MORI, S., MATSUYAMA, K., MORI, F. & NAKAJIMA, K. 2001. Supraspinal sites that induce locomotion in the vertebrate central nervous system. *Adv Neurol,* 87, 25-40.

MORRIS, R., TOSOLINI, A. P., GOLDSTEIN, J. D. & WHISHAW, I. Q. 2011. Impaired arpeggio movement in skilled reaching by rubrospinal tract lesions in the rat: a behavioral/anatomical fractionation. *J Neurotrauma,* 28, 2439-51.

MUIR, G. D., WEBB, A. A., KANAGAL, S. & TAYLOR, L. 2007. Dorsolateral cervical spinal injury differentially affects forelimb and hindlimb action in rats. *Eur J Neurosci,* 25, 1501-10.

MURRAY, H. M. & HAINES, D. E. 1975. The rubrospinal tract in a prosimian primate, Galago senegalensis. *Brain Behav Evol,* 12, 311-33.

NATHAN, P. W. & SMITH, M. C. 1955. Long descending tracts in man. I. Review of present knowledge. *Brain,* 78, 248-303.

NEAFSEY, E. J., BOLD, E. L., HAAS, G., HURLEY-GIUS, K. M., QUIRK, G., SIEVERT, C. F. & TERREBERRY, R. R. 1986. The organization of the rat motor cortex: a microstimulation mapping study. *Brain Res,* 396, 77-96.

NEWMAN, D. B., HILLEARY, S. K. & GINSBERG, C. Y. 1989. Nuclear terminations of corticoreticular fiber systems in rats. *Brain Behav Evol,* 34, 223-64.

NI, Y., NAWABI, H., LIU, X., YANG, L., MIYAMICHI, K., TEDESCHI, A., XU, B., WALL, N. R., CALLAWAY, E. M. & HE, Z. 2014. Characterization of long descending premotor propriospinal neurons in the spinal cord. *J Neurosci,* 34, 9404-17.

NISHIMARU, H., RESTREPO, C. E. & KIEHN, O. 2006. Activity of Renshaw cells during locomotor-like rhythmic activity in the isolated spinal cord of neonatal mice. *J Neurosci,* 26, 5320-8.

NOOR, R., WANG, C. X. & SHUAIB, A. 2003. Effects of hyperthermia on infarct volume in focal embolic model of cerebral ischemia in rats. *Neurosci Lett,* 349, 130-2.

NOWAK, D. A., GREFKES, C., AMELI, M. & FINK, G. R. 2009. Interhemispheric competition after stroke: brain stimulation to enhance recovery of function of the affected hand. *Neurorehabil Neural Repair,* 23, 641-56.

NUDO, R. J. 2006. Mechanisms for recovery of motor function following cortical damage. *Current Opinion in Neurobiology,* 16, 638-644.

NYBERG-HANSEN, R. 1965. Sites and Mode of Termination of Reticulo-Spinal Fibers in the Cat. An Experimental Study with Silver Impregnation Methods. *J Comp Neurol,* 124, 71-99.

Nyberg-Hansen R, Mascitti TA .1964. Sites +mode of termination of fibers of vestibulospinal tract in cat - experimental study with silver impregnation methods. *J Comp Neurol* 122:369.

ODA, Y. 1999. Choline acetyltransferase: the structure, distribution and pathologic changes in the central nervous system. *Pathol Int,* 49, 921-37.

O'LEARY, D. D. & TERASHIMA, T. 1988. Cortical axons branch to multiple subcortical targets by interstitial axon budding: implications for target recognition and "waiting periods". *Neuron,* 1, 901-10.

PALMER, E. & ASHBY, P. 1992. corticospinal projections to upper limb motoneurons in humans. *Journal of Physiology-London,* 448, 397-412.

PAXINOS, G. & WATSON, C. 2005. *The Rat Brain in Stereotaxic Coordinates.* 6th ed. Amsterdam: Academic Press.

PAXINOS, G., WATSON, C., PENNISI, M. & TOPPLE, A. 1985. Bregma, lambda and the interaural midpoint in stereotaxic surgery with rats of different sex, strain and weight. *Journal of neuroscience methods,* 13, 139-143.

PENDLEBURY, S. T., BLAMIRE, A. M., LEE, M. A., STYLES, P. & MATTHEWS, P. M. 1999. Axonal Injury in the Internal Capsule Correlates With Motor Impairment After Stroke. *Stroke,* 30, 956-962.

PERSSON, S., BOULLAND, J.-L., ASPLING, M., LARSSON, M., FREMEAU, R. T., EDWARDS, R. H., STORM-MATHISEN, J., CHAUDHRY, F. A. & BROMAN, J. 2006. Distribution of vesicular glutamate transporters 1 and 2 in the rat spinal cord, with a note on the spinocervical tract. *The Journal of Comparative Neurology,* 497, 683-701.

PETERSON, B. W. 1979. Reticulospinal projections to spinal motor nuclei. *Annu Rev Physiol,* 41, 127-40.

PETERSON, B., ANDERSON, M. & FILION, M. 1974. Responses of ponto-medullary reticular neurons to cortical, tectal and cutaneous stimuli. *Experimental Brain Research,* 21, 19-44.

PETRAS JM. 1967. Cortical, tectal and tegmental fiber connections in the spinal cord of the cat. *Brain Res,* 6, 275-324.

POMPEIANO, O. 1972. Spinovestibular relations: anatomical and physiological aspects. *Prog Brain Res,* 37, 263-96.

PORTER, R. & LEMON, R. N. 1993. *Corticospinal function and voluntary movement,* Oxford, UK, Clarendon.

PUIG, J., PEDRAZA, S., BLASCO, G., DAUNIS-I-ESTADELLA, J., PRADOS, F., REMOLLO, S., PRATS-GALINO, A., SORIA, G., BOADA, I., CASTELLANOS, M. & SERENA, J. 2011. Acute Damage to the Posterior Limb of the Internal Capsule on Diffusion Tensor Tractography as an Early Imaging Predictor of Motor Outcome after Stroke. *American Journal of Neuroradiology,* 32, 857-863.

PUSKÁR, Z., POLGÁR, E. & TODD, A. J. 2001. A population of large lamina I projection neurons with selective inhibitory input in rat spinal cord. Neuroscience,102,167-176

QUINLAN, K. A. & KIEHN, O. 2007. Segmental, synaptic actions of commissural interneurons in the mouse spinal cord. *J Neurosci,* 27, 6521-30.

RALSTON, D. D. & RALSTON, H. J., 3RD 1985. The terminations of corticospinal tract axons in the macaque monkey. *J Comp Neurol,* 242, 325-37.

REED, W. R., SHUM-SIU, A. & MAGNUSON, D. S. K. 2008. RETICULOSPINAL PATHWAYS IN THE VENTROLATERAL FUNICULUS WITH TERMINATIONS IN THE CERVICAL AND LUMBAR ENLARGEMENTS OF THE ADULT RAT SPINAL CORD. *Neuroscience,* 151, 505-517.

REED, W. R., SHUM-SIU, A., WHELAN, A., ONIFER, S. M. & MAGNUSON, D. S. K. 2009. Anterograde labeling of ventrolateral funiculus pathways with spinal enlargement connections in the adult rat spinal cord. *Brain Research,* 1302, 76-84.

REHME, A. K., FINK, G. R., VON CRAMON, D. Y. & GREFKES, C. 2011. The role of the contralesional motor cortex for motor recovery in the early days after stroke assessed with longitudinal FMRI. *Cereb Cortex,* 21, 756-68.

REN, K. & RUDA, M. A. 1994. A comparative study of the calcium-binding proteins calbindin-D28K, calretinin, calmodulin and parvalbumin in the rat spinal cord. *Brain Research Reviews,* 19, 163-179.

RIDDLE, C. N., EDGLEY, S. A. & BAKER, S. N. 2009. Direct and Indirect Connections with Upper Limb Motoneurons from the Primate Reticulospinal Tract. *The Journal of neuroscience : the official journal of the Society for Neuroscience,* 29, 4993-9.

ROBINSON, M., MACRAE, I., TODD, M., REID, J. & MCCULLOCH, J. 1990. Reduction of local cerebral blood flow to pathological levels by endothelin-1 applied to the middle cerebral artery in the rat. *Neurosci Lett,* 118, 269 - 72.

ROHL, L., OSTERGAARD, L., SIMONSEN, C. Z., VESTERGAARD-POULSEN, P., ANDERSEN, G., SAKOH, M., LE BIHAN, D. & GYLDENSTED, C. 2001. Viability thresholds of ischemic penumbra of hyperacute stroke defined by perfusion-weighted MRI and apparent diffusion coefficient. *Stroke,* 32, 1140-6.

ROSENZWEIG, E. S., BROCK, J. H., CULBERTSON, M. D., LU, P., MOSEANKO, R., EDGERTON, V. R., HAVTON, L. A. & TUSZYNSKI, M. H. 2009. Extensive spinal decussation and bilateral termination of cervical corticospinal projections in rhesus monkeys. *The Journal of Comparative Neurology,* 513, 151-163.

RUIGROK, T. J., PIJPERS, A., GOEDKNEGT-SABEL, E. & COULON, P. 2008. Multiple cerebellar zones are involved in the control of individual muscles: a retrograde transneuronal tracing study with rabies virus in the rat. *Eur J Neurosci,* 28, 181-200.

SAKAI, S. T., DAVIDSON, A. G. & BUFORD, J. A. 2009. Reticulospinal Neurons in the Pontomedullary Reticular Formation of the Monkey (Macaca fascicularis). *Neuroscience,* 163, 1158-1170.

SASAKI, S., ISA, T., PETTERSSON, L. G., ALSTERMARK, B., NAITO, K.,

YOSHIMURA, K., SEKI, K. & OHKI, Y. 2004. Dexterous finger movements in primate without monosynaptic corticomotoneuronal excitation. *J Neurophysiol,* 92**,** 3142-7.

SAVER, J. L. 2004. Number needed to treat estimates incorporating effects over the entire range of clinical outcomes: novel derivation method and application to thrombolytic therapy for acute stroke. *Arch Neurol,* 61**,** 1066-70.

SCHALLERT, T. & WHISHAW, I. Q. 1984. Bilateral cutaneous stimulation of the somatosensory system in hemidecorticate rats. *Behav Neurosci,* 98**,** 518-40.

SHAPOVALOV, A. I. & ARUSHANYAN, E. B. 1966. Effect of stimulation of brain stem and motor cortex on activity of spinal neurons. *Fed Proc Transl Suppl,* 25**,** 407-12.

SHAPOVALOV, A. I. & GUREVITCH, N. R. 1970. Monosynaptic and disynaptic reticulospinal actions on lumbar motoneurons of the rat. *Brain Res,* 21**,** 249-63.

SCHEPENS, B., STAPLEY, P. & DREW, T. 2008. Neurons in the pontomedullary reticular formation signal posture and movement both as an integrated behavior and independently. *J Neurophysiol,* 100**,** 2235-53.

SCHIEBER, MH (19900. How might the motor cortex individuate movements? *Trends Neurosci 13, 440-445*

SCHIEMANCK, S. K., KWAKKEL, G., POST, M. W., KAPPELLE, L. J. & PREVO, A. J. 2008. Impact of internal capsule lesions on outcome of motor hand function at one year post-stroke. *J Rehabil Med,* 40**,** 96-101.

SCHOEN, J. Comparative aspects of the descending fibre systems in the spinal cord. *Progress in Brain research,* 11, 203-22

SCREMIN, O.U. 2004. "Cerebral Vascular System" *The Rat Nervous System (Third Edition).* Burlington: Academic Press

SIESJO, B. K. 1992. Pathophysiology and treatment of focal cerebral ischemia. Part II: Mechanisms of damage and treatment. *J Neurosurg,* 77**,** 337-54

SOLEMAN, S., YIP, P. K., DURICKI, D. A. & MOON, L. D. 2012. Delayed treatment with chondroitinase ABC promotes sensorimotor recovery and plasticity after stroke in aged rats. *Brain,* 135**,** 1210-23.

SOTEROPOULOS, D. S., EDGLEY, S. A. & BAKER, S. N. 2011. Lack of Evidence for Direct Corticospinal Contributions to Control of the Ipsilateral Forelimb in Monkey. *The Journal of neuroscience : the official journal of the Society for Neuroscience,* 31**,** 11208-11219.

SOTEROPOULOS, D. S., EDGLEY, S. A. & BAKER, S. N. 2013. Spinal commissural connections to motoneurons controlling the primate hand and wrist. *J Neurosci,* 33**,** 9614-25.

SOTEROPOULOS, D. S., WILLIAMS, E. R. & BAKER, S. N. 2012. Cells in the monkey ponto-medullary reticular formation modulate their activity with slow finger movements. *The Journal of Physiology,* 590**,** 4011-4027.

STECINA, K., JANKOWSKA, E., CABAJ, A., PETTERSSON, L. G., BANNATYNE, B. A. & MAXWELL, D. J. 2008. Premotor interneurones contributing to actions of feline pyramidal tract neurones on ipsilateral hindlimb motoneurones. *The Journal of Physiology,* 586**,** 557-574

STECINA, K. & JANKOWSKA, E. 2007. Uncrossed actions of feline corticospinal tract neurones on hindlimb motoneurones evoked via ipsilaterally descending pathways. *The Journal of Physiology,* 580**,** 119-132.

STEPIEN, A. E., TRIPODI, M. & ARBER, S. 2010. Monosynaptic rabies virus reveals premotor network organization and synaptic specificity of cholinergic partition cells. *Neuron,* 68**,** 456-72.

STOECKEL, M. C. & BINKOFSKI, F. 2010. The role of ipsilateral primary motor cortex in movement control and recovery from brain damage. *Exp Neurol,* 221**,** 13-7.

STOKKE, M. F., NISSEN, U. V., GLOVER, J. C. & KIEHN, O. 2002. Projection patterns of commissural interneurons in the lumbar spinal cord of the neonatal rat. *The Journal of Comparative Neurology,* 446**,** 349-359.

STROEMER, P., PATEL, S., HOPE, A., OLIVEIRA, C., POLLOCK, K. & SINDEN, J. 2009. The neural stem cell line CTX0E03 promotes behavioral recovery and endogenous neurogenesis after experimental stroke in a dose-dependent fashion. *Neurorehabil Neural Repair,* 23**,** 895-909.

SUGIUCHI, Y., KAKEI, S. & SHINODA, Y. 1992. Spinal commissural neurons mediating vestibular input to neck motoneurons in the cat upper cervical spinal cord. *Neurosci Lett,* 145**,** 221-4.

TAKAKUSAKI, K., KOHYAMA, J., MATSUYAMA, K. & MORI, S. 2001. Medullary reticulospinal tract mediating the generalized motor inhibition in cats: Parallel inhibitory mechanisms acting on motoneurons and on interneuronal transmission in reflex pathways. *Neuroscience,* 103**,** 511-527.

TAKEUCHI, N., CHUMA, T., MATSUO, Y., WATANABE, I. & IKOMA, K. 2005. Repetitive transcranial magnetic stimulation of contralesional primary motor cortex improves hand function after stroke. *Stroke,* 36**,** 2681-6.

TAMURA, A., GRAHAM, D., MCCULLOCH, J. & TEASDALE, G. 1981. Focal cerebral ischemia in the rat: 1. Description of technique and early neuropathological consequences following middle cerebral artery occlusion. *J Cereb Blood Flow Metab,* 1**,** 53 - 60.

TAN, A. M., CHAKRABARTY, S., KIMURA, H. & MARTIN, J. H. 2012. Selective corticospinal tract injury in the rat induces primary afferent fiber sprouting in the spinal cord and hyperreflexia. *J Neurosci,* 32**,** 12896-908.

TATU, L., MOULIN, T., BOGOUSSLAVSKY, J. & DUVERNOY, H. 1998. Arterial territories of the human brain: cerebral hemispheres. *Neurology,* 50**,** 1699-708.

TEN DONKELAAR, H. J. 1988. Evolution of the red nucleus and rubrospinal tract. *Behavioural Brain Research,* 28**,** 9-20.

TERASHIMA, T. 1995. Anatomy, development and lesion-induced plasticity of rodent corticospinal tract. *Neuroscience Research,* 22**,** 139-161.

THOMALLA, G., GLAUCHE, V., KOCH, M. A., BEAULIEU, C., WEILLER, C. & RÖTHER, J. 2004. Diffusion tensor imaging detects early Wallerian degeneration of the pyramidal tract after ischemic stroke. *NeuroImage,* 22, 1767-1774.

TODD, A. J. 1997. A method for combining confocal and electron microscopic examination of sections processed for double-or triple-labelling immunocytochemistry. *Journal of Neuroscience Methods,*73,149-157.

TRAYSTMAN, R. J. 2003. Animal Models of Focal and Global Cerebral Ischemia. *ILAR Journal,* 44**,** 85-95.

TRUEMAN, R., HARRISON, D., DWYER, D., DUNNETT, S., HOEHN, M. & FARR, T. 2011. A Critical Re-Examination of the Intraluminal Filament MCAO Model: Impact of External Carotid Artery Transection. *Translational Stroke Research,* 2**,** 651-661.

TSUCHIYA, D., HONG, S., KAYAMA, T., PANTER, S. & WEINSTEIN, P. 2003. Effect of suture size and carotid clip application upon blood flow and infarct volume after permanent and temporary middle cerebral artery occlusion in mice. *Brain Res,* 970**,** 131 - 9.

UEDA, H. & FUJITA, R. 2004. Cell death mode switch from necrosis to apoptosis in brain. *Biol Pharm Bull,* 27, 950-5.

UENO, M., HAYANO, Y., NAKAGAWA, H. & YAMASHITA, T. 2012. Intraspinal rewiring of the corticospinal tract requires target-derived brain-derived neurotrophic factor and compensates lost function after brain injury. *Brain,* 135, 1253-67.

ULUÇ, K., MIRANPURI, A., KUJOTH, G. C., AKTÜRE, E. & BAŞKAYA, M. K. 2011. Focal Cerebral Ischemia Model by Endovascular Suture Occlusion of the Middle Cerebral Artery in the Rat. *Journal of Visualized Experiments : JoVE,* 1978.

UMEDA, T., TAKAHASHI, M., ISA, K. & ISA, T. 2010. Formation of Descending Pathways Mediating Cortical Command to Forelimb Motoneurons in Neonatally Hemidecorticated Rats. *Journal of Neurophysiology,* 104, 1707-1716.

VALERIANI, V., DEWAR, D. & MCCULLOCH, J. 2000. Quantitative assessment of ischemic pathology in axons, oligodendrocytes, and neurons: attenuation of damage after transient ischemia. *J Cereb Blood Flow Metab,* 20, 765-71.

VALTSCHANOFF, J. G., WEINBERG, R. J. & RUSTIONI, A. 1993. Amino acid immunoreactivity in corticospinal terminals. Exp Brain Res, 93, 95-103

VAN KAN, P. L. E. & MCCURDY, M. L. 2002. Contribution of Primate Magnocellular Red Nucleus to Timing of Hand Preshaping During Reaching to Grasp. *Journal of Neurophysiology,* 87, 1473-1487.

VERHEYDEN, G., NIEUWBOER, A., DE WIT, L., THIJS, V., DOBBELAERE, J., DEVOS, H., SEVERIJNS, D., VANBEVEREN, S. & DE WEERDT, W. 2008. Time course of trunk, arm, leg, and functional recovery after ischemic stroke. *Neurorehabil Neural Repair,* 22, 173-9.

VIRLEY, D., BEECH, J. S., SMART, S. C., WILLIAMS, S. C. R., HODGES, H. &

HUNTER, A. J. 2000. A Temporal MRI Assessment of Neuropathology After Transient Middle Cerebral Artery Occlusion in the Rat[colon] Correlations With Behavior. *J Cereb Blood Flow Metab,* 20, 563-582.

WARD, N. S. & FRACKOWIAK, R. S. J. 2006. The functional anatomy of cerebral reorganisation after focal brain injury. *Journal of Physiology-Paris,* 99, 425-436.

WEGENER, S., WEBER, R., RAMOS-CABRER, P., UHLENKUEKEN, U., WIEDERMANN, D., KANDAL, K., VILLRINGER, A. & HOEHN, M. 2005. Subcortical lesions after transient thread occlusion in the rat: T2-weighted magnetic resonance imaging findings without corresponding sensorimotor deficits. *Journal of Magnetic Resonance Imaging,* 21, 340-346.

WEIDNER, N., NER, A., SALIMI, N. & TUSZYNSKI, M. H. 2001. Spontaneous corticospinal axonal plasticity and functional recovery after adult central nervous system injury. *Proceedings of the National Academy of Sciences of the United States of America,* 98, 3513-3518.

WESSELS T, WESSELS C, ELLSIEPEN A, REUTER I, TRITTMACHER S & STOLZ E. 2006. Contribution of diffusion-weighted imaging in determination of stroke etiology. *AJNR Am J Neuroradiol*, 27(1), 35-9.

WHISHAW, I. Q., O'CONNOR, W. T. & DUNNETT, S. B. 1986. The contributions of motor cortex, nigrostriatal dopamine and caudate-putamen to skilled forelimb use in the rat. *Brain,* 109, 805-843.

WHISHAW, I. Q. & COLES, B. L. 1996. Varieties of paw and digit movement during spontaneous food handling in rats: postures, bimanual coordination, preferences, and the effect of forelimb cortex lesions. *Behav Brain Res,* 77, 135-48.

WIELOCH, T. & NIKOLICH, K. 2006. Mechanisms of neural plasticity following brain injury. *Curr Opin Neurobiol,* 16**,** 258-64.

WILSON, V. J., WYLIE, R. M. & MARCO, L. A. 1967. Projection to the spinal cord from the medial and descending vestibular nuclei of the cat. *Nature,* 215**,** 429-30.

YANG, H. W. & LEMON, R. N. 2003. An electron microscopic examination of the corticospinal projection to the cervical spinal cord in the rat: lack of evidence for cortico-motoneuronal synapses. *Exp Brain Res,* 149**,** 458-69.

ZAAIMI, B., EDGLEY, S. A., SOTEROPOULOS, D. S. & BAKER, S. N. 2012. Changes in descending motor pathway connectivity after corticospinal tract lesion in macaque monkey. *Brain,* 135**,** 2277-2289.

ZAGORAIOU, L., AKAY, T., MARTIN, J. F., BROWNSTONE, R. M., JESSELL, T. M. & MILES, G. B. 2009. A cluster of cholinergic premotor interneurons modulates mouse locomotor activity. *Neuron,* 64**,** 645-62.

ZAI, L., FERRARI, C., SUBBAIAH, S., HAVTON, L. A., COPPOLA, G., STRITTMATTER, S., IRWIN, N., GESCHWIND, D. & BENOWITZ, L. I. 2009. Inosine alters gene expression and axonal projections in neurons contralateral to a cortical infarct and improves skilled use of the impaired limb. *J Neurosci,* 29**,** 8187-97.

ZAPOROZHETS, E., COWLEY, K. C. & SCHMIDT, B. J. 2006. Propriospinal neurons contribute to bulbospinal transmission of the locomotor command signal in the neonatal rat spinal cord. *The Journal of Physiology,* 572**,** 443-458.

ZAROW, G. J., KARIBE, H., STATES, B. A., GRAHAM, S. H. & WEINSTEIN, P. R. 1997. Endovascular suture occlusion of the middle cerebral artery in rats: effect of suture insertion distance on cerebral blood flow, infarct distribution and infarct volume. *Neurol Res,* 19**,** 409-16.

<u>Appendix 1</u>: Formulae for common laboratory reagents

To prepare 4 L of 0.1 M phosphate buffer (PB) stock solution:
37.4 g of NaH2PO (2H2O) in 1200 ml H2O
84.9 g Na2HPO4 in 3000 ml H2O
Distilled water is added to bring the total volume to 4 L with buffered pH 7.4

To prepare 0.3 M phosphate buffer saline solution (PBS):
100 ml of 0.2 M PB in 1900 distilled water plus 36 g NaCl

PBST: 0.3% Triton X-100 in PB

Ringer solution:
Contains CaCl2 + KCl + NaCl + NaHCO3 + glucose in PB, buffered to pH 7.4

To prepare 1L of 4% paraformaldehyde fixative solution:
40 g paraformaldehyde
400 ml distilled H2O at ≈ 68°C
500 ml 0.2 PB
NaOH, to raise pH (few drops)
Solution is cooled and then filtered with enough distilled water added to bring the total
volume to 1 L with pH adjusted as necessary
pH = - log [H+]

C = Celsius; g = grams; L = litres; log = logarithmic, base 10; ml = millilitre;
M= molar (moles per litre).

Appendix 2: Primary antibody characterisation

The following summarises information regarding antibody specificity, controls, and application and is provided as per suppliers' data (referenced in Tables 4.1, 5.1, and 6.1 in chapters 4, 5 and 6 respectively).

CTb: Traces myelinated axons possessing the GM1 ganglioside, retrogradely and anterogradely. The specificity of antibody against CTb is demonstrated by the lack of staining in regions of the CNS that did not contain neurons that had transported the tracer and by the presence of immunostaining in neurons known to project to the injection sites.

ChAT: Neuronal enzyme that catalyses the synthesis of ACh from acetyl coenzyme and choline, therefore found primarily in cholinergic neurons. Positive controls include the presence of immunostaining in human placenta lysates, rat forebrain/rostral hypothalamus. Antiserum specificity routinely evaluated by Western blots on mouse brain lysates.

FG: Retrogradely transported fluorescent marker that accumulates in lysosomes of neurons. The specificity of antibody against FG is demonstrated by the lack of staining in regions of the CNS that did not contain neurons that had transported the tracer and by the presence of immunostaining in neurons known to project to the injection sites.

VGAT Functions in the uptake of GABA and glycine into synaptic vesicles. Marker of presynaptic GABAergic and glycinergic neurons. Antisera specificity is assured by Western blot on rat retina lysates. The immunogen peptide shows no significant homology with other known proteins.

VGLUT1 Mediates the uptake of glutamate into synaptic vesicles at presynaptic nerve terminals of excitatory neural cells. Antisera specificity assured by ICC on tissue sections from the rat CNS corresponding to the pattern described using other antisera to VGLUT1.

VGLUT2 localised in synaptic vesicles exhibiting excitatory features. Antisera specificity is assured by Western blots on rat brain lysate.

Calbindin: Member of a large family of intracellular calcium-binding proteins of the EF-hand related to calmodulin and troponin-C. Positive controls include the presence of specific staining of cerebellum Purkinje cells. It shows no cross-reactivity with other calcium-binding proteins e.g. calretinin

Calbindin: Calcium- binding protein that is expressed in central and peripheral nervous system and in many normal and pathological tissues. Positive controls include the presence of immunostaining in sensory ganglia and mesothelioma tissue.

Appendix 3: Protocol for paraffin processing of rat brains

Stage	Process	Time Period (h)
1	70% EtOH	2
2	80% EtOH	3
3	95% EtOH	4
4	Absolute EtOH 1	4
5	Absolute EtOH 2	5
6	Absolute EtOH 3	5
7	Absolute EtOH 4	6
8	50% Alcohol/50% Xylene	4
9	Xylene 1	5
10	Xylene 2	5
11	Paraffin wax 1	5
12	Paraffin wax 2	5
13	Paraffin wax 3	6

Appendix 4: Haematoxylin and Eosin staining procedure for paraffin embedded sections

Stage	Process	Time period (min)
1	Histoclear 1	5
2	Histoclear 2	5
3	Histoclear 3	5
4	Absolute EtOH 1	3
5	Absolute EtOH 2	3
6	90% EtOH	3
7	70% EtOH	3
8	Wash in running water	4
9	Haematoxylin staining	4
10	Wash in running water	2
11	Differentiation in acid EtOH	2 dips
12	Wash in running water	3
13	Scot's tap water substitute	2
14	Wash in running water	2
15	70% EtOH	2
16	90% EtOH	2
17	Alcoholic Eosin staining (95%)	4
18	Absolute EtOH 1	4
19	Absolute EtOH 2	4
20	Absolute EtOH 3	4
21	Histoclear 1	4
22	Histolclear 2	4
23	Histoclear 3	4

Appendix 5: No. of sham rats with impairments in each of the 11 subtests of the neurological score over 28 days

Sham (n=5)	No. of rats with impairments							
	Day -1	Day 1	Day 2	Day 3	Day 7	Day 14	Day 21	Day 28
Paw placement	0	0	0	0	0	0	0	0
Righting reflex	0	0	0	0	0	0	0	0
Horizontal bar	0	4	4	0	0	1	0	1
Inclined platform	0	4	1	0	0	0	0	0
Rotation	0	0	0	0	0	0	0	0
Visual fore-paw reaching	0	0	0	0	0	0	0	0
Contralateral reflex	0	0	0	0	0	0	0	0
Circling	0	0	0	0	0	0	0	0
Grasping	0	0	0	0	0	0	0	0
Motility	0	2	1	0	0	0	0	0
General condition	0	4	1	0	0	0	0	0

Appendix 6: **No. of MCAo rats with impairments in each of the 11 subtests of the neurological score over 28 days**

| MCAo (n=4)	No. of rats with impairments							
	Day -1	Day 1	Day 2	Day 3	Day 7	Day 14	Day 21	Day 28
Paw placement	0	4	4	3	3	3	3	2
Righting reflex	0	0	0	0	0	0	0	0
Horizontal bar	0	4	4	4	4	4	4	3
Inclined platform	0	4	3	3	2	2	2	2
Rotation	0	2	2	1	0	0	0	0
Visual fore-paw reaching	0	4	4	4	4	4	2	2
Contralateral reflex	0	0	0	0	0	0	0	0
Circling	0	2	2	1	1	1	1	1
Grasping	0	4	4	4	2	2	2	2
Motility	0	4	2	0	0		0	0
General condition	0	0	0	0	0	0	0	0

Appendix 7A : Example of CTb injection site in excluded MCAo rat with large infarct
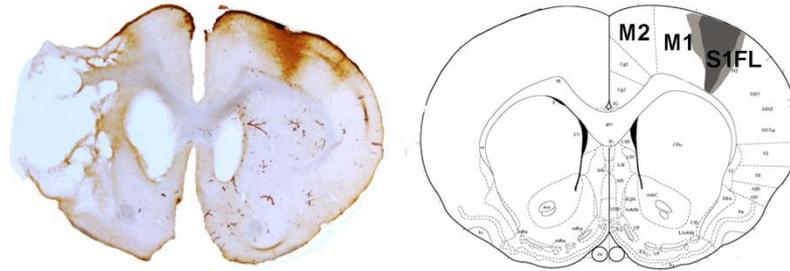
Note that the core of the injection site is lateral to M1 and M2

M1 = primary motor cortex; M2 = secondary motor cortex; S1FL = primary somatosensory-forelimb region

Appendix 7B: Reconstructed CTb injection sites for all sham and MCAo rats used in Chapter 4
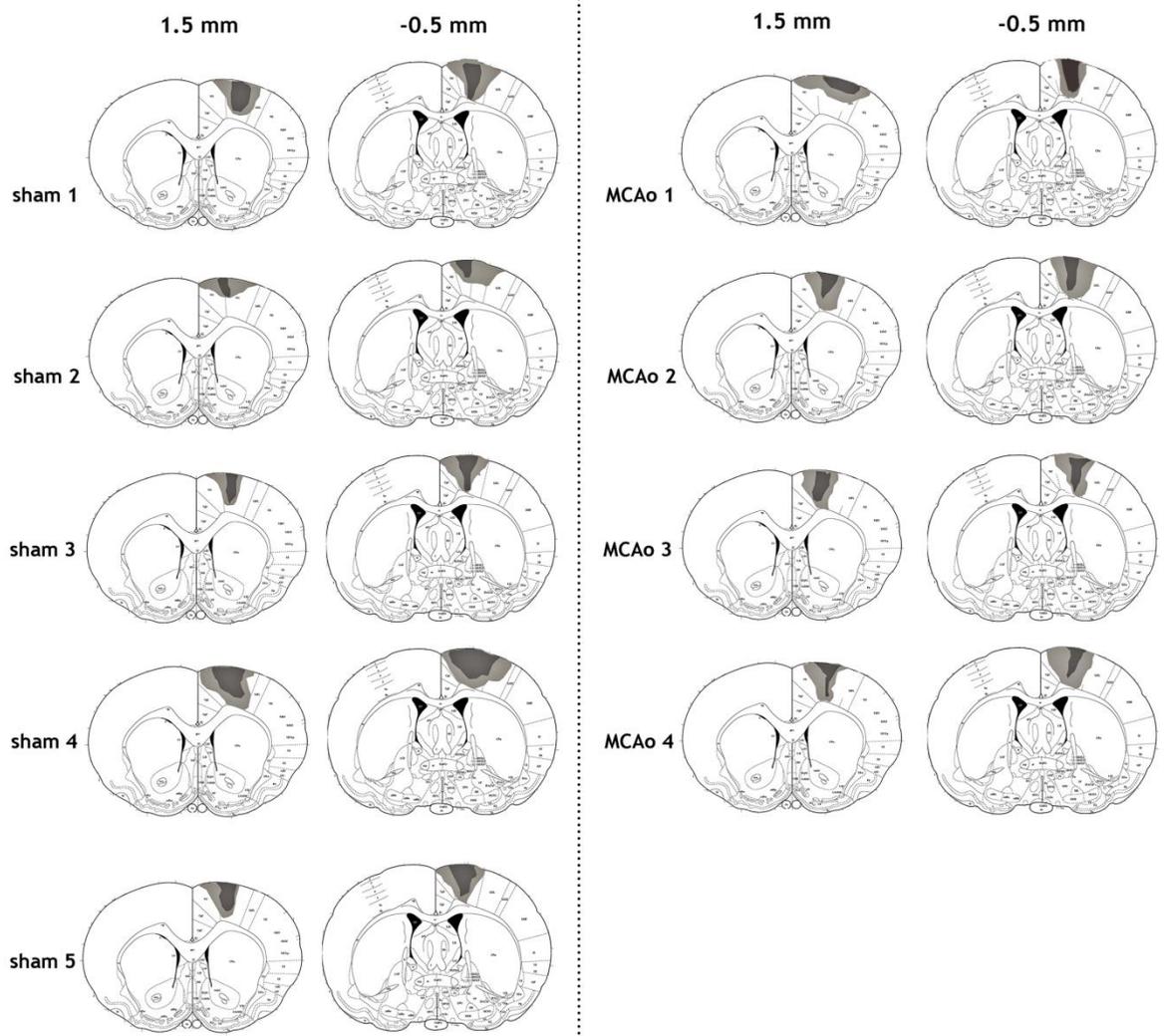
Appendix 8: Mean ± SDs for all three CTb-labelled terminal counting methods for sham and MCAo rats

	Segment		unaffected (left)	affected (right)	Ratio (affected/unaffected)
CTb-labelled terminal counts (automatic)	C3	sham	4522 ± 1900	430 ± 208	0.09 ± 0.03
		MCAo	4229 ± 3006	459 ± 344	0.11 ± 0.04
	C5	sham	5224 ± 1930	442 ± 192	0.09 ± 0.03
		MCAo	4632 ± 2402	486 ± 220	0.12 ± 0.04
	C7	sham	5263 ± 1566	520 ± 186	0.09 ± 0.02
		MCAo	4711 ± 2002	469 ± 270	0.1 ± 0.02
CTb$^+$ surface area	C3	sham	0.032 ± 0.011	0.002 ± 0.002	0.07 ± 0.06
		MCAo	0.026 ± 0.015	0.002 ± 0.002	0.10 ± 0.06
	C5	sham	0.041 ± 0.022	0.003 ± 0.002	0.06 ± 0.04
		MCAo	0.028 ± 0.014	0.002 ± 0.001	0.07 ± 0.05
	C7	sham	0.04 ± 0.025	0.003 ± 0.003	0.07 ± 0.04
		MCAo	0.028 ± 0.016	0.002 ± 0.001	0.08 ± 0.06
CTb-labelled terminal counts (manual)	C5	sham	90 ± 47	9 ± 5	0.09 ± 0.05
		MCAo	105 ± 48	9 ± 8	0.09 ± 0.06